SEISMIC BEHAVIOUR OF RC FRAME AND WALL-FRAME SYSTEMS SUPPORTED ON PILE FOUNDATIONS CONSIDERING SOIL-STRUCTURE INTERACTION

by

Nishant Sharma

DEPARTMENT OF CIVIL ENGINEERING
INDIAN INSTITUTE OF TECHNOLOGY GUWAHATI
GUWAHATI-781039, INDIA

December 2020

SEISMIC BEHAVIOUR OF RC FRAME AND WALL-FRAME SYSTEMS SUPPORTED ON PILE FOUNDATIONS CONSIDERING SOIL-STRUCTURE INTERACTION

A Thesis Submitted
in Partial Fulfillment of the Requirements
for the Degree of

DOCTOR OF PHILOSOPHY

by

Nishant Sharma

DEPARTMENT OF CIVIL ENGINEERING
INDIAN INSTITUTE OF TECHNOLOGY GUWAHATI
GUWAHATI-781039, INDIA

December 2020

CERTIFICATE

It is certified that the work contained in this thesis titled "*Seismic Behaviour of RC Frame and Wall-Frame Systems Supported on Pile Foundations Considering Soil-Structure Interaction"* by **Mr. Nishant Sharma** bearing roll no. 126104007, has been carried out under my supervision and submitted to Indian Institute of Technology Guwahati for the award of the degree of **Doctor of Philosophy**. This work has not been submitted elsewhere for a degree to the best of my knowledge and belief.

Date: 06 July 2020

Place: IIT Guwahati

Dr. Kaustubh Dasgupta
Associate Professor
Department of Civil Engineering
Indian Institute of Technology Guwahati
Guwahati-781039, Assam, India

Dr. Arindam Dey
Associate Professor
Department of Civil Engineering
Indian Institute of Technology Guwahati
Guwahati-781039, Assam, India

भारतीय प्रौद्योगिकी संस्थान गुवाहाटी
Indian Institute of Technology Guwahati

ABSTRACT

Construction of Reinforced Concrete (RC) buildings has gained considerable popularity, especially in the regions of economic development (mostly towns and cities). Most buildings in the urban areas comprise RC frame-type construction, with or without the presence of RC shear walls. The buildings in which the lateral force-induced due to the earthquake are resisted only by frame members are known as 'RC frame systems'. Similarly, the buildings in which the lateral forces are resisted by both the frame members as well as RC shear walls are known as 'RC wall-frame systems'. Governed by the prevailing strength and stiffness of the foundation soils, especially if they are relatively softer or weaker, these buildings require the support of pile foundations in most of the cases. For such systems, on being subjected to seismic motions, the soil influences the response of the structure and, vice-versa, the structure influences back the response of the soil, thereby initiating a mutual interacting phenomenon, which is termed as Soil-Structure Interaction (SSI). In such cases, depending on the relative stiffness of the footing substructure and foundation soil, soil-structure interaction (SSI) may intricately govern the combined response of the structure, footing, and the soil. Designers and analysts generally avoid considering complex SSI effects, owing to the expenses incurred in regards to the computational effort. Moreover, the prevalent notion that SSI effects are considered beneficial acts as a catalyst for ignoring SSI in such analyses and designs. However, if the supporting soil-pile foundation medium induces sufficient flexibility, then the structure can be considered flexible at the base, and SSI effects may significantly influence its elastic and inelastic response. The main aim of the present study and the dissertation work is to investigate the influence of soil-structure interaction (SSI) on the seismic behaviour of RC frame and RC wall-frame systems supported on pile foundations.

To realise the objectives of the present study, a rigorous numerical study has been carried out using the finite element (FE) based software framework (OpenSEES). Necessary convergence and validation studies are conducted to establish the efficacy of the numerical model. For numerical studies incorporating SSI, it is essential to model an appropriate extent of the soil domain, while simultaneously ensuring accuracy and computational efficiency. In the present study, it was asserted that the required lateral extent of the soil domain would not only depend on the dimension of the structure, but also on the extent of nonlinearity that is expected to arise within the soil inherently. Based on the

asymptotic reduction of the error in the SSI response (on increasing the soil domain length), simple relationships have been proposed for deciding an optimum lateral extent of the soil domain for different structural widths and levels of soil nonlinearity.

The incorporation of soil-pile foundation flexibility modifies the elastic and inelastic behaviour of the RC frame and RC wall-frame systems, which depends on several parameters of the structure and soil-pile foundation system. The elastic behaviour is assessed in terms of the modification of the fixed-base natural period (quantified in terms of modification factor, $MF = T_{SSI} / T_F$). Systems with larger stiffness contrast between the superstructure and foundation lead to a greater modification in the natural period and, subsequently, in the induced seismic forces. With the aid of Artificial Neural Network (ANN), predictive relationships are proposed for the quick and easy estimation of *MF*, which are further utilized for estimating effective natural period, T_{SSI}.

The influence of SSI on inelastic behaviour of the structures is assessed in terms of the ductility capacity and ductility demands. SSI modifies the yield and ultimate drifts, thereby leading to a modification in the ductility capacity of the RC frame and RC wall-frame systems. In general, SSI has a greater influence on ultimate drifts for RC frame systems. On the other hand, for RC wall-frame systems, the influence of SSI is greater on the yield drifts. Depending on the frame type, configuration, and soil condition, the extent of variation in ductility capacity under SSI is different. Incorporating shear walls in RC frame systems modifies its natural vibrational characteristics. This phenomenon alters its inelastic behaviour by increasing the possible allowance of ductility exhibition before the collapse, thereby modifying the ductility capacity.

SSI modifies the local and global ductility demands of the RC frame and RC wall-frame systems. Besides the properties of the superstructure and the soil-pile foundation system, the extent of modification is also dependent on the extent of nonlinearity experienced by the SSI system. The present study recommends conducting nonlinear SSI study and verifying the response of RC frame and RC wall-frame systems for which their corresponding fixed-base models exhibit inelasticity, and are represented by the inelastic response reduction factor $R_\mu > 2$. Incorporating shear walls causes a variation of the local demands (plastic hinge rotation) in the frame members at various storey levels that are prominently visible at the bottom and top storey levels.

Overall, this dissertation work reflects the importance of considering SSI in addressing the response of the RC frame and RC wall-frame buildings supported on pile foundations. It is recommended that consideration of SSI is especially inevitable for such building structures resting on a softer or weaker foundation medium. The guidelines provided in this study would aid the design engineers and analysts in their decision making as whether or not to consider the influence of seismic soil-structure interaction in the analysis of RC frame and RC wall-frame buildings.

Keywords: *Soil-structure interaction, RC frame, RC wall-frame, Nonlinear time-history analysis, Pushover analysis, Optimum soil domain length, Effective natural period, Ductility capacity, Ductility demands, ANN predictive model.*

This page has been left blank intentionally.

ACKNOWLEDGMENT

I would like to express my deep and sincere gratitude towards Dr. Kaustubh Dasgupta, and Dr. Arindam Dey for their warm encouragement and thoughtful guidance. It has been a great and memorable experience working under them. I value all their contributions in the form of time, suggestions, and ideas to make my Ph.D. experience a productive and stimulating one. I am especially grateful to them for their immense patience, friendly behaviour, care, coordination, understanding, and encouraging interactions, which has been a significant driving force for me to carry out my research work. Indeed, my supervisors will continue to remain my source of learning and inspiration. Through their interactions, I have learned many valuables inside as well as outside of the profession.

I am very thankful to the members of my doctoral committee for reviewing my work and providing valuable suggestions and comments. My sincere gratitude towards my Doctoral Committee (DC) chairperson, Prof. Hemant B. Kaushik, for his valuable suggestions while reviewing this research work. He has always been candid, caring, and provided immense support on any matter for my welfare. He shall always remain my source of inspiration and learning. I am thankful to Dr. Sandip Das, who has always been very kind to dispel my doubts and impart clarity of thought through his intriguing discussions that have always inspired me to learn from him. Dr. K. S. R. Krishna Murthy has been kind to provide his valuable comments and suggestions and is gratefully acknowledged.

My humble thanks to Prof. Ramgopal Upaluri and Dr. Snehal Kaushik for their encouragement, timely motivation, and valuable interactions. I shall forever cherish the personal love and care they have showered upon me.

I owe to my colleague cum friends, Mr. Biswajit Chand, Mr. Thainswemong Choudhury, and Mr. Nithin V. L., for their all-round support during my entire stay at IIT Guwahati. Indeed, they were a family away from family. I am grateful to Dr. Syed Humayun Basha for the warm friendship he has extended onto me during and after his stay at IIT Guwahati. The academic, as well as non-academic talks, shared with him, shall be cherished. The thoughtful and intriguing discussions with Dr. Kamaljyoti Nath will be irreplaceable. Special thanks to Dr. Rana Acharyya for introducing me to the concepts of Artificial Neural Networks and for sharing a warm friendship. The sincere friendship

extended by Miss Benazir Fatima Ahmed during my stay at IIT Guwahati is gratefully acknowledged.

I shall never be able to forget the delicious preparations made by my dear friend Biswajit's wife and his grandmother (Rashmi Ranjita Chand and Aai), which they used to feed with great love and affection. Their warm companionship alleviated the absence of family, felt while staying in the campus.

I would like to express my gratitude towards all my teachers at IIT Guwahati for imparting their wisdom and knowledge. My thanks are due to the staff, students, and research scholars at the Department of Civil Engineering who helped me and provided the necessary support.

The financial assistance provided by the Ministry of Human Resource Development (MHRD), Government of India, is gratefully acknowledged.

I would like to thank some of my close friends (Harsh, Pankaj, Vikas, Sridhar, Anjum, Sudeepta, Sandeep, Abhimanyu, Aditya, Abhay, Needhi, Anil) for their good wishes and support.

I would like to remember my Parents, Sisters, and Grandmother for their immense patience and unwavering support, which kept me moving through this long journey. I miss the presence of my late Grandfather, of whom I have fond memories. The constant support provided by my Uncles, Aunts, and Cousins is sincerely acknowledged. The caring attitude of my family has made my life happier and has helped me endure the testing times.

The blessing of my beloved Gurudev Late HH Bhakti Suhrid Paribrajak Maharaj, Late HH Bhakti Nista Sajjan Maharaj, and HH Hrishikesh Maharaj (Haricharan Prabhu) has been a guiding force, and I pray to always be guided through their instructions. Finally, I am grateful to Sri Gauranga and Sri Sri Radha Krishna for bestowing their causeless mercy directly and indirectly in the above form. I feel lucky and blessed to have received their mercy, and I shall remain forever grateful. I would like to pray for the good health and wellbeing of all.

Nishant Sharma

TABLE OF CONTENTS

LIST OF TABLES

This page has been intentionally left blank.

LIST OF FIGURES

LIST OF SYMBOLS AND ABBREVIATIONS

SYMBOLS

Symbol	Description
a_0, a_1	: Rayleigh damping coefficients
a_1, a_2	: Material constant in steel rebar
a_3, a_4	: Parameters determined experimentally in steel rebar
a_{itL}	: Acceleration response entity for location 'i' at time instant 't' corresponding to soil domain length 'L'
$a_{itL_{max}}$	: Acceleration response for location 'i' at time instant 't' corresponding to soil domain length 'L_{max}'
A	: Area of soil domain contributory to L-K boundary
A_c	: Cross-sectional area of the column
A_r	: Ratio of the cross-sectional area of the shear wall to the cross-sectional area of the column
A_w	: Cross-sectional area of shear wall
A_w	: Cross-sectional area of the shear wall
A_{we}	: Total effective area of shear walls in the first storey of the building
A_{wi}	: Effective cross-sectional area of the wall 'i' in the first storey of the building frame (in m^2)
b	: Ratio between the slope of the hardening and elastic branch
b''	: Width of confined core measured to outside of hoops
b_0	: Bias of the output node
b_h	: Bias of the hidden layer
C_1, C_2	: Ordinates of the branches of the bilinear fit
C_p	: Dashpot coefficient corresponding to the motion in the direction of primary wave
C_s	: Dashpot coefficient corresponding to the motion in the direction of shear wave
d	: Power of effective confinement ratio in shear modulus-confining pressure relationship.
d_b	: Diameter of longitudinal reinforcing bar
d_p	: Depth of pile
e_{itL}	: Error in the acceleration response for location 'i' at time instant 't' corresponding to soil domain length 'L'
E_0	: Initial slope in the compressive stress-strain relationship of concrete
E_c	: Elastic modulus of concrete
E_h	: Slope of the hardening branch in the stress-strain relationship in steel rebar
E_p	: Elastic modulus of the pile
E_s	: Slope of the elastic branch in the stress-strain relationship of steel rebar

E_s : Elastic modulus of the soil at depth equal to the diameter of the pile

E_{ts} : Elastic modulus of the tensile branch of concrete

ε_0 : Strain corresponding to the intersection of the elastic and yield asymptotic branches in the stress-strain relationship of steel rebar

ε_{20c} : Strain in confined concrete corresponding to 80% reduction in peak stress

ε_{50h} : Increase in strain in confined concrete corresponding to a 50% reduction in peak stress of unconfined concrete

ε_{50u} : Strain in concrete corresponding to a 50% reduction in peak stress of unconfined concrete

ε_c : Compressive strain in concrete

ε_{max} : Absolute maximum strain in steel rebar at the instant of strain reversal

ε_{psc0} : Concrete strain at the maximum compressive strength

ε_{pscU} : Concrete strain at crushing strength

ε_r : Strain corresponding to the point of reversal in the stress-strain relationship of steel rebar

ε_s : Strain in steel rebar

ε_u : Ultimate strain in steel rebar

ε_y : Yield strain in steel rebar

ε_y : Yield stress in steel rebar

f : Ricker wavelet function

f_0 : Characteristic frequency of the signal

f_c : Compressive strength of concrete

$f_c^{'}$: Compressive strength of concrete cylinder

f_{ck} : Grade of concrete

f_{lin} : Linear transfer function

f_{max} : Maximum frequency of input signal

f_N : N^{th} yield surface in multi-surface plasticity

f_{pc} : Concrete compressive strength at 28 days

f_{sig} : Sigmoid transfer function

f_t : Tensile strength of concrete

f_y : Yield stress of the steel reinforcing bar

f_y : Grade of rebar

f_{yh} : Yield strength of transverse steel

F : Shear force developed at the bedrock soil interface

F_v : Force at viscous boundary

g : Acceleration due to gravity

G : Shear modulus of soil

G_r : Reference low strain shear modulus of soil

G_{soil} : Shear modulus of the soil at depth equal to the diameter of the pile

H : Depth of the soil domain

H : Height of the building
H_s : Depth of the soil deposit
I : Importance factor of the structure
I_A : Arias Intensity
K : Ratio of peak confined and unconfined stress in concrete
K^* : Modal stiffness
K_e : Initial effective stiffness
K_x : Lateral stiffness of the foundation
$K_{x\phi}$: Coupled sway rotational stiffness of the foundation
K_ϕ : Rotational stiffness of the foundation
l : Distance between the point of the maximum moment to the point of zero moment
l : Distance between adjacent foundations
l_{max} : Maximum size of the mesh element
l_p : Plastic hinge length in frame members
L_p : Plastic hinge length in the shear wall
l_p : Length of pile
L : Lateral extent of soil or soil domain length
L_w : Length of shear wall
L_{wi} : Length of shear wall in the first storey in the direction of lateral forces (in m)
m_1, m_2 : Slopes of the branches of the bilinear fit
M / V : Shear span or moment to shear ratio
M^* : Modal mass
MF : Modification factor or ratio of effective to the fixed base natural period
MF_n : Normalized modification factor
MSE : Mean squared error
n : Number of data points
n : Number of neurons
n_p : Number of piles
N : Number of input variable
N : Total number of time instants
$NRMSE_L$: Normalized *RMSE* corresponding to a particular soil domain length L
$NRMSE_{PGA}$: Normalized *RMSE* corresponding to L_{min} normalized with respect to PGA_{max}
N_w : Number of shear walls in the considered direction of shaking
$p_0^{'}$, $p^{'}$: Effective confining pressure
$p_r^{'}$: Reference confining pressure
P : Axial force
R : Parameter influencing the shape of the elastic to yield transition curves in the stress-strain relationship of steel rebar

R : Response reduction factor

R_0 : Value of R during the first loading

R_1^2, R_2^2 : Coefficient of determination of the branches of the bilinear fit

$RMSE_{iL}$: Root mean square error at a particular location 'i' corresponding to soil domain length 'L'

$RMSE_L$: Cumulative $RMSE_{iL}$ corresponding to a particular soil domain length L

$RMSE_{L_{min}}$: Cumulative $RMSE_L$ corresponding to a smallest soil domain length L_{min}

R_μ : Response reduction factor

s_h : Spacing of hoops

s_i : First-order indices

s_t : Total effective indices

S_a : Spectral acceleration

S_H : Parameter for measuring pile foundation flexibility

t : Time in seconds

t_s : Time instant of the peak amplitude of the signal

T : Total time duration of the ground motion

T_a : Natural period of the structure

T_F : Fixed base natural period

T_s : Fundamental period of the soil layer

T_{SSI} : Effective natural period or natural period under the influence of SSI

u : Displacement

$\dot{u}$: Velocity

$\ddot{u}$: Acceleration

$\dot{u}_i$: Velocity of incident motion

$\ddot{u}_i$: Acceleration of the incident motion

U_0 : Amplitude of ricker wavelet

v_p : Primary wave velocity

v_s : Shear wave velocity of soil

v_{sH} : Shear wave velocity of the soil deposit at depth H_s

V : Shear at base of the superstructure

V_d : Design base shear

V_{max} : Maximum base shear

V_u : Shear corresponding to ultimate drift

V_y : Yield strength

W : Foundation width or structural width

W : Seismic weight of the structure

w_{HO} : Hidden-output weight

w_{IH} : Input-hidden weight

x : Location of incident motion

X : Input or output variable
Xm : m^{th} input variable
X_n : Normalized input or output variable
Y : Output variable
Z : Zone factor
αK_e : Post yield stiffness
γ : Shear strain
γ, β : Newmark's time step integration constants
δ, δ_{max} : Differential settlements
Δ : Roof drift
Δ_d : Roof drift demand
Δ_u : Ultimate drift
Δ_y : Yield drift
Δt : Time interval
ζ_n : Damping ratio corresponding to the n^{th} mode
θ_d : Rotational demand
λ : Ratio between unloading slope and initial slope in concrete stress-strain relationship
μ : Mean
μ_c : Ductility capacity
μ_c : Curvature ductility demand
$\mu_{c,FB}$: Curvature ductility demand under FB condition
$\mu_{c,SSI}$: Curvature ductility demand under SSI condition
μ_d : Displacement ductility demand
$\mu_{d,FB}$: Displacement ductility demand under FB condition
$\mu_{d,SSI}$: Displacement ductility demand under SSI condition
$\bar{\mu}_c$: Ratio of curvature ductility with SSI to that without SSI
$\bar{\mu}_d$: Ratio of displacement ductility with SSI to that without SSI
ξ : Absolute value of plastic strain corresponding to the preceding excursion in steel rebar
ρ : Mass density of soil
ρ_s : Ratio of the volume of transverse reinforcement to the volume of concrete core measured to outside of hoops
ρ_{sh} : Horizontal reinforcement ratio in the web of the shear wall
σ : Standard deviation
σ_0 : Stress corresponding to the intersection of the elastic and yield asymptotic branches in the stress-strain relationship of steel rebar
σ_r : Stress corresponding to the point of reversal in the stress-strain relationship of steel rebar
σ_s : Stress in steel rebar
σ_u : Ultimate stress in steel rebar

σ_y : Yield stress in steel rebar

$\sigma_1^{'}\ \sigma_2^{'}\ \sigma_3^{'}$: Effective stress along the three mutually perpendicular directions

σ_y^e : Change in yield stress in steel rebar due to reversal of load

τ : Shear stress

υ : Poisson's ratio

φ : Angle of internal friction of soil

$\phi_{d,avg}$: Average curvature demand

$\phi_{d,SSI}$: Average curvature ductility under SSI condition

ϕ_y : Yield curvature

Ω : Optimum lateral extent of soil domain

ω_n : Natural frequency of the soil domain corresponding to the n^{th} mode

[C] : Damping matrix

[K] : Stiffness matrix

[M] : Mass matrix

ABBREVIATIONS

Notation	Description
ANN	: Artificial Neural Network
AVR	: Absolute Value of Rotation
CP	: Collapse Prevention
FAR	: Fourier Amplitude Ratio
FB	: Fixed Base
IO	: Immediate Occupancy
ISD	: Inter-Storey Drift
LS	: Life Safety
MDOF	: Multi Degree Of Freedom
PBI	: Perfectly Bonded Interface
PGA	: Peak Ground Acceleration
RC	: Reinforced Concrete
SDOF	: Single Degree Of Freedom
SPF	: Soil Pile Foundation
SSI	: Soil-Structure Interaction

Chapter 1
INTRODUCTION

CONTENTS

1.1 OVERVIEW

Construction of Reinforced Concrete (RC) buildings has gained considerable popularity, especially in the regions of economic development (mostly towns and cities). Most buildings in the urban areas comprise RC frame type construction, with or without the presence of RC shear walls. In severe seismic zones, the provision of a shear wall contributes to the increase in the lateral load capacity and the lateral stiffness of the building. In the event of an earthquake, these concrete walls attract substantial lateral force and maintain the lateral drift of the building within reasonable limits. Buildings in which the lateral forces, induced due to the earthquake, are resisted by frame members only are known as 'RC frame systems'. Similarly, the buildings in which the lateral forces. are resisted by both the frame members as well as reinforced concrete walls are known as 'RC wall-frame systems'. Depending on the type of soil at the site, these buildings are supported by either shallow footings or pile foundations. Shallow foundations may suffice when the supporting soil condition is rocky or possess sufficiently high stiffness. However, in most cases, governed by the prevailing nature of relatively softer or weaker soils (having comparatively lower consistency or lesser relative density, respectively), these buildings are required to be supported by pile foundations. In such cases, depending on the relative stiffness of the foundation substructure and foundation soil, soil-structure interaction (SSI) may intricately

govern the combined response of the structure, footing, and the embedding soils. Past studies have highlighted the importance of SSI on the seismic behavior of a building supported on pile foundations embedded in relatively softer soils (Carbonari et al., 2011 and 2012; Hokmabadi et al., 2014). In the event of an earthquake, the soil-foundation system gets shaken up due to which the structure is set into motion. The response of the structure, to the shaking of the soil, in turn, influences the motion of the soil by introducing deformations into the soil. This process in which the response of the soil influences the motion of the structure and, subsequently, the response of the structure influences the motion of the soil, is referred to as soil-structure interaction (SSI).

1.2 MAJOR CONCERNS AND NEED OF THE STUDY

Foundations resting on rocky medium imparts a high degree of restraint, and the assumption of considering building as fixed-at-the-base holds good. However, if the supporting medium comprises predominantly weaker or softer soils, then the building can be considered to be flexible at the base and be influenced by SSI effects. In the latter case, the natural period of the building gets increased as compared to that obtained by assuming the building to be fixed at the base. Design engineers generally avoid considering complex SSI effects, which is attributed to the following reasons. There is an ever-existing lack of availability of easy access to information with regard to modelling aspects of complex SSI effects. Moreover, the incorporation of complex SSI effects in practical problems is computationally time consuming and expensive. Even if the designers accept to undergo the arduous effort of incorporating the complex phenomenon of SSI in modelling, there is no surety that the results could be relied upon as they confront a lack of substantiation with the literature. Additionally, the prevalent notion of SSI effects to be beneficial acts as a catalyst for the designers to resort to the codal suggestion that the seismic forces can be evaluated conservatively by ignoring soil-structure interaction effects (BSSC-97) and consider the system without foundation flexibility (i.e., fixed at its base). This is attributed to the consideration that SSI introduces flexibility in the soil-structure system, thereby resulting in an increase of the natural period of the structure and reduction of the design forces. However, past studies have shown that considering SSI to be beneficial is an oversimplification made by the codes, and the same may lead to the unsafe design of the structure and foundation (Mylonakis and Gazetas, 2000). Moreover, situations where SSI can be beneficial, the simplification of ignoring SSI may lead to an uneconomic design. Either way, it becomes essential to investigate and evaluate the SSI effects on the structure

and incorporate guidelines into the seismic codes so as to have safe as well as economic design criteria.

According to the present-day seismic design philosophy, the RC buildings are designed to resist only a percentage of the actual lateral forces mobilized onto the structure during an earthquake. The remainder of the forces is dissipated by means of large inelastic deformations, on account of material distress. Under the fixed-base condition, the inelastic behavior of the superstructure contributes towards the exhibition of ductility. However, on incorporating substructure flexibility, the inelastic behaviour of the superstructure is modified on account of the contributions of the foundation in the inelastic response of the SSI system. A wealth of knowledge exists on studies considering SSI effects with simplifications such as linear or equivalent linear behaviour of soil and structure, and idealizations in regard to the structure and foundation (Kausel, 2010). However, very limited studies are available that address the complexities (involving nonlinearity of structure and soils, as well as the complex geometry of the structure-foundation system) associated with the incorporation of SSI in such problems (Lou et al., 2011). It is worth mentioning that a great deal of the research has focused on structures supported on shallow foundation, and less attention has been paid to that supported on pile foundations. Moreover, the inclusion of nonlinearity in the building and soil for the evaluation of the seismic response of the structure has not received much attention and needs significant study. In most cases, the behaviour of soil is highly nonlinear, and, in the event of a major earthquake, the structure unquestionably produces an inelastic response. Studies of buildings on pile foundations have been less and only limited to incorporating elastic behavior.

1.3 Scope of the Present Study

Considering the limited research, the main aim of the present study is to investigate the influence of soil-structure interaction (SSI) on the seismic behaviour of RC frame and RC wall-frame systems supported on pile foundations. The seismic behaviour can be classified as elastic and inelastic. The elastic behaviour is studied by investigating the influence of SSI on the natural period, and a predictive relationship for quick and easy estimation of the effective natural period (natural period under the influence of SSI) is developed. The inelastic behaviour is studied by considering the influence of nonlinear SSI on the lateral load behaviour so as to understand the modification that would arise with respect to the

conventional fixed-base analysis and thereby investigate its influence on the ductility capacity and demands.

1.4 ORGANIZATION OF THE STUDY

The present study is divided into eight chapters, including the present one, which gives a brief introduction to the topic. Chapter 2 provides a concise state-of-the-art review of the Seismic Soil-Structure Interaction (SSI) studies related to building structures. Several studies related to the methodology, various computational procedures, and the modelling of the soil domain that are found integral to any seismic SSI technique has been presented with a view to developing a basic understanding of the subject. Moreover, the seismic SSI studies, along with guidelines presented in various codes of design practice, have been reviewed. Finally, the gap areas that have not received their due attention in the past SSI studies related to buildings have been highlighted. Based on the gap areas, the objectives of the present study are formulated.

Chapter 3 presents the various aspects of numerical modelling (nonlinear material models, boundary conditions, analysis procedures, and other components) adopted in the present study. The validation studies of the developed numerical models are elucidated to establish their efficacy and adoption for further analysis.

Nonlinear dynamic soil-structure interaction analysis using the finite element method requires the single-step direct method of analysis that necessitates modelling of the entire soil continuum together with the structural system. Theoretically, considering an infinite (as large as possible) lateral extent of soil domain would be ideal. However, such a choice leads to heavy computational expense and is not practically feasible. Therefore, it is important to justifiably define the lateral extent of the soil domain to be used for dynamic SSI analysis that would ensure computational efficiency without loss of accuracy of the system response. Chapter 4 outlines an approach for deciding on an optimal horizontal extent of soil domain to be used for dynamic SSI analysis. Based on the study, a simple generalized set of relationships has been prescribed, which are used for developing the numerical model to be used in the following chapters.

Chapter 5 investigates the effect of SSI on the natural period of RC frame and RC wall-frame systems supported on pile foundation. The effect of SSI on RC frames and RC wall-frame systems has been studied for various configurations of the superstructure and

soil-pile foundation systems. To overcome the shortcomings of past studies, a robust relationship for predicting the effective natural period (T_{SSI}) of RC frame and RC wall-frame system supported on pile foundation is proposed.

In Chapter 6, the influence of SSI on the inelastic lateral load behavior of RC frame and RC wall-frame systems is investigated. Subsequently, the modification in the inelastic behaviour is studied, and the variation in the ductility capacity due to SSI effects is assessed. Finally, some attention is given to study the role of the shear wall in modifying the ductility capacity of an RC frame system.

During the shaking of an earthquake, a structural system is subjected to inelastic deformations. The imposition of the inelastic deformations onto a structural system can be assessed by evaluating the ductility demands both at the local (elemental) and the global (structural) level. For the same shaking, the ductility demands are modified due to SSI effects. Chapter 7 investigates the influence of SSI on the inelastic response of the plastic hinge regions within the superstructure, and subsequently, the influence of SSI on the local and global ductility demands is assessed.

Finally, the study is summarized, and the conclusions drawn from the present study are presented in Chapter 8, along with the possible scope of future work.

This page has been intentionally left blank.

Chapter 2
REVIEW OF LITERATURE

CONTENTS

2.1 OVERVIEW

This chapter aims to provide a concise state-of-the-art review of the seismic Soil-structure interaction (SSI) studies related to building structures. Irrespective of the type of structure, other associated works are also presented that are considered as essential and integral for SSI studies. Noted researchers working in the field of SSI expressed different types of views with regard to the adoption and beneficial effects of seismic SSI. However, as evidenced by the literature, there exist contradictory opinions about its necessity, benefits, as well as its detrimental effects. The inconclusiveness of the reports triggers the necessity to critically study the issues and aspects of seismic SSI and examine the various available codal guidelines in detail. The same has been reported in the present chapter. Certain relevant studies related to the methodology, various computational procedures, and the modelling of the soil domain that are found integral to any seismic SSI technique has been presented with

a view to developing a basic understanding of the subject. Finally, the seismic SSI studies, along with guidelines present in various codes of design practice, have been reviewed. Moreover, the gap areas that have not received their due attention in the past SSI studies related to buildings have been highlighted. Based on the gap areas, the objectives of the present study are highlighted. Overall, this chapter provides a basic insight into the area of seismic SSI and the studies related to building structures supported on shallow and deep foundations. The present chapter focuses on illuminating the areas that have not received due attention in the earlier studies.

2.2 PAST REVIEWS ON SOIL-STRUCTURE INTERACTION STUDIES

The earliest review on dynamic soil-structure interaction (DSSI) was reported by Hadjian et al. (1974). The study was made in the light of two primary approaches in solving SSI problems, namely the continuum approach (lumped parameter) and the finite element approach. An intricate comparison of the two approaches was provided, highlighting the efficacies and shortcomings of each. Based on the prevalent state-of-the-art on dynamic SSI of that period, it was concluded that further research should be focused on the application of each of the methods in order to address justifiably the several unresolved issues related to the adequacy, efficacy, and suitability of each of the methods for SSI analysis. Modern-day advancements in computational techniques aided in expanding the knowledge related to the features and capabilities of both the continuum and finite element approaches. It has been understood that both the methods prove to be relevant in their own extents of applicability and usefulness.

Kausel (2010) has documented an excellent review of static and dynamic SSI along with their early histories. A treatise was presented, highlighting the various research works conducted in the fields of static and dynamic SSI. The pioneering works focused on obtaining the fundamental analytical solutions to the problems of disk loading (representative of shallow circular foundations) and rectangular foundations resting on elastic half-space. Apart from citing most of the pioneering and other noteworthy works, a compilation of the research works dedicated to the interaction phenomenon of an overlying structure with the underlying soil was presented. In this regard, a critical discussion on the contradictory aspects of SSI was provided, primarily debating on the necessity or redundancy of conducting an SSI analysis for various problems. However, it is observable

that most of the works reviewed were from 'the era bereft of powerful digital computers and the very versatile numerical methods' (Kausel, 2010).

Lou et al. (2011) presented a concise review of the studies carried out in the recently emerged area concerning the analysis and evaluation of Structure-Soil-Structure-Interaction (SSSI), the basic concepts of which holds similar relevance to conventional SSI studies. Analytical works involving the presence of multiple discs located on the surface of an elastic half-space (representing multiple shallow circular foundations) were presented in detail. A critical appraisal was provided related to solution approaches for the SSSI studies involving the Finite Element Method (FEM) and its more advanced variant, the Boundary Element Method (BEM). The review points out that only a meagre contribution has been made in the area of SSI that takes into account the relevant engineering complexities. It was also stated that significant understanding is required to address the practical engineering design and analysis problems, such as the presence of complex structural models in the nonlinear and inhomogeneous foundation soil.

More recently, Roesset (2013) presented a review of the early stages of SSI, focusing on the development of the subject. The documentation critically highlighted the prevailing contradictions related to the advantages and disadvantages of two prevalent methods of SSI analysis, namely the 'Direct' method and the method of 'Sub-structuring'. Along with this, studies related to the interaction effects among piles in a group have also been illustrated. With regard to the highlighted topics, the review provided a very fruitful chronological insight over the decades, until the mid-eighties of the twentieth century. Although the review focused on the studies related to the design of nuclear power plants, most of the highlighted works have been pioneering and paved the way for the present-day understanding of the subject. Kavitha et al. (2016) presented a review on the SSI analysis of laterally loaded piles in which they concluded that there are various factors affecting the soil-pile-structure system. The governing factors are (a) soil property, (b) soil profile, (c) gradient of ground surface, (d) pile geometry, and (e) pile arrangement. The review emphasised on the fact that accurate prediction of the structural response is dependent on proper accounting of these governing factors.

From these earlier review documentations, it is noticeable that the phenomenon and the effects of dynamic SSI should not be ignored, especially for particularly important structures such as nuclear containment facilities and offshore establishments. Even for

various building typologies, especially for tall structures accompanied by deep foundations, there is an utmost necessity to investigate and consider the effects of dynamic SSI during design and analysis. However, in this regard, considering the present state of practice, most of the design guidelines fail to provide any clearly defined criteria related to SSI and its consideration for the most common and worldwide prevalent building typologies. Since, in general, the relative flexural rigidity of soil is comparatively lesser than that of the overlying structure, BSSC (1997) provisions suggest ignoring the effects of SSI to prevent the overall system to become flexible. ASCE 7-05 (2006) considers the effect of SSI, although only accounting for the beneficial effect of SSI, by incorporating an overall reduction in the seismic design forces due to the increased flexibility of the system. However, the 1985 Mexican earthquake proved that such a design consideration could be quite detrimental. During this event, an entirely reverse phenomenon was noted, wherein the presence of soft soil led to a substantial increase in the seismic forces. As a consequence, the low-to-mid-rise buildings (for which the consideration of SSI effects was deemed unimportant) suffered the maximum damage resulting in a massive loss of life and property. In this regard, Mylonakis and Gazetas (2000) showed that it is not always justified to consider SSI as beneficial. It is important to note that most of the developments on seismic/dynamic SSI studies were based on the safety assessment of the nuclear containment facilities founded mostly on shallow mat/raft foundations, aptly idealized as discs resting on the surface of soil that was treated as an elastic half-space. Governed by the structural and geotechnical characteristics, buildings are either founded on shallow or pile foundations. In the event of an earthquake, the shaking of the relatively flexible surrounding foundation soil results in the excitation of overlying or embedded structure, thus consequently exhibiting a mutual interaction to render flexibility to the structure. In the event of an earthquake, the response of any such structure-foundation system is contributed by a combination of the ground motion, type of foundation, and natural period of the structure. Yegian et al. (2001) highlighted that over the last decade of the twentieth century, the direction of research in the field of SSI mostly got oriented from shallow to pile-supported structures. However, it was clearly pointed out that many relevant unaddressed questions and issues were still existent, the most debated one being the identification of the beneficial and detrimental scenarios of seismic SSI.

The objective of this chapter is to provide a concise review of the various studies related to the effects of considering SSI on the response of buildings, with special emphasis

to buildings supported on pile foundations. The review has been presented in segments encompassing different relevant aspects of the said topic with highlights on the evidence of SSI, along with the available computational and analysis techniques accounting for the modelling issues of soil domain and foundation interaction. A critical appraisal of the available literature on SSI effects on buildings has been provided, and the existing codal provisions around the world, related to the consideration of SSI, have been elaborated. The tune of this review has been set based on the recommendation of (Kausel, 2010) where it is quoted as "In all likelihood, however, such future reviews will have to focus much more narrowly on sub-disciplines given the significant breadth of that the subject of SSI has now attained".

2.3 EVIDENCES OF SOIL-STRUCTURE INTERACTION

As already mentioned, seismic soil-structure interaction has been deemed to be important for the design of only some particular types of structures. A persistent debate exists in the structural/geotechnical fraternity as to whether or not to emphasize on SSI for semi-important structures as well. With the aid of cited evidences, many available literatures have judged the above-stated debate in favour of consideration of SSI. This inclination originates from the glaring example of the significant and widespread damage to the common and ordinary low-to-mid-rise building structures during the 1985 Mexico City earthquake, owing to the effects of soil-structure interaction. However, at the same time, it was also stated that such a disaster might especially be associated with the typical site condition that prevails in the region of Mexico City. This proposition prepared the pathway rendering the consideration of SSI investigation to be almost unnecessary for structures located in regions where site effects are absent. However, several other literatures illustrate that observations, as cited for Mexico City, have also been noted for other sites comprising of soft soil as the primary foundation material. Therefore, it becomes imperative to compile such evidential information from earlier documentation, thereby highlighting the effects of seismic soil-structure interaction on the building structures. In this regard, a compiled evidential documentation is presented in the following part of this chapter.

In-situ instrumentation of a building structure aids in capturing its field response when subjected to ambient and/or seismic motions, the analyses of which can lead to the identification of SSI effects on buildings. Although evidence of seismic SSI is ample, very few literatures exist that involve the diagnosis from instrumented buildings. Luco et al.

(1988) reported about the forced vibration test results based on the experimentations conducted on the instrumented Millikan Library Building (Pasadena), thus attempting to estimate the fixed-base natural frequencies and superstructure modal damping ratios. It was revealed that the interaction between the soil and the structure substantially influenced the response of the building. The influence was up to the extent that the induced rigid body motion associated with the translation and rocking motions of the building exceeded the roof response by more than 30%. The deformations of the superstructure, as well as the fundamental frequencies of the structure-foundation-soil system, were exhibited to be solely governed by the inertial forces generated during translational and rocking motions of the base. Based on the data records from the accelerometers placed at different floor levels of the Hachinohe Technical College, Yamahara (1970) showed that the motion recorded for the ground adjacent to the building was significantly different from that of the building foundation. Such an observation clearly indicated the influence and effect of the presence of a building on the free-field ground response. It was also pointed out that the ground motions having shorter periods (wavelength shorter than the base dimension of the building) do not produce severe response in the building due to the filtering out of the shorter periods present in the ground motion, thereby reducing the energy of the input motion incumbent on the building. This phenomenon is termed as 'filtering of frequencies', and is attributed to the kinematic interaction effects of soil-structure interaction. A similar observation was made by Aldea et al. (2007) with respect to the seismic response of an instrumented high-rise building located at Bucharest, Romania, having a dual reinforced concrete structure and comprising of the multi-level basement. Compared to the motions recorded at the adjacent free-field ground surface, it was reported that there was a significant reduction of the motion in the third level basement of the building, especially in the frequency range of 2-3Hz, which has been again attributed to the kinematic SSI effects.

Apart from the kinematic interactions, rocking motions have also been found to pose significant influence on the response of superstructures, with the effect being especially pertinent for the tall structures. Subjected to the 1989 Loma Prieta earthquake, acceleration record response obtained from the 60-storey high vertically tapered pyramidal Transamerican building at San Francisco revealed the rocking aspect of SSI in the building response (Celebi and Safak, 1991). Fourier analysis of the accelerograms obtained at the ground and basemat levels indicated a rocking frequency of the building to be present at 2 Hz, acting around the N-S and E-W axes. It was pointed out that although the rocking

amplitude was small, it had a significant influence on the motions at basement and ground, and would, in turn, further affect the developments of the Design Response Spectrum. From the observations, it was concluded that the rocking motion of buildings need not necessarily be prompted by a single frequency, or might not be present within a single band; rather, it is possible that the rocking motion could be excited at various distinct frequencies or bands. Based on the response of two seismically-instrumented buildings (JAL building in Mexico City and SIS building in Acapulco) located on soft soils, Muria-Vila et al. (2004) observed that there were several frequencies associated with the rocking movement of the instrumented buildings. An obscure relation of the rocking frequency with the amplitude of the input motion was noted. This was attributed to the uncertain development of the contact pressures at the soil-foundation interface, owing to the averaging effect of the incident wave, as well as the formation of new sources of vibration from the foundation movements and temporal contact loss. It was concluded that the contribution of the rocking component on the total response of the structure or the SSI effects should not be ignored; rather, pile group effects, contact loss and dependency on frequency amplitude should be included in future building codes.

With regard to the seismic SSI studies, ground surface amplification of the input motion also referred to as 'Site Amplification', is another factor that significantly influences the response of structures. The amplification is a manifestation of the local site effects. At the same time, the site amplification is affected by the presence of the structure. Limited literature is available, highlighting the conditions influencing the site effects in the presence or absence of existing structures. Heidebrecht et al. (1990) highlighted the unusual attributes of the Mexico City site that resulted in the large site amplification during the 1985 earthquake. Apart from the soil being characterized by very high moisture content and plasticity index, the accompanying low shear modulus and damping, low intensity of rock-level excitation (ensuring elastic response of the soil) and the proximity of the predominant frequency of the soil layer to the excitation motion were adjudged as the major factors resulting in the significant site amplification. Emphasis was laid on the importance of identification and recognition of those situations that ensures a greater possibility of high amplification of the base shears for the structures located on soft clay sites in the regions of low seismicity. Such understanding is required to be implemented further for the modification of the existing codes and design practices. It was also found that the high-intensity excitations, rather, aid in the decrement of the spectral amplification due to the

nonlinear characteristics of the soil. From the recordings of the JAL building in Mexico, located on a thick soft clay bed, Meli et al. (1998) observed that the amplification of the motion at the ground surface was, on average, 2.6 times the motion recorded at the base of the soft soil deposits. At the same time, the motion at the roof of the building was observed about thrice to that obtained at the ground surface. The researchers concluded that due to the high flexibility of the building, only moderate inertial effect of SSI was observed. Additionally, significant kinematic interaction effects were observed only for the higher frequencies of excitation, typically observed for pile groups in heterogeneous soils. The large amount of damage caused at the Mexico City site during the 1985 earthquake was also attributed to the duration of the motion, apart from its amplitude. Guéguen and Bard (2005) confirmed the propositions of the past researchers advocating that the free field motion can be contaminated by the presence of the building when subjected to ground shaking. Their study substantiated the explanation provided by Guéguen et al. (2002), on the lengthening of ground motion records at sites similar to the Mexico City site and, hence highlights the greater need to focus in the field of Soil-Structure-Soil-Interaction (SStSI). From the presented critical appraisal, it is confirmed that there exists evidence highlighting the influences of seismic soil-structure interaction on the response of the building structures. Hence, it is of utmost necessity to advocate consideration of SSI effects for the common building structures resting on different types of soils.

2.4 COMPUTATIONAL PROCEDURES AND METHOD OF ANALYSIS

This section briefly outlines the computational procedures that have been used for SSI studies. Emphasis has been laid on the three popular approaches for solving a typical SSI problem, namely the Finite Element Method (FEM), Finite Difference Method (FDM), and Boundary Element Method (BEM). FEM has proved to be the most versatile tool for conducting numerical analyses since its applicability is not problem-specific, rather widespread and applicable to a variety of class of problem. FEM has the ability to address real and complex problems with significant intricacies (Cook et al., 1989). However, it is worth mentioning that although FEM has proved to be a versatile solution tool, solving complex problems requires sufficient time and computational memory. Hence, in order to make the solution technique more robust and computationally inexpensive, researchers have tried to develop and establish coupled methods for SSI analysis. For solving dynamic SSI problems related to the modelling of buried structures subjected to transient stress, Stevens and Krauthammer (1988) proposed an analysis technique based on a hybridization of Finite

Element Method (FEM) and Finite Difference method (FDM). FDM is well suited for the analysis of wave propagation in continuous media with nonlinear properties and subjected to large strain deformation, while FEM is well suited for analysing the structure and its response under various scenarios. The proposed hybrid method, although with scope for further improvement, providing a balance between the accuracy and the computational effort required for solving SSI problems. It is worth mentioning that FEM falls short of representing accurately unbounded media, as it is not possible to model an infinite medium using traditional finite element formulation. In this regard, Godbole et al. (1990) pioneered the static SSI analysis of surface strip footings using infinite elements; wherein, the finite elements were coupled with the infinite elements, having shape functions, resulting in a model response entity (e.g., settlement, vertical stress, and contact pressure) to approach the far-field characteristics at infinite distance. The geometry describing these coupled elements is such that one side of the element is positioned at infinity. The method was successful for static cases; however, verification for the dynamic case was not provided.

Apart from the finite element and finite difference methods, the Boundary Element Method has been used by many researchers to represent the infinite extent of the soil boundary. With regard to the embedded foundations, Wolf and Darbre (1984) showed that among the various formulations of the BEM (the weighted residual formulation, the indirect BEM and the direct BEM), the indirect BEM led to comparatively accurate results. Moreover, the symmetry of the dynamic stiffness matrix of the soil was ensured along with the easy computation of the displacements due to applied loads. In order to solve for the dynamic response of rigid foundations through the sub-structure approach, Celebi et al. (2006) employed the BEM in the frequency domain to develop the impedance functions for surface-supported footings and embedded foundations. A good agreement was achieved between the numerical and analytical solutions over a wide range of frequency factors for various modes of vibration of the foundation (horizontal, vertical, rocking, and torsional vibrations). BEM has been used in conjunction with FEM to obtain the solution to the governing differential equations of various SSI problems such as transient analysis of DSSI subjected to horizontally propagating shear waves or SH waves (Eilouch and Sandhu, 1986), DSSI of coupled shear walls (Capuani et al., 1995) and DSSI of nearby piled buildings (Padrón et al., 2009). Wang (1992) made use of coupled boundary and finite elements for 3D foundation-soil interaction in which the soil media was represented by boundary elements. The continuity of both elements was established through equilibrium

and continuity conditions along with the soil-structure interface. For considering various SSI effects, Chuhan et al. (1999) developed a coupling of Finite Element (FE)-Boundary Element (BE)-Infinite Element (IE)-Infinite Boundary Element (IBE) method. It was shown that the method could be applied to conduct a seismic design and analysis of nuclear structures founded on layered soil deposit, the system being solved in the frequency domain. The coupled model allows the nonlinearity of the near-field soil to be represented by equivalent linear characteristics, thereby reducing the computational effort. The model is also capable of incorporating the angular wave incidence from the far-field. The adopted boundary elements allow the reduction of the spatial dimension by one, thereby reducing the degrees of freedom compared to those prevalent with finite elements; thus, consequently reducing the computational effort. However, BEM is not well suited for inhomogeneous and anisotropic media. Moreover, for obtaining the solution of the concerned problem, fundamental solutions are required that satisfy the governing differential equations. Often these analytical solutions are very complicated and difficult to obtain (Wolf, 2003). Hence, researchers attempted to establish a method that would combine the advantages of both the finite element method and the boundary element method. This led to the development of the Scaled Boundary Finite Element Method (SB-FEM), a semi-analytical approach. Wegner et al. (2005) modified an existing program (DSSIA-3D) by implementing a new procedure where a substructure method was used, in which the unbounded soil was modelled using SBFEM and the structure using the conventional FEM. More recently, Syed and Maheshwari (2017) employed the coupled FEM-SBFEM method for conducting nonlinear analysis of soil-pile system.

Apart from the above-mentioned methods, Bielak et al. (2003) developed the Domain Reduction Method (DRM). In this method, the entire domain was subdivided into two sub-domains, namely (a) the one that simulates the earthquake source and propagation path effects wherein the localized features are removed, and (b) the one that models the local site effects. Although the method involved the assumption of non-dissipative nature and linear characteristics of the material, it had the advantage of being applied to problems in which the causative faults were quite far from the actual site. A significant reduction in the size of the analysis domain was also achieved. As compared to the conventional absorbing boundaries with viscous dashpot systems, analysis with DRM led to a 50% reduction in computational time as well (Zdravkovic and Kontoe, 2008).

In a particular method of analysis, SSI problems can be treated in two ways; either by including the soil domain along with the structure or by utilizing a reduced representation of soil and foundation system in the form of impedance. This broadly leads to three analysis techniques for SSI problems, namely (i) single-step method (ii) multistep method, and (iii) substructure method. The first two methods involve the inclusion of the soil in the analysis. The single-step method is the most straightforward method to solve an SSI problem in which the solution to the problem is obtained in a single step, as the name suggests. The multi-step method involves breaking up the problem into two separate problems of Kinematic interaction and Inertial Interaction and subsequently obtaining the solution by combining the response from the two separate problems. Since this method involves the principle of superposition, the multistep method is applicable at most to equivalently linear problems (Kramer, 1996). On the contrary, the single-step method can be applied to nonlinear problems as well, since no superposition is required. The disadvantage of the single-step method is that the response of a small portion is dependent on a large domain. In other words, to obtain the SSI solution of a structure of width *W*, a soil domain of width several times the width (alpha×*W*) of the structure is required to be solved, thus making the method computationally expensive (Datta, 2010). The substructure method of analysis can also be used to find the solution of the inertial interaction by representing the foundation soil with the aid of complex functions simulating its dynamic stiffness and damping characteristics (Datta, 2010). These functions are known as impedance functions and are defined as the ratio of the steady-state forces (or moments) to the steady-state displacements at the base of the massless foundation. Gazetas (1991a) presented a complete set of algebraic formulae and dimensionless charts for the computation of the components of impedance functions and are in extensive use until date. The applicability of the above-mentioned methods for solving an SSI problem is dependent on the type of the problem as well as on the effects that are to be evaluated and, thus, the judgment for the choice of method has to be taken accordingly.

2.5 Soil Domain Modelling

Most of the research in the area of soil-structure interaction has been carried out to model the soil domain and boundary conditions. Modelling of the soil using a lumped spring approach is the simplest way to account for soil flexibility. In this approach, springs are attached to the centre of gravity of the foundation corresponding to each degree of freedom. Gazetas (1991a) has prescribed the value of the stiffness of these springs based on the

assumption that the foundation rests on homogenous elastic half-space. As the stress distribution in the soil mass below the footing may not be accurately determined using the lumped spring model, distributed spring model is resorted to in which the soil medium is represented as a system of identical, but mutually independent, closely spaced, discrete, linearly elastic springs (Dutta and Roy, 2002). Makris and Gazetas (1992) used the Winkler model with frequency-dependent springs and dashpots for pile-soil-pile interaction. Nonlinear Winkler spring model is also capable of capturing the failure of soil in terms of gapping and separation phenomena as presented for rigid caisson foundations (Gerolymos and Gazetas, 2006). Raychowdhury and Singh (2012) showed that the nonlinear Winkler model has good capability to capture the characteristics of building resting on shallow foundations (dynamic variation of the moment, shear force and settlement of foundation with rotation and sliding of the same) and observed a good agreement between experimental and simulation results. Apart from the nonlinear Winkler spring model being well suited for the FEM approach, the same finds affirmative applicability with the BEM approach. Kampitsis et al. (2013) implemented the nonlinear Winkler spring model in BEM to exhibit various effects in the soil-pile-structure interaction problem (geometrical nonlinearity, rotary inertia, shear deformation as well as nonlinear P-δ effects). Although a lesser computational effort was required, the results were sufficiently accurate as compared with the response of the full 3D FE model. Although the distributed spring model proves to be an improvisation over the lumped spring model, the former is not devoid of certain disadvantages. Gajan et al. (2010) compared the response of a building resting on shallow foundation using the contact interface model and the nonlinear Winkler model. It was observed that the computed maximum forces, stiffness, and energy dissipation were comparable for both the models. However, the sliding displacements predicted by the nonlinear Winkler model were comparatively greater, primarily due to the uncoupled behaviour of the lateral and vertical springs. To overcome the disadvantages of the Winkler spring model, several modifications have been suggested by various researchers and have been documented in detail in the available literature (Dutta and Roy, 2002).

In comparison to the Winkler approach, a more precise and rigorous behavioural response of the soil for a soil-structure interaction problem can be obtained by modelling the soil as a continuum. The concept of elastic continuum initiated from the estimation of static stresses by Boussinesq's theory in which the soil domain was assumed semi-infinite, homogeneous, isotropic, linear elastic solid. Advancement in the finite element methods

aided in the detailed modelling of semi-infinite soil domain by finite domain analysis through the proper imposition of the boundary conditions. Kausel et al. (1975) pointed out that the elementary boundaries (i.e., with roller supports) is effective only when located substantially far from the region of interest (where the response of the system is primarily evaluated) and when internal damping of the system is relatively high. However, the adoption of this boundary condition does not reduce the domain size noticeably and hence, requires a lot of computational effort. In order to overcome the shortcoming of the earlier model, the consistent boundary formulation (Lysmer and Waas, 1972) was developed. In this case, the boundaries could be placed at the edge of the foundation, and sufficiently accurate results could be obtained with significantly lesser computational effort. Researchers showed that the viscous boundaries produced good results when placed at an appropriate distance from the area of interest (Roesset and Ettouney, 1977; Wolf and Somaini, 1986). Moreover, it was understood that elongated elements would introduce large errors in rocking compliance and consistent boundaries would produce sufficiently accurate results for linear or equivalently linear analysis. Kausel (1988) analyzed the various types of well-known absorbing boundaries (Lindman-Engquist-Majda boundary, Lysmer-Kuhlemeyer boundary, Ang-Newmark boundary, Modified Smith boundary, and Liao-Wong boundary) and concluded that these various boundaries were essentially subtle variations to understand the same mechanism at the boundary and in the immediate vicinity. Chen (1985) concluded that nonlinearity of the soil should be given due importance while choosing transmitting boundaries since the nonlinear shaking of the soil can significantly alter the travelling waveform. The nonlinearity of the soil being further dependent on the shear strength of the soil, the selection of placement of transmitting boundaries should be based on the shear strength profile at the site, or as a safer alternative, can be rather as deep as possible. In FEM modelling of the soil domain for SSI studies, the extent of the soil domain, size of the elements, and boundary condition are crucial for proper representation of the soil.

In FEM modelling of the soil domain for SSI studies, the extent of the soil domain, size of the elements, and boundary condition are crucial for proper representation of the soil. The most popular and versatile boundary conditions that can be applied to the soil model are the Lysmer–Kuhlemeyer boundary conditions (LK boundaries) represented by dashpots with appropriate damping coefficients. Jingbo and Yandong (1998) highlighted that among the various boundaries, the viscous boundaries were the most convenient to use

during the time-domain analysis. They concluded that the viscous–spring boundaries had the advantage of simulating elastic recovery capacity of the soil in the far-field, which is not possible to be simulated by the viscous boundaries. Gentela (2011) showed that proper application of the L-K boundary conditions with a finite soil domain led to a close matching of the fundamental period obtained from Eigen analysis and the proposed recommendations by Kramer (1996). Kramer (1996) highlighted that the fundamental period of a soil domain of an infinite extent could be easily obtained, provided the soil depth and the shear wave velocity of the stratum are known *a-piori*. Zhang et al. (2008) used two criteria to decide upon the adequacy of the horizontal extent of the soil domain, viz. (a) soil response away from the boundary should be as close to that of a shear soil column made of the same material under linear elastic undamped condition, and; (b) nonlinear vertical soil response at any location in the computational domain should remain small as compared to the horizontal response at that location.

The type and size of the elements also play a vital role in the precision and feasibility of the obtained results from an SSI analysis. The inappropriate size of the elements used for the discretization of the soil-structure domain does not ensure a proper wave propagation phenomenon to take place within the computational geometry. Kuhlemeyer and Lysmer (1973) recommended that the size of the elements must be less than one-eighth of the minimum wavelength (or maximum frequency) of the seismic waves propagating through the medium. This criterion ensures proper scientific representation of the propagation of the shortest wavelength through the soil media. As already mentioned, the Lysmer – Kuhlemeyer conditions are appropriate for the modelling of the boundary conditions. However, there are other available techniques as well to model the boundary conditions for simulating the condition of radiation damping or representing the non-reflecting boundaries.

As already mentioned, Godbole et al. (1990) exhibited the application of infinite elements in SSI analysis. Based on the observation of non-reflectance of an outgoing circular dilatational pulse to its point of origin (in contrary to that observed in the case of a fixed boundary), Häggblad and Nordgren (1987) manifested the good acceptability of the absorbing capabilities of infinite elements in a 2D problem. Yun et al. (2000) developed the frequency-dependent dynamic infinite elements for modelling the far-field of a two-dimensional layered half-space for SSI analysis. Since the formulation was frequency-based, a nonlinear analysis was not possible. Smith (1974) proposed a method for

cancellation of the single boundary reflection by the superposition of independent solutions of free and fixed boundary assumptions. Cundall et al. (1978) incorporated constant velocity and constant stress boundary conditions for the cancellation of the wave reflection from the boundaries. Kunar and Rodriguez Ovejero (1980) modified the earlier models for non-reflecting boundaries by superposing two boundary grids independently connected to the main mesh, accompanied by the provision of viscous dashpots at the base of the model where the seismic excitation is applied. Such a provision makes the non-reflecting boundaries to respond only to the radiation waves generated because of SSI, and let it remain inert to the motion caused by the vertical propagation of the input seismic waves. Such modification aided in obtaining the proper response of the soil domain subjected to vertically propagating shear waves, contrary to the 1D response obtained with conventional absorbing boundaries. Moreover, the boundary variables were averaged after a specific time duration was elapsed. Since these boundaries involved superposition, they were applicable only to equivalent linear analysis. Deeks and Randolph (1994) developed a frequency-independent axisymmetric absorbing boundary that agreed closely to the frequency-dependent plane strain boundaries. These boundaries implemented simple mechanical models (spring, dashpot, mass system). The boundary condition being frequency independent and simple to formulate with substantial accuracy, these boundaries provided useful consequence in comparison to the then-existing time-domain truncating boundaries in axisymmetric situations. Nakamura (2009) proposed the transformation of frequency-dependent energy transmitting boundary conditions in the time-domain for nonlinear analysis.

From the foregoing discussion, it is amply clear that the type of model and modelling adopted for the representation of the soil domain largely affects the SSI response. Further, the finite element considerations related to the discretization of the soil domain and boundary conditions are the various factors that govern and significantly influences the SSI analysis. Once again, it is important to mention that each type of method is unique and would produce results accordingly. The above illustration concisely outlines the various methods of modelling of the soil domain that may be applicable to evaluate SSI on building structures.

2.6 FOUNDATION INTERACTION

In any SSI analysis, two components of the substructure comprise the entire problem, the foundation, and the soil. Inarguably, the foundation is the most important part of the SSI studies that play a crucial role in advocating the behaviour of the entire system, as it is primarily the interacting component, through which the structure communicates with the surrounding soil. Many early studies on soil-structure interaction were devoted to the estimation of the impedance functions of the foundation resting on the soil. Kausel (2010) highlighted that a lot of research had been devoted to the evaluation of the fundamental solution of the circular disks resting on elastic half-space and subjected to harmonic vertical loads. Gradually, more and more complicated situations were being addressed, and obtaining the fundamental solution to these problems had become progressively difficult. This led the researchers to try to obtain approximate solutions to the problems. Meek and Veletsos (1974) presented an approximate steady-state analysis of rigid massless disk resting on the surface of an elastic half-space. The analysis implemented the cone models, which is based on the assumption that only a portion of the half-space, in the form of a truncated cone is effective in transmitting the energy imparted to the disk. Nagendra and Sridharan (1984) provided the solutions of equation for foundations with a rigid base and subjected to horizontal vibration, based on the assumption that no vertical stress would be developed due to the applied horizontal dynamic load. The solutions were provided for uniform and parabolic contact shear distributions considering the variation of the relative rigidity of the foundation.

As the solutions for the fundamental differential equations became more and more complicated, much of the research carried out was directed to the exploration and definition of alternative approximate solutions. A very important contribution in the field of SSI was the calculation of the dynamic stiffness of the shallow footings. In the earlier years, researchers have developed and presented charts to obtain the dynamic stiffness for rectangular and circular footings resting on elastic half-space. Dobry and Gazetas (1986) presented formulae to compute the dynamic stiffness and dashpot coefficients of arbitrarily shaped foundations resting on a reasonably homogeneous thick soil stratum. In general, the foundations do not simply rest on the surface of the ground, rather, they are embedded into the soil. Moreover, the soil below the foundations is layered in most instances. Gazetas (1983) presented a complete set of algebraic formulae and dimensionless charts for the computation of dynamic stiffness and damping coefficients for harmonic oscillations that

are in extensive use until date. Gazetas (1983) presented a comprehensive review of the dynamic analysis of the machine foundation and provided an evaluation of the dynamic stiffness and damping coefficients of foundations (circular, strip, rectangular, and arbitrarily shaped ones) supported by three variants of idealized soil profiles. The above-stated research studies highlighted in this section did not attempt to account for the nonlinear hysteretic behaviour of the soil. Chatterjee and Basu (2008) presented the estimation of lateral dynamic stiffness of the footing resting on elastic-perfectly plastic nonlinear hysteretic soil without considering the rocking behaviour of the foundation. With the aid of centrifuge modelling, Weissman and Prevost (1991) studied the influence of the frequency of the superstructure on the foundation embedment, foundation shape, and radiation damping, and illustrated the SSI effects for a structure resting on a soil layer overlying the bedrock. The study highlighted that the classical formulae for stiffness and damping parameters, as found in conventional literature, were sufficiently accurate for surface footings. All the studies highlighted so far in this section were dedicated to the shallow foundations and their interaction. These studies aided in building up the various important concepts and methods (analytical and approximate) that helped in the eventual understanding of the various aspects of foundation interaction related to different categories of foundation.

Apart from the conventionally used shallow footings for lightly loaded structures resting on soils with reasonable bearing capacity, pile foundations are more prevalent in the construction of moderate-to-large high-rise structures resting on compressible and poor subsoil conditions. Now-a-days, the utilization of pile foundations for buildings has become a common practice. The geometric properties of the piles can significantlty affect the natural properties of the SSI system. In this regard, Roy et al., (2018) showed that pile diameter and length have significant influence on the natural frequencies of pile raft foundations. Additionally, the interaction of pile foundation also influences the natural properties of the SSI system. Blaney and O'Neill (1986) conducted a dynamic lateral load test on a cantilevered mass supported by pile embedded in stiff overconsolidated clay. A shift in the resonant frequency was observed due to the formation of permanent gaps at the pile-soil interface. It was further observed that at lower loads, lesser hysteretic damping was exhibited. Randolph (1981) stated that the effective length, or the critical length, for the statically loaded pile is nearly ten times the diameter of the pile embedded in the soils that can be treated as an elastic continuum. For dynamically loaded piles, the effective length of

the piles increases depending on the frequency of the excitation (Krishnan et al., 1983). Gazetas (1984a) conducted a numerical study on the seismic response of end-bearing piles subjected to vertically propagating S-waves. Subsequently, the results were presented in the form of dimensionless graphs for the estimation of the kinematic and inertial interaction factors for a wide range of geometrical and material parameters. Just as observed for the case of shallow foundations, the stiffness and damping coefficient of the pile foundation also comprise of dynamic and static counterparts. Gazetas and Dobry (1984b) evaluated the lateral dynamic stiffness of flexible pile embedded in various types of soil profiles, which can be used in the SSI analysis by accounting proper modification of the same for the flexible soil-pile system. This method of replacing the soil and pile system by impedance functions (spring stiffness and dashpot coefficients) is extremely convenient and easy to use, and, hence, have become the most popular and computationally efficient method to model the soil-pile interaction. The adopted procedure is commonly termed as 'Analysis of Beams on Dynamic Winkler foundation (BDWF)'. The primary reason for the popularity of BDWF is that this method of modelling is relatively computationally inexpensive, and its results are noted to have been in accord with the rigorous finite element (FE) predictions of deflections and moments within a maximum deviation of 15% in the flexural responses. This technique is able to handle complex conditions of geometry, soil, and excitation (Dezi et al., 2009; Kavvadas and Gazetas, 1993). In BDWF method, soil is represented by springs and dashpots, distributed along the length of the pile. The springs can be assigned suitable *p-y* response curves. The dashpot coefficients should be such that they are able to account for material and radiation damping (Gazetas and Dobry, 1984c). Using the principle of superposition on the kinematic and inertial response, Mylonakis et al. (1997) implemented the BDWF for determining the kinematic response of a single pile embedded in an assumed equivalent linear soil. Berger et al. (1977) adopted the two-dimensional pile-soil model to estimate the radiation damping coefficients of a laterally oscillating pile, which is an analogous representation of a fully 3D system. It was assumed that a horizontally moving pile section of effective width and thickness generated 1D P-waves travelling in the direction of shaking and 1D SH waves travelling in the orthogonal direction to shaking. Such an adoption aided in the analysis of the complex three-dimensional wave propagation phenomenon through a comparatively inexpensive computational technique of 1D wave propagation. Gazetas and Dobry (1984c) pointed out that the above analogical 1D model for radiation damping would predict constant frequency-independent coefficients that are in contradiction to the results of rigorous wave propagation analyses. This led to the

proposition of radiation damping coefficients for a 2D and 3D problem using the truncated quarter-plane model.

For pile groups, the dynamic impedance cannot be computed by simply adding the impedances of individual piles, since additional deformations are transmitted from adjacent piles in the group. Dobry and Gazetas (1988) presented a simple method of obtaining the dynamic impedances of floating rigidly capped pile group, in which the interference of cylindrical wave fields originating along each pile shaft was considered to be spreading radially outward. Based on superposition, Makris and Gazetas (1992) presented a three-step method to obtain the dynamic response of the piles. Pile-soil-pile interaction can also be accounted for with the use of Green's functions. Dezi et al. (2009) made use of the elasto-dynamic Green's functions to express the soil displacement due to interaction. The nonlinear analysis of the pile-soil continuum system under the influence of seismic motions can be performed with the help of FEM or FDM. Reducing the computational expense is always a prime issue while performing studies using FEM. Badry and Satyam (2016) showed the applicability of the Equivalent Pier Method (EPM), originally proposed by Poulos and Davis (1990), in reducing the computational cost of the SSI problem when solving using FEM. The BNWF (Beam on Nonlinear Winkler Foundation) method stands out to be a very versatile method of analysis because of its computational efficiency and several advantages over other simplified methods (Boulanger et al., 1999). Methodologies have been developed wherein the soil around the pile is categorized into two separate zones, i.e., (a) near-field (plastic zone), where nonlinear soil pile interaction occurs, and (b) the far-field zone, where primarily linear elastic behaviour is prevalent (Nogami et al., 1992; Novak and Sheta, 1980). The methodology was developed based on the concept of series radiation damping, which was found to be in reasonable agreement with the preliminary centrifuge results by Wang et al. (1998). Hokmabadi et al. (2014) conducted a fully nonlinear analysis of a mid-rise building resting on a floating pile through numerical FDM simulation. The model was validated against a scaled model of the same that was experimentally tested on a shake table. It was reported that the lateral deformations of the structure resting on a shallow footing were higher when compared with the deformation of the structure supported by piles. An important conclusion of the study was that SPSI (soil-pile-structure-interaction) could also increase inter-storey drifts when compared with the fixed-base structure. This, in turn, may affect the performance level from life-safety to near-collapse, the damage intensity being higher for structures on shallow foundations. Hence,

from the various research studies highlighted in the current section, pertaining to the modelling of the shallow and deep foundations, it can be said that modelling of the foundation is a critical component, and requires due attention for the successful evaluation of soil-structure interaction effects in various structures.

2.7 SSI STUDIES ON BUILDINGS

The most widely built structure in the construction industry comprises of the buildings supporting human habitation and workplace. For all practical purposes, it becomes imperative to study the effect of SSI on buildings to get a thorough understanding of their response. This section deals with the application of SSI studies to buildings, as available in the existing literature. Studies on the natural period of the structure have been carried out in the past. Bhattacharrya and Dutta (2004) assessed the effect of soil-structure interaction on the change in natural periods of the building frames resting on isolated and grid foundations. Balkaya et al. (2012) carried out finite element analysis (FEA) of the shear wall dominant buildings under the influence of different types of soil conditions. The vibrational periods and mode shapes of the structures were evaluated, and it was pointed out that the code-based method of prediction of the periods was quite misleading. Nateghi and Rezaei-Tabrizi (2013) showed that the proximity of the period of the structure to that of the free-field period of the soil significantly affects the nonlinear response of the adjacent structure. Renzi et al. (2013) presented an approximate method of analysis for which it was concluded that the wave parameter (a measure of the relative stiffness of the foundation and the superstructure) significantly influences the lengthening of the period of the structure. Vivek and Raychowdhury (2017) conducted experiments on steel moment resisting frames supported on shallow foundations to show the elongation in the natural perod of the buildings under the influence of SSI. All these studies show that the period of the structure may play a significantly important role in the soil-structure interaction analysis. Veletsos and Meek (1974) showed that the effect of soil-structure interaction was to decrease the resonant frequency of the system. At the same time, it modifies the peak response of the short-squatty structures and tall structures by, respectively, decreasing and increasing the response. Bielak (1978) studied the behaviour of nonlinear systems with the compliance of the soil foundation. It was observed that the resonant amplitudes increased for a compliant base when compared with those of a rigid foundation. Although these research studies were some of the pioneering works aimed at SSI analysis of the building structures, the inherent

assumptions and idealizations render them unsuitable for the modern-day scenario where very advanced methods are available.

A considerable amount of research has displayed the validity of the fixed-base (FB) analysis for SSI cases and the deviation from the actual scenario brought about by such assumptions. Han (2002) showed that analysis of tall buildings fixed on a rigid base does not represent the real seismic response of the structure since the stiffness is overestimated, and damping is underestimated. Sáez et al. (2013) highlighted the fact that soil reaches the limit of elasticity under weak to moderate shaking, and inferred that the analysis of the structures with FB or with linear soil was highly inconsistent. Hence, the researchers studied the 2D moment-resisting frames by conducting the modelling with nonlinear soil and concluded that the effects of inelastic SSI resulted in a variation of the computed structural response compared to that obtained with the fixed-base condition. Kraus and Džakić (2013) highlighted that the assumption of a fixed-base analysis is valid in situations wherein the foundation soil has relatively higher stiffness in comparison to the structure; this is attributed to the simple reason that the deformations at the soil interface would be negligible. It was showed that the behaviour of low-rise building is different from that of the high-rise building, which is apparent in the distribution of the storey shear profile of the buildings, and that the same could be detrimental for the low-rise buildings. However, the conclusion drawn needs substantiation with further studies by incorporation of soil nonlinearities into the analysis. Dutta et al. (2004) also concluded that soil-structure interaction played a significant role to increase the seismic base shear of low-rise building frames, and the effect was strongly influenced by the frequency content of the earthquake ground motion. It was also highlighted that the fixity of the structure is dependent on the amount of load transferred from the building to the ground and will govern the size of the footing. This, in turn, will affect the flexibility of the soil due to which various natural frequencies may become closely spaced leading to an increase in the cross-modal coupling terms contributing to the overall seismic response. From these studies, it is clear that although the practice is to reduce the design forces for the design of buildings under the influence of SSI, such a concept is not valid or acceptable for all classes of buildings. For those buildings against which the validity exists, the relative distribution of the forces and the various profiles of the design entities are significantly different from that of a fixed-base structure. This change in the profile of forces/displacements could be critical for the estimation of the ductility of the building members, an important parameter in the design.

Halabian et al. (2002) showed that for towers resting on soils having low shear wave velocity, the ductility requirements of individual sections of the freestanding tower are affected by the foundation flexibility. The foundation flexibility may have strong unfavourable effects on the response of the tower and on the development of internal forces in the flexible parts of the structure. Although the study was conducted for towers, the analogy can be extended for a slender building since it may behave in a similar fashion, and the ductility requirements at certain storey levels may be similarly affected.

El Ganainy and El Naggar (2009) highlighted that no separate provisions were available for the seismic analysis and design of buildings with underground stories. For performance-based design, SSI has become an integral part of the method. It was shown in the study that the incorporation of SSI in the analysis resulted in increased moments and shear demands for buildings founded on soft soil. The effect of SSI was observed to reduce with the increasing number of underground stories. Another class of buildings for which the conclusions from the fixed-base analysis cannot be applied is the RC wall-frame buildings, in which there exist regions of significant stiffness (due to the presence of wall) as well as quite flexible regions. The presence of a stiffness gradient in the same structure would produce different behaviour in comparison to a structure devoid of such a huge non-uniformity of this gradient. Oliveto and Santini (1993) presented two methods for the dynamic analysis to decipher the response of the RC frame-wall plane system and made an account of different modes of vibration using frequency domain analysis. From the study, it was concluded that the amplification of the structural response is related to the reduction of the effective damping ratio in the first mode when the phenomenon occurs in the form of rocking motion. Nadjai and Jhonson (1996) used the discrete force method for the elastic analysis of the shear wall system subjected to lateral loads while modelling the base flexibility using vertical and rotational springs. Foundation flexibility was found to affect significantly the behaviour of the shear wall and the core assembly, especially the stresses in the lower portion of the wall. The method developed was appropriate for the reduction in computational effort. However, due to the consideration of the flexibility in a lumped fashion, the real scenario might not have been reproduced. Moreover, nonlinearity, hysteresis damping, and radiation damping were not accounted for.

Subjected to moderate earthquakes and considering the influence of linear SSI, Carbonari et al. (2011) evaluated the response of coupled RC wall-frame structures on pile

foundations, while accounting for soil-pile interaction and radiation damping. It was observed that rocking of the wall foundation, related to the vertical dynamic impedance, depends significantly on the soil and increases rapidly with the decrease in the stiffness of the soil deposit. Moreover, it was observed that the seismic base shear in the columns increased while the same in the wall decreased when compared with fixed-base results. Such observation implied that the migration of shear forces from the wall to the frame strongly increases with the decrement of soil stiffness. Carbonari et al. (2012) extended the earlier understanding of nonlinear behaviour of the structure. The SSI was accounted for using the substructure method in which nonlinear properties of the soil were taken into consideration in terms of equivalent linear properties. In the study, it was seen that the incorporation of SSI increased the lateral deformability of the structure. The rocking of the foundation significantly affected the response of the couple RC wall-framed structures, the effect of which was to reduce the shear at the base of the wall and increase the same at the frame base. Raychowdhury and Singh (2012) noted that SSI was not accounted into the-then present design practice due to its apparent consequence of leading to a conservative design and due to the absence of reliable nonlinear modelling technique. The researchers evaluated the response of a steel moment-resisting frame considering nonlinear soil-foundation interface behaviour using the BNWF approach. It was concluded that linear and nonlinear SSI effects reduced the global force demand and increased roof displacement. It was concluded that SSI could significantly alter seismic demands, ignorance of which can lead to uneconomic design. From these studies, it is clear that the response of an RC wall-frame building is significantly different from that of a moment-resisting frame building and that the presence of rocking response (under the wall) plays a key role in the relative distributions of forces in various members of the structure. Moreover, the response of any structure resting on soil with linear elastic behaviour is quite different from that resting on soil with nonlinear behaviour. Under such cases, each of the conclusions drawn from a linear SSI should not be considered universally valid for the real scenarios, in which the soil exhibits nonlinearity even under very small strains.

It is worth mentioning that the effects of soil-structure interaction not only depend on the type of the superstructure, but also on the type of foundation that exists underneath the superstructure. The behaviour of the buildings supported by shallow foundations differs from that of the deep foundations (e.g., pile foundation). Kutanis and Elmas (2001) performed 2D linear and nonlinear SSI analyses of a tall building on a shallow foundation

using the method of sub-structuring. Sound results obtained from the method made it relevant for application to important structures. After a scrutiny of the results of the roof displacement, which exhibited higher values for fixed-base analysis, the contrasting behaviour of the tall buildings supported on deep and shallow foundation could be aptly illustrated (Kutanis and Elmas, 2001; Han, 2002). The roof displacement of tall buildings supported on shallow foundation exhibits higher displacements for fixed-base analysis and lowest for nonlinear SSI, while the vice-versa is noted for tall buildings supported on pile foundation. Lu et al. (2003) analyzed a 12-storied building (with additional basement) supported on a pile-raft foundation. It was observed that a change in the shear modulus of the adopted soil with equivalent linear elastic behaviour resulted in a change in the response of the structure, having no straightforward correlation with each other. As observed previously, the effect of consideration of SSSI on the linear elastic behaviour of the structure increased the peak value of displacement in the structure but reduced the peak values of acceleration, inter-storey drift, shear, and overturning moment of the structure. The importance of the relative stiffness of the structure and the soil is highlighted in the change of peak displacements. Han (2002) conducted a study on a 20-storied building supported on pile foundations comprising a rigid base, along with linear and nonlinear soil pile systems. The boundary zone model proposed by Novak and Sheta (1980) was incorporated in the modelling of soil nonlinearities in the periphery of the pile. The structure-soil-foundation was analyzed for various conditions of the foundation, as stated earlier. It was concluded that the behaviour of the building supported on pile foundation is notably different from that of fixed-base or that supported on shallow foundation. It was also stated that for safe and economical design, a judicious seismic analysis is required.

Along with the type of structure and foundation, the soil type and ground motion decisively influence the response of the structure and the forces that are developed in it. Depending on the nature of the ground motion and the nature of the soil, the amplification and de-amplification of the seismic waves take place and govern the unique response of the structure. Matinmanesh and Asheghabadi (2011) studied the amplification of seismic waves as they propagate from bedrock to the surface, supporting a high-rise and a low-rise building on mat foundations. It was observed that ground motions (frequency content), type of soil, and type of the structure (natural period of the structure) contribute simultaneously in the determination of the amplification level of the seismic waves at the surface. The study was based on the elastic behaviour of both the soil and the structure and, hence, the conclusions

drawn may change with the incorporation of soil nonlinearity. Tabatabaiefar et al. (2013) highlighted the increased need to incorporate site-dependent dynamic analysis for the evaluation of the response of a structure to cater to the site effects as observed in many earthquakes (Mexico 1985, Christchurch 2011, Tohoku 2011). SSI study on a 10-storey moment-resisting frame (supported on shallow foundation) was carried out using Flac 2D (a finite difference software) in which nonlinearities of the structure, soil, and interface were incorporated. It was found that the ratio of the base shear as obtained from the flexible base model and the fixed-base model was less than unity, which was alleviated to near unity values on incorporating the structural inelasticity. The inter-storey drifts of the flexible base models on soft soils were observed to increase, thereby pushing the structure into the near collapse performance level. This rendered that the assumption of the negligence of SSSI effects, as manifested in the current codal design practices, was conservative and inadequate for a safe and reliable design of moment-resisting frames. Yegian et al. (2001) mentioned that SSI analysis, with the inclusion of the overall structure-foundation-soil system, was yet to receive due attention. The inclusion of nonlinearities of the soil and superstructure and the clear distinction on the merits and demerits of various methods available for the analysis is still comfortably unavailable to the practicing engineering community.

2.8 CODAL PROVISION ON SOIL-STRUCTURE INTERACTION

As already mentioned, a lot of studies have been carried out to show the influence of soil-structure interaction on the seismic behaviour of the buildings. It is important to know which of these aspects are relevant for proper structural design. It is equally important to understand under what situation the SSI effects should not be ignored. With this aim, this section provides a review of various codal provisions related to the consideration of the soil-structure interaction. Apart from the design codes of various countries, a few international guidelines are also reviewed.

Apart from NIST GCR 12-917-21 (2012), only a few international codes have guidelines regarding SSI and only a handful among them makes a mandatory consideration of SSI in the design. Eurocode 8 Part 1(2004) suggests that the SSI effects must be mandatorily taken into account for the following cases, namely (a) when the second-order effects (P-δ effects) play a significant role, (b) when the structure is slender and tall, (c) when the structures are supported on very soft soils, or (d) when the structures have deep-seated foundations such as the pile foundations. The code mentions the conditions under

which SSI should be considered, however, it does not provide any specific guidelines on the computation of SSI effects. Eurocode 8 Part 1 (2004) makes a special mention of a typical soil type that has a very low value of shear wave velocity, low internal damping, and an abnormally extended range of linear behaviour. The code recommends a special study to define the seismic actions as this type of soil produces abnormal site amplification. Japanese guidelines (JSCE, 2007) mandates the consideration of SSI effects wherever the interaction effects cannot be ignored. However, it does not specify the situations for which the interaction effects should be regarded. ASCE 7-05 (2006) allows for consideration of SSI effects either by modifying the results from the fixed-base analysis or by incorporating the soil flexibility by equivalent linear stiffness. The Indian standard for earthquake resistant design, IS 1893 Part 1 (2016), exempts consideration of SSI for the analysis of structures supported on rock and rock-like material. No mention, however, is made in the guidelines if SSI is to be considered in the analysis and design procedure for foundations in other types of soils. IS 1893 Part 1 (2016) does not also suggest the use of other international guidelines and standards for considering SSI in the designs.

The Mexican code (del Distrito Federal G, 2004) allows for an approximate inclusion of SSI by evaluating a modified time period of the structure (Root-mean-square, or RMS, of the time period of the structure with fixed-base conditions, the time period of the structure allowing only lateral movement, and the time period of the structure only allowing rocking movement). The result is an increased time-period of the system. In order to include the SSI effects, FEMA 450 (2003) and ASCE 7-05 (2006) allow for a reduction in the base shear force by considering a modified time period and damping of the fixed-base structure. Alternatively, the codes suggest the consideration of foundation flexibility as an option and recommend representation of soil flexibility by considering equivalent linear stiffness. This method requires modification of the seismic input motion at the base of the structure and, in that regard, the former method (reducing the base shear based on the modified time-period and damping of the fixed base structure) can be considered to be rather convenient for design purposes. FEMA 440 (2005) provides the guidelines on the modification of the foundation input motion and can be used in conjunction with the guidelines of FEMA 356 (2000) and ATC 40 (1996). In comparison to the fixed-base foundation models, the mentioned guidelines primarily address on reducing the shaking induced demand on the structure, caused due to kinematic interaction or foundation damping effects.

Among the various international codes and guidelines, the Japanese guidelines (JSCE, 2007) prescribe, as a general rule, the use of time-history analysis for the verification of earthquake resistance of structures. Those structures are considered that allow the consideration of nonlinearity of the structural members and soil, except for the situations wherein it is obvious that the response of the structure and member will be in the elastic region. The code recommends direct modelling of the soil along with the structure for seismic SSI analysis unless there are cases where interaction effects can be neglected. It suggests the consideration of a sufficiently large region and the usage of boundary conditions to allow for the proper propagation of ground motion. Moreover, when the separation of ground and structure is supposed to affect the response of the structure, the code recommends the usage of 'joint elements' to represent the effects of separation and sliding between structure and the ground. Constitutive models are recommended to capture the characteristics of the plastic behaviour of the foundation soil. From the review of various codes and standards, it is amply clear that the American (FEMA 356, 2000; FEMA 440, 2005) and Japanese standards (JSCE, 2007) are much more advanced in terms of provisions related to SSI and guidelines for its consideration. The American standard focuses more on design procedures and other linear models for SSI, whereas the Japanese code suggests modelling of SSI as accurately as possible considering various constitutive models and interface nonlinearity. Unfortunately, Indian standard codes do not grant any dedicated provisions related to SSI that can be used for the design and analysis of structures with embedded foundations.

2.9 PREVAILING GAPS IN THE LITERATURE AND MOTIVATION OF THE STUDY

Based on the understanding from the available literature, it can be understood that it is extremely important to orient the research towards the avenues of evaluation of the effects of SSI on the structure and in the identification of the scenarios that give rise to detrimental effects of SSI. Past reviews from the last century provide a good insight into the origin and developments related to the various issues that existed in the subject of soil-structure interaction. It is evident that a great deal of work has been done to comprehend the effects of dynamic SSI. It has been hypothetically assumed that, for most cases, SSI can be considered beneficial for the multi-storeyed residential and/or commercial buildings, adjudged as the most common types of civil engineering structures. Many researchers have proved this hypothesis to be erroneous in different situations. Many pieces of evidence exist that display the effects of seismic soil-structure interaction on the response of the structures

and have highlighted significant contributions due to SSI. Moreover, ground motion amplification plays a key role in the response of the structures. There exist various methods for evaluating the effects of seismic SSI, and each method has its own applicability and extent of usefulness. Various issues related to the modelling of the soil and foundation interaction have been discussed. It is observed that significantly less amount of research has been devoted to nonlinear modelling of soil and foundation interaction for seismic soil-structure interaction studies.

The natural period of the building plays a significant role in the response of the structure for seismic SSI studies. It has been observed that the validity of the fixed-base analysis can be used for flexible bases only restrictively if the foundation comprises stiff soils. It is noted that the behaviour of low-rise and high-rise buildings are different from each other. In the same manner, the behaviour of moment-resisting frame buildings is different from that of the wall-frame buildings, wherein rocking plays a key role in the behaviour of the latter type. The type of foundation plays a significant role in determining the response of the building superstructure. The behaviour of buildings supported on shallow foundations is different from those supported on piles and pile groups. Site characteristics and ground motion significantly influence and govern the damaging response of the buildings in the event of an earthquake. Thus, it is evident that a lot of issues are intricately involved and required to be known for a better understanding of the seismic SSI.

From the review, it is clear that a lot of studies have been carried out that give the overall picture of the effects of SSI. However, studies that focus on the comparative application of various methods to a particular type of building typology and structure has been very few. Such studies should be undertaken to understand the localized and specific effects of SSI, which would be beneficial in comprehending the detrimental scenarios or causes that may arise due to SSI. The following are the issues that require attention and needs to be addressed:

- Codes provide inadequate guidelines related to SSI for buildings and need to play a greater role in the inclusion of SSI into the analysis and design procedure of the building structures.
- A great deal of the research has focused on structures supported on shallow foundation, and less attention has been paid to those supported on pile foundations. Although a few researchers have pointed to the detrimental effects of SSI, there is a need to address the

question in scrutinized detail to identify the beneficial and detrimental scenarios for seismic soil-structure interaction. The presence of the phenomenon of ground motion amplification demands the need for such identification and recognition by various international codes and seismic guidelines.

- For the nonlinear modelling of the soil domain, detailed studies related to the guidelines of the discretization of the horizontal and vertical extent of soil domain do not exist. To be considered for the SSI analysis, this aspect needs attention so that an optimum balance could be achieved between the accuracy of the solution and computational efficiency.
- The inclusion of nonlinearity in the building and soil for the evaluation of the seismic response of the structure has not received much attention and needs significant study. In most cases, the behaviour of soil is highly nonlinear, and, in the event of a major earthquake, the structure unquestionably produces an inelastic response. Studies of buildings on pile foundations have been less and only limited to incorporating elastic behaviour.
- Studies on RC wall-frame buildings have been substantially scarce.
- The effects of ground motion incorporating the effect of SSI are significantly different in comparison to the situations where SSI effects are disregarded. Proper identification of the parameters that modify these ground motions has not been considered in SSI studies. Much attention needs to be given to identify the scenarios wherein inclusion of SSI proves to be beneficial and/or detrimental.
- The development of code-based procedures (empirical or semi-analytical) needs attention. Although there are a few methods available for the inclusion of SSI in code-based design, with the advancement of powerful computing, the methods need to be improved or new methods need to be developed that take into account the significant details (ground motion characteristics, soil nonlinearity, etc.).

2.10 Objectives and Scope of the Present Study

Based on the highlighted gaps in the literature, the objective of the present study encompasses ‘Seismic Behaviour of RC Frame and RC Wall-frame Systems Supported on Pile Foundations Considering Soil-Structure Interaction’. In order to meet the prescribed objective, the following scopes have been outlined with regard to RC frame and RC wall-frame systems supported on pile foundations:

- Prescribe appropriate horizontal extents of the soil domain, to be used for dynamic SSI analysis.
- Investigate the influence of seismic soil-structure interaction on the natural period and develop a predictive relationship for quick and easy estimation of the effective natural period of the SSI system.
- Consider the influence of nonlinear SSI on the lateral load behaviour to understand the modification that would arise with respect to the conventional fixed-base analysis.
- Study the effect of nonlinear SSI on the global and local ductility demands.
- Outline possible recommendations for incorporating seismic soil-structure interaction in assessing structural response.

Chapter 3
NUMERICAL MODELLING AND VALIDATION STUDIES

CONTENTS

3.1 OVERVIEW

To realise the outlined objectives, a numerical study is carried out using the Finite Element Method (FEM) and the various aspects of modelling adopted in the present study are discussed in this chapter. For conducting realistic SSI studies, it is important to simulate the material characteristics and appropriate boundary conditions. For simulating the soil and structural behaviours, existing models incorporating material nonlinearity have been adopted. Proper boundary conditions are imposed and to ensure the simulation of radiation damping in the SSI model. Staged gravity analysis has been conducted for developing a proper state of stress within the soil under gravity loads prior to conducting the seismic analysis. The numerical model for SSI analysis is validated by comparing its results with those available in the literature. The entire study is conducted with the help of a finite element-based software framework, OpenSEES (Mazzoni et al., 2009).

3.2 MATERIAL MODELLING

To conduct a seismic soil-structure interaction study, the assignment of appropriate material characteristics to the components (soil and structure) is essential for simulating proper behaviour. Both soil and reinforced concrete may undergo large inelastic deformation during earthquake shaking. Thus, the adopted material models should be able to capture the peak and hysteretic stress-strain response during cyclic behaviour. The following subsections describe the material models used in the present study for simulating the nonlinear behaviour of soil and reinforced concrete.

3.2.1 Constitutive Model for Soil

To represent soil of varying stiffness, in the present study, cohesionless soil is considered corresponding to four different relative densities. The basic properties of those soils are given in Table 3.1, wherein S1, S2, S3, and S4 represent loose, medium, medium dense, and dense sands, respectively. Thus, S1 and S4 correspond to the soils of minimum and maximum stiffness, respectively. Pressure-dependent constitutive behaviour (Yang et al., 2008) has been used for the simulation of the nonlinear characteristics of the soil. In this model, the monotonic and cyclic response of the soil at a particular depth depends on the confining pressure at that depth. Plastic behaviour is based on multi-surface plasticity (Prevost, 1985; Iwan, 1967; Mroz, 1967), shown in Figure 3.1a, wherein the hardening zone is defined by several yield surfaces possessing a common apex (at $p_0^{'}$) along the hydrostatic axis. The outermost surface, also termed as the failure envelope, is the envelope of peak shear strength. For hysteretic response under arbitrary cyclic shear loading, the material model employs a purely kinematic deviatoric hardening rule (Parra, 1996; Yang, 2000). Figure 3.1b shows the flow rule of the material model, which is capable of simulating contraction and dilational volumetric response. The boundary between contraction and dilation is defined by the phase transformation (PT) surface. The flow rule adopted is such that the soil response is contractive within PT surface (phase 0-1) and dilative outside PT surface (phase 2-3). During unloading, the response is contractive (phase 3-4) until specific effective confinement is achieved. Possible liquefaction-induced perfectly plastic phase is induced during phase 1-2 before the initiation of dilation. The selected constitutive model is able to simulate response that is dependent on the instantaneous confining pressure as well as capture the typical characteristics of cohesionless soil such as dilatancy (based on non-associative flow rules) and liquefaction (Yang et al., 2003, Elgamal et al., 2003).

Table 3.1 Basic properties and constitutive parameters of the soil for the present study

Type of soil	ρ (kN/m^3)	φ (°)	υ	v_s (m/s)	G_r (kPa)	γ_{max}	d	Φ_T (°)
Loose (S1)	17	29	0.33	193	5.5×10^4	0.1	0.5	29
Medium (S2)	19	33	0.33	212	7.5×10^4	0.1	0.5	27
Medium Dense (S3)	20	37	0.35	240	1.0×10^5	0.1	0.5	27
Dense (S4)	21	40	0.35	270	1.3×10^5	0.1	0.5	27

Note: ρ is the mass density of the soil, φ is the angle of internal friction, v is the Poisson's ratio, $v_s = \sqrt{G/\rho}$ is the average shear wave velocity, G_r and γ_{max} are the reference low-strain shear modulus at and peak shear strain respectively at reference pressure $p_r^{'}$ = 80 kPa, d is the coefficient that describes the relationship $G = G_r(p^{'}/p_r^{'})^d$, $p^{'}$ is the instantaneous effective confinement pressure, G is the instantaneous shear modulus and Φ_T is the phase transformation angle.

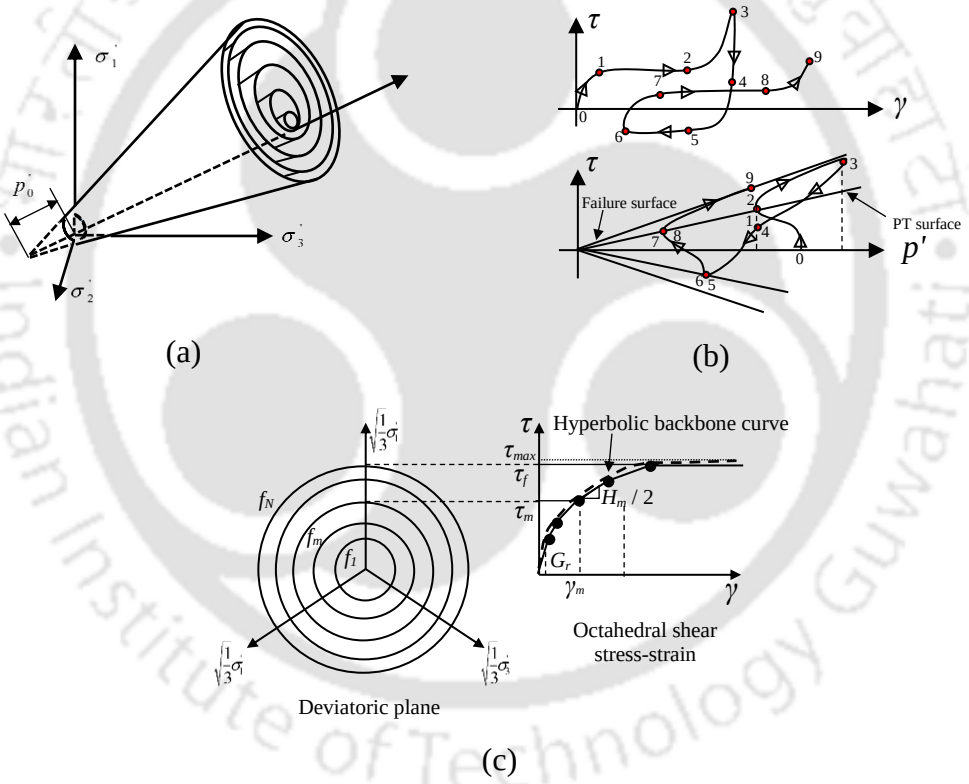

Figure 3.1 Pressure dependent soil material (Yang et al., 2003): (a) yield surface configuration in principle effective stress space (b) shear stress-shear strain curve and effective stress path, and (c) hyperbolic backbone curve and its piecewise-linear representation for the octahedral stress-strain response (Prevost, 1985; Parra, 1996).

The mentioned constitutive behaviour of soil is implemented with the help of *PressureDependMultiYield* model available in OpenSEES. The octahedral stress-strain characteristics are represented by a hyperbolic backbone curve with a piecewise linear approximation for each yield surface interval (Figure 3.1c). In the present study, 20 yield

surfaces have been used for simulation of soil behaviour. The intention of considering a pressure-dependent constitutive model for the soil is to simulate the following two aspects:

a. *To model a realistic shear wave velocity profile of the soil domain*: Realistically, the shear wave velocity increases with an increase in the depth of the soil deposit. At a particular depth, the shear wave velocity of the soil is a function of its shear modulus. The considered constitutive model simulates the shear modulus as per the relationship shown in Table 3.1 [$G = G_r (p^{'} / p_r^{'})^d$ where $p^{'}$ is the instantaneous effective confinement pressure and G is the instantaneous shear modulus]. According to this relationship, the shear modulus is a function of pressure that in turn is a function of the depth of the soil deposit. Moreover, the shear wave velocity at any particular depth is obtained using the relationship $v_s = \sqrt{G / \rho}$. Hence, the chosen material model for soil allows the modelling of an increase in the confinement pressure ($p^{'}$), thereby exhibiting an increase in the shear modulus (G) and the shear wave velocity (v_s) with an increase in the depth of the soil deposit (see Figure 3.5).

b. *To simulate the appropriate confining action of the soil onto the piles*: Appropriate modelling of soil profile characteristics is of particular importance to piles embedded in granular/cohesionless soil. This is because the piles experience an increase in the confining pressure as the embedment length increases. The confining action ultimately governs the stiffness exhibited by the pile foundations embedded into the soil. The chosen material model for soil is capable to capture the increase in the confining action onto the pile with the increase in the embedment length and hence allows for the simulation of appropriate confining action of the soil onto the piles.

3.2.2 Constitutive Model for Concrete

In any load-bearing RC member, concrete exhibits varying behaviour as it may or may not exhibit increased strengths and ductility, depending on whether or not it undergoes confinement action. Under compressive loads, transverse reinforcement imparts confinement action to the core concrete owing to which the strength and ductility are significantly increased. Comparatively lesser strength and ductility are mobilised in the cover concrete due to the absence of such confining action. It is, therefore, essential to

account for the confined and unconfined behaviours of concrete in the material characteristics by providing appropriate stress-strain relationships. In the present study, the uniaxial stress-strain behaviour of unconfined concrete is modelled using the Kent-Park model (Kent and Park, 1971), and that of confined concrete is modelled using the modified Kent-Park model (Scott et al., 1982). The characteristics of the stress-strain curve for confined and unconfined concrete are shown in Figure 3.2.

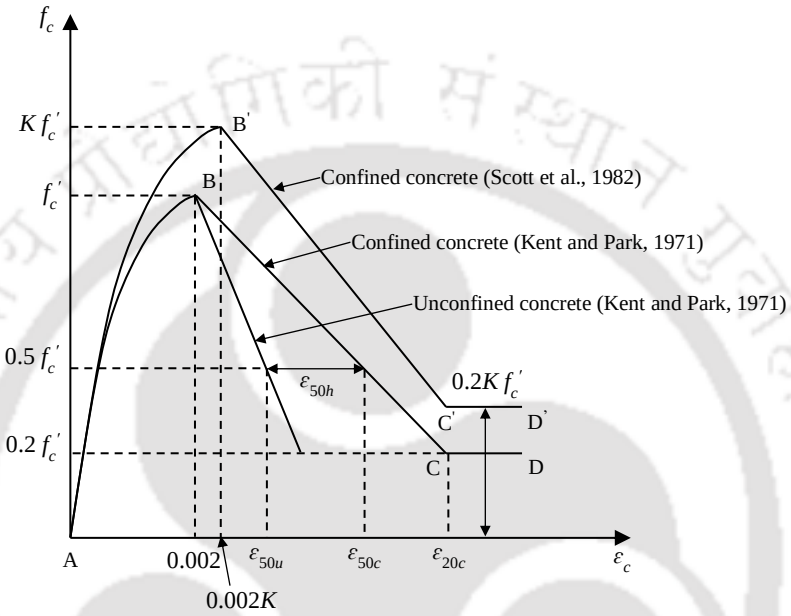

Figure 3.2 Stress-strain curves for confined concrete for Kent and Park (Kent and Park, 1971) and Modified Kent and Park (Scott et al., 1982) models.

In unconfined concrete, prior to the development of peak stress (region AB), the stress-strain relationship is described as shown in Eq. 3.1. The stress-strain relationship immediately after the peak stress has a linear descent. The slope of this branch can be obtained by determining the strain corresponding to the 50% reduction in peak unconfined stress using Eq. 3.2, and the failure stress in unconfined concrete is limited to $0.2 f_c'$.

$$f_c = f_c' \left[\frac{2\varepsilon_c}{0.002} - \left(\frac{\varepsilon_c}{0.002} \right)^2 \right] \tag{3.1}$$

$$\varepsilon_{50u} = \frac{3 + 0.002 f_c'}{f_c' - 1000} \tag{3.2}$$

In the above Eqs., f_c is stress in concrete (in psi); ε_c is the strain in concrete; f_c' is the concrete cylinder strength (in psi).

On account of confining action, the strength and the ductility of concrete are increased. As shown in Figure 3.2 (region BCD), the Kent-Park model is able to account for the increase in ductility of concrete, however, it does not account for an increase in strength due to confinement. To overcome that, drawback, Scott et al. (1982) proposed the modified Kent-Park model. According to this model, prior to the development of peak stress, the confined stress-strain relationship is similar to that of the Kent-Park model, with the only difference being in the magnitude of peak stress and the corresponding strain (region AB'). The values of maximum stress and its corresponding strain are given by $K f_c'$ and $0.002K$, respectively (i.e., K times the respective values of the Kent-Park model), and the expression for K is given by Eq. 3.3.

$$K = 1 + \frac{\rho_s f_{yh}}{f_c'} \tag{3.3}$$

In the above equation, ρ_s is the ratio of the volume of transverse reinforcement to the volume of concrete core measured to outside of hoops f_{yh} is the yield strength of transverse steel. In the post-peak region, the stress-strain relationship is confined concrete of the modified Kent-Park model is determined in two steps. In the first step, the post-peak stress-strain relationship corresponding to the Kent-Park model is determined. The strain in confined concrete given by the Kent-Park model, corresponding to a 50% reduction in peak stress, is obtained by accounting for the increase in strain due to ductility, using Eq. 3.4.

$$\varepsilon_{50h} = \frac{3}{4}\rho_s \sqrt{\frac{b''}{s_h}} \tag{3.4}$$

In Eq. 3.4, b'' is the width of confined core measured to outside of hoops and s_h is the spacing of hoops. This provides the slope of the post-peak confined stress-strain relationship in the Kent Park model. The stress at any strain, beyond peak (region BC), can be obtained using the expression given in Eqs. 3.5 and 3.6.

$$f_c = f_c'[1 - Z(\varepsilon_c - 0.002)] \tag{3.5}$$

$$Z = \frac{0.5}{\varepsilon_{50u} + \varepsilon_{50h} - 0.002} \tag{3.6}$$

These relationships are further utilized for estimating ε_{20c}, i.e., the strain corresponding to 80% reduction in the peak confined stress of the Kent-Park model. In the second step, the post-peak confined stress-strain relationship in the modified Kent-Park model is obtained. The strain corresponding to an 80% reduction in peak confined stress (ε_{20c}) of the modified Kent-Park model is the same as that of the Kent-Park model. However, the value of confining stress in the modified Kent-Park model, at and above this strain (region C'D'), is '*K* times' that of the Kent-Park model. Further, the stress-strain relationship in the region B'C' is one with a linear descent. The residual strength of confined concrete (region C'D') is limited to $f_c = 0.2K f_c'$.

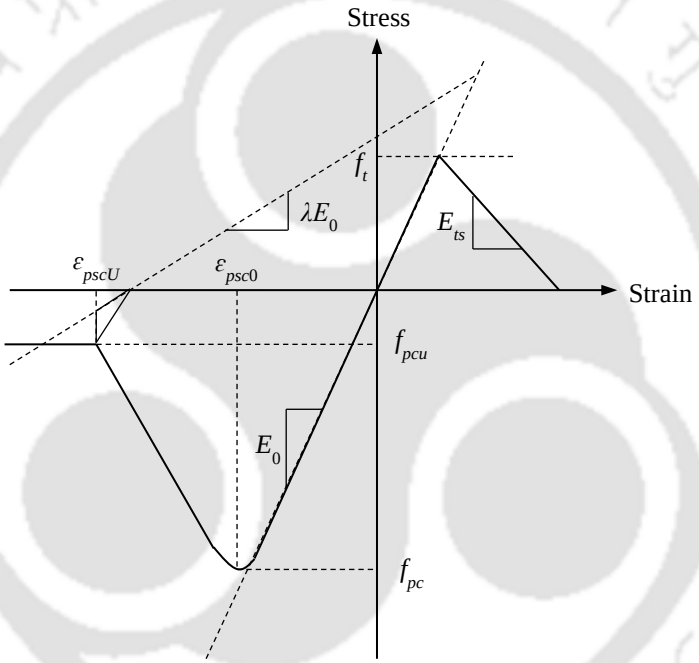

Figure 3.3 Stress-strain curve for uniaxial material *Concrete02* (Mazzoni et al., 2009).

In the present study, the *Concrete02* material model available in OpenSEES has been utilized for the modelling the stress-strain behaviours of confined and unconfined concrete. The material model is capable of displaying cyclic strength degradation and hysteretic behaviour and possesses linear tension softening. The elastic modulus of the tensile branch is assumed as shown in Eq. 3.7.

$$E_{ts} = f_t / 0.002 \tag{3.7}$$

In Eq. 3.7, $f_t = 0.7\sqrt{f_{pc}}$ is the tensile strength of the concrete, and f_{pc} is the concrete compressive strength in 28 days. The generic stress-strain behaviour, followed by the

model, is shown in Figure 3.3, where ε_{psc0} is the strain in concrete at maximum compressive strength; E_0 is the initial slope for the compressive stress-strain curve; ε_{pscU} is the strain in concrete at crushing strength; and, λ is the ratio between unloading slope and initial slope.

3.2.3 Constitutive Model for Steel Rebar

During strong earthquake shaking, the inelastic behaviour in the members of RC buildings gets concentrated in the plastic hinge regions. Once the concrete members undergo cracking, the response of the RC sections may be substantially influenced by the reinforcement. Therefore, accurate modelling of the reinforcement behaviour (in terms of stress-strain relationship) becomes important. The model should be capable of simulating the elastic and hardening branch. It should be capable of accounting for a reduction in the yield stress, after a load reversal, which should increase in proportion with the amount of plastic strain exhibited by the immediate foregoing excursion. Simultaneously the curvature in the transition zone between the elastic and plastic branches must decrease, which is known as the Bauschinger effect. The model should also be capable of exhibiting an increase in the envelop curve proportional to the plastic strain developed in the preceding excursion. This phenomenon is termed as isotropic hardening.

In the present study, the material model used for modelling of the steel rebar is that proposed by Menegotto and Pinto (1973) and modified by Fillippou et al. (1983), which is capable of simulating the above-mentioned essentials expected from an accurate material model for rebar. This model has been widely used by various researchers to simulate rebar behaviour in different types of RC structures. The characteristics of the monotonic behaviour are governed by Young's modulus (E_s), strain hardening ratio ($b= E_h /E_s$, i.e., the ratio between the slope of the hardening branch and elastic branch), strain and stress at yield point (ε_y, σ_y), and the strain and stress at the ultimate point (ε_u, σ_u) (Figure 3.4).

The cyclic stress-strain relationships of this model simulate curved transitions between the linear asymptotes of the elastic branch (with slope E_s) and the hardening branch (with slope E_h). The points where the two asymptotes meet are indicated by the strain ε_0 and stress σ_0 corresponding to the branches under consideration (Figure 3.4). Similarly, the point, corresponding to the strain reversals under consideration, is indicated by strain ε_r and stress σ_r. Mathematically, the stress-strain (σ_s–ε_s) relationship is shown in Eq. 3.8,

$$\sigma^* = b\varepsilon^* + \left[\frac{(1-b)\varepsilon^*}{\left(1+(\varepsilon^*)^R\right)^{1/R}}\right] \tag{3.8}$$

where,

$$\sigma^* = \frac{\sigma_s - \sigma_r}{\sigma_0 + \sigma_r} \tag{3.9}$$

$$\varepsilon^* = \frac{\varepsilon_s - \varepsilon_r}{\varepsilon_0 + \varepsilon_r} \tag{3.10}$$

$$R = R_0 - \frac{a_1\xi}{a_2 + \xi} \tag{3.11}$$

In Eq. 3.8, R is the parameter that influences the shape of the transition curve and varies with the strain history and is defined as shown in Eq. 3.11. In this equation, ξ is the absolute value of plastic strain corresponding to the last excursion; a_1 and a_2 are material constants, and R_0 is the value R during first loading.

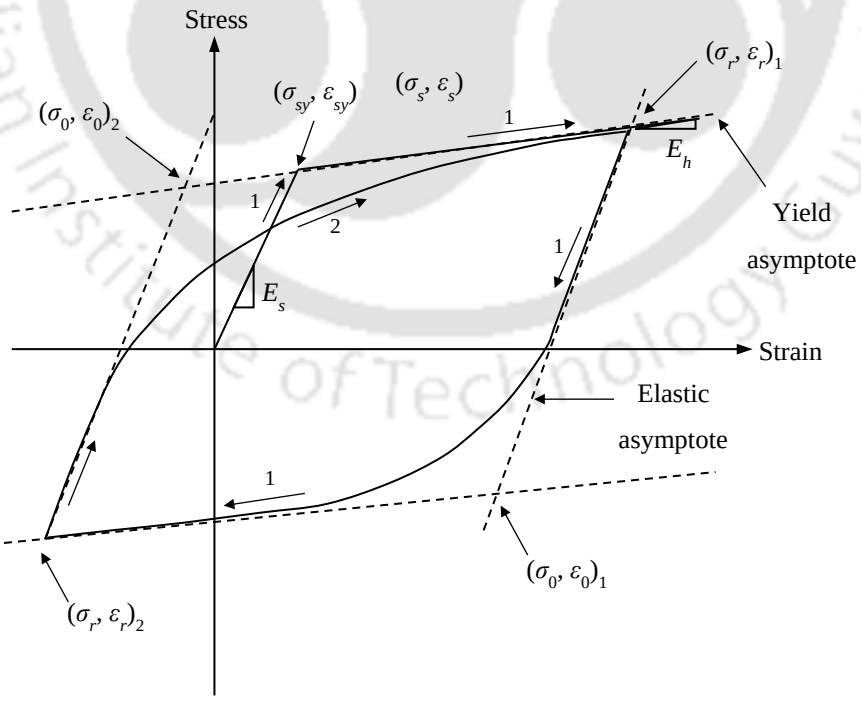

Figure 3.4 Menegotto-Pinto model for cyclic behaviour of steel rebar.

The model, as described above, although capable of reproducing experimental results quite well, it does not allow the incorporation of isotopic hardening. This drawback was addressed by Fillippou et al. (1983) by incorporating a change in the yield stress after every load reversal, which is dependent on the amount of plastic strain incurred in the previous excursion. Mathematically, the change in the yield stress, σ_y^e, is expressed in Eq. 3.12.

$$\sigma_y^e = \sigma_y a_3 \left\{ \frac{\varepsilon_{\max}}{\varepsilon_y} - a_4 \right\} \tag{3.12}$$

In Eq. 3.12, a_3, and a_4 are parameters determined experimentally, ε_{max} is the absolute maximum strain at the instant of strain reversal, ε_y and σ_y are the yielding strain and yielding stress. The mentioned model is implemented in OpenSEES using *Steel02* material.

3.3 GEOMETRIC MODELLING

In numerical studies, the numerical solution of a field problem is obtained, which provides the spatial distribution of the desired variables (e.g., force, displacement, stress, strain, etc.) over the specified geometry of the problem. This is achieved numerically by discretizing the geometry of the problem using multiple elements. The behaviors of soil and the structure are governed by different material characteristics. Furthermore, specific boundary conditions need to be defined for the soil domain for simulating the phenomenon of radiation damping. Moreover, depending on the field problem, certain idealizations may be required while modelling material behaviour. For example, in the present study, the inelastic behavior in the superstructure is limited to definite zones called 'plastic hinge regions'. The following subsections describe the various element types and the idealizations made over the spatial geometry of the problem.

3.3.1 Modeling of Soil

The present study intends to evaluate the in-plane seismic behaviour of RC frame and RC wall-frame systems under the influence of SSI. Therefore, in the present study, the two-dimensional soil domain is considered with a depth of 30 meters. The choice of selection of modelling of top 30 meters of the soil profile is in line with the prescription of ATC-40 (ATC-40, 1996) and various other past studies (Tomeo et al., 2018; Nguyen et al., 2016; Tabatabaiefar et al., 2013; Tabatabaiefar and Massumi, 2010). ATC-40 recommends site

characterization to be based on the shear wave velocity of the top 30 meters of the soil profile. Moreover, it also suggests considering the average soil properties of the top 30 meters of the soil. The idealised shear wave velocity profile and their average values (estimated based on the recommendations of ATC-40) for the various soil types, considered in the present study, are shown in Figure 3.5.

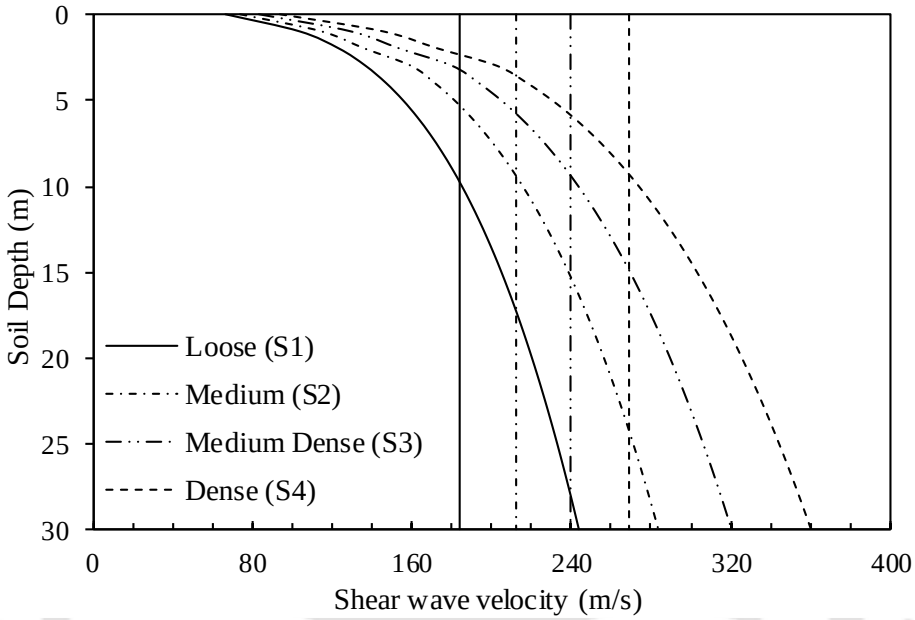

Figure 3.5 Shear wave velocity profile of soil types considered.

In the present study, the water table is not considered in the soil profile, and the bedrock is assumed to lie at a depth of 30 meters from the ground surface level. The in-plane seismic action causes insignificant variation in the out-of-plane strain within the soil. Hence, the soil domain is discretized using four noded plain strain bilinear isoparametric quadrilateral elements, with four gauss integration points. The simulation of inertial mass within the soil is done by means of bulk density, which is taken into account by these elements.

3.3.1.1 Modelling of Horizontal and Vertical Boundaries

During earthquake shaking, seismic waves shake up the foundation first, and then the shaking is propagated in the superstructure. The vibration of the superstructure produces waves that travel back into the soil medium. As those waves travel back into the soil medium, their amplitudes get reduced due to the spreading of the waves over a large volume of soil mass (Kramer, 1996). This phenomenon is termed as ‘radiation damping’ or ‘geometric damping’ and is distinct from ‘material damping’ in which energy is dissipated

due to hysteretic behaviour. For numerical simulation, a truncated soil domain with proper boundary conditions needs to be considered for optimizing the computational time and effort. The soil domain can be assigned with boundary conditions such that either the displacement is zero that is addressed by fixing the boundary nodes against displacement, or by providing zero-stress boundary conditions with the use of rollers at the boundary nodes. However, such boundaries have the property to reflect the waves. Thus, the waves do not radiate away from the soil domain but rather get trapped, resulting in a "box effect" (Kramer, 1996). This phenomenon leads to unrealistic behaviour and incurrence of significant errors. Therefore, to accurately model the effect of radiation damping, non-reflecting 'Lysmer-Kuhlemeyer' boundaries (also known as 'L-K boundaries') are used at the horizontal and vertical edges of the soil domain (Lysmer and Kuhlemeyer, 1969). These boundaries employ viscous dashpots to prevent the reflection of seismic waves back into the soil medium after being incident on them. On the vertical edge (i.e., the far lateral boundaries), the L-K boundaries consist of dashpots in the horizontal as well as the vertical direction, having dashpot coefficients[†] as $C_p = \rho v_p A$ and $C_s = \rho v_s A$ respectively. Since the motion applied to the SSI system is at the base and is essentially a shear wave propagating in the vertical direction. Therefore, only horizontal dashpots were attached at the horizontal edge (i.e., at the bottom boundary) having a coefficient $C_s = \rho v_s A$. The primary wave velocity (v_p) can be obtained from shear wave velocity (v_s) and Poisson's ratio (υ) as $v_p = \{2v_s(1-\upsilon)/(1-2\upsilon)\}^{0.5}$. It is worth mentioning that without these boundaries, it would not be possible to truncate the soil domain to a finite extent and model the effect of radiation damping.

3.3.2 Modeling of Structure

3.3.2.1 Superstructure

To model the frame members (beams and columns) of the RC frame and RC wall-frame systems, two noded beam-columns elements having three degrees of freedom at each node are used. Corresponding to each node, the three degrees of freedom consists of two in-plane translations and one in-plane rotation. Based on the exact interpolation of the internal forces, the flexibility (or force-based) approach is used in the formulation of this element (Spacone

[†] The dashpot coefficient corresponoding to the to the motion in the direction of primary wave is denoted by C_p, and that corresponding to the motion in the direction of shear wave is denoted by C_s. The area of soil domain contributory to dashpots in the L-K boundary is dentoed by A.

et al., 1996a and 1996b). ATC-40 specifies the Equivalent Frame Method (EFM) approach as an appropriate methodology for modelling of slender shear wall in which the shear effects can be conservatively ignored. Hence, in the present study, the RC shear walls are modelled with the help of the EFM approach. In this method, the shear wall behaviour is captured by modelling a beam-column element possessing the sectional properties as that of the actual wall section. The element is placed along the centre-line of the width of the shear wall (Figure 3.6). The monolithic behaviour of the shear wall, with the end columns as its boundary elements, is modelled with the help of rigid elements. The EFM model is capable of satisfactorily representing the axial-flexure behaviour of the shear wall.

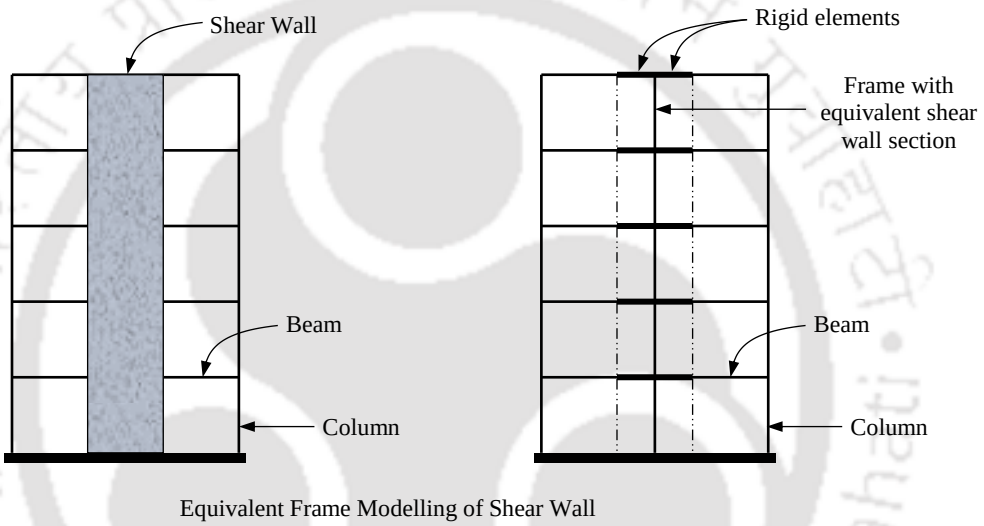

Figure 3.6 Modelling of frame members and idealization of the shear wall as an equivalent frame.

To simulate the inertial forces within the superstructure, the mass of the superstructure is lumped at every floor level as shown in Figure 3.7. The figure shows a representative diagram of the scheme adopted for lumping of the mass (dead load as well as live load) related to the various components of the structure. It can be seen from the Figure 3.7 that apart from the in-plane elements, the mass is lumped for the out-of-plane elements (for half-width of the bay in the out-of-plane direction) such as beams and slabs at the respective nodes for all the storeys. Similarly, the masses of the pile and pile cap elements are lumped at their respective nodes.

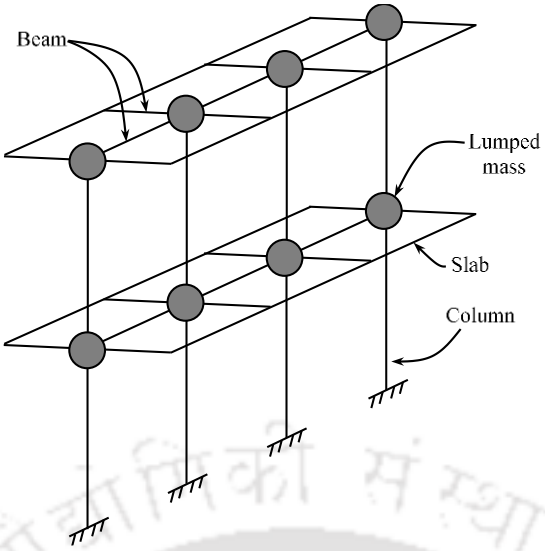

Figure 3.7 Lumping of structural mass at frame nodes (Representative diagram).

3.3.2.2 Substructure

To model the the substructure foundation elements (pile and pile cap) of the RC frame and RC wall-frame systems, two noded beam-columns elements having three degrees of freedom at each node are used. Corresponding to each node, the three degrees of freedom consists of two in-plane translations and one in-plane rotation. At the top of the pile foundation, pile caps are modelled to connect them with other piles and the superstructure. As the pile caps are rigid concrete elements, they are assigned linear elastic sectional properties for the entire study. In the present study, the interface nonlinearity was not considered and a Perfectly Bonded Interface (PBI) modelling is used for the modelling of soil-pile foundation interfaces. The perfectly bonded interfaces do not allow any separation or sliding between the soil and pile surfaces. For cohesionless soil, the adopted modelling approach is a satisfactory one, since under compressive loads the soil exhibits confining action onto the piles. Additionally, in this regard, a study was conduted by Mondal et al. (2012) wherein it was exhibited that the PBI modelling showed only 5-10% variation with the results of nonlinear interface model. Due to the incompatibility of the number of nodal degrees of freedom in the soil and pile elements[§], a direct node-to-node contact between the two cannot be established (Kolay 2009). For this, a set of dummy nodes possessing the same number of degreees of freedom need to be introduced between the soil and pile nodes. These dummy nodes were constrained to possess the same motion as that of the corresponding soil node in the horizontal and vertical directions. Further, in order to eatablish the soil-pile

[§]At each node, the soil elements used in the present study possess 2 degrees of freedom whereas the beam column elements, used for modelling the pile foundations, possess 3 degrees of freedom.

interaction mechanism, the dummy nodes were connected to the corresponding pile nodes with the help of zero-length rigid link elements. The rigid links ensure a complete transfer of the motion developed at the soil nodes onto the pile nodes and vice-versa. It is worth mentioning that the soil nodes, corresponding structure nodes, and the corresponding dummy nodes are at the same physical location. A schematic represetntation of the same is shown in Figure 3.8.

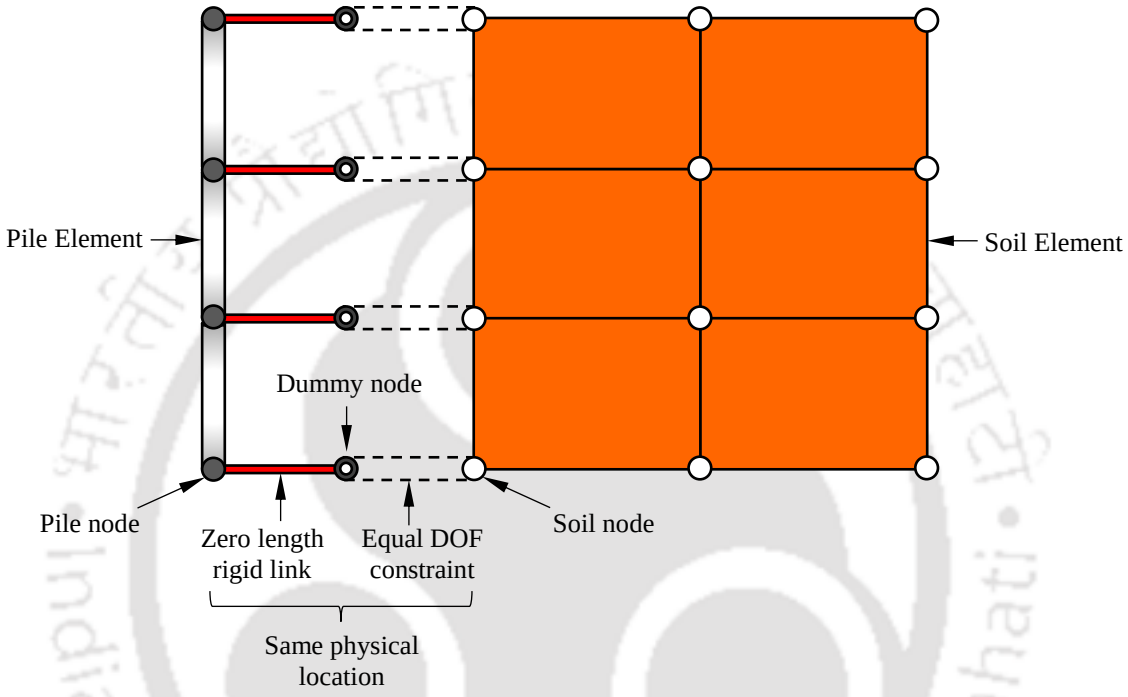

Figure 3.8 Schematic representation of the Perfectly Bonded Interface approach used for the modelling of the pile-soil interface.

3.3.2.3 Idealization for Inelastic Structural Behaviour

Depending on the expected structural behaviour in a study, the structural modelling may involve idealization either for only elastic behaviour or for both elastic and inelastic behaviours. For example, to obtain the natural period of a structure-foundation-soil system, the elastic behaviour of the entire system should be ensured. However, for actual performance evaluation of the same system, appropriate modelling should be implemented to capture inelastic behaviour. Additionally, within the members of a structural system (beams, columns, shear wall, and piles), the inelastic behaviour tends to localize in certain regions. This feature calls for appropriate modelling in those limited regions where inelasticity is most likely to be mobilized. In the present study, linear elastic sectional properties were used for the segments of the study wherein the structural system is required to behave elastically (discussed in Chapters 4 and 5). For those segments where the

structural system is required to behave inelastically (discussed in Chapters 6 and 7), fibre sections are assigned with nonlinear material properties for concrete and rebar (discussed in the previous sections). For the members in the superstructure (beam, column, and shear wall), the characteristics for possible inelastic behaviour are assigned in the 'plastic hinge region', that is predefined at the two ends of each element by means of a parameter called 'plastic hinge length'. Depending on the cross-sectional properties, the plastic hinge length in the beams and the columns is determined using the relationship proposed by Paulay and Priestley (1992) as shown in Eq. 3.13.

$$l_p = 0.08l + 0.022 d_b f_y \tag{3.13}$$

In Eq. 3.13, l_p is the plastic hinge length (in m), l is the distance between the point of the maximum moment to the point of zero moment in m, d_b is the diameter of longitudinal reinforcing bar in m, and f_y is the yield stress of the reinforcement in MPa. Similarly, the plastic hinge length in the shear wall is determined using the relationship proposed by Kazaz (2010) as,

$$L_p = 0.27 L_w \left(1 - \frac{P}{A_w f_c^{'}}\right)\left(1 - \frac{f_y \rho_{sh}}{f_c^{'}}\right)\left(\frac{M/V}{L_w}\right) \tag{3.14}$$

where L_p is the plastic hinge length of the shear wall, L_w is the length of the shear wall, P/A_w $f_c^{'}$ is the axial force ratio (ratio of the axial load P to the load resisted by the concrete in the shear wall cross-sectional area, A_w), ρ_{sh} is the horizontal reinforcement ratio in the web of the shear wall and M/V is the shear span. For piles, the nonlinearity is distributed over the entire length, since the closed-form equation of plastic hinge length in piles is not presently available in the literature.

3.4 SEISMIC INPUT MOTION

In the present study, as already mentioned, the soil is assumed to be underlain by bedrock, which is significantly stiffer than the overlying soil layers. This ensures that the bedrock mass behaves as an infinite linear elastic half-space. The seismic excitation to the SSI system is applied in the form of equivalent nodal shear forces at the bedrock level. The forces, at the bedrock level, are estimated based on one-dimensional wave propagation through homogenous, linear elastic, and undamped soil medium (Joyner and Chen, 1975).

The expression for shear forces (Zhang et al., 2008) developed at the bedrock soil interface is shown in Eq. 3.15.

$$F(x,t) = -C_s \dot{u}(x, t) + 2C_s \dot{u}_i (t + x/v_s) \tag{3.15}$$

In Eq. 3.15, $\dot{u}_i (t + x/v_s)$ is the velocity of incident motion, $\dot{u}(x, t)$ is the velocity of the soil particle motion, and C_s is the coefficient of dashpot. The first term on the right-hand side in Eq. 3.15 is the force generated by the dashpot, and the second term is the equivalent nodal shear force that is proportional to the velocity of the incident motion. The same methodology has been applied by Kolay (2009) and Mondal et al. (2012) for the analysis of bridge abutment-soil system and soil-well-pier system under seismic excitation, respectively.

3.5 STAGES OF ANALYSIS

As stated in the previous section, pressure-dependent constitutive model has been used to simulate the behaviour of the soil. According to this model, to develop the requisite strength and mobilization of proper stress state within the soil, it is essential to introduce lateral confining action. However, the assignment of the L-K boundaries does not provide any confining action as they do not provide any restraint. Therefore, to develop a proper state of stress within the soil, 'stage-wise gravity analysis' is carried out prior to conducting the dynamic analysis. This ensures that the soil media is subjected to the requisite confining action even with the imposition of L-K boundaries. The procedure for the staged analysis has been outlined by Zhang et al. (2003) and adopted by Kolay et al. (2013) with some modifications. For the sake of completeness, the analysis steps are described as follows and is pictorially shown in Figure 3.9.

Stage 1: Elastic gravity analysis

The SSI model, consisting of the soil-pile-structure system, is developed with the base restrained in both the horizontal and vertical directions. The vertical boundaries are restrained only in the horizontal direction and are kept free to displace in the vertical direction. The material model of soil is considered as elastic and the gravity loads in the structure and soil are applied. A single-step analysis is performed to achieve equilibrium.

Stage 2: Plastic gravity analysis

The material constitutive model is changed to plastic, and the SSI system is brought into equilibrium through multiple iteration steps. Once the equilibrium is achieved, the reactions on the horizontal and vertical boundaries are recorded.

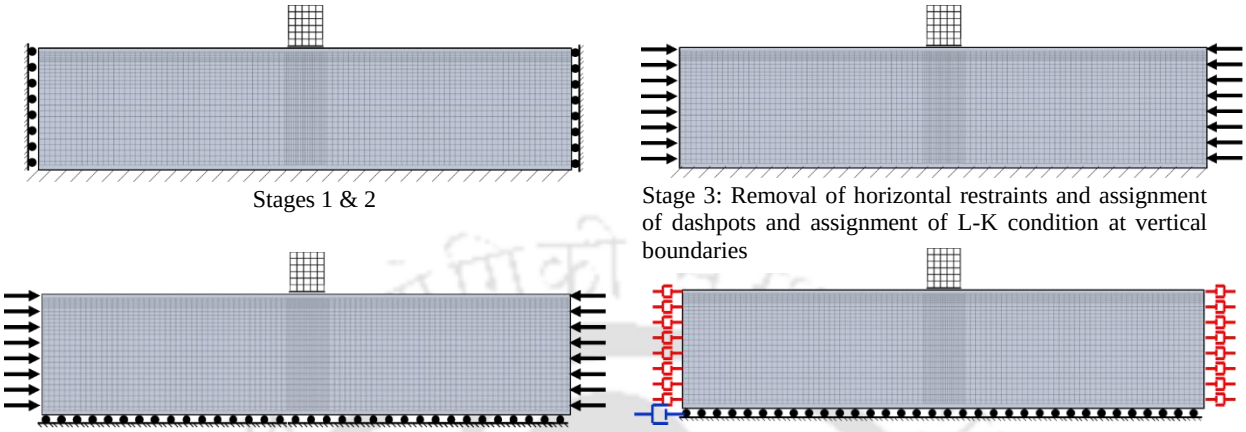

Figure 3.9 Staged Gravity analysis of the soil-pile-structure system.

Stage 3: Assignment of L-K boundary condition to the vertical boundaries

For the vertical (or, the far lateral) boundaries of the soil domain, the restraint along the horizontal direction is removed, and the reactions obtained in the previous stage are applied. The model is brought into equilibrium through iterations. Subsequently, L-K boundaries are assigned along with both horizontal and vertical directions.

Stage 4: Assignment of L-K boundary condition to the horizontal boundary

For the base boundary of the SSI model, the restraint along the horizontal direction is removed, and the reactions obtained in Stage 2 are applied. The model is brought into equilibrium iteratively, and the L-K boundaries are assigned in the horizontal direction.

Stage 5: Dynamic analysis

Once the boundary conditions have been successfully applied, the SSI model is subjected to seismic excitation that is applied as equivalent nodal shear forces at the base of the FE model. The equation of motion of the SSI model is obtained as shown in Eq. 3.16,

$$[\mathrm{M}]\{\ddot{u}(t)\} + [\mathrm{C}]\{\dot{u}(t)\} + [\mathrm{K}]\{u(t)\} = \{\mathrm{F}(t)\} + \{\mathrm{F}_v\} \tag{3.16}$$

where [*M*], [C] and [K] are the global mass, damping, and stiffness matrices of the SSI system respectively; $\{\ddot{u}\}$, $\{\dot{u}\}$ and $\{u\}$ represent the nodal acceleration, velocity, and displacement vectors respectively; $\{\mathrm{F}(t)\}$ represents the input nodal shear force vector, and

$\{F_v\}$ is the force vector assigned at the viscous boundaries during the staged gravity analysis. For the present study, Newmark's method for time-step integration has been adopted, for which the values of γ and β are considered 0.6 and 0.3025, respectively. The initial condition of the SSI model is considered to be 'at rest'.

3.6 Discretization, Meshing and Convergence Study

In the finite element method, proper meshing of the numerical model is of utmost importance before arriving at rigorous inferences from the study. In SSI studies, the size of the soil elements used for discretization affects the accuracy of the response of various parameters. As the softest soil is expected to be the most critical case for studying the influence of meshing on the response, a soil column located on a virgin free field (Figure 3.10), with properties corresponding to the softest soil, is considered. The acceleration response of the soil column, over the depth, is obtained corresponding to an input time-history of a Ricker wavelet. The acceleration function of a Ricker wavelet is shown in Eq. 3.17.

$$f(t) = U_0(2a^2 - 1)e^{-a^2} \tag{3.17}$$

In Eq. 3.17 U_0 is the amplitude of the Ricker wavelet; $a = \pi f_0 (t - t_s)$ wherein f_0 is the characteristic frequency of the signal, t is time in seconds, and t_s is the time of the peak position of the signal. The considered Ricker wavelet attains peak acceleration at a time instant of 0.5 seconds. The characteristic frequency of the Ricker wavelet is selected to be 3.9 Hz. The time history of the generated input is shown in Figure 3.11.

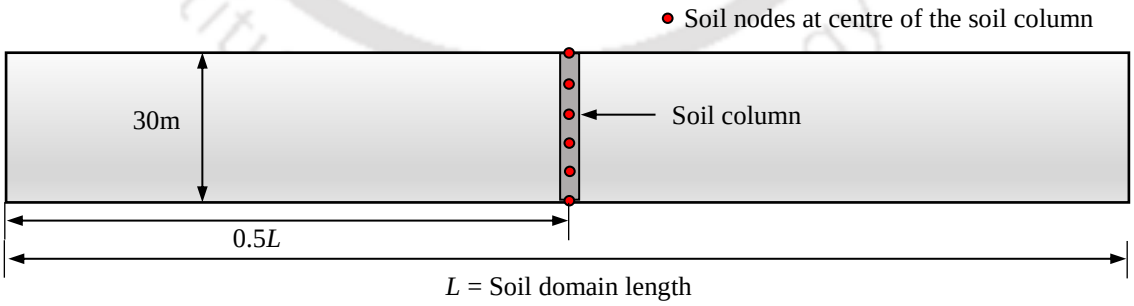

Figure 3.10 Location of soil nodes and the column in the virgin soil domain.

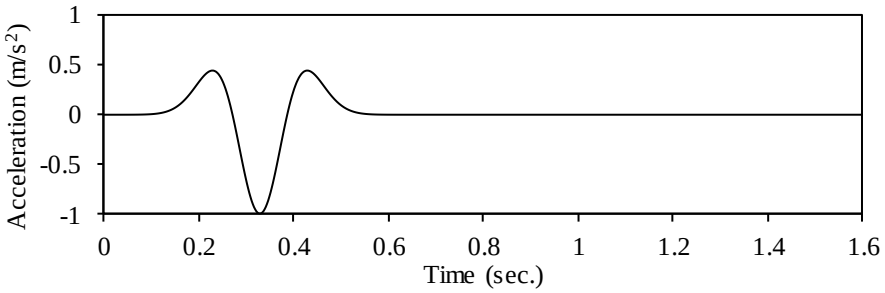

Figure 3.11 Acceleration time history of the adopted Ricker wavelet.

In the present study, an optimum biased meshing of the soil domain has been adopted, wherein the size of the mesh elements is varied in the vertical and horizontal directions, to ensure accurate response with minimized computational effort. The vertical size of the mesh elements is estimated based on the recommendation of Kuhlemeyer and Lysmer (1973) as shown in Eq. 3.18,

$$l_{\max} = 0.125 f_{\max}^{-1} (G\rho^{-1})^{0.5} \tag{3.18}$$

where, $l_{\max}$ is the maximum size of the soil elements; $f_{\max}$ is the value of maximum frequency of input motion (typically considered as 15 Hz); G is the shear modulus of the soil specified at a particular soil depth that corresponds to a mean effective confining pressure at the specified depth, and ρ is the mass density of the soil.

The intention of Eq. 3.18 is to ensure the transmission of the shear wave with the highest possible frequency, from the bedrock to the surface, in its direction of propagation. This calls for a biased mesh discretization scheme where the size of the mesh varies from finer at the surface to coarse at larger depths (specifically, since G is considered to increase with depth). Horizontally, it is understood that finer discretization of the mesh is desirable in the vicinity of the structure and the size of the elements can be increased gradually towards the far lateral boundaries.

Figure 3.12a shows an example of the optimized meshing adopted in the present study. The smallest and the largest element sizes adopted for the study are 0.375 m × 0.5 m and 1.5 m × 1.5 m, respectively. The aspect ratio of the soil elements is restricted to a maximum value of 4, which is well within the safe upper limit from modelling aspects (Reddy, 1993). The acceleration response in the soil column with the adopted meshing is determined and is compared with that obtained from the uniformly discretized mesh of different sizes (Figure 3.12b). It can be observed that the acceleration response (across the

depth of the soil domain at an interval of 5 m) obtained from the adopted meshing is very close to that provided by a fine uniform meshing scheme (mesh size of 0.75 m). Hence, it can be said that the adopted optimized meshing scheme provides satisfactory results, and the same can be adopted for further analysis.

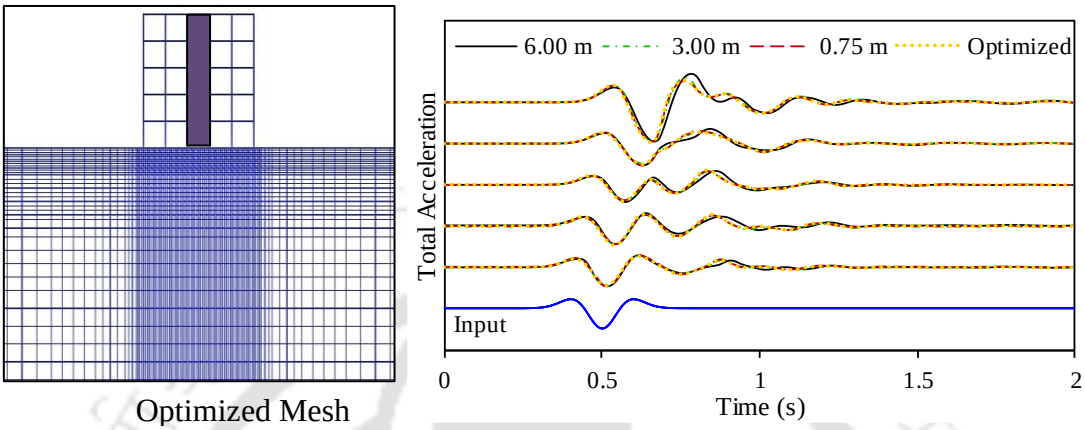

Figure 3.12 Mesh discretization: (a) optimized meshing adopted in the study, and (b) convergence study for the performance of the optimized mesh in comparison to the uniform mesh discretizations.

3.6.1 Capturing Spuriousness

For very small-sized elements, it is possible for the numerical solution to exhibit spuriousness during the nonlinear analysis of soil. Figure 3.13 shows the effect of variation of mesh element size on the acceleration response of soil nodes in the selected soil column with linear elastic and nonlinear characteristics. For soil with linear elastic characteristics (Figure 3.13a), the reduction in mesh element size from 6 m to 3 m produces some change in the response, while on further reducing the mesh size to 1.5 m, no change in the response is observed. For soils with nonlinear properties (Figure 3.13b), with a reduction in mesh size, spurious oscillations tend to increase in the response due to the combined effect of nonlinear soil behaviour and excitation of higher frequency modes. This has also been observed and reported by Hilber et al. (1977). To capture these oscillations, numerical damping can be incorporated using the HHT-α method (Hilber et al., 1977) or by using a value of $\gamma > 0.5$ in the Newmark method for time step integration. However, even after the incorporation of the numerical damping, the spurious oscillations may not necessarily be captured (as observed in the present case).

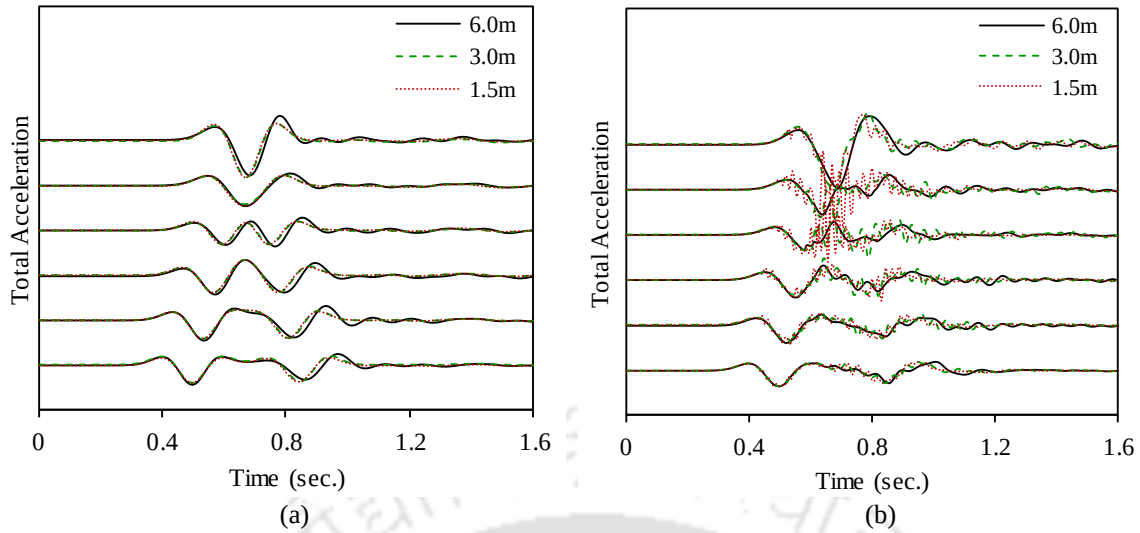

Figure 3.13 Effect of varying mesh sizes on nodal acceleration response at the center of the soil domain for soil with (a) linear elastic, and (b) nonlinear properties.

In the present study, a small amount (2%) of Rayleigh damping has been incorporated for capturing the spurious oscillations generated in the soil response. Rayleigh damping requires the specification of damping ratios corresponding to two modes In the present study, the first two modes are considered for the stated purpose. Based on the damping ratios and the frequency of the modes, the coefficients a_0 and a_1 are estimated (Chopra, 2011) for forming the damping matrix as shown in Eq. 3.19.

$$C = a_0[\mathrm{M}] + a_1[\mathrm{K}] \tag{3.19}$$

In Eq. 3.19, [M] is the mass matrix, and [K] is the stiffness matrix of the system. Assuming ω_i and ω_j to be the natural frequencies corresponding to two modes '*i*' and '*j*'. Then, the modal damping ratios for the two modes, ζ_i, and ζ_j are related to the coefficients a_0 and a_1 as shown in Eqs. 3.20 and 3.21.

$$a_0 = 2\zeta_i\omega_i \tag{3.20}$$

$$a_1 = 2\zeta_j / \omega_j \tag{3.21}$$

The fundamental frequencies of the soil domain can be obtained as (Kramer, 1996)

$$\omega_n = v_s\pi(0.5+n)/H \tag{3.22}$$

where v_s is the average shear wave velocity of the soil deposit, ω_n is the angular frequency of the mode number n, and H is the depth of the soil domain. Figure 3.14 shows the acceleration response of the soil nodes within the soil column with incorporated Rayleigh damping. It can be observed that Rayleigh damping is very much effective in capturing the spurious oscillations in the response of the soil with nonlinear behaviour (Figure 3.14b) even when the size of the elements is reduced to sufficiently low values.

Additionally, from Figure 3.13, it can be observed that the proposition made by Kuhlemeyer and Lysmer (1973) provides adequate accuracy in the results. Moreover, once the condition for the maximum mesh size is satisfied, there is no further requirement of refining the mesh, and the coarsest mesh is sufficient to capture the features of wave propagation through the medium.

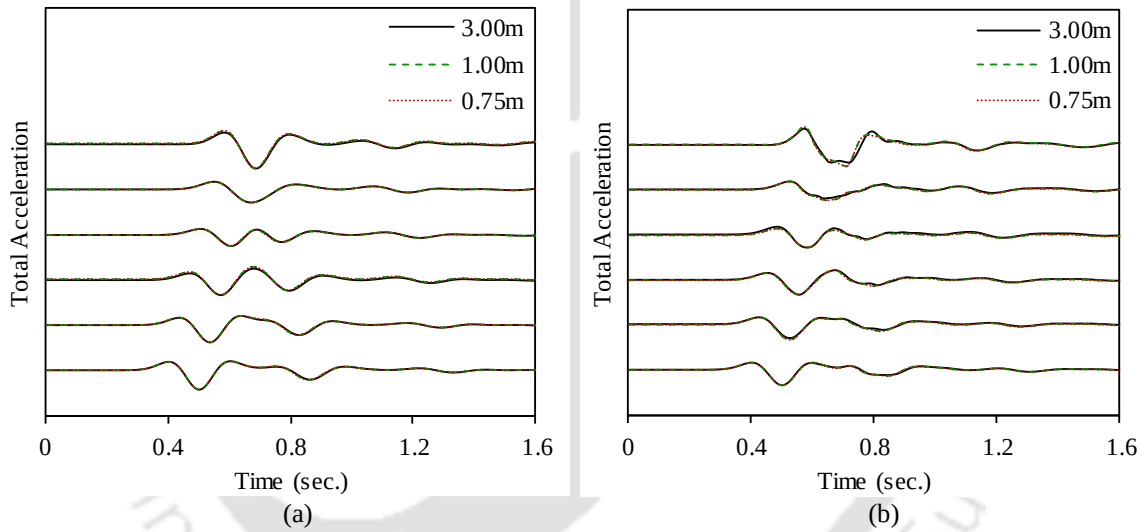

Figure 3.14 Effect of Rayleigh damping and mesh size on the acceleration response of soil column with (a) linear elastic, and (b) nonlinear properties.

3.7 VALIDATION OF THE NUMERICAL RESPONSE

For the simulation of reliable and accurate response in any numerical study, a validation study needs to be carried out prior to conducting rigorous analyses. As already mentioned, before conducting a dynamic analysis of the SSI model, it is a prerequisite to carry out static gravity analysis in a staged manner. In order to validate the dynamic soil response with the incorporated boundary conditions, the results of the developed numerical model are validated with those available in the literature. In the present study, a sine wavelet is provided as an input at the base of the soil domain. The corresponding acceleration response is obtained across the depth of a soil column located centrally in the soil domain, and the results are compared with those in existing literature (Figure 3.15a). Close agreement of the

results indicates the successful application of the different stages of the analyses, as described in the previous section. The boundary conditions applied to the soil domain, are also automatically validated. Thus, the adopted numerical modelling approach for soil can be further used for rigorous dynamic analysis.

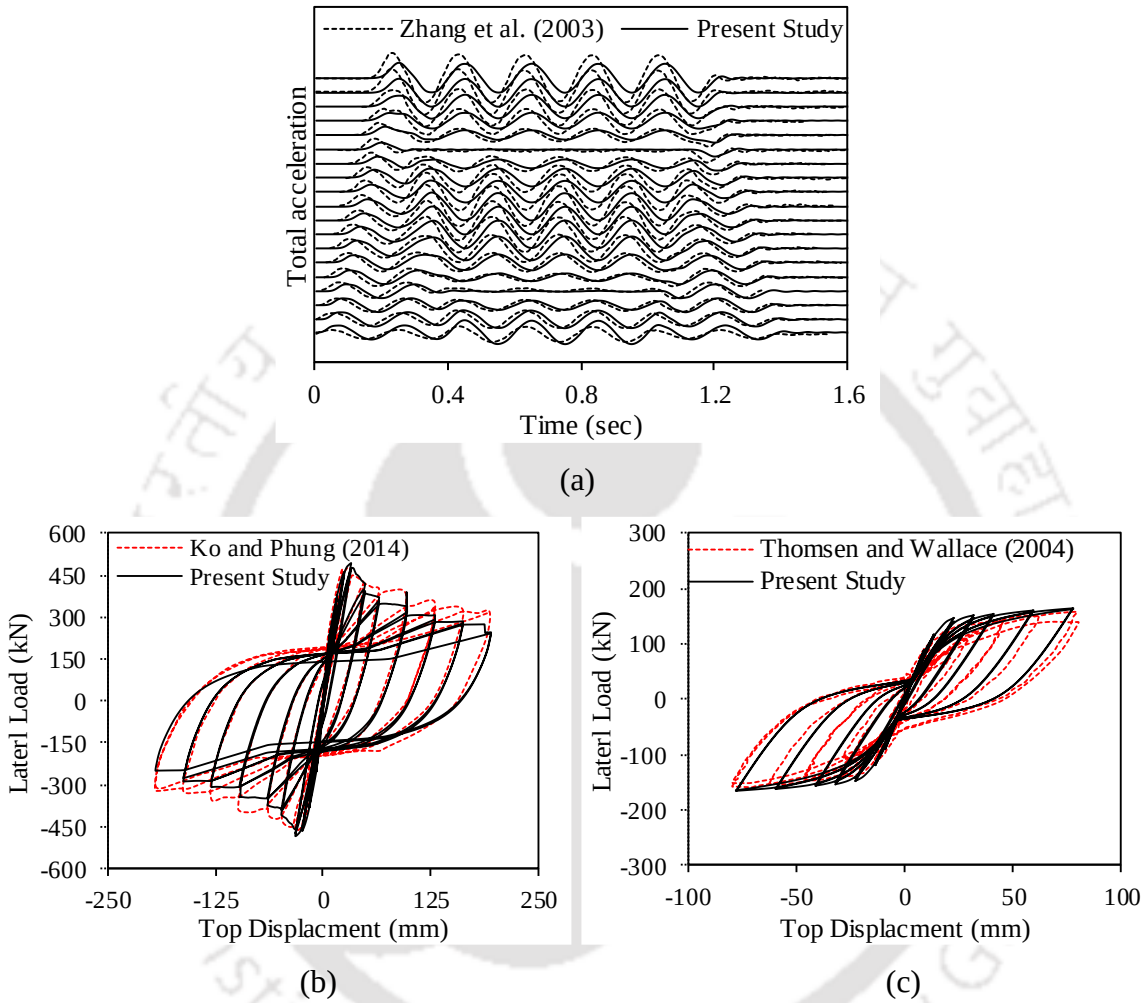

Figure 3.15 Validation of numerical response: (a) soil column response to sine wavelet; nonlinear cyclic behaviour of (b) an isolated column, and (c) isolated slender shear wall (using EFM).

Apart from the soil response, it is also necessary to affirm the accuracy and reliability of the nonlinear behaviour of the structural members using the material models and elements adopted in the present study. For this purpose, the adopted modelling approach is validated using the nonlinear cyclic behaviours of an isolated column and an isolated shear wall. Displacement-controlled cyclic pushover analysis of a cantilever column of 3.25 m height (Ko and Phung, 2014) has been carried out using the program OpenSEES and the results are validated with those of the original study (Figure 3.15b). The FE modelling approach of the shear wall, as stated earlier, is validated by numerical simulation of a

slender shear wall with a height of 3.65 m. Displacement-controlled cyclic pushover tests on a similar wall specimen were carried out earlier by Thomsen and Wallace (2004). For the purpose of validation, the modelling technique prescribed by Tang and Zhang (2011) is followed. From Fig. 3.14c, it can be observed that the numerical behaviour of the tested shear wall is satisfactorily simulated. Based on the comparatives, it can be inferred that the adopted modelling strategy can be applied for further analysis of the building frame with shear walls. The details of the members and loading can be found in the respective studies and have not been reproduced here for the sake of brevity.

3.8 SUMMARY

In this chapter, the modelling aspects utilized for the present study are discussed in detail. The finite element modelling of the SSI system has been outlined with reference to the material and geometric modelling. The method of seismic input and the staged analysis procedure have been described in detail. A small study pertaining to the most critical soil characteristics has been carried out to arrive at an optimized meshing scheme. Further, the effect of incorporation of a small amount of Rayleigh damping has been shown to eliminate spurious oscillations. Finally, the numerical response of the soil domain and the structural elements have been validated with those available in the literature. The results provide the confidence for adopting the mentioned numerical modelling approach for further rigorous analysis of the SSI system.

This page has been intentionally left blank.

Chapter 4
OPTIMUM LATERAL EXTENT OF SOIL DOMAIN FOR DYNAMIC SSI OF RC FRAMED STRUCTURES

CONTENTS

4.1 OVERVIEW

Nonlinear dynamic soil-structure interaction analysis, using the finite element method, requires the use of a single-step direct method of analysis. The advantage of this method is that a time-domain approach is followed, and hence the nonlinearity of the soil or the structure can be directly incorporated (Ghosh and Wilson, 1969). This method necessitates modelling of the entire soil continuum together with the structural system. Theoretically, considering an infinite (as large as possible) lateral extent of soil domain would be ideal as it produces a response free from the boundary effects, yet accounting for the radiation damping. However, such a choice leads to heavy computational expense and is not practically appreciable from the finite element point of view. To overcome this difficulty, it is a common practice to model the SSI system with a finite length of soil domain, while using radiation boundaries at the lateral extents. However, even with the incorporation of these boundaries, the estimation of model response may be inaccurate if the length of the domain is not optimally sufficient. Additionally, the requisite extent of the horizontal soil domain may vary for different soil conditions, the intensity of earthquake shaking, and

widths of the supported structural systems. Therefore, it is important to justifiably define the lateral extent of the soil domain (also referred to as 'soil domain length' in the present study) to be used for dynamic SSI analysis that would ensure computational efficiency without loss in accuracy of the system response. In the present chapter, an approach for deciding on an optimal horizontal extent of soil domain to be used for dynamic SSI analysis is outlined. Based on the study, a simple generalized set of relationships has been prescribed for the horizontal extent of soil domain being expressed as a function of structural (or foundation) width and the PGA of the strong motion. The developed relationships are used for developing the numerical model to be used in further SSI studies.

4.2 LATERAL EXTENT OF SOIL DOMAIN CONSIDERED BY PAST RESEARCHERS

Although there have been a few recommendations by past researchers on the soil domain length to be used for dynamic SSI studies, they are primarily based on simple SSI models analyzed as a single degree of freedom systems (SDOF) and with linear soil characteristics. Moreover, most studies focused on shallow or mat foundation, and such recommendations for structures supported on pile foundations are not readily available. In the available recommendations, foundation/structural width has been considered as the prime factor for estimating the lateral extent of the soil domain. Ghosh and Wilson (1969) recommended a horizontal extent of soil domain as $4W$ (W is the base width of the foundation or the structural width). Roesset and Ettouney (1977) recommended a domain length of $5W$ for soils with high internal damping and $10W$ to $20W$ for soils with low internal damping. Matinmanesh and Asheghabadi (2011) used a domain length of $60W$, whereas that used by Pala et al. (2008) was $155W$. Table 4.1 shows the values of the normalized lateral extent of the soil domain used in the more recent studies as a function of structural or foundation width (W). It can be observed that there exists an absence of concordance concerning the lateral extent of the soil domain to be considered for conducting numerical dynamic SSI studies. Hence, the lateral extents adopted in the past studies may not always be conveniently utilized depending on the governing factors of the problem being analyzed. In cases, the adoption of the lateral extents, proposed by the past researchers that have proved to be useful in the purview of their respective studies, may provide grossly inaccurate results owing to the significantly different modeling factors and requirements of the SSI problem being handled. The adoption of many of the previous recommendations becomes more restricted for framed structures supported on pile group foundations. Moreover, it would

not be prudent enough to adopt an extremely large extent of the soil to satisfy accuracy while significantly compromising on computational efficiency.

Table 4.1 Lateral extent of soil domain used in past studies

Past studies	W (m)	H (m)	L/W	Remarks
Lu et al. (2003)	14.1	-	10.00	PF/EL/VB/FE
Pala et al. (2008)	9.0	25-100	155.00	SF/L/VB/FE
Rayhani and El-Naggar (2008)	5.5	-	5.00	SF/NL/EB/FD
Matinmanesh and Asheghabadi (2011)	10.0	50	60.00	SF/L/SD/FE
Tabatabaiefar and Massumi (2010)	8.0	-	7.50	SF/L/EB/FE
	12.0	-	11.25	SF/L/EB/FE
Tabatabaiefar et al. (2013)	12.0	-	5.00	SF/NL/VB/FD
Nateghi and Rezaei-Tabrizi (2013)	40.0	-	10.00	SF/L/EB/FE
Saez et al. (2013)	6.0	30	6.67	SF/NL/O/FE
	10.0	-	7.00	SF/NL/O/FE
Hokmabadi et al. (2014)	15.0	30	4.00	SF&PF/NL/VB/FD
Nguyen et al. (2016)	15.0	30	9.33	SF/EL/IE/FE
Ghandil and Behnamfar (2017)	20.0	45	4.00	PF/EL/VB/FE

Note: remarks provide additional information about the study and abbreviations used are given under.
General: W is foundation/structural width; H is the depth of soil; L/W is the normalized soil domain length; L is the length of horizontal extent of soil domain.
Foundation type: SF = shallow foundation; PF = pile foundation.
Soil characteristics: L = linear; EL = equivalent linear; NL = nonlinear;
Boundary system: EB = elementary; VB = viscous; SB = spring-dashpot; IE = infinite elements; O = others.
Analysis formulation: FE = finite element; FD = finite difference

4.3 Estimating the Lateral Extent of the Soil Domain

Standard definitions of domain extent that are available for static cases cannot be succinctly used for dynamic or seismic loading as the extent would be substantially influenced by structural width, type of soil, and its nonlinear characteristics, as well as the intensity of shaking. A simplistic approach to determine the horizontal extents of the soil domain, based on stress or displacement contours, is helpful only for static cases. For dynamic cases, the stress contours change at every time step of the applied earthquake motion. If an analysis involves multiple varying parameters (such as several structural configurations, soil types, shaking intensities), then the determination of an appropriate soil domain length for each case proves to be a cumbersome task. To overcome this problem, a fair judgement is needed to be made based on some study that would provide the necessary confidence on the adopted lateral extent of the soil domain. In this regard, in the present chapter, a numerical study is undertaken to arrive at an appropriate horizontal extent of the soil domain for various

structure-soil-loading conditions, which is reported in the present chapter and further utilized for rigorous studies to be reported in the succeeding part of the thesis.

4.3.1 Methodology

As already highlighted, structural/foundation width (W) is a prime factor governing the lateral extent of soil domain (L) and can be measured in terms of the normalized length of soil domain (L/W). Wolf (1986) suggested for an increment in the soil domain length by placing the artificial boundary farther away from the structure to improve the accuracy. Therefore, it can be said that the results corresponding to a very large lateral extent would provide accurate results as the influence of the boundaries would be the least. However, a random selection of a very large lateral extent may prove to be computationally uneconomical. In the present study, the influence of the variation of the soil domain length on the SSI response of RC framed structure is studied. For all practical engineering purposes, a particular length of soil domain can be identified, which would provide sufficiently accurate results and simultaneously prove to be computationally economical. This normalized length is termed as the 'optimum normalized length of soil domain', and is denoted by Ω. To account for the influence of various factors such as structural width, soil type, and shaking intensity, parametric variations have been conducted. Based on the observations, generalized relationships for the optimum lateral extent of soil domain have been proposed. These relationships are useful for deciding upon an optimum lateral extent of the soil domain for any individual scenario.

4.3.2 SSI System Considered in the Present Study

For the present study, the structure considered is a two-dimensional RC building frame supported on pile foundations. The structure-foundation system is positioned in the center of the soil domain. A representative illustration of the typical plan and elevation of the building considered is shown in Figure 4.1. The typical floor-to-floor storey heights and the bay widths are considered as 3 m. For estimating the sizes of the frame members in this study, the out-of-plane width and height of the structure are considered constant as 15 m (5 bays) and 36 m, respectively (Figure 4.1). The response of an SSI system may be different for different widths of the structure. Hence, three different configurations have been considered for the structure, by varying the number of bays in the direction of the in-plane structural width (W), rendering the total width of the structure as 15 m (5 bays), 27 m (9 bays) and 45 m (15 bays), respectively. As per the guidelines specified in IS 456 (2000), it

is mandatory to provide an expansion joint at every 45 m. For larger structural widths, this expansion joint separates the two portions of the structure, and the Structure-Soil-Structure-Interaction (SSSI) response of the two portions are to be separately analyzed. Hence, the width of the structure in the present study is limited to 45 m, which encompasses the conventional widths of the 'individually standing' structures. The out-of-plane width of each of the adopted configurations is the same. For a particular width of the structure, the SSI response may vary for different soil conditions. Therefore, each structural configuration is considered founded on three different types of soil, namely loose (S1), medium (S2), and medium dense (S3) soil. The structure is assumed to be located in Seismic Zone V (as per the seismic zoning map of India, i.e., IS 1893 Part 1 (2016). It is supported on pile foundations and has been designed with the help of relevant Indian standards (IS 13920, 2016; IS 456, 2000) after considering the gravity and lateral loading as per IS 1893 Part 1 (2016), IS 875 Part 2 (1987) and IS 2911 Part 1/Sec 1 (2010). The loading on the structure, apart from the self-weight, is shown in Figure 4.1. The modulus of elasticity of the concrete is taken to be 25 GPa.

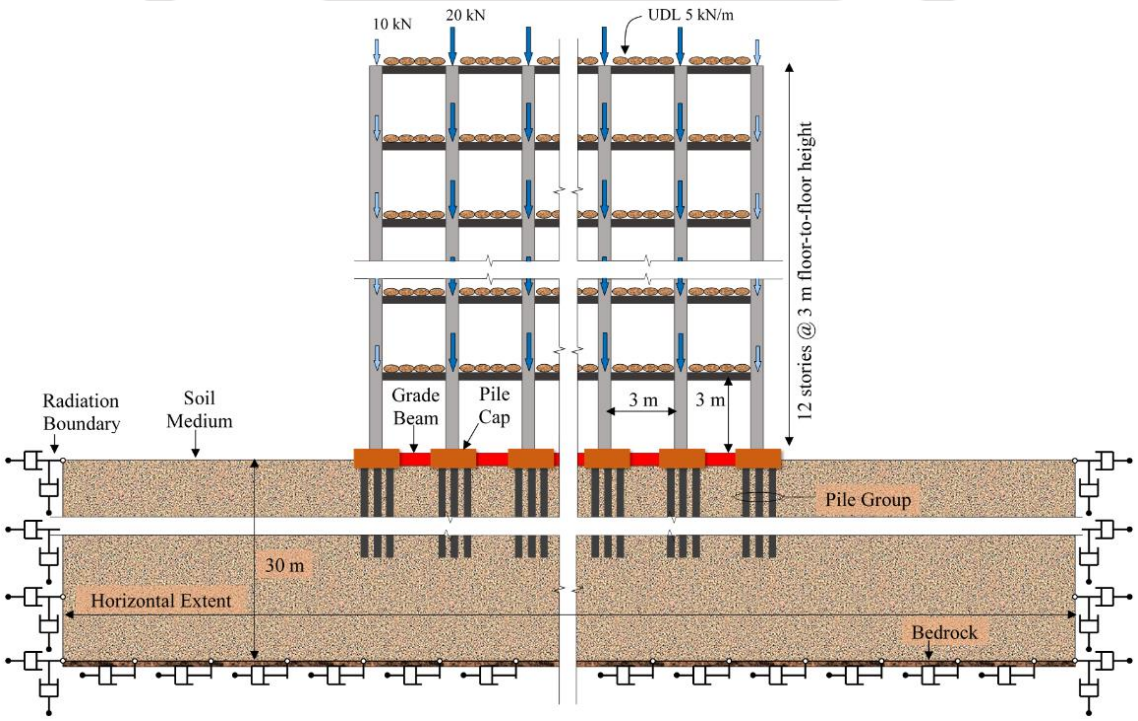

Figure 4.1 Representative illustration of the SSI model considered for the present study.

The size of the column is 500 mm × 500 mm until the sixth storey, above which the dimensions are reduced by 100 mm along both the directions. For all storey levels, the width of the beam is 250 mm, and the overall depth is 400 mm. The size of the square grade beam

is taken as 400 mm × 400 mm. The pile foundations have been designed in accordance with three different soil conditions. Distance between adjacent piles in a group is considered three times the diameter of the individual pile (i.e., $3d_p$, where d_p is the diameter of the individual pile). The stiffness of the pile group is estimated, and a single equivalent pile possessing the same stiffness as that of the pile group is modelled beneath the columns, to account for the out-of-plane stiffness provided by the pile group. This methodology has been successfully applied in the past (Zhang et al., 2008). The details of the pile groups and equivalent piles are shown in Table 4.2. The discretization of the pile has been carried out, ensuring connectivity between the pile nodes and the adjacent soil nodes.

Table 4.2 Details of the pile group

Type of soil	Dia. of individual pile (m)	Length of individual pile (m)	No. of plies in a group	Dia. of equivalent pile (m)
Loose (S1)	0.50	15	3	1.47
Medium (S2)	0.45	15	3	1.32
Medium dense (S3)	0.40	15	3	1.17

4.3.3 Seismic Input Motion

Based on the categorization provided in Uniform Building Code (1997), three ground motions (one near field motion M1, two far-field motions M2 and M3), belonging to different seismic events, have been selected for conducting the study. The corresponding accelerograms are shown in Figure 4.2a, 4.2c, and 4.2e, respectively. M1 is recorded during the 1995 Kobe earthquake at station KJMA, M2 is recorded during the 1980 Mammoth Lakes earthquake at station Long Valley Dam, and M3 is recorded during the 1994 Northridge earthquake at station Malibu-Point. The input strong motions have been taken from the PEER ground motion database (PEER Database). It can be observed that the motions are characteristically different, in particular reference to their PGA and the duration of motion. It is assumed that the motions have been recorded at the rock outcrop-level, and hence, the same motions are used as input without any scaling down by 50%, as recommended by Kramer (1996). The analyses are performed for the significant duration of each motion (as per the proposition by Trifunac and Brady, 1975), which is calculated based on the Arias Intensity (Kempton and Stewart, 2006). Arias Intensity (I_A) is a measure of the intensity of the shaking ground motion and is obtained, as shown in Eq. 4.1,

$$I_A = \frac{\pi}{2g}\int_0^T \ddot{u}_i^2(t)dt \tag{4.1}$$

where, $\ddot{u}_i$ is the acceleration of the incident motion at any time t, and g is the acceleration due to gravity. The significant duration is the time duration corresponding to 5% I_A - 95% I_A. The Arias Intensity, as well as the significant duration of the selected motions, are also shown in Figures 4.2b, 4.2d, and 4.2f, respectively.

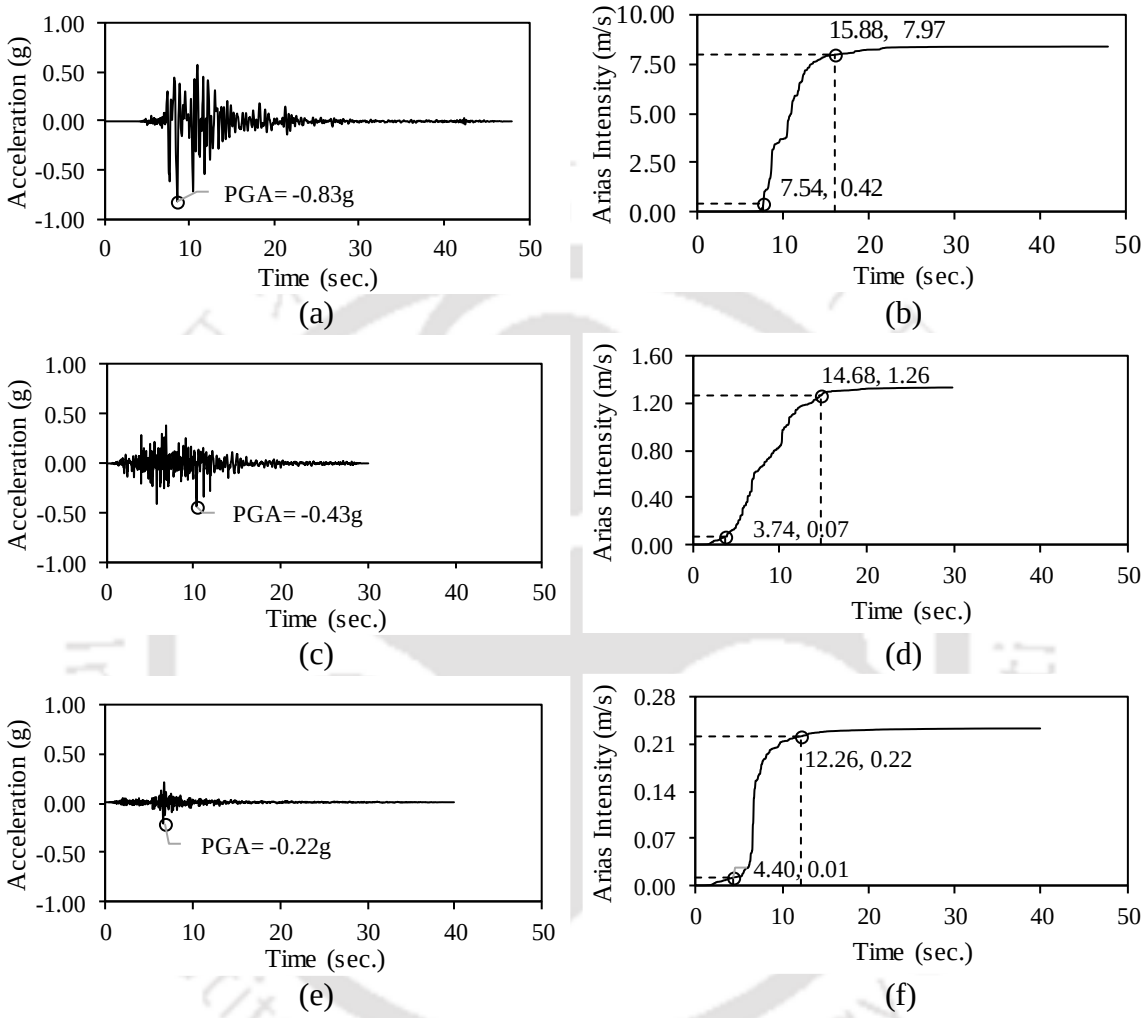

Figure 4.2 Seismic input motions: (a) accelerogram of M1, (b) Arias intensity of M1, (c) accelerogram of M2, (d) Arias intensity of M2, (e) accelerogram of M3, and (f) Arias intensity of M3.

4.3.4 Analysis Cases and Response Locations

For the estimation of optimum size of soil domain for SSI analysis, it is important to study the effect of soil domain length on response of the SSI system. Instead of estimating the response at just one specific location (as conventionally selected at the mid-length of the lateral extent), the effect should be ascertained at various locations, including the desired points of interest in the computational domain. Moreover, the response may be different for different widths of the structure and may vary with the different levels of seismic shaking.

In the present study, three structural-foundation-soil systems have been selected, which are different from each other in their in-plane widths (W), while having the same out-of-plane width. Each structural configuration is founded on three different types of soil, as described earlier. For a particular configuration, various lengths of soil domain are considered to define the SSI system. A particular SSI system is then subjected to the previously selected three different strong motions. Table 4.3 shows the various soil domain lengths, corresponding to the structural widths, and motions considered for which the SSI analysis is carried out. The values in the table indicate the computational time[2] required for completion of the analysis, thereby indicating the relative complexity of the various SSI models analyzed. The effect of soil domain length on the response of the SSI system is evaluated by monitoring the acceleration response at various locations in the system. The various nodal locations selected for this purpose are (i) soil column very near the structure (Loc. A), (ii) soil at pile location (Loc. B), (iii) pile location (Loc. C), (iv) soil column near the boundary (Loc. D). and (v) superstructure (Loc. E). For each location, multiple points have been selected for recording the response over the depth or height of the substructure or superstructure, respectively. All the mentioned locations are depicted in Figure 4.3.

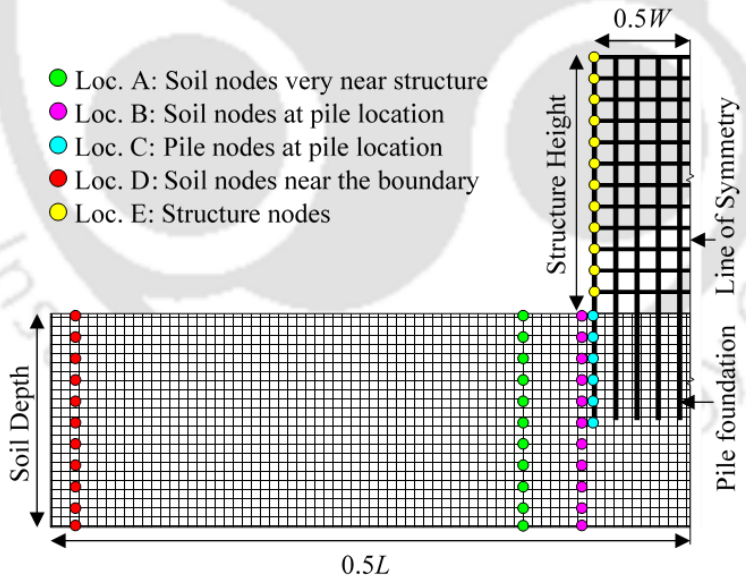

Figure 4.3 Details of the response locations chosen for monitoring the acceleration response.

[2] The system utilized for this study possesses Intel Core i7 quadcore processor having a clock speed of 3.6 GHz, and a RAM of 16 GB.

Table 4.3 Details of the analysis cases and computational time for various cases

Domain length (m)	Computational time required for analysis (in hours)								
	Motion 1 (M1)			Motion 2 (M2)			Motion 3 (M3)		
	S1	S2	S3	S1	S2	S3	S1	S2	S3
Structural width 15 m									
753	12.23	15.35	15.38	8.23	8.51	8.50	44.58	43.63	42.41
681	8.00	11.81	14.56	6.57	8.91	7.63	35.86	33.82	33.65
603	7.86	9.00	11.00	5.13	8.03	7.52	27.57	26.51	26.25
543	5.40	7.02	8.09	5.15	7.27	6.23	22.53	18.02	21.93
483	4.00	5.56	4.91	4.23	6.58	5.42	18.46	17.89	17.66
423	3.28	4.13	3.46	3.15	4.53	3.69	14.96	13.61	14.25
363	2.50	3.06	2.63	2.75	3.64	2.79	12.03	10.78	11.28
303	1.75	`2.23	1.86	1.68	2.65	2.12	9.08	8.08	8.58
243	1.42	1.55	1.47	1.18	1.18	1.18	6.26	5.75	5.95
183	0.83	1.03	0.83	0.78	0.83	0.83	4.07	3.83	3.97
153	0.75	0.75	0.75	0.55	0.55	0.55	3.19	3.07	3.05
123	0.53	0.56	0.54	0.27	0.27	0.27	2.23	2.18	2.16
93	0.46	0.48	0.47	0.23	0.23	0.23	1.58	1.52	1.45
75	0.33	0.35	0.34	0.17	0.17	0.17	1.28	1.12	1.08
63	0.21	0.23	0.22	0.12	0.12	0.12	1.03	0.96	0.87
45	0.14	0.13	0.12	0.06	0.06	0.06	0.61	0.60	0.57
33	0.05	0.05	0.05	0.03	0.03	0.03	0.41	0.41	0.36
Structural width 27 m									
1353	34.23	33.78	32.50	32.23	29.155	33.90	282.33	245.17	201.22
1215	29.68	28.96	27.68	24.16	24.56	26.36	218.90	190.46	155.42
1083	24.56	23.93	23.27	20.17	20.39	20.84	166.00	142.59	116.70
975	20.56	19.34	19.92	16.23	17.42	17.79	120.63	107.35	90.45
867	17.26	15.56	15.67	13.56	13.88	14.34	106.20	82.81	66.52
759	10.25	8.37	7.69	8.56	6.03	8.59	78.35	56.18	42.13
651	8.56	5.13	6.31	6.75	4.76	6.32	56.65	38.35	35.52
543	6.58	3.74	4.57	4.49	3.43	4.14	38.56	26.82	24.89
435	4.56	2.68	3.02	2.09	2.25	2.71	24.35	18.35	17.59
327	2.36	1.74	1.82	1.55	1.13	1.64	15.63	11.33	11.46
273	1.56	1.29	1.22	1.16	0.87	1.00	12.36	8.72	8.78
219	1.15	0.64	0.60	0.71	0.67	0.74	10.63	6.17	6.52
165	0.96	0.45	0.43	0.48	0.45	0.48	6.35	3.97	4.73
135	0.65	0.36	0.36	0.34	0.35	0.21	4.35	2.93	3.15
111	0.43	0.29	0.28	0.14	0.16	0.17	2.48	2.19	2.45
81	0.23	0.15	0.20	0.10	0.12	0.12	1.15	1.38	1.53
57	0.10	0.06	0.13	0.06	0.07	0.07	0.15	0.83	0.92
Structural width 45 m									
2253	117.5	114.98	371.28	123.18	104.24	96.10	197.26	252.97	207.12
2025	87.66	82.60	244.26	99.5	75.06	71.24	139.37	199.74	147.73
1803	65.44	58.72	145.82	73.30	48.96	51.27	100.56	152.36	109.61
1623	50.72	42.82	129.82	59.83	50.26	60.58	76.64	116.56	80.93
1443	37.34	37.08	95.40	46.89	40.71	24.92	58.35	87.25	61.66
1263	29.73	30.00	49.21	35.26	29.87	24.24	43.48	62.12	48.69
1083	23.80	23.97	49.65	15.63	18.45	19.22	30.15	41.07	35.27
903	16.84	18.17	26.78	10.90	10.04	13.70	19.33	27.14	25.65
723	10.71	11.66	20.00	5.57	7.24	9.20	12.17	16.96	15.21
543	5.78	6.33	10.26	3.16	4.78	3.90	7.72	8.66	7.23
453	2.40	3.63	7.13	2.33	3.58	2.55	5.19	5.03	5.13
363	1.75	2.34	5.23	1.41	1.53	1.99	3.13	4.22	3.28
273	1.24	1.47	3.50	0.89	1.01	1.17	2.53	2.21	2.13
225	0.98	0.89	2.97	0.59	0.80	0.88	1.21	1.14	1.17
183	0.76	0.64	2.33	0.47	0.60	0.59	0.51	0.50	0.48
135	0.51	0.43	2.02	0.30	0.25	0.36	0.30	0.31	0.29
93	0.33	0.26	1.44	0.19	0.16	0.20	0.12	0.18	0.15

Values in the table indicate the analysis duration (in hours) for various domain lengths considered.
S1: Soft Soil; S2: Med Soil; S3: Medium Dense soil

4.4 RESULTS AND DISCUSSION

The following sections discuss in detail the results of various analyses, the methodology adopted for obtaining the optimum length of the soil domain, and the various relationships proposed for practical usage.

4.4.1 Effect of Soil Domain Length on the Response of SSI System

Figures 4.4, 4.5, and 4.6 show the effect of the horizontal extent of soil domain on the acceleration response at different locations in the SSI system for structural widths W = 15 m, 27 m, and 45 m, respectively. It can be observed that there is a noticeable difference in the response of the SSI system corresponding to the smallest and the largest domain lengths. As the domain length increases, the response gradually approaches to that illustrated by the larger domain lengths. Additionally, minute scrutiny shows that the change in the response is more sensitive for smaller domain lengths, and it is otherwise for the larger domain lengths. For example, in Figure 4.4a, it can be observed that when the domain length is increased from 33 m to 63 m, there is a significant change in the response, whereas the same is comparatively lesser when the domain length is increased from 183 m to 753 m. It implies that beyond a particular length of soil domain, there is a marginal change in the response. The observation holds good for the different soil types, motions, and structural widths selected in the present study. Hence, it can be said that for all practical engineering purposes, there exists a particular length of soil domain, which would be sufficient enough to consider the obtained results as accurate, and the same is termed as the optimum lateral extent of soil domain. Identifying the optimum length of the soil domain would be helpful in significantly reducing the computational expense incurred for SSI analysis without compromising on the accuracy of the response. In this regard, a quantitative estimation of the change in the response at various locations in the SSI system has been determined, and the same has been used to define the guidelines. The methodology is described in the next section.

4.4.2 Quantification of the Change in Response and Optimum Domain Length

To quantify the change in the system response due to the increase of soil domain length, a particular foundation-structure system is analyzed with different horizontal extents of the soil domain, as highlighted in Table 4.3. Let 'a_{itL}' be the acceleration response at a particular nodal location 'i', at a given time instant 't', and for a particular length of soil domain 'L'. For example, Figure 4.4a shows the acceleration response for 'i' as Loc. B (0 m depth) at different time instants 't' of the ground motion, for various domain lengths 'L' (L = 33 m,

45 m, 63 m, 183 m, and 753 m). Similarly, the other subplots of Figures 4.4, 4.5, and 4.6 show likewise. The system response corresponding to the largest domain size can be considered as the most accurate, as it is primarily unaffected by the boundaries by virtue of a very large extent of soil domain length. For smaller domain lengths, it is observed that there is a significant influence of the nearness of the boundaries on the response. Hence, the response corresponding to the largest domain length is considered as a benchmark of accuracy. It must be pointed out that the largest domain length considered in the study is 50 times the structural width (W), which is quite large for producing a response free from the boundary effects. On the other hand, a particular length of soil domain is said to be sufficient if it is small enough to produce a response within an acceptable margin of tolerance with respect to the benchmark values ($a_{itL_{max}}$), and yet maintaining a restriction on the computational expense. The instantaneous absolute difference between the most accurate response and that obtained from a specific length of soil domain is termed as the error in the response entity, and is expressed as shown in Eq. 4.2.

$$e_{itL} = a_{itL_{\max}} - a_{itL} \tag{4.2}$$

Once the error at all the time instants is obtained, the Root Mean Square Error (*RMSE*) at a particular location 'i' and for a particular length of soil domain 'L' is estimated as shown in Eq. 4.3.

$$RMSE_{iL} = \sqrt{\frac{\sum_{t=0}^{T} e_{itL}^2}{N}} \tag{4.3}$$

In Eq. 4.3, T is the significant time duration of the ground motion, e_{itL} is the instantaneous absolute error at a particular time instant 't', location 'i' and for a particular soil domain length 'L' (evaluated as per Eq. 4.2), and N is the total number of time samples in the ground motion ($N=T/\Delta t$, Δt is the sampling interval). Subsequently, the *RMSE* at various locations (Figure 4.3) is summed up to produce the cumulative *RMSE* corresponding to a particular domain length of soil, as shown in Eq. 4.4.

$$RMSE_L = \sum RMSE_{tL} \tag{4.4}$$

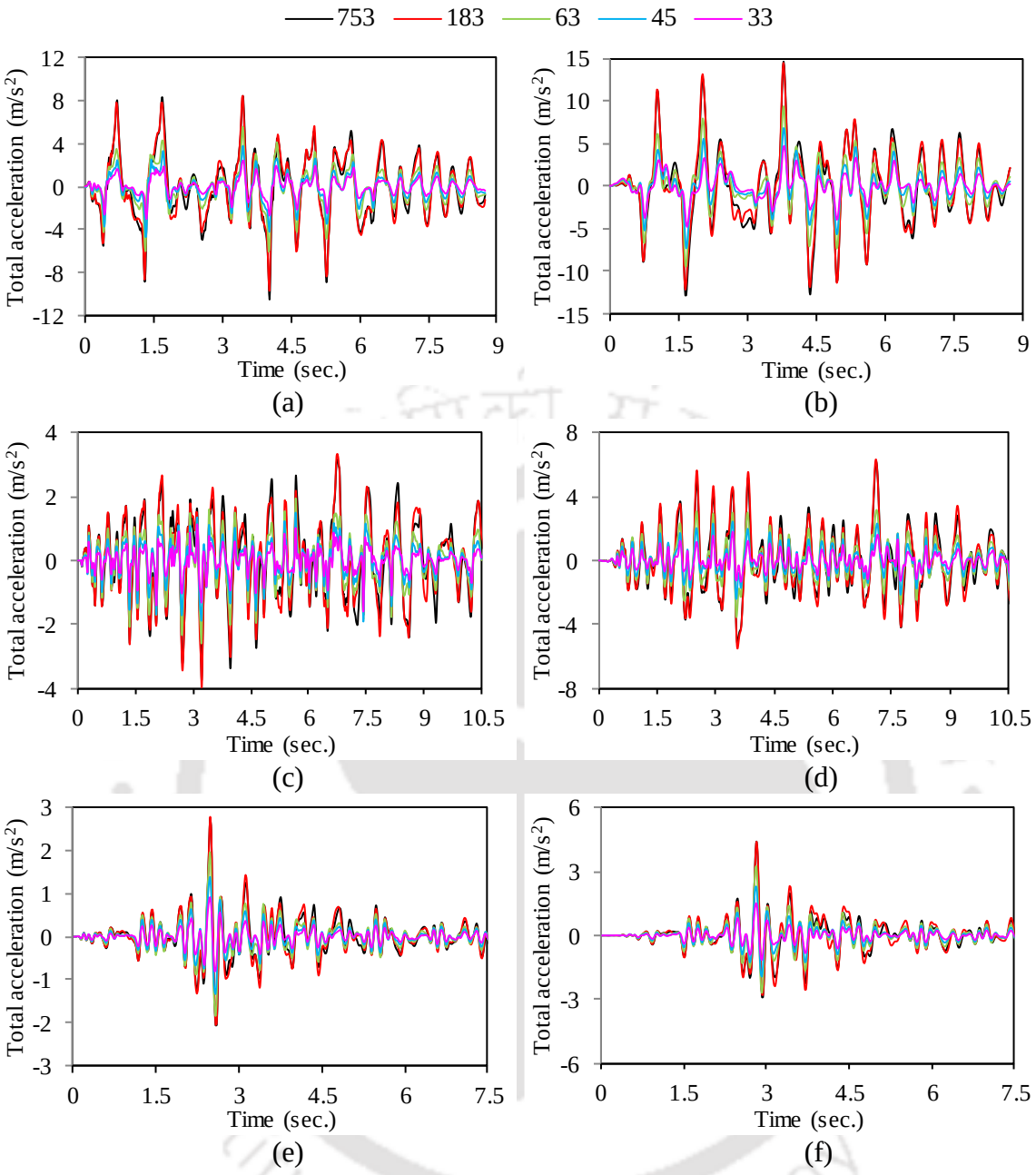

Figure 4.4 Acceleration response for B = 15 m structural width and soil TY-I at (a) Loc. B for M1, (b) Loc. E for M1, (c) Loc. B for M2, (d) Loc. E for M2, (e) Loc. B for M3, and (f) Loc. E for M3.

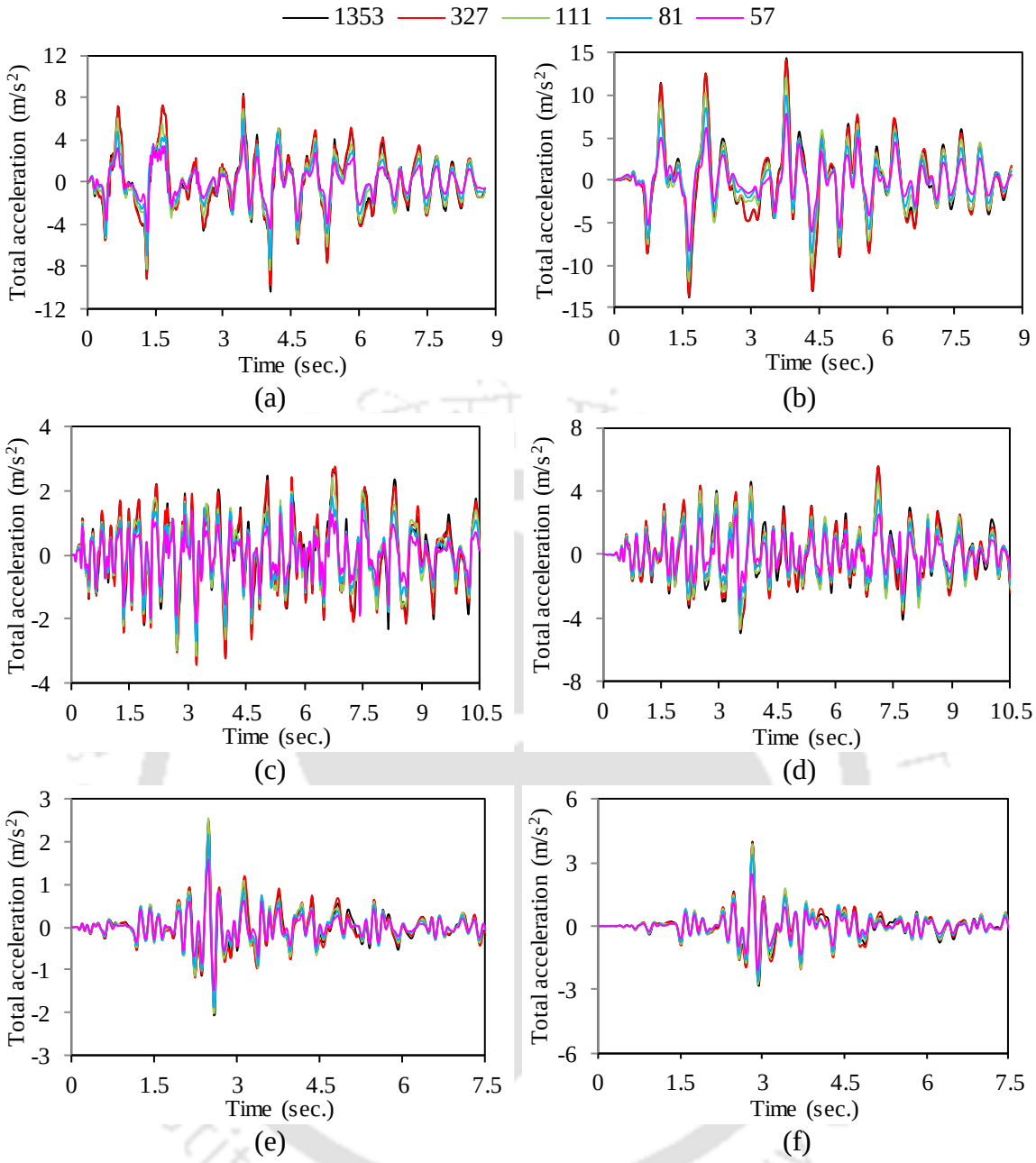

Figure 4.5 Acceleration response for B = 27 m structural width and soil TY-I at (a) Loc. B for M1, (b) Loc. E for M1, (c) Loc. B for M2, (d) Loc. E for M2, (e) Loc. B for M3, and (f) Loc. E for M3.

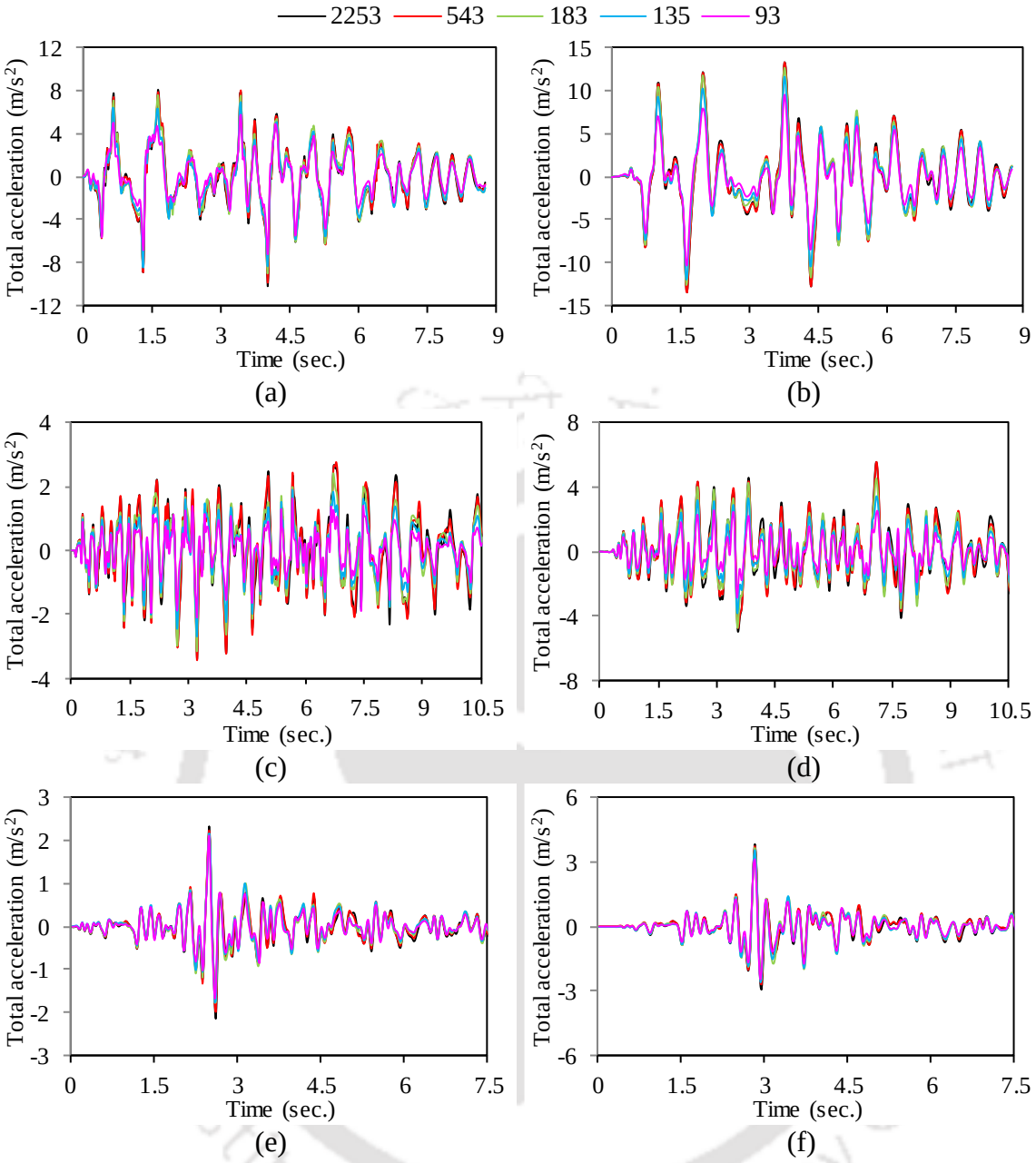

Figure 4.6 Acceleration response for B = 45 m structural width and soil TY-I at (a) Loc. B for M1, (b) Loc. E for M1, (c) Loc. B for M2, (d) Loc. E for M2, (e) Loc. B for M3, and (f) Loc. E for M3.

Figure 4.7 shows the variation of normalized *RMSE* with the normalized domain length (L/W) for SSI systems of varying structural widths (15 m, 27 m, and 45 m) resting on different soil types (S1, S2, and S3) and subjected to various strong motions (M1, M2 and, M3). The normalized *RMSE* is obtained by normalizing $RMSE_L$ by the largest value, i.e., corresponding to the smallest domain length $RMSE_{L_{min}}$, as shown in Eq. 4.5.

$$NRMSE_L = \frac{RMSE_L}{RMSE_{L_{min}}} \tag{4.5}$$

It is observed that all the curves have similar trend characteristics. The initial portion of these curves is very steep, which gradually takes the shape of horizontal asymptote with an increase in the domain length. The trend suggests that progressively increasing domain lengths have a successively lesser influence on the system response. The reduction in the change of the response with an increase in normalized domain length is indicative of the reduction in the overall error in the acceleration response of the SSI system.

4.4.3 Optimum Lateral Extent of Soil Domain for SSI Studies

Based on the qualitative trends as observed in Figure 4.7, it can be generalized that there are two distinct zones, one represented by a steep decrement of normalized *RMSE* with increasing domain length, followed by a near-asymptotic trend of normalized *RMSE*. Therefore, the *RMSE* curves can be justifiably approximated with a bilinear fit, as shown in Figure 4.8. The intersection of the two branches provides the magnitude of the normalized soil domain length beyond which the change in the system response can be considered insignificant. The normalized domain length corresponding to the optimum point is termed as the optimum normalized length of soil domain (Ω). The identified extent of Ω would be sufficient for a computationally inexpensive SSI analysis, and at the same time, help in estimation of the system response within an adequate tolerance with the benchmark responses.

In order to observe the effect of ground motion intensity (PGA), the various *RMSE* curves are shown by normalizing with respect to the curve obtained for the motion with the highest PGA level (M1) for various soil domains as shown in Eq. 4.6.

$$NRMSE_{PGA} = \frac{RMSE_L}{RMSE_{L_{min}}\big|_{PGA_{\max}}} \tag{4.6}$$

Figure 4.9 shows the various normalized *RMSE* curves along with their bilinear idealizations for different soil types, structural widths, and ground motions. The details of the idealized bilinear curves along with the estimated optimum normalized domain lengths are provided in Table 4.4.

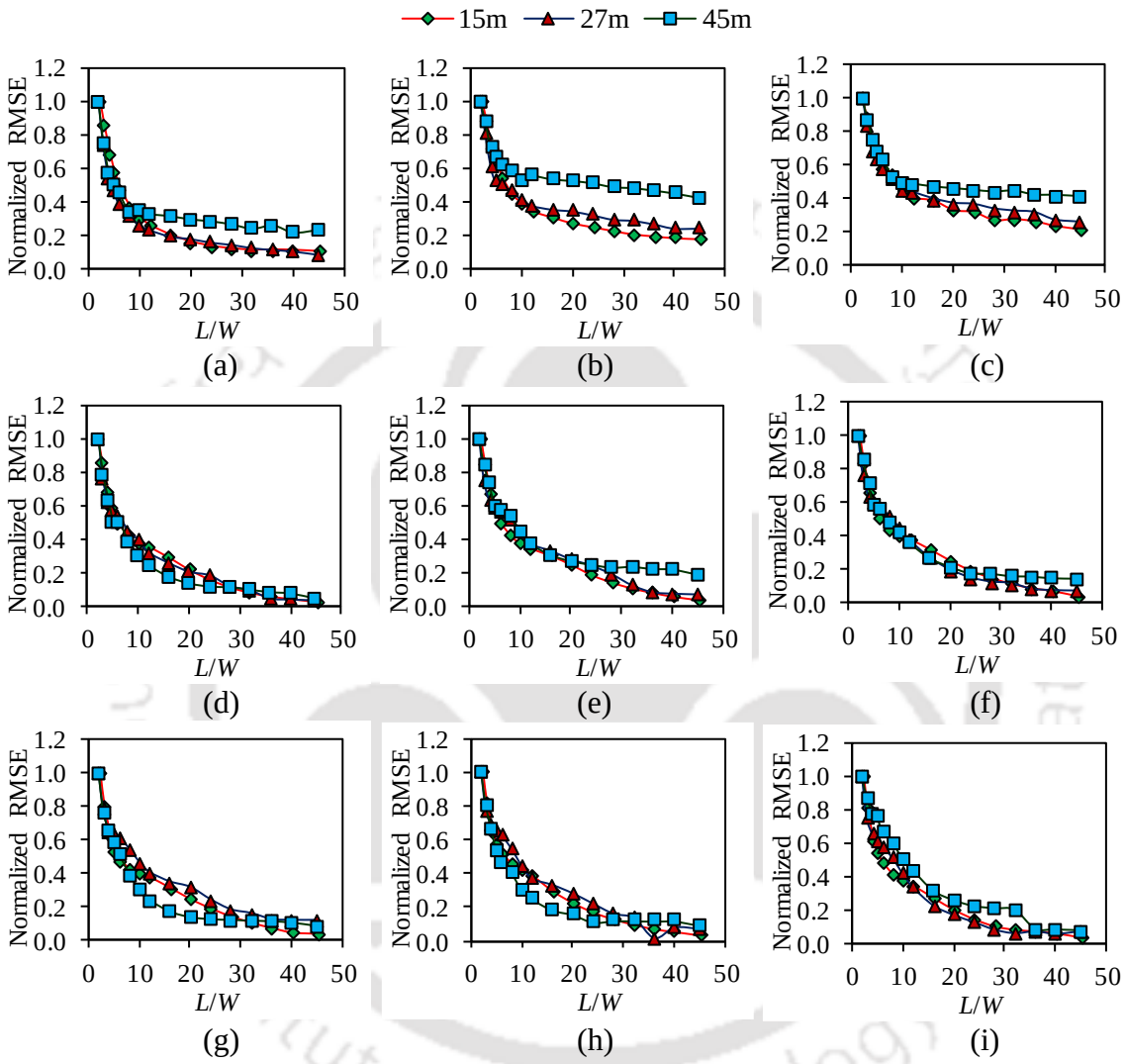

Figure 4.7 Variation of normalized RMSE with normalized domain length (*L*/*W*) for (a) soil TY-I and M1, (b) soil TY-II and M1, (c) soil TY-III and M1, (d) soil TY-I and M2, (e) soil TY-II and M2, (f) soil TY-III and M2 (g) soil TY-I and M3 (h) soil TY-II and M3, and (i) soil TY-III, M3.

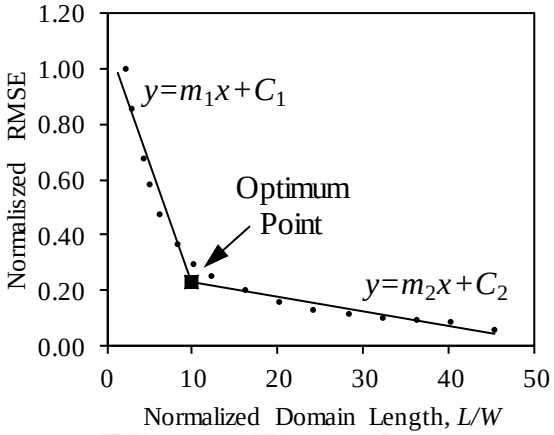

Figure 4.8 Bilinear fit for RMSE for locating the optimum point.

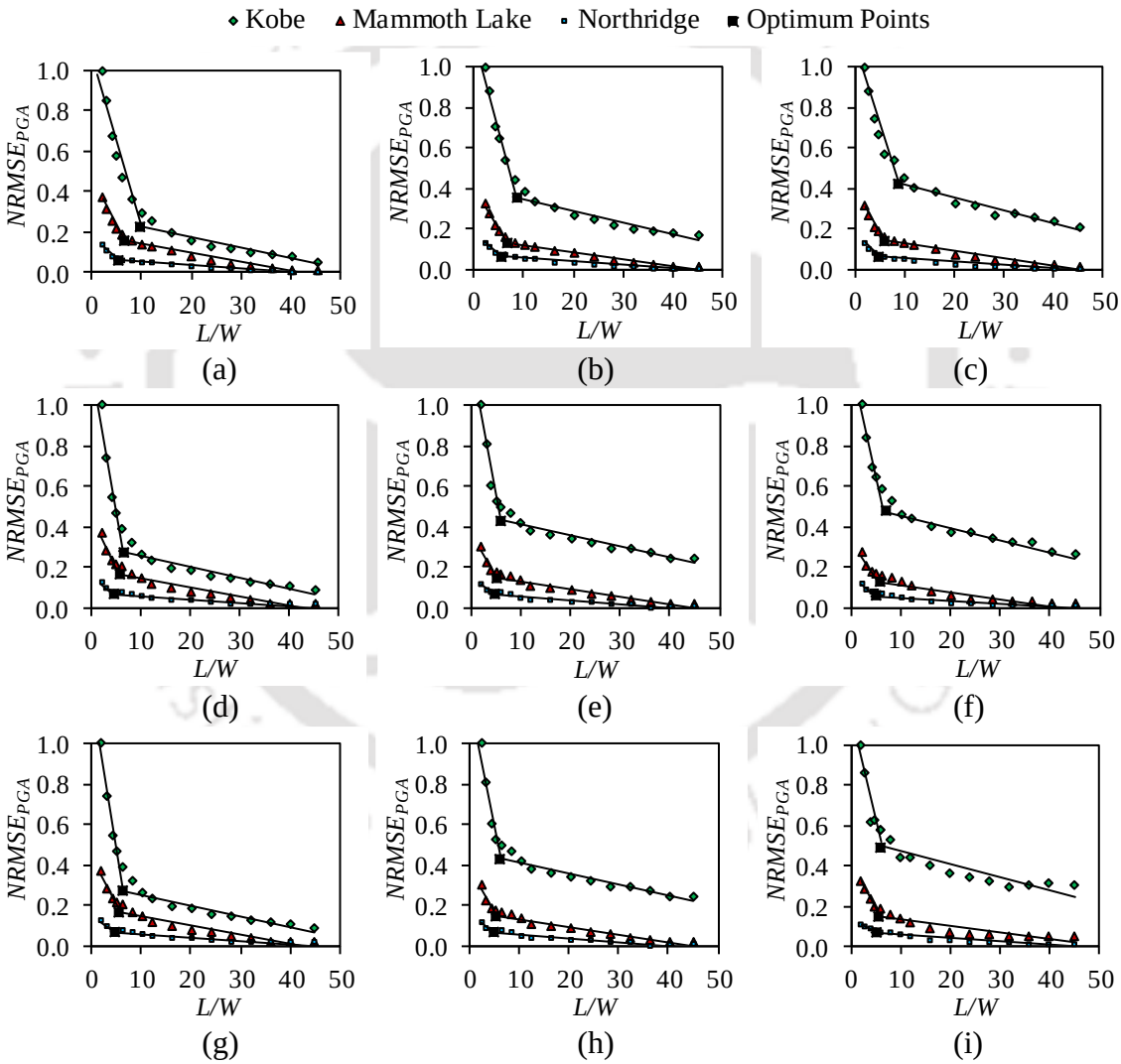

Figure 4.9 Normalized RMSE curves along with their bilinear idealizations showing the optimum points for (a) W = 15 m and soil TY-I (b) *W* = 15 m and soil TY-II, (c) *W* = 15 m and soil TY-III, (d) *W* = 27 m and soil TY-I, (e) *W* = 27 m and soil TY-II, (f) *W* = 27 m and soil TY-III (g) *W* = 45 m and soil TY-I, (h) *W* = 45 m and soil TY-II, and (i) *W* = 45 m and soil TY-III.

Table 4.4 Details of the bilinear fits of various normalized *RMSE* curves and the estimated optimum normalized domain length

Structural width, *W*	Soil type	Ground motion	m_1	C_1	m_2	C_2	R_1^2	R_2^2	Ω
15 m	S1	M1	-0.0860	1.0862	-0.0052	0.2819	0.91	0.90	9.95
	S1	M2	-0.0474	0.4663	-0.0044	0.1862	0.97	0.93	6.51
	S1	M3	-0.0221	0.1813	-0.0016	0.0698	0.98	0.96	5.44
	S2	M1	-0.0929	1.1503	-0.0058	0.4058	0.95	0.91	8.55
	S2	M2	-0.0410	0.4015	-0.0034	0.1515	0.97	0.97	6.65
	S2	M3	-0.0205	0.1774	-0.0017	0.0715	0.97	0.93	5.63
	S3	M1	-0.0775	1.1087	-0.0063	0.4815	0.90	0.93	8.81
	S3	M2	-0.0446	0.4056	-0.0037	0.1651	0.97	0.95	5.88
	S3	M3	-0.0258	0.1894	-0.0016	0.0679	0.99	0.90	5.02
27 m	S1	M1	-0.1492	1.235	-0.0054	0.3088	0.92	0.90	6.44
	S1	M2	-0.0522	0.4586	-0.0045	0.1885	0.91	0.90	5.62
	S1	M3	-0.0208	0.1631	-0.0016	0.0758	0.96	0.91	4.55
	S2	M1	-0.1279	1.2095	-0.0054	0.4646	0.91	0.92	6.08
	S2	M2	-0.0416	0.3696	-0.0038	0.1704	0.90	0.94	5.23
	S2	M3	-0.0181	0.1518	-0.0018	0.0736	0.91	0.90	4.80
	S3	M1	-0.1037	1.1712	-0.0062	0.5201	0.93	0.92	6.68
	S3	M2	-0.0362	0.3288	-0.0034	0.1461	0.91	0.85	5.57
	S3	M3	-0.0197	0.1541	-0.0016	0.0651	0.91	0.81	4.92
45 m	S1	M1	-0.1341	1.2002	-0.0044	0.4036	0.90	0.80	6.14
	S1	M2	-0.0695	0.5572	-0.0040	0.1742	0.98	0.75	5.85
	S1	M3	-0.0305	0.2224	-0.0017	0.0769	0.98	0.91	5.19
	S2	M1	-0.1019	1.1841	-0.0036	0.5955	0.96	0.91	5.98
	S2	M2	-0.0475	0.4484	-0.0035	0.2076	0.99	0.71	5.47
	S2	M3	-0.0252	0.1998	-0.0017	0.0732	0.97	0.78	5.38
	S3	M1	-0.1079	1.1702	-0.0063	0.5331	0.85	0.80	6.27
	S3	M2	-0.0454	0.4183	-0.0035	0.1749	0.98	0.81	5.81
	S3	M3	-0.0120	0.1337	-0.0017	0.0771	0.98	0.88	5.49

Note: Ω is the optimum value of normalized soil domain length; R_1^2 is the coefficient of determination of the vertical branch and R_2^2 is the coefficient of determination of the horizontal branch

4.4.4 Relationship of Optimum Lateral Extent of Soil Domain with PGA

Once the optimum normalized length of soil domain is obtained, their relationships with PGA for different structural widths and soil types are investigated. Figures 4.10a-4.10c show the relationship between PGA and the optimum normalized length of soil domain (Ω) for structure resting on S1, S2, and S3 soils, and having structural widths, W = 15 m, 27 m, and 45 m, respectively. It is observed that for a particular structural width (W) and PGA, the value of Ω does not vary significantly for different soil types. For different soil types, corresponding to the structural width of W = 15 m, the value of Ω corresponding to 0.82g PGA level lies in the range of 8.55-9.95, and that corresponding to 0.22g PGA level lies in the range of 5.02-5.63; similar feature is noted in all the other cases shown in the figures. Moreover, it is observed that rather than soil type, PGA has a more dominant influence on the variation of Ω. For the structural width of W = 15 m and TY-I soil, the value of Ω varies in the range of 5.44-9.95 for 0.22g-0.82g PGA levels; a similar feature is observed in the

other cases as well. Considering negligible influence of the soil type, an average curve is drawn to establish a relationship between PGA level and Ω (Figures 4.10d to 4.10f) for structural widths 15 m, 27 m, and 45 m, respectively. It is observed that a linear relationship provides a very good fit indicated by sufficiently high R^2 value. In all the figures, it is observed that the requirement of domain length increases with an increase in the PGA level. For larger structural widths, the requirement of Ω at high PGA level is less as compared to that corresponding to smaller structural widths. For e.g., at the PGA level of 0.8g, Ω is 8.9 for W = 15 m; however, Ω is 6.1 for the structural width of 45m at the same PGA level. For lower PGA levels, Ω is approximately similar. For the 0.2g PGA level, for different structural widths, Ω lies within 4.7-5.4. The obtained relationships have been assessed with the help of sensitivity analysis. For such studies, various approaches are available in the literature. Vu-Bac et al. (2016) developed a software framework for conducting uncertainty and sensitivity analysis of computationally expensive models. Hamdia et al. (2017) presented a methodology for the stochastic modelling of a problem by incorporating uncertainty in the input and constructing a PCE (Polynomial Chaos Expansion) surrogate model and finally showing its effectiveness in sensitivity analysis. Hamdia et al. (2018) implemented three methodologies for conducting sensitivity analysis in their study, namely, MOAT (Morris One At a Time), PCE-Sobols' and EFAST (Extended Fourier Amplitude Sensitivity Test). Due to the limited scope of the present study, a simplistic sensitivity analysis is presented for the different soil types considering two variables, the width of the structure (W) and PGA of the input motion.

The PGA level is considered to follow a normal distribution with mean (μ) as 0.49g and standard deviation (σ) as 0.25g, and W is considered uniformly distributed within a range of 15 m to 45 m. The results of the sensitivity analysis using MOAT and Sobols' method are shown in Figures 4.11a and 4.11b, respectively. From Figure 4.11a, it can be observed that for soil type S3, Ω shows greater sensitivity to PGA, whereas for soil types S1 and S2, both W and PGA are found influential. The total effect indices (s_t) and first-order indices (s_i) for the variables considered are shown in Figure 4.11b. It can be observed that corresponding to soil S1, the sensitivity indices for W and PGA are nearly equal in value. This indicates that both the parameters are influential for soil S1. For soil S2, the indices have a considerable difference. This indicates that for soil S2, W has more influence compared to PGA. Similarly, for soil S3, the indices have a considerable difference.

However, in this case, PGA exhibited more influence than *W* in the determination of the optimum length of the soil domain for soil S3.

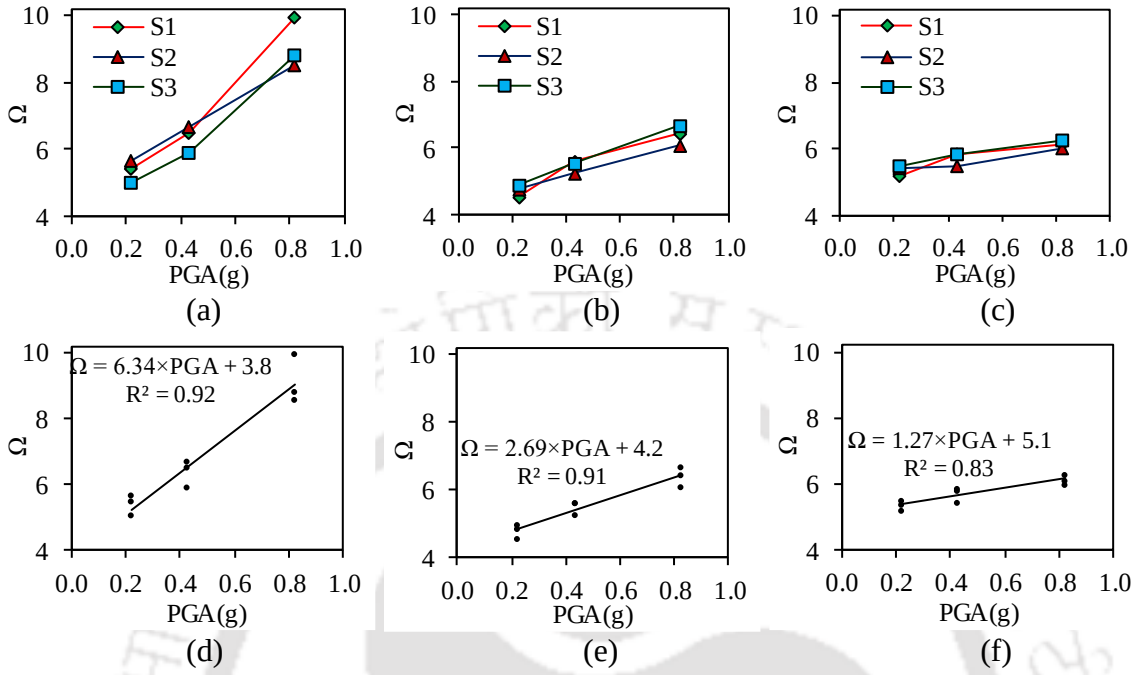

Figure 4.10 Variation of optimum normalized domain length (Ω) with PGA for (a) *W* = 15 m, (b) *W* = 27 m and (c) *W* = 45 m for various soil types; variation of linear fitted Ω with PGA for (d) *W* = 15 m, (e) *W* = 27 m, and (f) *W* = 45 m.

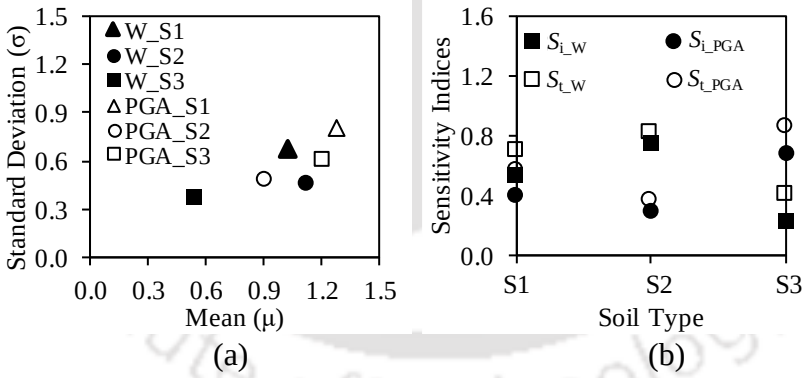

Figure 4.11 Sensitivity analysis: (a) MOAT method, and (b) Sobols' method.

4.5 Engineering Application

In the previous section, the relationship between the optimum normalized length of soil domain and PGA of the strong motions is established for individual structural/foundation widths (15 m, 27 m, and 45 m). However, for engineering purposes, it would be required to develop numerical models to investigate the seismic SSI aspect. In this regard, it would be more fruitful to develop relationships to ascertain the optimum normalized length of soil domain required to conduct such studies for various structural or foundation widths. Based

on the observations and estimates obtained from the present study, engineering relationships with linear trends are developed for various levels of PGA (Figure 4.12) and are expressed in Eqs. 4.7-4.9.

$$\Omega = -0.1W + 11.5 \qquad \vee PGA = 0.82g \tag{4.7}$$

$$\Omega = -0.03W + 7.5 \qquad \vee PGA = 0.43g \tag{4.8}$$

$$\Omega = 5.5 \qquad \vee PGA = 0.22g \tag{4.9}$$

In Eqs. 4.8 and 4.9, the parameter W is expressed in meter (m). For intermediate PGA levels, linear interpolation can be sought. It is noted that the proposed relationships satisfy all the observations of the analyses, such as:

1. Higher the PGA, higher is the value of Ω for a particular structural/foundation width (W), and vice versa.
2. For larger structural/foundation widths (W), Ω is less, and vice-versa.
3. For low PGA level, Ω is nearly the same and independent of different structural/foundation widths (W).
4. In the previous sections, it has already been established that the influence of soil type on Ω is insignificant, and hence this parameter is not included in the expressions.

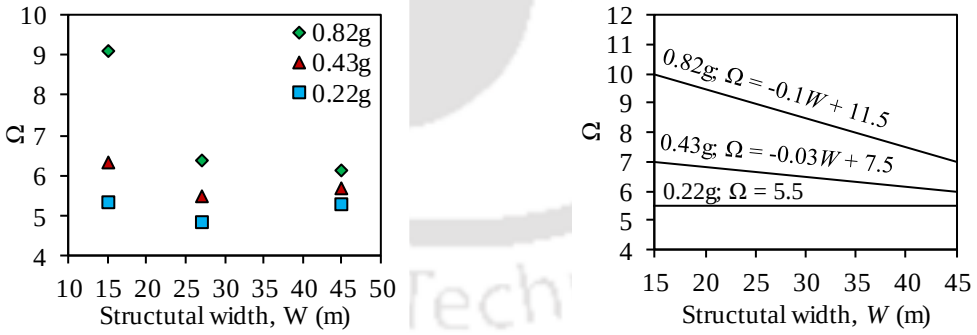

Figure 4.12 (a) Averaged optimum normalized length of soil domain for varying structural width (W) for different PGA levels, and (b) proposed relationships of optimum domain length with varying structural width for different PGA levels.

The practical applicability of the prescribed relationships is judged based on their performance in comparison to a similar model developed with a very long soil domain (e.g., 50×W, i.e., $L/W = 50$). Corresponding to the three selected structural widths and PGA levels,

various optimum normalized lengths of soil domain are obtained, and dynamic analysis is carried out. Table 4.5 shows the percentage difference in the estimated peak acceleration response recorded at (i) soil node at the surface very near to the structure, (ii) pile node at the top of the outermost pile, and (iii) structure node at the roof level. It is observed that the maximum error obtained is less than 10%, which is quite acceptable for practical engineering purposes. Moreover, the percentage of the computational time required for performing the analysis is below 5% of the time required for performing exact analysis, which definitely indicates the computational proficiency of the adopted values.

Table 4.5 Percentage error in the estimate of peak acceleration response

Structure width, W	PGA (g)	Ω	$\Omega \times W$ (m)	Difference in peak acceleration, %			Computational time[#] %
				Soil node	Pile node	Structure node	
15 m	0.82	10.00	150	2	9	5	4.3
	0.43	7.06	106	4	4	7	3.5
	0.22	5.53	83	1	2	4	2.0
27 m	0.82	8.81	238	5	7	4	3.3
	0.43	6.70	181	4	6	1	2.2
	0.22	5.52	149	1	4	6	1.0
45 m	0.82	7.00	315	2	4	1	1.0
	0.43	6.15	277	8	6	4	0.9
	0.22	5.51	248	9	9	9	0.8

[#]Ratio of the computational time required for analysis with domain length $\Omega \times W$ to that required with domain length $50W$ in percentage

In the past, there have been a few recommendations for the horizontal extent of the soil domain to be used for SSI studies. Some researchers have also adopted specific values of the horizontal extent of the soil domain as suitably required for their purpose without any comprehensive study. Figure 4.13 shows a comparison of the prescribed relationships from the present study and the soil domain lengths considered by past researchers. It is observed that the values and the relationships used by past researchers fall within an agreeable zone of the relationships proposed in the current study.

It is to be noted that the relationships prescribed in the present study are more rigorous since they are inclusive of various factors such as structural width, PGA level, and soil type. These relationships are more helpful in deciding about the length of the soil domain to be considered for soil-structure interaction studies when various factors are to be accounted. It is observed that the relationships proposed by previous researchers are mostly independent of the structural width, which in different cases prove to be computationally inefficient owing to significant underestimation or overestimation of system response and computational effort, respectively. Hence, based on the present findings and relevant

comparisons, it can be stated that the prescribed estimates for soil domain length are computationally efficient as well as suitable enough to provide the system response. Thus, these relationships are credible for practical use in the future SSI analysis. For any random structural width and PGA of input seismic motion, the optimum normalized length of soil domain length can be arrived at by a suitable linear interpolation. The relationships proposed in the present study, thus, provide a guideline for arriving at the horizontal extent of the soil domain to be chosen for SSI analysis.

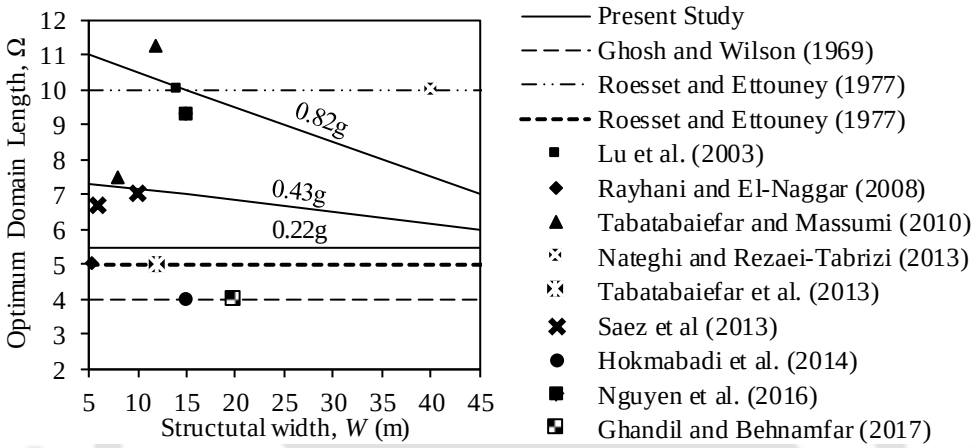

Figure 4.13 Comparison of the proposed relationship of the optimum normalized length of soil domain with past studies, for different PGA levels and structural widths.

4.6 SUMMARY

In the present chapter, a strategic approach has been outlined to arrive at the optimum normalized length of soil domain to be considered for soil-structure interaction studies. Based on exhaustive finite element simulations, the normalized root mean square error (*NRMSE*) for various domain lengths is obtained for structures comprising various structural widths and resting on different soil types. With the aid of bilinear fit to the *NRMSE* plots, normalized optimum lengths of soil domain have been obtained. Any length beyond the optimum domain length produces an insignificant change in the overall response of the SSI system with the percentage difference in the results being less than 10%, but leading to a drastic saving in the computational expense (minimum of 96% is observed in this study). The optimum domain lengths for various causes have been obtained, based on which a generalized set of relationships has been prescribed. The prescribed relationships correlate the horizontal extent of the soil domain as a function of structural (or foundation) width and the PGA of the strong motion. It is observed that the domain length to be used for rigorous SSI studies is virtually independent of the soil type. It is concluded that larger

extents of soil domain are required for SSI studies considering higher PGA strong motion, and vice versa. SSI analyses comprising of smaller structural widths require larger normalized domain lengths (Ω), and vice versa. In comparison to the correlations of the domain length provided by earlier researchers, the one prescribed herein proves to be more robust (being inclusive of various factors such as soil type, structural or foundation width, and PGA level of input motion), practically feasible and computationally efficient. The developed relationships from the present research can be credibly used as guidelines for numerical modelling in SSI studies.

Chapter 5
INFLUENCE OF SSI ON NATURAL PERIOD OF RC FRAME AND WALL-FRAME SYSTEMS

CONTENTS

5.1 OVERVIEW

During any earthquake shaking, the magnitude of seismic forces induced within the structure depends on its natural period of vibration. This is also reflected in the design codes of various countries. For the estimation of the natural period, the conventional approach is to assume the base of the building as fixed, and the estimate is termed as the fixed-base natural period (T_F) of the system. Foundations resting on rocky medium imparts a high degree of restraint, in which case the assumption of the fixed-base building holds good. However, if the supporting medium comprises relatively soft and deformable soil, the building can be considered having a flexible base, and the same is supposedly influenced by SSI effects. In the latter case, the natural period of the building is increased in comparison to that obtained for an assumed fixed-base building system. The natural period of the building under the influence of SSI is termed as the effective natural period (T_{SSI}). For the same structure, a variation in foundation-soil conditions would result in the variation of the

effective natural period. As highlighted in the available literature, the modification in the fixed-base natural period leads to a modification in the level of seismic forces that could be detrimental towards the seismic safety of structures. In this regard, the estimation of the natural period of the structure under the influence of SSI has been one of the focus areas as far as the subject matter is concerned. Expressions for the determination of effective natural period are available in the literature. The general format of the expressions is shown in Eq. 5.1, wherein *MF* is a modification factor that depends on the structural, soil, and foundation properties.

$$T_{SSI}=T_F\times MF \tag{5.1}$$

Although useful, these expressions are developed considering one or more of the following simplifications: (a) the structure is idealized as a single degree of freedom, SDOF, oscillator, (b) the structural system is considered supported on shallow foundation, and (c) equivalent springs, or single lumped pile, is used to represent the stiffness of the pile foundation. These simplifications could possibly lead to inaccurate estimates of the effective natural period, mainly due to two reasons. Firstly, SDOF representation is not suitable for modelling the rocking behaviour of the building. In a building frame, the rocking behaviour is non-uniform under the vertical members. However, the SDOF system is only capable of modelling the uniform rocking behaviour. Secondly, the flexibility imparted by piles, distributed under the columns and shear wall, is noticeably different from that of a lumped single pile or an equivalent spring.

The present chapter investigates the effect of SSI on the natural period of RC frame and RC wall-frame systems supported on pile foundation. In contrast to the usage of simplified models with SDOF system and foundation considered as single lumped piles or equivalent springs, in the present study, a detailed Finite Element (FE) modelling using OpenSEES has been used to attempt an accurate estimation of the effective natural period (T_{SSI}). The effect of SSI on RC frames and RC wall-frame systems has been studied for various configurations of the superstructure and soil-pile foundation systems. To overcome the shortcomings of past studies, it is essential to develop a relationship for the prediction of the effective natural period, capable of capturing the complex phenomenon of soil-structure interaction without simplifying assumptions. Artificial Neural Networks (ANNs) have gained popularity over the past decades, as they are capable of delineating and deciphering the complex relationships between multitudes of input parameters and output

entities. In the present study, an ANN model has been trained to develop a relationship for the modification factor (*MF*) that is useful in predicting the effective natural period (T_{SSI}) of RC frame and RC wall-frame system supported on pile foundation. The reasonable agreement of the outcomes from the proposed relationship with those available in literature demonstrates its usefulness and applicability to identify the effective natural period of the RC frame and RC wall-frame building systems.

5.2 DESCRIPTION OF THE RC FRAME AND RC WALL-FRAME CONFIGURATIONS

In the present study, two types of systems, viz., (i) RC frame and (ii) RC wall-frame, have been considered. The floor-to-floor height and bay width are considered 3 m. For each structure type, four different storey heights have been considered comprising 3-storeys (9 m), 6 -storeys (18 m), 9-storeys (27 m), and 12-storeys (36 m). For each height of the building frame, four configurations of structural width of 9 m (3-bays), 15 m (5-bays), 27 m (9-bays), and 45 m (15-bays) are considered. As in the previous chapter, the maximum considered width of the superstructure has been limited to 45 m. Figure 5.1 shows the representative illustrations of the various configurations considered in the present study. Each configuration is labelled using an alphanumeric nomenclature to represent system type, number of storeys and number of bays, in the stated order. For e.g., the label F3-15 corresponds to an RC frame system comprising 3-storeys and 15-bays. Similarly, W12-9 represents an RC wall-frame system having 12-storeys and 9-bays. Each building system is considered founded on four different soil conditions (viz., S1, S2, S3, and S4) and one fixed-base condition (FB). For all the cases, the superstructure design remains the same, while only the foundation design is modified as per the supporting soil type. For a particular configuration, the design of the frame members (column, beam, and shear wall) is varied with height as per the design requirements. Moreover, for a particular structure-soil combination, the columns are considered supported by three different arrangements of pile foundation, namely (a) single pile (b) two-pile group, and (c) three-pile group.

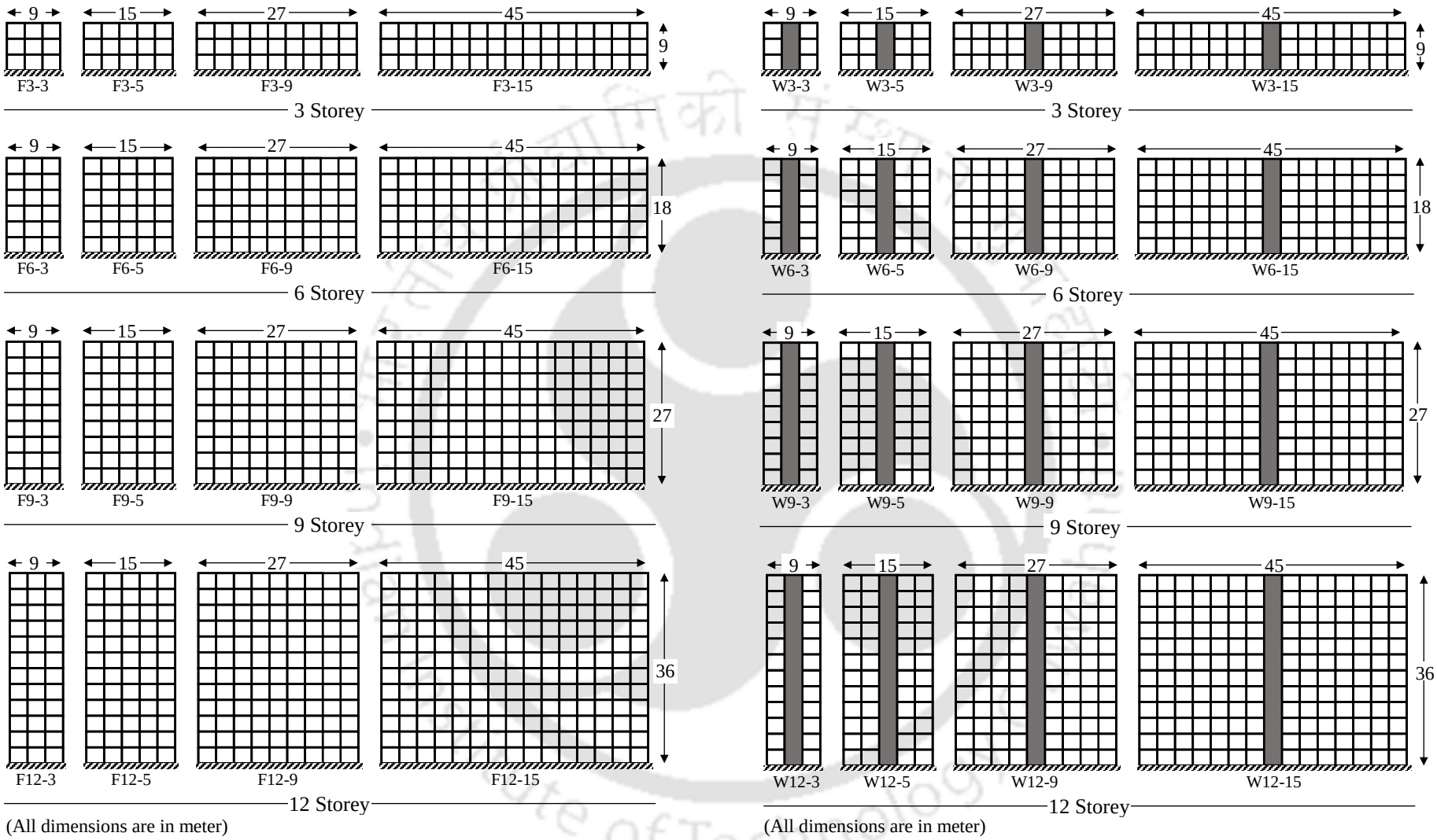

Figure 5.1 Details of the configurations considered in the present study.

As shown in Figures 5.2a and 5.2b, corresponding to a particular configuration, the only difference between the frame and wall-frame system is marked by the shear wall incorporated in the central bay, which is supported by the corresponding pile group system that is different from those supporting the columns. The pile group under the shear wall is not varied in its configuration and is maintained the same even though the pile configuration under the columns is varied. The details of the superstructure and pile foundations for the various configurations are provided in Appendix A. For the study carried out in this chapter, the material characteristics in the superstructure and pile foundation elements are considered 'linear elastic'.

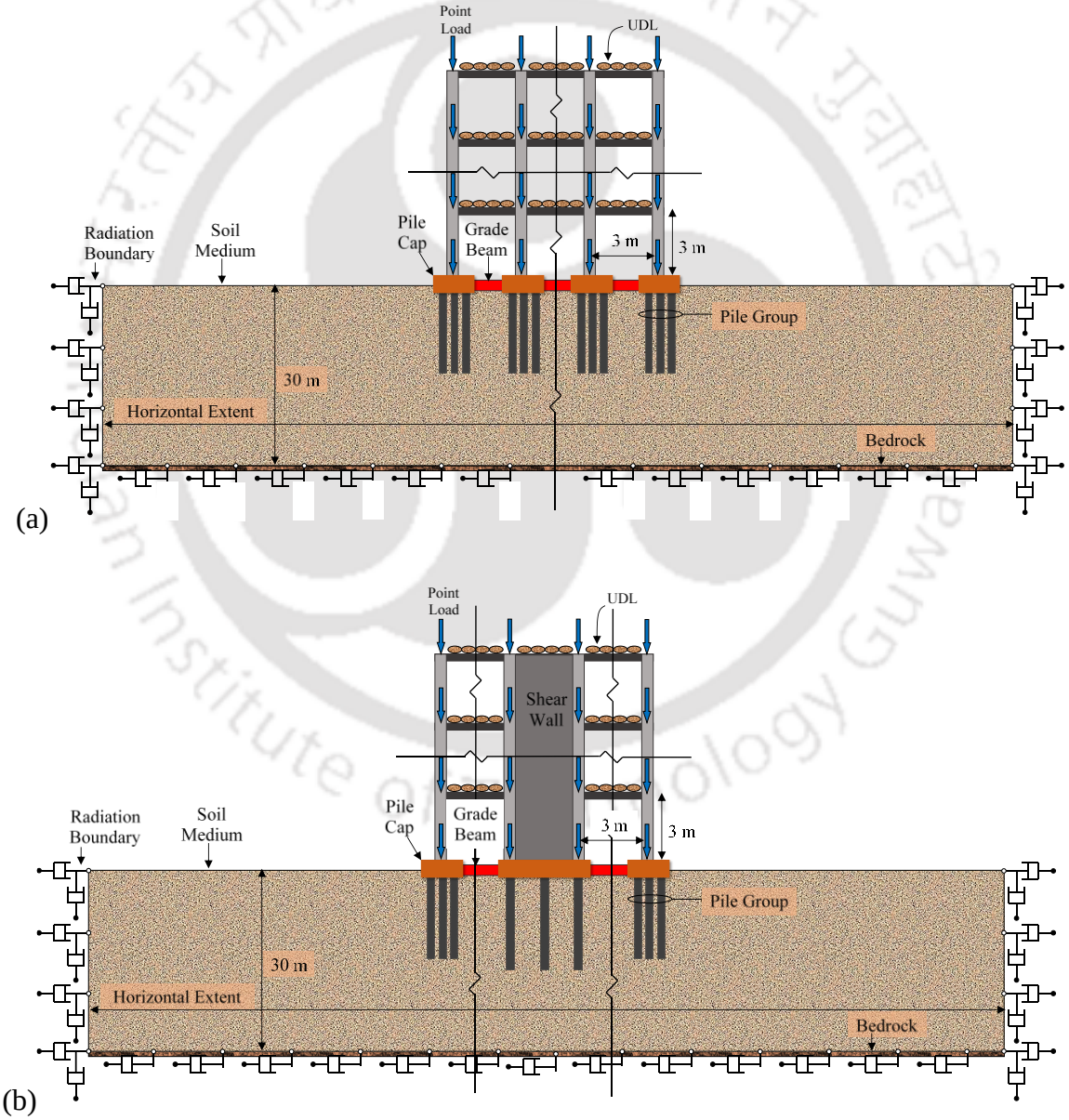

Figure 5.2 Representative illustration of the SSI model for (a) RC frame system, and (b) RC wall-frame system.

5.3 METHODOLOGY AND INPUT

As already explained in Chapter 3, the radiation boundaries do not provide lateral/horizontal restraint, thereby are unable to generate lateral confining action essential for mobilization of strength and development of a proper state of stress within the soil. The state of static stresses influences the confinement action imparted to the pile foundation, which in turn governs the flexibility of the soil-pile foundation system. Depending on the imparted flexibility, the fixed-base natural period of the structural system is modified. To ensure the development of a proper confining state of stress within the soil, 'staged gravity' analysis is carried out. The SSI model without horizontal restraints possesses a singular stiffness matrix. Under such circumstances, the eigenvalue analysis does not show appropriate results, as there is a display of rigid body displacements for the first mode. Further, the natural period estimates by eigenvalue analysis are influenced by the size of the considered soil domain. For e.g., a 3-storey 3-bay structure resting on soil would exhibit a different natural period if the horizontal extent of the soil domain is changed from 200 m to 250 m, or if the depth of the soil domain is modified from 30 m to 40 m. This is attributed to the modification of the stiffness matrix and mass matrix of the SSI model (used for estimating natural period using eigenvalue analysis) upon changing the dimensions of the soil domain, thus producing a different estimate of the natural period. However, the response of the structural system under soil-pile flexibility should depend only on the confinement action provided by the soil in the vicinity of the pile foundations. Therefore, to obtain the natural period of the structure under the influence of SSI, the vibrational response of the system is obtained by conducting time history analysis.

Most soils tend to exhibit inelastic behavior even under small strains, and hence, even the application of gravity loads may induce a marginal inelastic response in the soil. The inelastic behavior directly influences the state of stresses developed within the soil, thereby influencing the confining action onto the piles. This, in turn, influences the flexibility induced to the soil-pile foundation system. Thus, it is essential to incorporate the nonlinear behavior of the soil during gravity analysis and maintain the state of confinement for estimating the natural period of the SSI system. The change in the natural period of the structural system under the influence of SSI, primarily, should be governed by the flexibility of the soil-pile foundation system. However, assessment of the modification in the natural period with the incorporated soil nonlinearity might be intermingled with the inelastic behaviour of the soil. This may lead to inaccurate estimates of *MF* (increase in the natural

period due to the incorporation of soil-pile flexibility). Therefore, it becomes highly essential to delineate the influence of soil nonlinearity on the estimates of the effective natural period. Additionally, it is to be ensured that the vibrational input excites the natural frequencies of the SSI system. Hence, in the present study, the SSI system is dynamically excited using a 'White Noise' of very low amplitude (peak acceleration of 0.0005g) to obtain the vibrational response. The low amplitude of the excitation prevents the development of nonlinearity within the soil material. The time history and frequency distribution of the input motion are shown in Figures 5.3a and 5.3b, respectively. The response at the top storey level of the superstructure in the SSI system is obtained and the effective natural period is identified by locating the lowest frequency corresponding to the dominant peaks in the transfer function (in the form of Fourier Amplitude Ratio, FAR, i.e., the ratio of the output to input Fourier amplitude at a particular frequency). The dominant peaks in the Fourier Amplitude Ratio (FAR) spectrum indicate the location of the natural frequencies of the SSI system. A similar methodology has been successfully adopted in the past (Zhang et al. 2008) for evaluating the natural period of an integral abutment bridge under the influence of SSI.

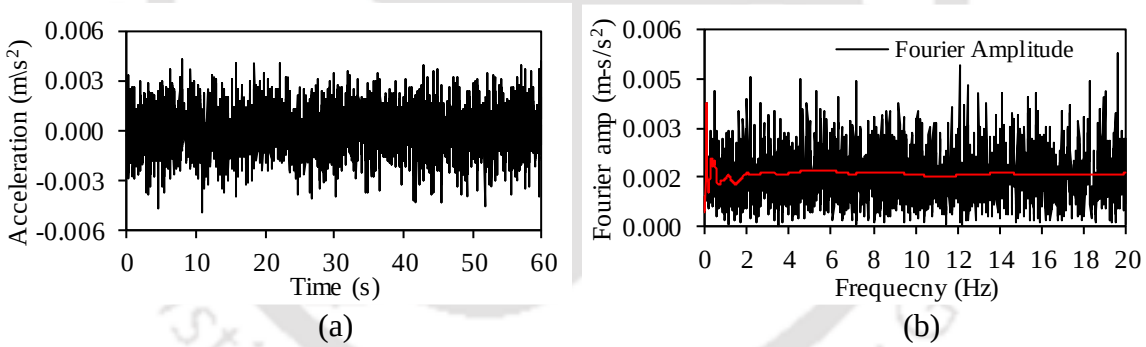

Figure 5.3 Characteristics of the selected white noise motion: (a) accelerogram time history, and (b) fourier amplitude spectrum.

5.4 Results and Discussion

5.4.1 Natural period of Free-Field Soil and Fixed Base Superstructure

Before proceeding to analyse the coupled SSI systems, the methodology is applied on the free field soil system and fixed-base superstructure system. The free-field soil model (without the structure), with Lysmer-Kuhlemeyer (L-K) boundaries, is subjected to the considered 'white noise' motion. The free-field response is obtained at the ground surface, and the transfer functions (based on the FAR spectrum) are obtained. Distinct peaks in the FAR spectrum highlight the natural frequencies of the free field soil layer. Figures 5.4a-

5.4d show the FAR spectrum, thereby indicating the natural frequencies corresponding to the first four modes of vibration for the different soil types considered in the study. The theoretical expression, as available in the literature (Gazetas, 1991b), for obtaining the fundamental natural period of a free field soil domain is shown as shown in Eq. 5.2,

$$T_s = 4.48\frac{H_s}{v_{sH}} \tag{5.2}$$

where T_s is the fundamental period of the soil layer, v_{sH} is the shear wave velocity of the soil domain at the depth H_s (bottom of the soil deposit), and H_s is the thickness of the soil deposit. The above expression is applicable for soil layers having a parabolic increase in shear modulus with depth. Using Eq. (5.2), the fundamental natural periods of the free field soil domain are obtained for the different soil types, and the same are compared with those obtained by time-history analysis of the finite element (FE) model (Figure 5.4e). As observed, a fairly good agreement is attained between the two approaches.

Similarly, the structural systems under fixed-base conditions are subjected to the considered 'white noise' motion, and the roof level response of the structure is obtained. The FAR spectrum over a range of frequencies shows distinct peaks corresponding to the natural frequencies of the superstructure. Figures 5.5a and 5.5b show the FAR spectrum of configurations F6-5 and F12-5, respectively. Similarly, Figures 5.6a and 5.6b show the FAR spectra of configurations W6-5 and W12-5, respectively. Figures 5.5c and 5.5d show the comparison of the natural periods corresponding to the first three modes, obtained from conventional eigenvalue analysis and the adopted methodology for F6-5 and F12-5, respectively. Similarly, Figures 5.6c and 5.6d show the comparison of the natural period corresponding to the first three modes for W6-5 and W12-5, respectively. It can be seen that a very good match is existent between the results from both the analysis procedures. Thus, the methodology adopted is capable of providing satisfactory and appropriate results and can be convincingly applied for further analysis. Hence, the same is used for obtaining the natural periods of the coupled structure-pile-soil system.

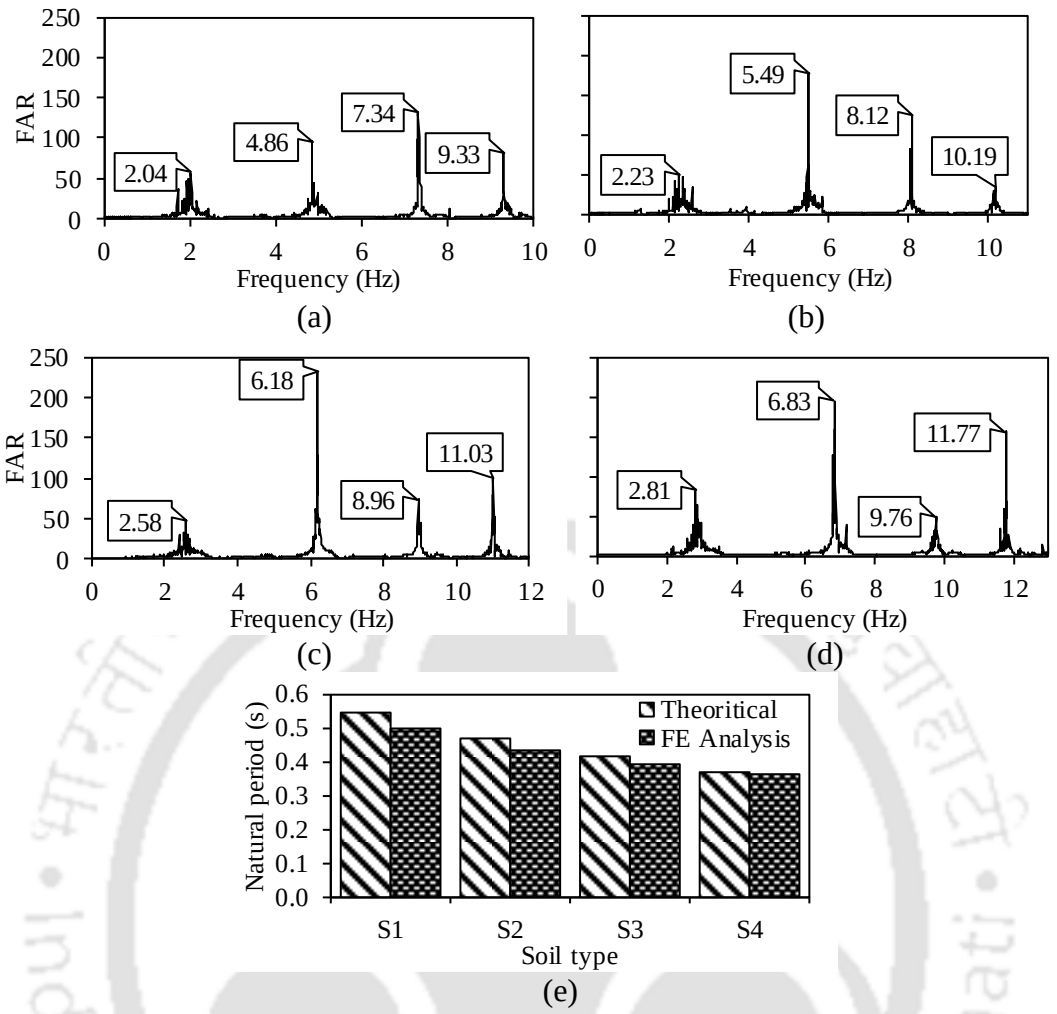

Figure 5.4 Identification of natural period from transfer functions of the free field soil response for soil types (a) S1, (b) S2, (c) S3, and (d) S4; (e) Comparison of fundamental natural periods obtained theoretically and using FE analysis for the mentioned soil types.

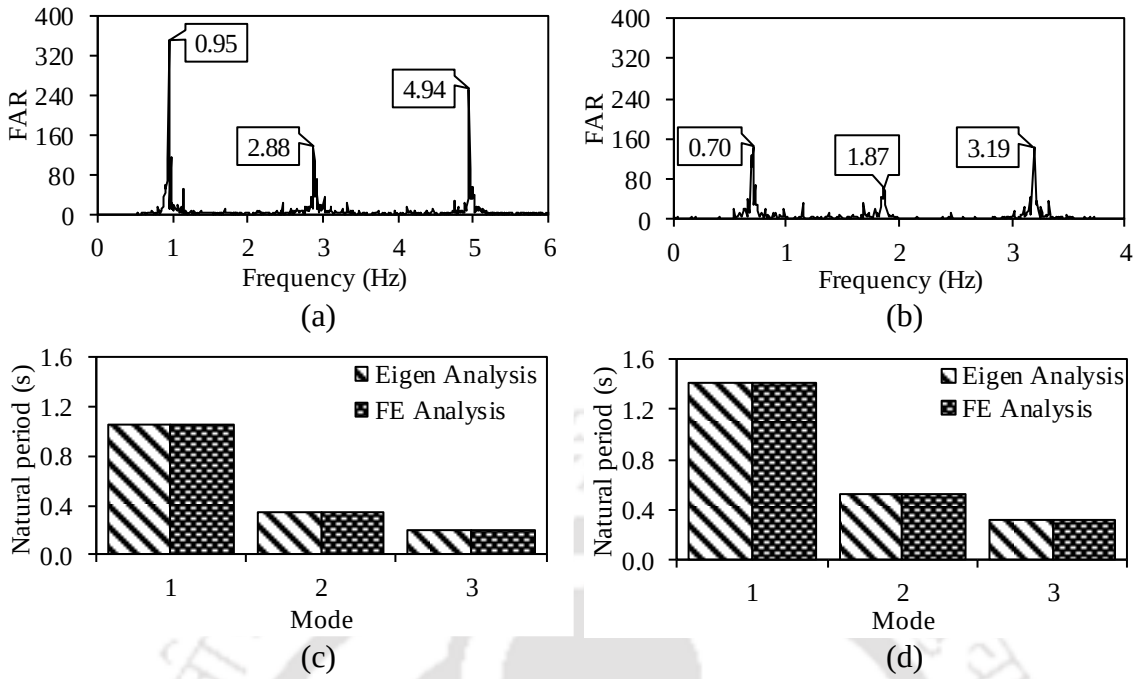

Figure 5.5 Fourier amplitude ratio spectrum of the roof-level response for (a) F6-5, and (b) F12-5; comparison of natural periods from Eigenvalue and finite element (FE) analysis for (c) F6-5, and (d) F12-5.

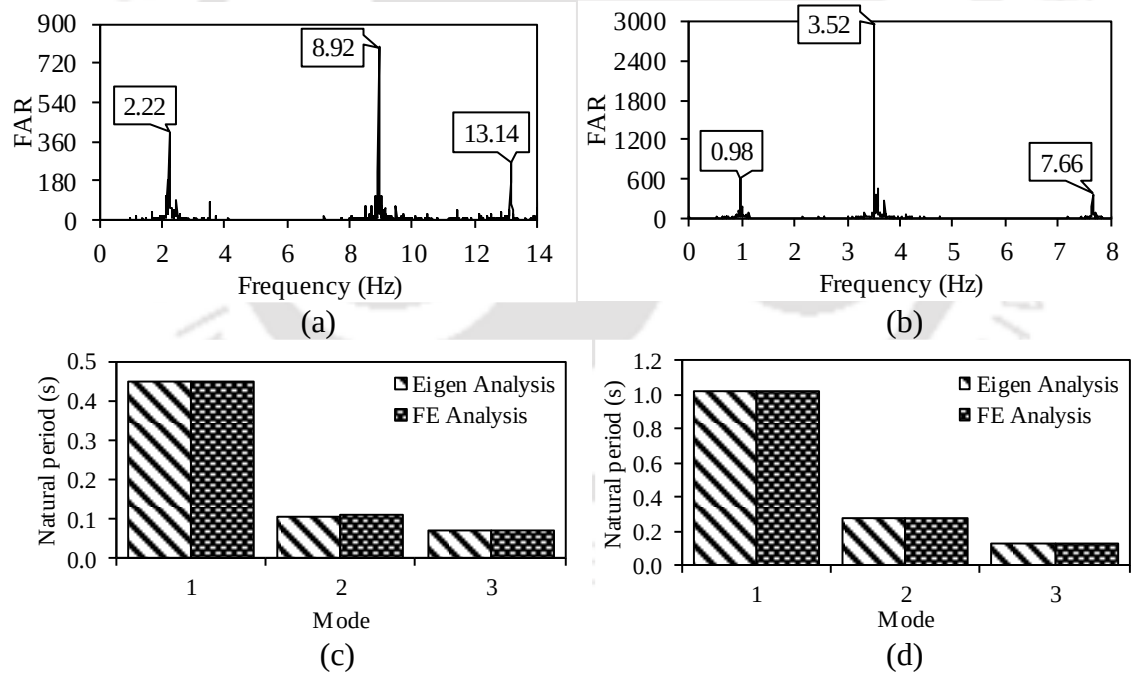

Figure 5.6 Fourier amplitude ratio spectrum of the roof-level response for (a) W6-5, and (b) W12-5; comparison of natural periods from Eigenvalue and finite element (FE) analysis for (c) W6-5, and (d) W12-5.

5.4.2 Effective Natural Period of SSI System

The SSI system is subjected to the considered 'white noise' motion to induce dynamic excitations, and the acceleration response at the roof level is obtained. The FAR spectrum is obtained, and the first dominant peak indicates the effective natural frequency of the SSI system. Figures 5.7a-5.7d show the FAR spectra indicating the effective natural frequency of F6-5 for S1-S4 soil types, respectively. Similarly, Figures 5.8a-5.8d show the FAR spectra indicating the effective natural frequency of W6-5 under S1-S4 soil types, respectively. The effective natural period (T_{SSI}) of different configurations under various soil-pile foundation conditions is thus obtained from the effective natural frequency of the SSI system, and the results are discussed in the following subsections.

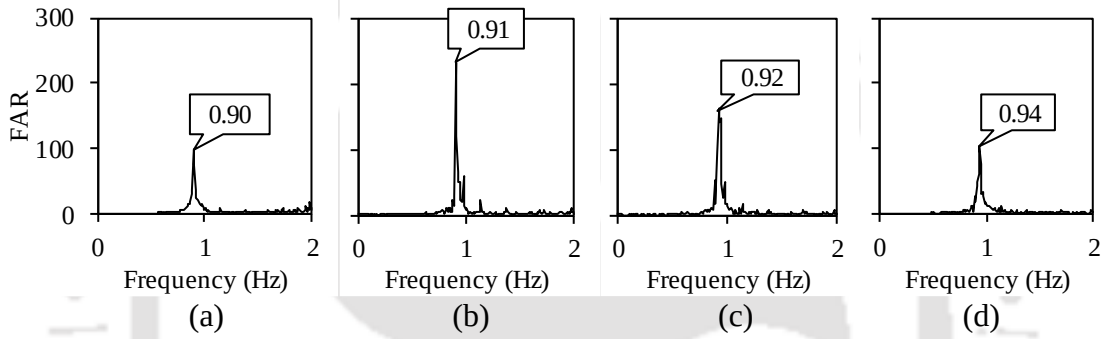

Figure 5.7 Identification of the fundamental natural frequency of F6-5 with pile foundations supported on soil types (a) S1, (b) S2, (c) S3, and (d) S4.

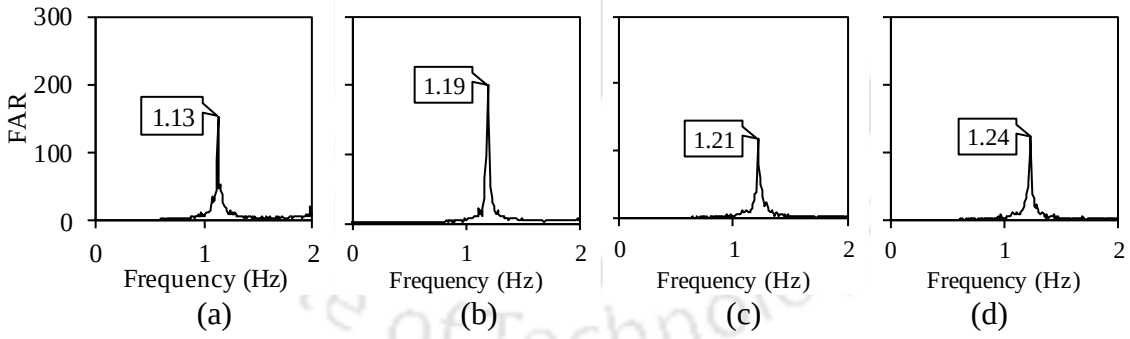

Figure 5.8 Identification of the fundamental natural frequency of W6-5 with pile foundation supported on soil types (a) S1, (b) S2, (c) S3, and (d) S4.

5.4.3 Influence of Significant Parameters on *MF*

The results obtained are presented in this section to discuss the parameters that govern the change in the fixed-base natural period of the RC frame and RC wall-frame systems due to SSI effects. The various configurations of the building frames have been analysed under the fixed-base condition to obtain the fixed-base natural period (T_F), and under four different soil-pile foundation conditions to obtain their respective effective natural periods (T_{SSI}). The

amount of change in the natural period (from T_F to T_{SSI}) is a measure of the SSI effects on the system and is quantified in terms of the modification factor (*MF*) as shown in Eq. 5.1. Higher *MF* is indicative of greater SSI effects, and primarily, the properties of the structure, foundation, and soil are the influential parameters.

5.4.4 RC Frame System

Any particular building frame is characterized by its natural period under fixed-base condition (T_F), which varies as per the structural configuration. Depending on the structural configuration (height and width), T_F may vary, which will, in turn, influence *MF*. Figures 5.9a and 5.9b show the influence of the width of the building frame on *MF* under different soil conditions for short (3-storeyed) and tall (12-storeyed) frames, respectively. It can be observed that for short frames (3-storeyed), increasing the width from 9 m to 45 m increases the T_F from 0.70s to 0.73s. The variation of *MF* for narrow (9 m) frame under different soil conditions is about 1.10 (S1) to 1.05 (S4), and that for wider (45 m) frame, it is about 1.16 (S1) to 1.06 (S4). For taller frames (12-storeyed), increasing the width from 9 m to 45 m decreases the T_F from 1.47s to 1.41s. The variation of *MF* for narrow (9 m) frames under different soil conditions is about 1.22 (S1) to 1.11 (S4), while that for wider (45 m) frames, it is about 1.15 (S1) to 1.05 (S4). Similarly, Figures 5.10a and 5.10b show the influence of the height of the building frame on *MF* under different soil conditions for narrow (9 m) and wider (45 m) configurations, respectively. For narrow frames (9 m), on increasing the height from 3-storeys to 12-storeys, T_F increases from 0.70s to 1.47s. The variation of *MF* for short (3-storeyed) frames under different soil conditions is about 1.11 (S1) to 1.05 (S4), and that for taller (12-storeyed) frames, it is about 1.22 (S1) to 1.10 (S4). For wider frames (45 m), increasing the height from 3-storeys to 12-storeys, T_F is increased from 0.73s to 1.41s. The variation of *MF* for short (3-storeyed) frames under different soil conditions is about 1.16 (S1) to 1.06 (S4), while that for taller (12-storeyed) frames, it is about 1.15 (S1) to 1.05 (S4). It can be observed that for any particular structural configuration, SSI effects are highest (higher *MF*) for soft soil (S1) and are reduced for relatively stiffer soil conditions (S2, S3, and S4). Increase in the width of the frame results in an increase or decrease in the fixed-base natural period (T_F), which depends on the frame height attributed to the addition of mass and stiffness to the structural system. In short frames, being inherently stiff in nature, an increase in width results in the dominant addition of mass, thereby causing the wider frames to be more flexible as compared to the narrower ones. Taller frames are

flexible by nature, thus an increase in the width results in the dominant addition of stiffness; and consequently, the wider frames turn out to be stiffer as compared to the narrower ones. The SSI effects are observed to be marginally larger for frames with extreme configuration (e.g., 'very short and wide' or 'very tall and narrow' frames). Increasing the height of the frames (corresponding to a fixed-width) leads a system to be more flexible. Moreover, for narrow frames, the SSI effects increase with larger heights; however, for wider frames of different heights, the SSI effects are comparable.

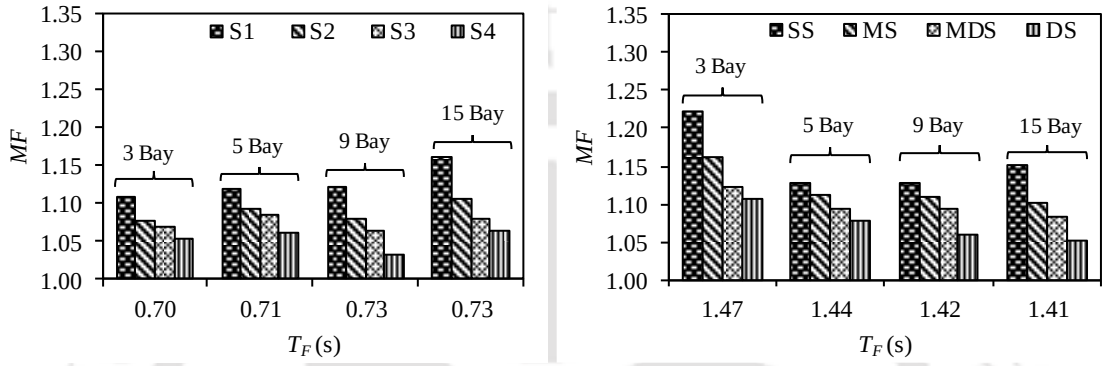

Figure 5.9 Variation of *MF* with number of bays for (a) 3 storeyed, and (b) 12 storeyed RC frame systems.

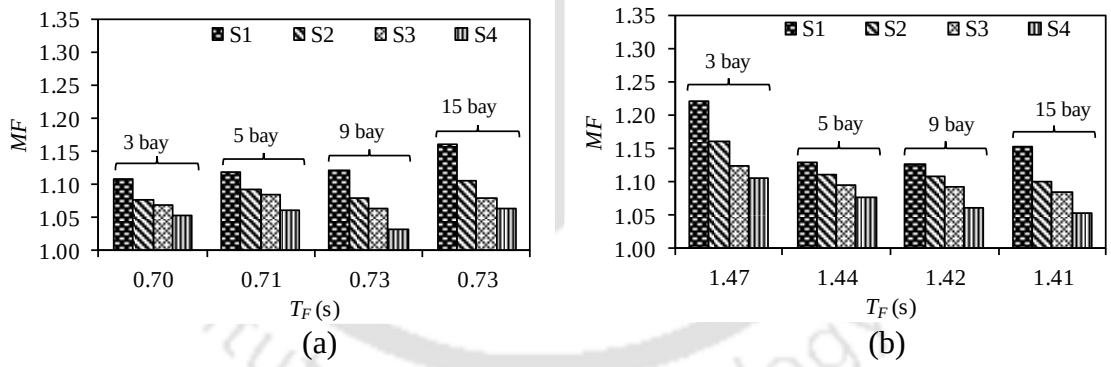

Figure 5.10 Variation of *MF* with number of storeys for RC frame system having widths of (a) 9 m, and (b) 45 m.

Apart from the structural configuration, the soil-foundation characteristics also influence *MF*. Corresponding to a particular soil condition, the column members of the RC building frame can be supported by pile foundations, which may consist of a single large diameter pile or multiple piles of smaller diameter. For the same structure-soil combination, variation in the foundation system might result in a variation of *MF*. Figures 5.11a and 5.11b show the variation of *MF* under different pile foundation configurations for F3-15 and F12-15 RC frame systems, respectively, with various soil conditions. As observed, for

the different pile foundation configurations, *MF* increases as the stiffness of the soil decreases. Moreover, in comparison to the building frame supported on single piles, the building frames supported by a 2-pile or 3-pile group exhibit a slight reduction in *MF*. This is attributed to the fact that in contrast to a single pile, a pile group is more effective in capturing the rocking behaviour, and impart additional rocking stiffness under the columns due to group action. Hence, the *MF* is relatively larger for structures supported on single piles as compared to the piles in a group.

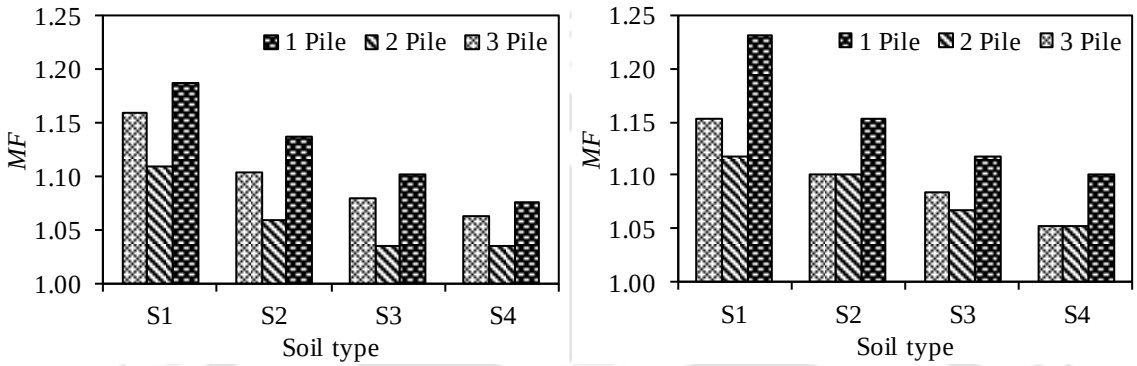

Figure 5.11 Variation of *MF* with pile configuration for (a) F3-15, and (b) F12-15 RC frame systems under different soil conditions.

For a particular foundation configuration, the type of soil governs the design of the foundation. In the present study, for soils of lesser stiffness, the size of the pile foundation increases in diameter (d_p) and/or length (l_p), as shown in Table A.3 of Appendix A. The properties of the pile foundation in conjunction with the soil determine the flexibility of the soil-pile foundation system. Figures 5.12a and 5.12b show the variation of *MF* with the average dimensions of pile (length and diameter) for short (3-storeyed) and tall (12-storeyed) RC building frames, respectively. It is observed that *MF* increases with the increase in pile length and diameter. Increase in both pile length and diameter indicates less stiff soil conditions, which ultimately leads to greater soil-pile foundation flexibility (thus higher *MF*). Although the size of the pile has been segregated in terms of length and diameter, however, the two parameters are correlated through pile deformability. Therefore, a dimensionless parameter has been used as a measure of pile foundation flexibility (Rovithis et al., 2009), and is expressed as shown in Eq. 5.3,

$$S_H = (l_p / d_p)(E_p / E_s)^{-0.25} \tag{5.3}$$

where E_p is the elastic modulus of the pile, and E_s is the elastic modulus of soil at a depth equal to the diameter of the pile. Stiffer piles possess smaller S_H, while flexible piles possess higher S_H. Figures 5.13a and 5.13b show the variation of *MF* versus average S_H of the pile foundation for various frame widths corresponding to the short (3-storeyed) and tall (12-storeyed) frames respectively. It is observed that for all structural configurations, the effect of SSI increases (*MF* increases) with the flexibility of piles. Moreover, the influence of pile foundation flexibility on short (3-storeyed) frame is greater for wider (45 m) configuration, while that for taller (12-storeyed) frame, it is greater for narrower (9 m) configuration. The results discussed herein are corresponding to the RC frame system, wherein the columns are supported by 3-pile group. Other configurations of pile foundation show similar trends and hence are not discussed for the sake of brevity.

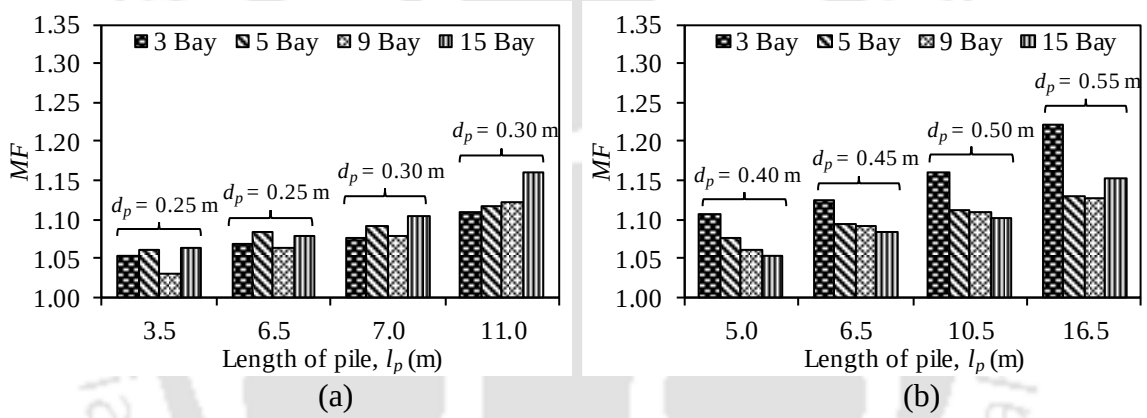

Figure 5.12 Variation of *MF* with pile length for (a) 3 storeyed, and (b) 12 storeyed RC frame systems.

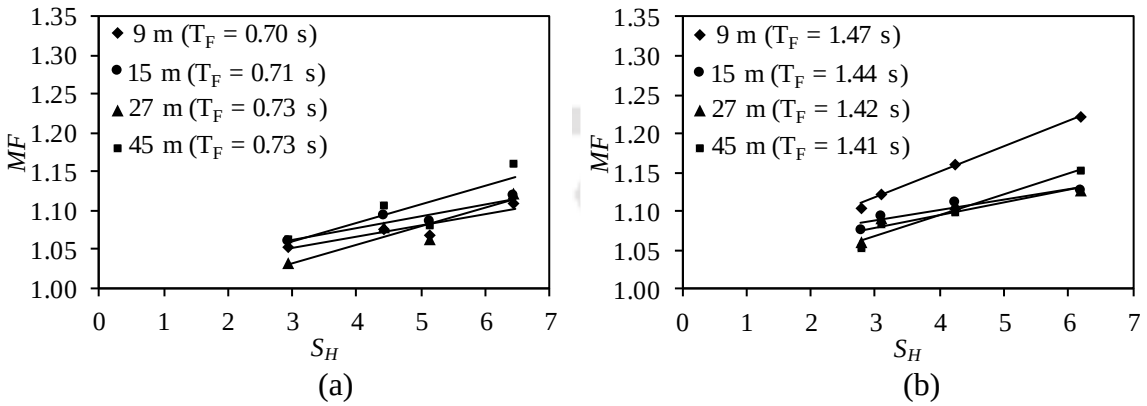

Figure 5.13 Variation of *MF* with S_H for (a) 3 storeyed, and (b) 12 storeyed RC frame systems.

5.4.5 RC Wall-frame System

The results obtained for RC wall-frame systems are presented in this section to discuss the parameters that govern the change in the fixed-base natural period due to SSI effects. In the present study, the shear wall is located in the central bay. Upon increasing the width of the frame, the shear wall area ratio (ratio of the cross-sectional area of the shear wall to the cross-sectional area of columns, $A_r = \sum A_w / \sum A_c$) reduces with a simultaneous increase in the overall mass of the RC wall-frame system. For the same height of the RC wall-frame system, this leads to an increase in the fixed-base natural period of the system.

Figures 5.14a and 5.14b show the influence of width on *MF* under different soil conditions for short (3-storeyed) and tall (9-storeyed) building frames, respectively. It can be observed that for 3 storeyed frames, upon increasing the width from 9 m (3-bay) to 45 m (15-bay), T_F increases from 0.12 s to 0.26 s. The variation of *MF* for narrow configuration (3-bay), under different soil conditions, is about 4.5 (S1) to 3.74 (S4), while that for a wider configuration (15-bay), it is about 2.9 (S1) to 2.5 (S4). For 9 storeyed frames, on increasing the width from 9 m to 45 m, T_F increases from 0.63 s to 0.90 s. The variation of *MF* for narrow configuration (3-bay), under different soil conditions, is about 1.73 (S1) to 1.61 (S4), while that for wider configuration (15-bay), it is about 1.43 (S1) to 1.27 (S4). Similarly, Figures 5.15a and 5.15b show the influence of height on *MF* under different soil conditions for the frames with narrow (3-bay) and wide (15-bay) configuration, respectively. For narrow configurations (9 m), on increasing the height from 3-storeys to 12-storeys, T_F increases from 0.12 s to 0.94 s. The variation of *MF* for 3 storeyed (short) frame, under different soil conditions, is about 4.5 (S1) to 3.74 (S4), while that for 12-storeyed (taller) frame, it is about 1.51 (S1) to 1.45 (S4). For wider frames (45 m), on increasing the height from 3 storeys to 12 storeys, T_F increases from 0.26 s to 1.17 s. The variation of *MF* for 3 storeyed (short) frame, under different soil conditions is about 2.9 (S1) to 2.5 (S4), while that for 12-storeyed (taller) frame, it is about 1.28 (S1) to 1.18 (S4). It can be observed that for stiffer frames, the SSI effects are greater, as indicated by higher *MF*. Increasing the width and height of an RC wall-frame system causes it to become flexible (increase in T_F), which reduces the SSI effects (smaller *MF*). For a particular RC wall-frame system, the SSI effects are highest for soft soil (S1) and reduce for stiffer soil conditions (S2, S3, and S4). Moreover, RC wall-frame systems with higher relative stiffness (ratio of structural stiffness to soil stiffness) exhibit greater SSI effects, i.e., stiffer frames

on softer soil conditions exhibit higher *MF*. A Similar observation has been reported by Renzi et al. (2013) when studying the effect of SSI on ordinary buildings resting on raft foundations.

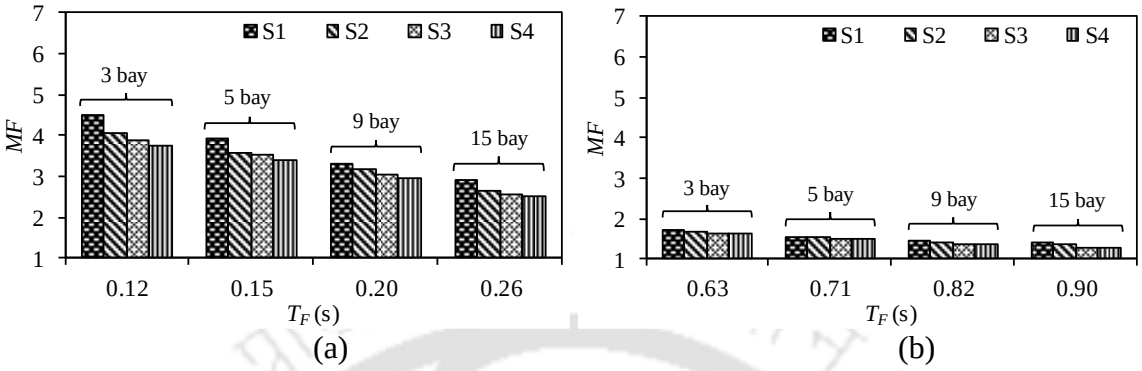

Figure 5.14 Variation of *MF* with T_F for (a) 3-storeyed, and (b) 9-storeyed building RC wall-frame systems

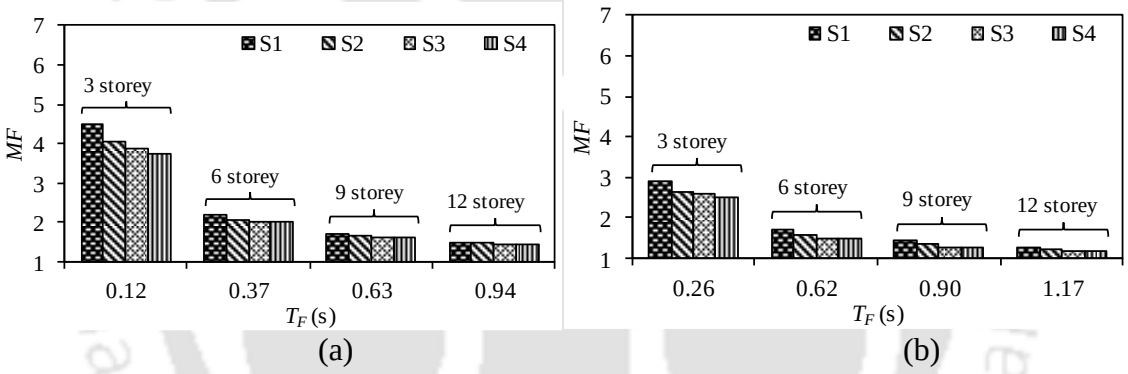

Figure 5.15 Variation of *MF* with T_F for RC wall-frame systems having widths of (a) 9 m, and (b) 45 m.

As for RC frame systems, in RC wall-frame systems as well, corresponding to a particular soil condition, the column members of the RC wall-frame system can be supported by pile foundations, which may consist of a single large diameter pile or multiple piles of smaller diameter (i.e., pile groups). For the same structure-soil combination, this may result in the variation of *MF*. Figures 5.16a and 5.16b, respectively, show the variation of *MF* for different configurations of pile foundation for W3-15 and W12-15 systems supported by various soil conditions. For the different pile foundation configurations, *MF* increases with a reduction in the stiffness properties of the soil. Moreover, in comparison to the building frame supported on single piles, the building frames supported by 3-piles or 2-piles group exhibit a slight reduction in *MF*. This is attributed to the fact that piles in a group are more effective in capturing the rocking behaviour and impart additional rocking

stiffness under the columns due to group action. Hence, *MF* is higher for structures supported by single piles and smaller for pile groups.

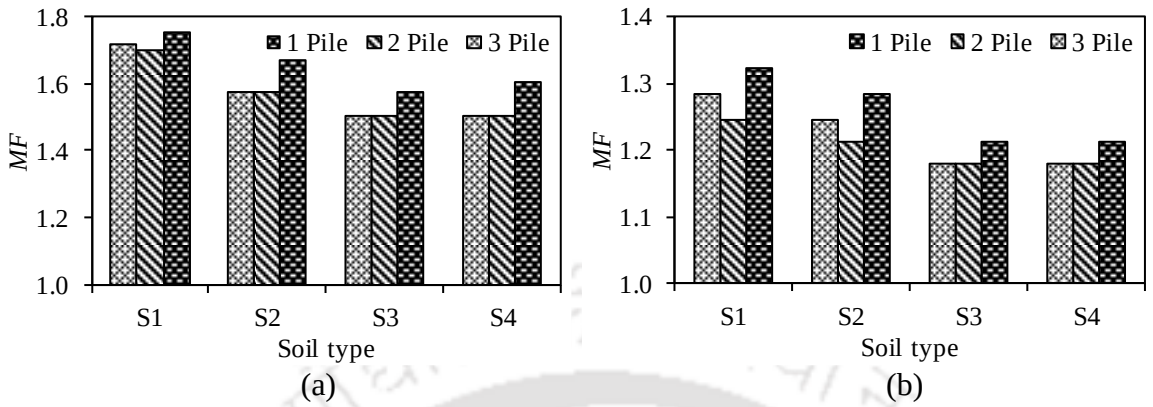

Figure 5.16 Variation of *MF* with pile configuration for (a) W3-15, and (b) F12-15 frame systems under different soil conditions.

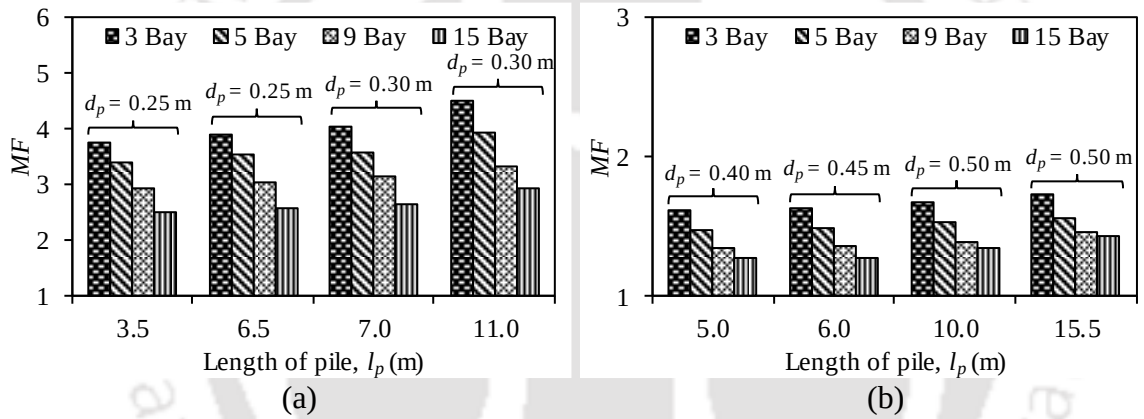

Figure 5.17 Variation of *MF* with pile length for (a) 3-storeyed, and (b) 9-storeyed RC wall-frame systems.

Figures 5.17a and 5.17b show the variation of *MF* with average dimensions (length and diameter) of the piles for 3-storeyed and 9-storeyed RC wall-frame systems, respectively. It can be observed that *MF* increases with the increase in pile length and diameter. An increase in both pile length and diameter indicates less stiff soil conditions, which ultimately leads to greater flexibility in the soil-pile foundation system, thus leading to higher *MF*. Figures 5.18a and 5.18b show the variation of *MF* against the average S_H of the pile foundation for various T_F corresponding to 3-storeyed and 9-storeyed RC wall-frame systems, respectively. It can be observed that for all structural configurations, the effect of SSI increases (*MF* increases) with an increase in flexibility of the piles. Moreover, this increase is greater for stiffer frames. For e.g., for a 3-storey frame with T_F = 0.12 s, as S_H increases from 3.23 to 6.97, *MF* increases from 3.74 to 4.5. However, for 3-storeyed

frames with T_F = 0.26 s, as S_H increases from 3.0 to 6.58, *MF* increases from 2.49 to 2.91. A Similar observation can be made for 12-storeyed RC wall-frame system. Hence, stiffer building frames on flexible pile foundation exhibit greater SSI effects. The results discussed herein are corresponding to the RC wall-frame system wherein the columns are supported by a group of three piles. Other configurations of pile foundation show similar trends and hence are not discussed for the sake of brevity.

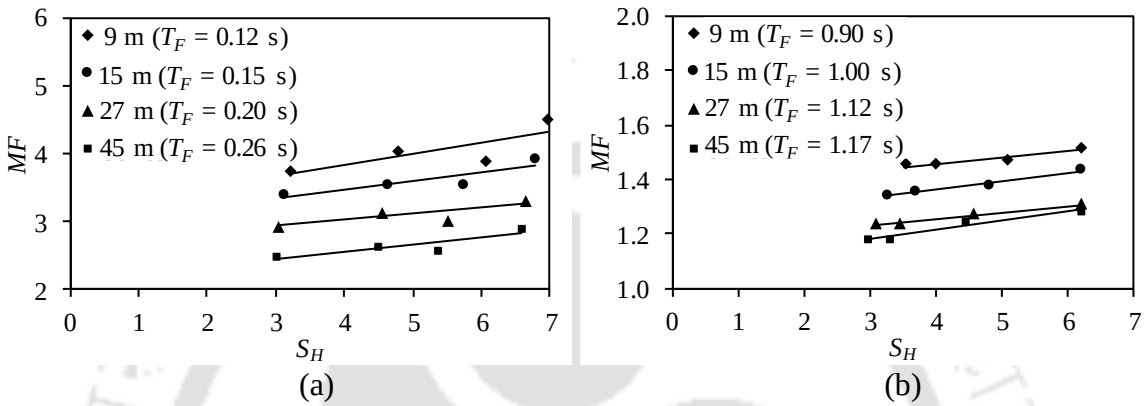

Figure 5.18 Variation of *MF* with S_H for (a) 3-storeyed, and (b) 12-storeyed RC wall-frame systems.

5.5 Development of ANN Model for Estimation of *MF*

An artificial neural network (ANN) architecture model is developed for the estimation of *MF* to be used in Eq. 5.1. A neural network architecture is subdivided into layers (viz., input layer, an output layer, and hidden layer), similar to the structure of the biological neural network in the human brain. These layers establish a complex relationship between the input and the output with the help of nodes known as neurons. Each neuron communicates with all other neurons in the different layers. In the input layer, these nodes are the input parameters, whereas, in the output layer, the nodes are representatives of the output. The nodes in the hidden layer represent mathematical functions defining the complex relationship between the input and the output parameters. Depending on the complexity and suitability, there may be multiple sublayers within the hidden layers. In the past, several studies have been carried out wherein multiple hidden layers have been used. However, although captivating, it has been found in many studies that ANN models with single hidden layer are good enough for modelling the input-output relationship for most problems (Momeni et al., 2014; Behera et al., 2013a & 2013b; Pala et al., 2008; Das and Basudhar, 2006; Mansour et al., 2004; Lee, 2003).

For any ANN model, a learning rule needs to be applied for the training of the hidden neurons. The most widely used learning rule is the Levenberg-Marquardt learning rule and is observed to be appropriate for most of the prediction problems (Hagan and Menhaj, 1994; Behera et al., 2013a). This rule follows a feedforward backpropagation algorithm. 'Tan sigmoid' is mostly used as the transfer function as it is adjudged as one of the most efficient in representing the biological behaviour of neurons (Acharyya et al., 2018). In the present study, the ANN model has been developed using MATLAB v2016a (MathWorks, 2001). A prerequisite for developing the ANN model is to ensure that equal weightage is given to each input and output variable. This is done by preprocessing the input and output data. The data is normalized to vary within the range from -1 to 1, using Eq. 5.4. This ensures that equal weightage is given to the input and output variable at the development stage of the ANN model.

$$X_n = \frac{2(X - X_{\min})}{(X_{\max} - X_{\min})} - 1 \tag{5.4}$$

In Eq. 5.4, X_n is the normalized value, $X_{\max}$ and $X_{\min}$ are the maximum and minimum values of the variable X. Subsequently, the determination of the number of neurons in the hidden layer is done with the aid of Eq. 5.5, so that the *MSE* (Mean Squared Error) of the output is minimum.

$$MSE = \frac{\sum_{i=1}^{n} (MF_{simulated} - MF_{predicted})^2}{n} \tag{5.5}$$

In Eq. 5.5, *MSE* is the mean of the squared error between the simulated and predicted output estimates, i.e., $MF_{simulated}$ and $MF_{predicted}$, respectively, and n is the number of data points. This ensures that an optimum number of neurons is selected as required in the ANN model to avoid underfitting or overfitting of the data. For this, a convergence study has been performed, and the plot of the *MSE* with the number of neurons in the hidden layer is shown in Figure 5.19a. It can be observed that for the dataset, the value of *MSE* is minimum corresponding to 6 neurons in the hidden layer. This results in a 9-6-1 architecture of the ANN model, as shown in Figure 5.19b. The input parameters considered are corresponding to the soil, pile foundations, and frame systems. The governing parameters for soil and foundation considered are the shear modulus (G_{soil}) corresponding to the depth equal to the

average diameter of the pile (d_p), the average length of the pile (l_p), and the number of piles (n_p). The superstructure system is described using five input parameters, namely the effective first mode modal stiffness of the building frame (K^*), effective first mode modal mass of the building frame (M^*), the height of the building frame (H), the width of the building frame (W) and the shear wall area ratio of the RC wall-frame (A_r). The output considered in the ANN architecture is the modification factor (MF) that has already been discussed in the earlier sections.

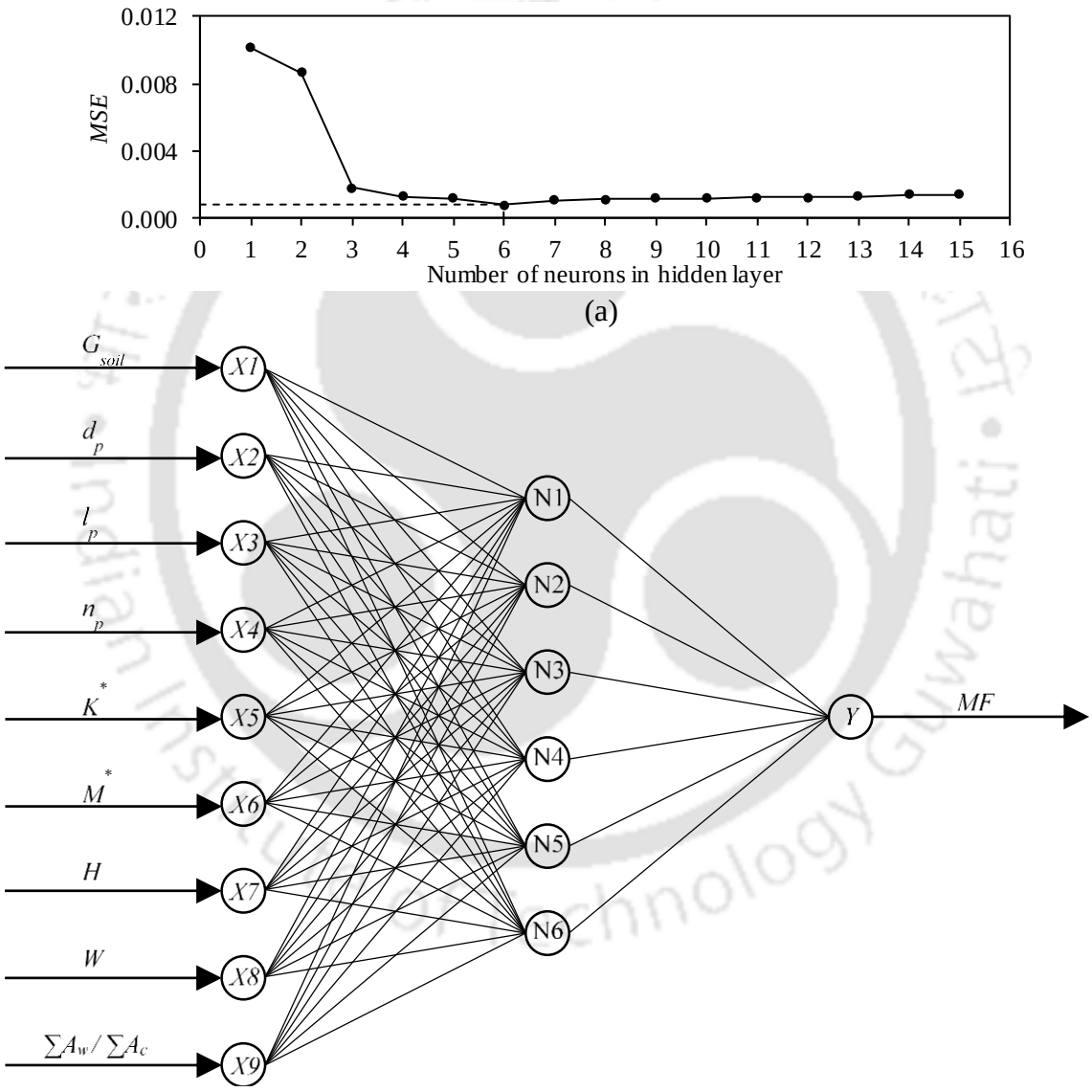

Figure 5.19 (a) Variation of MSE with varying numbers of hidden layer neurons; (b) A 9-6-1 ANN architecture used as a predictive tool for the present study.

Based on the FE simulations, a dataset comprising 384 input-output combinations are generated. The segregation (Ghaboussi et al., 1994) of the data is done such that 60%

of the complete dataset is used for the purpose of training and the remaining 40% for verification of the ANN model. The data used for verification is further subdivided into two equal halves, which is used for validation and testing. The weights and biases of the ANN model are adjusted such that the error between the predicted and simulated values of the output (in this case, the modification factor, *MF*) is minimum. It is important to stop the training at an optimum stage when the model is trained just enough to generalize the relationship without overfitting or underfitting the data. The training is stopped when the error, after reaching a minimum, subsequently increases for a certain number of iteration steps. In the present study, this optimum stage is achieved with the help of early stopping criteria (Acharyya and Dey, 2018; Momeni et al., 2014), in which the error corresponding to training data and testing data is obtained at each epoch (iteration) and is compared to the preceding epoch. This ensures the model is trained so that it is capable of generalizing the relationship without underfitting or overfitting of the data.

The performance of the developed ANN model during the training phase, validation phase, and testing phase are shown in Figures 5.20a, 5.20b, and 5.20c, respectively. It can be observed that the model is able to predict the values of the output quite well even when exposed to the testing dataset (dataset to which the model is not exposed while developing the model). The coefficient of efficiency R^2 for training, validation, and testing phases are found to be 0.99. Figures 5.20d and 5.20e show the performance of the developed model for RC frame and RC wall-frame systems respectively. The percentage error in the predicted values of *MF* is estimated using Eq. 5.6 and is shown in Figures 5.20f and 5.20g for RC frame systems and RC wall-frame systems, respectively.

$$\text{Error}_{MF} = \frac{MF_{simulated} - MF_{predicted}}{MF_{simulated}} \times 100\% \tag{5.6}$$

It can be observed that the maximum error in the output is less than 10% for both the systems. From the figures, it can be seen that the capability of the model to predict *MF* is quite sound and is equally good for the RC frame and RC wall-frame systems.

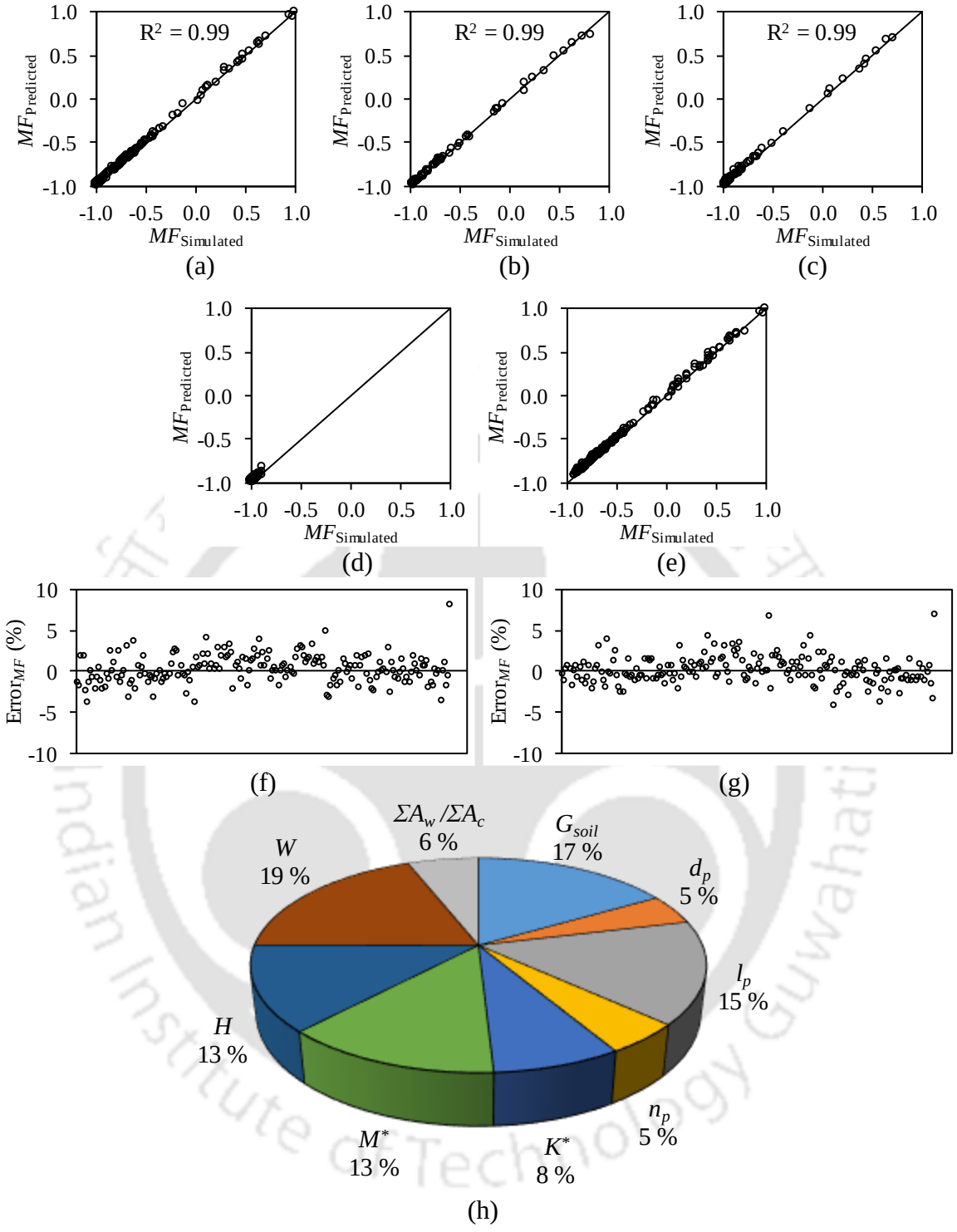

Figure 5.20 Performance of ANN model (a) training phase, (b) validation phase, (c) testing phase, (d) RC frame systems, and (e) RC wall-frame system; Error in *MF* for (f) RC frame systems, and (g) RC wall-frame systems; (h) Outcome of sensitivity analysis.

5.5.1 Sensitivity Analysis

A sensitivity analysis is essential to ascertain the influence of each input variable on the output. This is possible by estimating the relative importance of each variable with respect to each other. Garson's algorithm (Garson, 1991) has been employed to study the sensitivity of the various input variables on the modification factor (*MF*). As per Garson's algorithm, the connection weights (weights for input-hidden and hidden-output connections) are partitioned. The absolute values of the partitioned weights are then utilized for the determination of the relative importance of the input variables using Eq. 5.7,

$$\text{Relative Importance}_{Xm} = \sum_{j=1}^{n} \frac{\left| {}^{m}w_{IH}^{j} \right|}{\left(\sum_{k=1}^{N} \left| {}^{k}w_{IH}^{j} \right| \right) \left| w_{HO}^{j} \right|} \tag{5.7}$$

where *Xm* is the m^{th} input variable for which the relative importance is to be obtained, w_{IH} is the weight of the input-hidden connection, w_{HO} is the weight of the hidden-output connection, N (N = 9) is the total number of input variables and n (n =6) is the total number of neurons in the hidden layer. Table 5.1 shows the weights between the input layer and the hidden layer nodes. Table 5.2 shows the weight between the hidden layer nodes and the output node. Table 5.3 lists the biases of the input and output neurons after training. The relative importance and ranking of the various input parameters are shown in Table 5.4. The relative importance rank of individual variables highlights the fact that modification factor (*MF*) is highly influenced by the width (*W*) of the superstructure, shear modulus of the soil (G_{Soil}), followed by the length of the pile (l_p). The effective modal mass (M^*) and the height (*H*) of the superstructure, followed by its stiffness (K^*) are moderately influential. Shear wall area ratio ($A_r = \sum A_w / \sum A_c$), followed by the number of piles (n_p) and average diameter of the pile (d_p) have the least influence on the value of the modification factor (*MF*) in the developed model. The contribution of the importance percentage is shown in Figure 5.20h. It can be seen that approximately 42% of contribution is from the properties of the soil-pile foundation system, and 58% contribution is from the properties of the superstructure system.

Table 5.1 Weights of the neurons connecting the Input and hidden layer nodes

Input Variable		w_{IH} (input-hidden neuron weights)					
		N1	*N2*	*N3*	*N4*	*N5*	*N6*
X1	G_{Soil}	0.01	0.16	0.38	0.52	-0.86	1.34
X2	d_p	-0.20	0.12	0.30	0.61	-0.09	0.34
X3	l_p	-0.10	0.20	0.34	0.40	0.87	-0.25
X4	n_p	-0.04	0.09	0.28	0.28	-0.17	0.47
X5	K^*	-0.67	-1.81	-0.11	-0.67	0.10	-1.13
X6	M^*	0.54	-0.02	-0.96	-0.08	-0.59	-0.38
X7	*H*	0.45	-0.73	-1.03	-0.22	0.45	-0.86
X8	*W*	0.14	-0.13	0.004	-0.47	1.15	0.52
X9	$\sum A_w/\sum A_c$	-0.14	-0.76	-0.47	0.45	0.14	-0.06

Table 5.2 Weights of the neurons connecting the hidden and output layer nodes

Output *MF*	w_{HO} (hidden-output neuron weights)					
	N1	*N2*	*N3*	*N4*	*N5*	*N6*
Y	-0.97	-0.41	0.18	0.25	0.04	-0.44

Table 5.3 Biases of the neuron after training

b_0 (Bias of output node)	b_h (Bias of hidden layer neurons)					
	N1	*N2*	*N3*	*N4*	*N5*	*N6*
0.21	1.31	-2.32	-0.65	1.33	-1.35	2.67

Table 5.4 Weights of hidden input neurons

Input Variable		Outcome of Garson's sensitivity analysis	
		Relative Importance	Rank
X1	G_{Soil}	7.315	2
X2	d_p	1.991	9
X3	l_p	6.786	3
X4	n_p	2.052	8
X5	K^*	3.378	6
X6	M^*	5.710	4
X7	*H*	5.654	5
X8	*W*	8.300	1
X9	$\sum A_w/\sum A_c$	2.637	7

5.5.2 ANN-Based Predictive Relationship

The input-output relationship of the developed ANN model can be expressed in the form of a predictive mathematical relationship. Past studies have shown the usefulness of such relationships, and various researchers have developed ANN-based predictive relationships corresponding to different problems (Acharyya and Dey 2018; Garson 1991; Goh 1994; Das and Basudhar 2006). The general form of the normalized ANN equation is shown in Eq. 5.8.

$$MF_n = f_{lin}\left\{b_0 + \sum_{j=1}^{n}\left[w_{HO}^{j}\, f_{sig}\left(b_{hj} + \sum_{k=1}^{N} w_{IH}^{j} X_k \right)\right]\right\} \tag{5.8}$$

In Eq. 5.8, MF_n is the normalized output variable (MF) varying from -1 to 1, f_{sig} is the Tan sigmoid transfer function, f_{lin} is the linear transfer function, b_0 is the bias at the output layer, b_{hj} is the bias at the j^{th} neuron of the hidden layer, w_{IH} is the input-hidden weight, w_{HO} is the hidden-output weight, N (N = 9) is the total number of input variables, and n (n = 6) is the total number of neurons in the hidden layer. The developed equation utilizes the weights and biases obtained after training of the data, as shown in Tables 5.1 to 5.4. The normalized ANN equation needs to be expressed in a denormalized form for practical application. The final form of the developed ANN relation is shown in the following equation (Eq. 5.9),

$$MF = 0.5(MF_n + 1)(MF_{\max} - MF_{\min}) + MF_{\min} \tag{5.9}$$

where MF_{max} = 4.54, MF_{min}= 1.02, MF_n is the normalized modification factor and is expressed in Eq. 5.10.

$$MF_n = 0.21 + B_1 + B_2 + B_3 + B_4 + B_5 + B_6 \tag{5.10}$$

The expressions for B_1 to B_6 are shown in Eqs. 5.11a-5.11f,

$$B_1 = -0.97\left(\frac{e^{A_1} - e^{-A_1}}{e^{A_1} + e^{-A_1}}\right) \tag{5.11a}$$

$$B_2 = -0.41\left(\frac{e^{A_2} - e^{-A_2}}{e^{A_2} + e^{-A_2}}\right) \tag{5.11b}$$

$$B_3 = 0.18\left(\frac{e^{A_2} - e^{-A_2}}{e^{A_2} + e^{-A_2}}\right) \tag{5.11c}$$

$$B_4 = 0.25\left(\frac{e^{A_4} - e^{-A_4}}{e^{A_4} + e^{-A_4}}\right) \tag{5.11d}$$

$$B_5 = 0.04\left(\frac{e^{A_5} - e^{-A_5}}{e^{A_5} + e^{-A_5}}\right) \tag{5.11e}$$

$$B_6 = -0.44\left(\frac{e^{A_6} - e^{-A_6}}{e^{A_6} + e^{-A_6}}\right) \tag{5.11f}$$

where, A_1 to A_6 can be obtained from Eqs. 5.12a-5.12f.

$$A_1 = 0.01G_{Soil} - 0.2d_p - 0.1l_p - 0.04n_p - 0.67K^* + 0.54M^* + 0.45H + 0.14W - 0.14A_r + 1.31 \tag{5.12a}$$

$$A_2 = 0.16G_{Soil} + 0.12d_p + 0.2l_p + 0.09n_p - 1.81K^* - 0.02M^* - 0.73H - 0.13W - 0.76A_r - 2.32 \tag{5.12b}$$

$$A_3 = 0.38G_{Soil} + 0.3d_p + 0.34l_p + 0.28n_p - 0.11K^* - 0.96M^* - 1.03H + 0.004W + 0.47A_r - 0.65 \tag{5.12c}$$

$$A_4 = 0.52G_{Soil} + 0.61d_p + 0.4l_p + 0.28n_p - 0.67K^* - 0.08M^* - 0.22H - 0.47W + 0.45A_r + 1.33 \tag{5.12d}$$

$$A_5 = -0.86G_{Soil} - 0.09d_p + 0.87l_p - 0.17n_p + 0.1K^* - 0.59M^* + 0.45H + 1.15W + 0.14A_r - 1.35 \tag{5.12e}$$

$$A_6 = 1.34G_{Soil} + 0.34d_p - 0.25l_p + 0.47n_p - 1.13K^* - 0.38M^* - 0.86H + 0.52W - 0.06A_r + 2.67 \tag{5.12f}$$

5.6 Comparison of the Proposed Model with Past Studies

As already mentioned, a few past studies in the past have prescribed relationships for T_{SSI} and the corresponding expressions for *MF* are given in Table 5.5. Recapitulating, *MF* is described as the ratio of the effective natural period of the SSI system (T_{SSI}) to the fixed-base natural period (T_F). The expression for the effective natural period adopted by ATC 3-06 (1978) had been developed by Veletsos and Meek (1974) with the assumption that the structure is supported on shallow foundation. Gazetas (1996) provided an improved version of the expression provided in ATC 3-06 (1978) by including additional sway rocking stiffness component. Kumar and Prakash (2004) recommended a modified expression of the version given in ATC 3-06 for the estimation of effective natural period of the structures supported on pile foundations. The estimates of *MF* using the proposed ANN predictive relationship are compared with those available in the literature and with that obtained from

finite element simulations. These expressions require the estimation of foundation stiffness, and standard expression has been utilized (Gazetas 1991b) for the same. The results shown in this section are corresponding to the building frame system wherein the columns are supported by a group of three piles. Other configurations of pile foundation show similar trends and hence, are not discussed for the sake of brevity.

Table 5.5 T_{SSI} relationships proposed in past studies

Past Study	Expression	Remark
Veletsos and Meek (1974)	$MF = \frac{T_{SSI}}{T_F} = \sqrt{1+\frac{K^*}{K_x}+\frac{K^*H^2}{K_\phi}}$	Analytical equation developed for surface footings. Most widely used and adopted by seismic code e.g. ATC 3 (1978).
Gazetas (1996)	$MF = \frac{T_{SSI}}{T_F} = \sqrt{1+\frac{K^*}{K_x}+\frac{K^*H}{K_{x\phi}}+\frac{K^*H^2}{K_\phi}}$	Semi-empirical relation with additional sway rocking component.
Kumar and Prakash (2003)	$MF = \frac{T_{SSI}}{T_F} = \sqrt{1+\frac{60}{H}\left(\frac{K^*}{K_x}+\frac{K^*H^2}{K_\phi}\right)^{1.5}}$	Semi-empirical relationship proposed specifically for structure on pile foundation

MF = Ratio of fixed effective natural period to the fixed-base period of the system
T_{SSI} = Natural period of the structural system under the influence of SSI
T_F = Fixed-base natural period of the superstructure
H = Effective height of the superstructure
K^* = Effective stiffness of the superstructure under fixed-base condition
K_x = Lateral stiffness of the foundation
K_ϕ = Rotational stiffness of the foundation
$K_{x\phi}$ = Coupled sway rotational stiffness of the foundation

Figures 5.21a and 5.21b show a comparison of the estimates of *MF* for a few RC frame systems resting on S1 and S4 types of soil, respectively. Similarly, Figures 5.21c and 5.21d show a comparison of the estimates of *MF* for a few RC wall-frame systems resting on S1 and S4 types of soil, respectively. It can be observed that the estimates of *MF* using the proposed ANN equation show a very good and close agreement with those obtained from the finite element simulations. This is because the expressions have been developed using advanced finite element SSI models, considering several input parameters that are interrelated by means of a complex network. The expression given by past researchers provide estimates of the *MF* with a relatively larger difference from the FE simulated values when compared with the estimates provided by the proposed ANN relation. It can be observed that the expression adopted by ATC 3-06 (1978) and Gazetas (1996) provide lower estimates of the *MF* for the various cases considered. Although the expression proposed by Gazetas (1996) is an improved version of that given in ATC 3-06 (1978), still there exists a large difference in the estimates of *MF* with those obtained from the

simulations. This is due to the fact that these expressions are more appropriate for structures supported on shallow foundations. Similar observations have also been made in other studies (Kumar and Prakash, 2004; Rovithis et al., 2009).

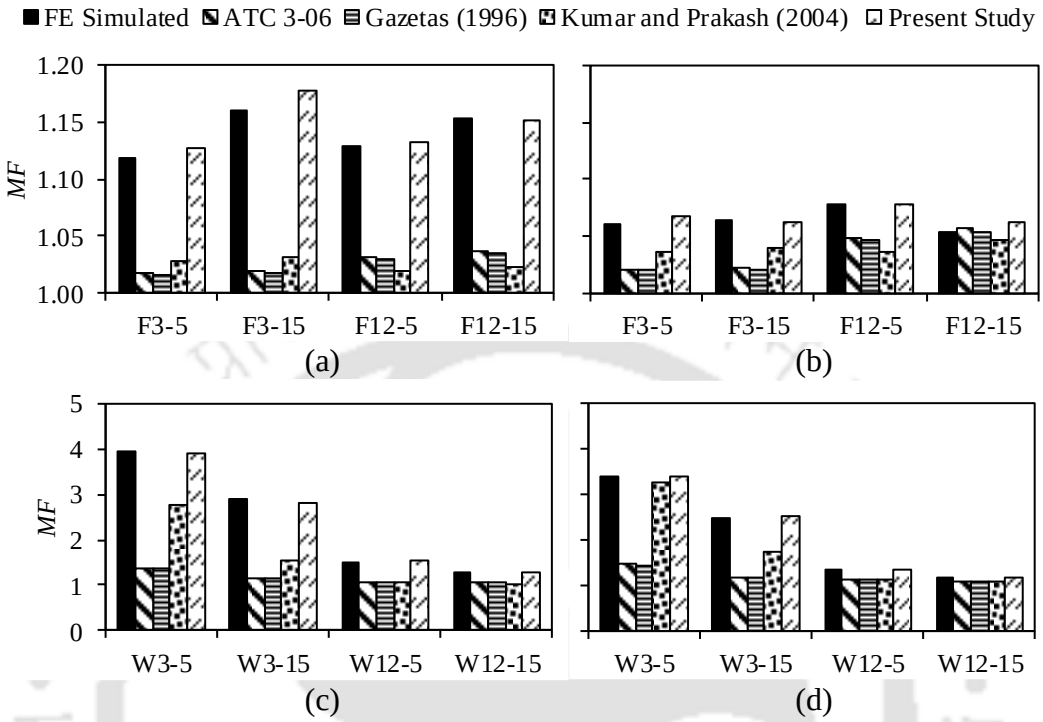

Figure 5.21 Comparison of the estimates of *MF* from the proposed relation with that from past studies for selected samples: (a) RC frame system on S1, (b) RC frame system on S4, (c) RC wall-frame system on S1, and (d) RC wall-frame system on S4.

The estimates of *MF* using the expression provided by Kumar and Prakash (2004) are relatively closer to the simulated values for many cases when compared with the estimates provided by ATC 3-06 (1978) and Gazetas (1996). This is because the expression provided by Kumar and Prakash (2004) is applicable to structures supported on pile foundations. However, the observed deviation from the FE simulated results is because the expression of Kumar and Prakash (2004) has been developed using a simplified‡ model and

‡ In the simplified modelling approach, the soil foundation system is not explicitly modelled, rather equivalent representation of the soil-foundation system is adopted in the form of impedance functions. The simplified approach for modelling requires the substructure method of analysis wherein the soil-foundation and structure response are evaluated separately. In the present study, the modelling approach adopted is a detailed one wherein the soil-pile foundation system is explicitly modelled along with the superstructure. In this method, single step technique is used for the analysis. The advantage of the simplified method is that it is computationally efficient although it is applicable for linear-elastic analysis. On the other hand, the detailed modelling, although computationally expensive, provides the advantage of considering inelasticity and allows the possibility of explicitly modelling and studying the soil-foundation behaviour

a small dataset. Additionally, for developing the regression-based relationships, Kumar and Prakash (2004) have utilized a very small dataset (60 cases). On the other hand, the dataset utilized for the training and validation of the ANN prediction model in the present study consisted of results obtained from finite element simulations, thereby comprising a significant number of dataset (384 cases) obtained from a detailed modelling approach. Hence, performance of the proposed ANN prediction model was observed to be much better as compared to the corresponding estimates from the relationships proposed by other researchers.The results presented here highlight the robustness of the ANN-based expressions proposed in the present study.

5.7 SUMMARY

Natural period is an important parameter of any structural system for characterizing the dynamic behaviour of the system. Thus, it has significant relevance in the context of the seismic behaviour of the structural system. The conventional practice is to use the fixed-base natural period (T_F) of the system. However, the presence of the soil-foundation system inevitably induces SSI effects onto the structural system, thereby leading to a change in the natural period. In this chapter, the SSI effects on the natural period of RC frame and RC wall-frame systems supported on pile foundation have been reported. Detailed finite element modelling of the superstructure and the soil-pile foundation system has been carried out to provide accurate estimates of the effective natural period (T_{SSI}) of several configurations of the superstructure and soil-pile foundation systems. The change in the fixed-base natural period under the influence of SSI for the frames was quantified in terms of the modification factor (*MF*). *MF* is the ratio of the effective natural period (T_{SSI}) to the fixed-base natural period (T_F) of the building frame. A parametric study was conducted to identify the influence of various input parameters of the SSI system on *MF*. A higher magnitude of *MF* indicated greater effects of SSI. Subsequently, a feed-forward back-propagation artificial neural network (ANN) model has been developed to form a predictive relationship for obtaining the modification factor (*MF*) for the determination of effective natural period (T_{SSI}) of RC frame and RC wall-frame systems supported on pile foundations.

The main summaries are as follows:

- In general, RC frame and RC wall-frame systems resting on loose soil exhibit greater SSI effects that reduce for stiffer soil conditions.

- In RC frame systems, an increase in the width of the structure does not result in a noticeable increase in *MF*. However, increasing the height of the structure causes a relatively larger increase in *MF*. Moreover, systems with extreme configurations (such as very short and wide or very tall and narrow frames) exhibit marginally greater SSI effects.
- In RC wall-frame systems, an increase in the width and the height was characterized by an increase in fixed-base natural period of the system. Systems with stiffer characteristics exhibited greater SSI effects as compared to the relatively flexible ones.
- RC frame and RC wall-frame systems whose columns are supported by single pile foundation system exhibit greater SSI effects as compared to those supported on group of two or three piles. When placed in a group, the piles are more effective in capturing rocking behavior and thereby impart additional rocking stiffness under the columns due to group action.
- The flexibility of the pile foundation, along with soil stiffness, plays a determining role in SSI effects. Building frames on pile foundations having greater flexibility (S_H) exhibit greater SSI effects that increase for systems with larger fixed-base stiffness. Thus, stiffer systems on flexible pile foundation exhibit greater SSI effects.
- The ANN prediction model is able to predict the modification factor (*MF*) accurately for the RC frame and RC wall-frame systems within a maximum tolerance level of 10%.
- Sensitivity analysis of the developed ANN model that the overall influence of the input parameters on the *MF* can be segregated as 42% provided by the soil-pile foundation properties, while the remaining 58% contribution is from the structural properties.
- The proposed ANN equation is able to provide relatively accurate estimates of *MF* when compared with those obtained using the expressions available in the literature. The observed differences are attributed to the fact that the expressions proposed by past researchers were developed either for SDOF on shallow foundation or for frame structures on pile foundations represented by simplified soil-foundation models. In the present study, the proposed ANN equation is developed using advanced finite element modelling and considers the intricate relationship between the various input parameters and the output. The developed model can be easily coded in any programing language or MS-Excel. Based on the known input parameters, the same can be used for quick

assertion whether or not the SSI effects would be important or negligible for a given RC frame and RC wall-frame system.

This page has been intentionally left blank.

Chapter 6
INFLUENCE OF SSI ON INELASTIC BEHAVIOUR: ASSESSMENT OF DUCTILITY CAPACITY

CONTENTS

6.1 OVERVIEW

Past studies on the seismic response of multi-degree-of-freedom (MDOF) systems under ultimate loading conditions have highlighted the inadequacies of force (strength) based design. It was observed in many cases that the design philosophy was inadequate to ensure the non-exceedance of structural strength. However, the actual seismic response of the buildings during strong earthquake shaking showed that along with the deficiency in strength, the inability of the buildings to undergo large inelastic deformations also led to severe damage or collapse. These observations paved the way for the present-day philosophy of earthquake-resistant design for RC structures. According to the design philosophy, during an earthquake, the overall seismic resistance of the RC buildings comprises of (a) strength capacity which resists fraction of the actual seismic demand on the structure and (b) deformation capacity which accounts for dissipation of seismic energy through inelastic deformations without significant reduction in strength. This ability of the building structure to offer resistance under large inelastic deformations, without significant

reduction in strength, is termed as 'ductility'. Under the fixed-base condition, the inelastic behavior of the superstructure contributes towards ductile behaviour. However, on incorporating the flexibility of foundation and soil, the inelastic behaviour of the superstructure gets modified because of the contributions of the pile foundations towards the inelastic response of the overall SSI system. This modification in the inelastic behaviour may modify the ductility capacity of the building system under SSI effects. The present chapter investigates the influence of SSI on the inelastic lateral load behavior of several[‡] RC frame and RC wall-frame systems. Subsequently, the modification in the inelastic behaviour is studied, and the variation in the ductility capacity due to SSI effects is assessed. Finally, some attention is given to study the role of shear wall in modifying the ductility capacity of an RC frame system.

6.2 Methodology for Assessing Inelastic Behaviour and Ductility Capacity

Displacement-controlled nonlinear static analysis has been carried out for assessing the inelastic behaviour of the RC frame and RC wall-frame systems with incorporated SSI effects. The adopted lateral load distribution adopted is corresponding to the first translational mode of the system that is incrementally applied by means of a displacement-controlled strategy. The mode shape profiles of RC frame and RC wall-frame systems are provided in Appendix B. To judge the performance of the SSI system under the lateral loads, an evaluation criterion needs to be defined. Past researchers (Mondal et al., 2013) have utilized inter-storey drift (ISD) limits, prescribed in codal guidelines (e.g., ATC 40, 1996; FEMA 356, 2000) for the evaluation of the global performance of structural systems. These limits are prescribed for various levels of damage states corresponding to different types of structural systems. Table 6.1 shows the various inter-storey drift limits corresponding to three different levels of damage states for different types of vertical elements of the RC structural system considered in the present study. For RC frame systems, the columns act as the primary lateral load resisting elements, and the global performance of the system is very much dependent on the storey level performance of these elements. Hence, for RC frame systems, the limits corresponding to concrete frames have been utilized. Similarly, for RC wall-frame systems, the damage incurred in the structural wall at a storey level (which provides a large share in the lateral load resistance) significantly affects the global

[‡]Note: The various configurations have been introduced in Chapter 5, and from this chapter onwards, the study is focused on the systems supported by pile foundation with group of three piles.

performance. Hence, for the RC wall-frame systems, the limits corresponding to concrete walls have been utilized for the purpose of performance evaluation.

Table 6.1 Lateral drift limits for performance evaluation (FEMA 356, 2000)

Element type	Performance levels		
	Immediate occupancy (IO)	Life safety (LS)	Collapse prevention (CP)
Column frames	1%	2%	4%
Concrete walls	0.5%	1%	2%

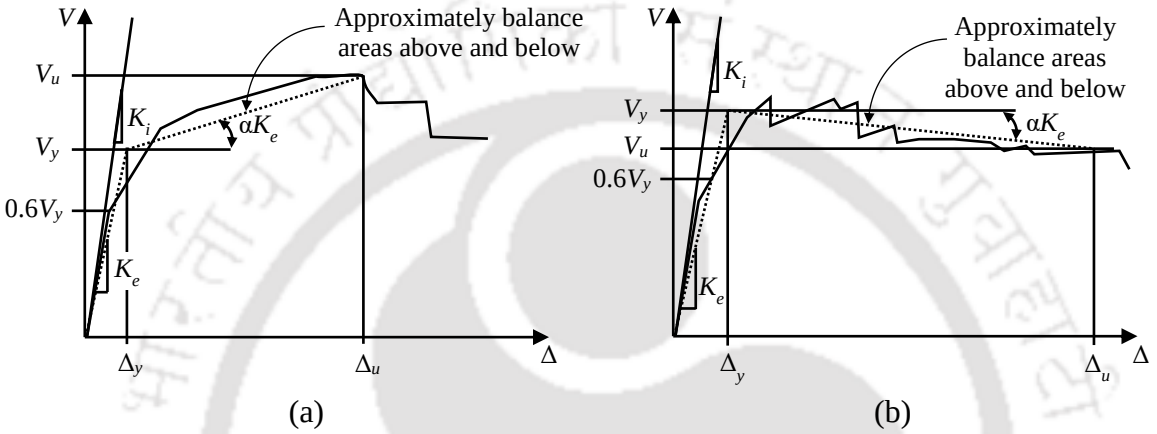

Figure 6.1 Bilinear idealization of pushover curves with (a) positive post-yield slope, and (b) negative post-yield slope (FEMA 356, 2000).

The outcome of the nonlinear static analysis is plotted in the form of roof drift (Δ, i.e., roof displacement with respect to the base and normalized with respect to the height of the superstructure) on the abscissa of a cartesian plot, and the shear force developed at the base of the superstructure (V) on the ordinate. To assess the global ductility capacity of the SSI system, the yield and ultimate performance states have been identified on the corresponding pushover curves of the system. The inter-storey drifts at each storey level are checked against the limits shown in Table 6.1 at every analysis step. The superstructure is considered to have achieved the ultimate state when, at a particular storey level, the inter-storey drift corresponding to the collapse prevention state (CP) is mobilized. The roof drift corresponding to this analysis step is recorded as the ultimate drift (Δ_u) of the structural system. For identification of the yield drift (Δ_y) of the structural system, the obtained pushover curves are bilinearized in accordance with the guidelines provided in FEMA 356. Figures 6.1a and 6.1b show the bilinear idealization of representative pushover curves having positive and negative post-yield slopes, respectively. The initial and post-yield slopes (K_e and αK_e) are determined iteratively, to simultaneously satisfy two criteria. The

criteria are stated as (a) approximate balance of the area above and below the actual and the idealized pushover curves, and (b) equating the effective lateral initial stiffness of the idealized curve to the secant stiffness of the actual curve corresponding to 0.6 times the yield strength (V_y). Once the ultimate and yield drifts are obtained, the global ductility capacity of the structural system can be obtained ($\mu_c = \Delta_u / \Delta_y$).

6.3 BEHAVIOUR OF SUPERSTRUCTURE SYSTEM

As already discussed, the various configurations of the RC frame and RC wall-frame systems subjected to lateral loads, have been analysed to obtain the inelastic behaviour while considering the influence of SSI. The results have been compared with the outcome from the fixed-base (FB) systems. The influence of SSI on the superstructure system is studied in terms of base shear, inter-storey drift, and plastic hinge rotation, which are discussed in the following subsections.

6.3.1 RC Frame System

Figures 6.2a-6.2d show the bilinear pushover curves of a few selected RC frames under the different soil-pile foundation conditions. The pushover curves are plotted in the form of base shear, which is normalized with respect to the weight of the superstructure, and lateral roof drift. The respective inter-storey drift profiles at the ultimate state are shown in Figures 6.2e-6.2h.

It can be observed that the influence of SSI on the maximum base shear is marginal, and its value for the SSI-incorporated case does not vary significantly from that of the fixed-base (FB) system (Figures 6.2a-6.2d). For e.g., V_{max} in F3-3 varies between 0.20-0.19 for S1 to FB conditions, while that corresponding to F3-15 is almost constant at 0.17. For F12-3, V_{max} varies between 0.15-0.14 for S1 to FB conditions, while that for F12-15, it varies between 0.16-0.14. The variation in the yield drift (Δ_y) for the frames have been observed to be quite insignificant. For e.g., Δ_y for F3-3 is observed to vary between 0.74-0.72 for S1 to FB conditions, while that for F3-15, the same varies between 0.68-0.7. For F12-3, slightly larger variation in Δ_y is observed, between 0.74-0.60 for S1 to FB conditions; however, for F12-15, the variation is yet negligible, ranging between 0.53-0.5. Insignificant variation in ultimate drifts (Δ_u) is observed for F3-3 (2.8-2.85 for S1 to FB conditions) and F3-15 (1.92-2.01 for S1 to FB conditions). However, discernible variation in Δ_u can be observed for F12-3 (2.69-2.14 for S1 to FB conditions) and F12-15 (1.25-0.96 for S1 to FB conditions).

From the foregoing observations, it can be noted that for short frame (3 storey), Δ_u under FB condition is relatively larger as compared to that obtained considering SSI conditions. For instance, under FB condition, Δ_u for F3-3 and F3-15, is 2.85 and 2.01, respectively, which is correspondingly reduced to 2.8 and 1.92 under S1 condition. For the taller frame (12 storey), the trend is reversed, wherein Δ_u is relatively lesser under FB condition compared to that observed under SSI condition. For e.g., under FB condition, Δ_u for F12-3 and F12-15, is 2.14 and 0.96, respectively, which is correspondingly increased to 2.69 and 1.25 under S1 condition. It is worth highlighting that for a particular height of RC frame system, under a given soil-pile foundation condition, increasing the width causes a reduction in the ultimate drifts. For e.g., Δ_u for 3-storeyed RC frame system under S1 condition reduces from 2.8 to 1.92 on increasing the width from 3 bays to 15 bays. Similarly, for 12-storeyed RC frame system, under S1 condition, on increasing the width from 3 bays to 15 bays, Δ_u reduces from 2.69 to 1.25.

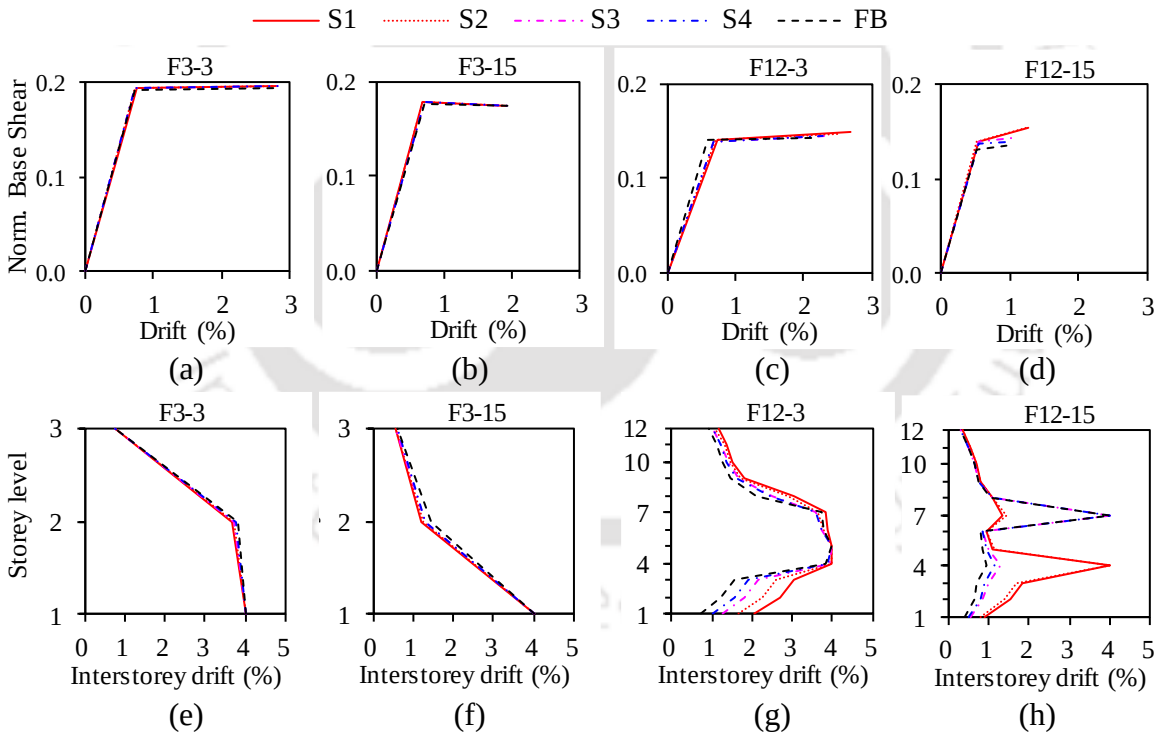

Figure 6.2 Influence of SSI on lateral load behaviour: pushover curves for (a) F3-3, (b) F3-15, (c) F12-3, and (d) F12-15; Inter-storey drift profiles for (e) F3-3, (f) F3-15, (g) F12-3, and (h) F12-15.

Figures 6.2e and 6.2f respectively show the inter-storey drift (ISD) profile for F3-3 and F3-15, under different soil-pile-foundation (SPF) conditions. For these frames, the peak ISD under different foundation conditions develops at storey level 1 (L1). Although the

variation under the different soil-pile foundation conditions is not significant, however, it can be observed the ISD profiles possess the largest and lowest values under FB and S1 conditions, respectively. This is the reason that the ultimate drifts of the short 3-storey frames under SSI conditions are observed to be lower than that under FB condition. Similarly, Figures 6.2g and 6.2h, respectively, show the ISD profile for F12-3 and F12-15 under the various considered SPF conditions. For F12-3, it can be observed that the peak ISD develops at L4 for all the SPF conditions. For F12-15 under S1 and S2 conditions, the peak ISD develops at L4; however, for other SPF conditions (S3, S4 and FB), the same develops at L7. Moreover, the ISD profile of these frames possesses highest values under the maximum SSI influence and lowest under FB condition (for F12-15, in contrary to the ISD profiles of S3, S4 and FB exhibiting the peak at L4, the other two SPF conditions, i.e., S1 and S2, the ISD profiles develop peak at L4). This causes the ultimate drifts of the taller frames (12 storey) under SSI condition to be higher, while the same is relatively lower for FB conditions. On comparing the ISD profiles of the 3-storeyed frames having narrow (F3-3) and wide (F3-15) configurations, it can be observed that compared to the narrower configuration, the wider configuration exhibits lower values of ISD under all SPF conditions. Similar observation is made for narrow and wide configurations of the 12-storeyed frame system. Wider frames, having a larger number of members at each storey level, possess larger redundancy. Consequently, they thereby inhibit large ISD values, except at the storey developing the impending collapse. Hence, once yielding begins, the inelasticity aggravates at a storey level, without the development of large ISD values at other storey levels. Narrower frames, on the other hand, develop large ISD values at the storeys where collapse is not imminent as well. This causes the frames with narrower configurations to exhibit larger Δ_u, which reduces upon increasing the width of the frames corresponding to a fixed height.

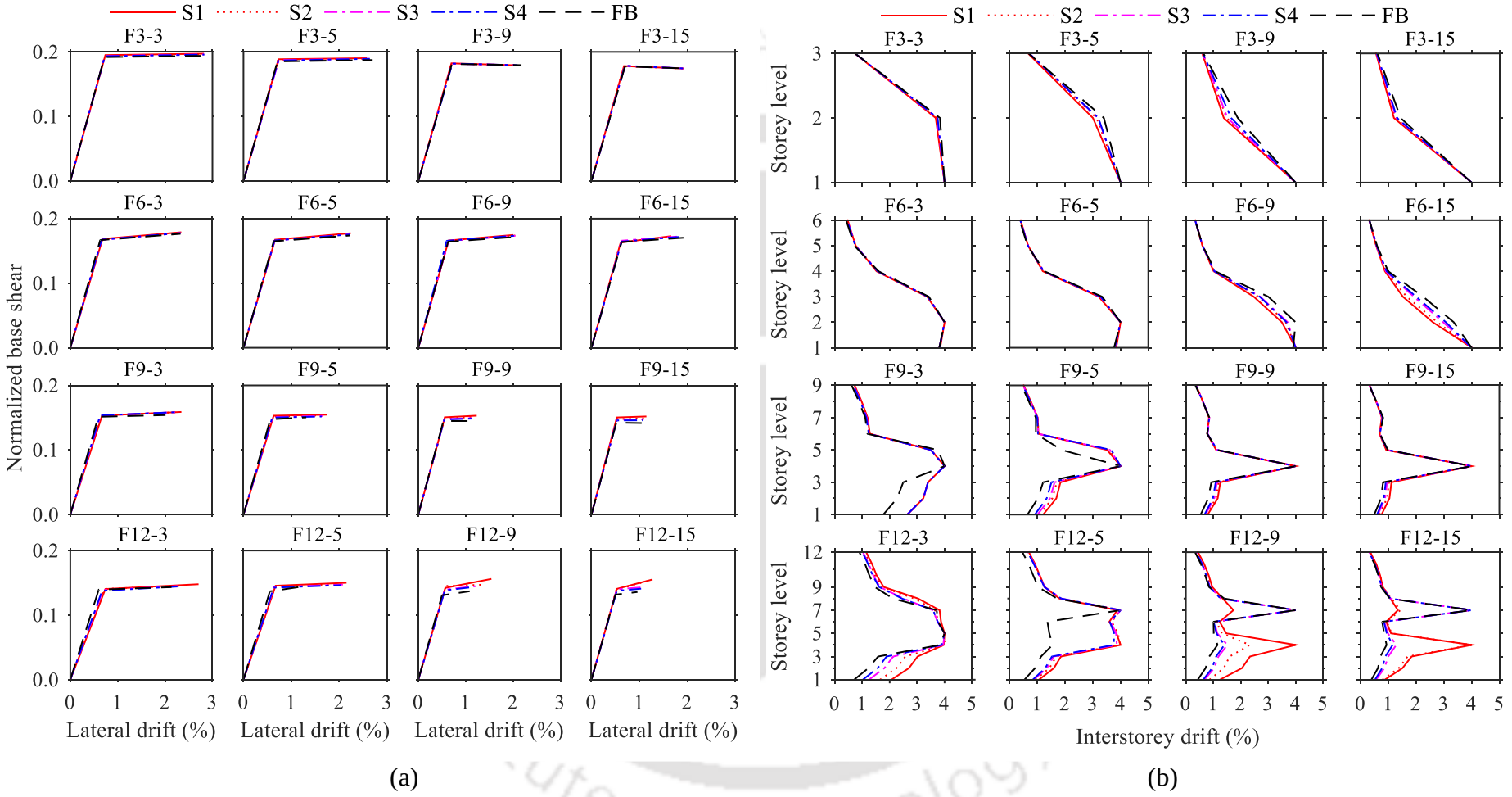

Figure 6.3 Influence of SSI on inelastic behaviour of RC frame systems of the various configuration shown in the form of (a) pushover curves, and (b) inter-storey drift profiles.

The foregoing discussion was limited to a few selected frames. The pushover curves and ISD profiles of the other configurations of the RC frame system are shown in Figures 6.3a, and 6.3b, respectively, and a qualitative discussion is presented in the following. From Figure 6.3a, it can be observed that for almost all the configurations, the influence of SSI on base shear is negligible. The influence of SSI on Δ_y and Δ_u is also quite marginal for most of the configurations, however, it is somewhat observable for a few configurations (F9-3, F9-5, F12-3, F12-5, F12-9, and F12-15). From Figure 6.3b, it can be observed that the variation of the ISD profile is negligible for some frames (F3-3, F3-15, F6-3, F6-5, F9-9and F9-15), while for others (F3-5, F3-9, F6-9, F6-15, F9-3, F9-5, F12-3, F12-5, F12-9 and F12-15) it is quite discernible. Corresponding to the frame systems with smaller height (3-storeyed and 6-storeyed frames), the development of peak ISD is at the lowermost storey level (for F6-3 and F6-5, peak ISD is at L2). Moreover, for these frames, when compared with FB condition, the ISD profiles possess lower values under the influence of SSI (lowest for S1). This leads to Δ_u to be lower under the influence of SSI. For taller frames (9-storeyed and 12-storeyed frames), peak ISD develops at higher storey levels (L4 for 9-storeyed frames; L4 and L7 for 12-storeyed frames). When compared with the FB condition, the ISD profiles possess larger values under the influence of SSI (highest for S1 condition). The observed phenomenon causes Δ_u to be larger under the influence of SSI. For a fixed height of the frame, increasing the width causes a reduction in the ISD values at storey levels adjacent to the one where collapse is imminent (the reason for such a behaviour has been discussed previously). This observation is true for all the considered SPF conditions. For a few frames (F12-3, F12-5, and F12-15), SSI causes a shift in the location of imminent collapse developed at a storey.

Although ISD has been utilized as a criterion for the performance evaluation, it provides only an approximate estimate of the plastic hinge rotation developed at each storey level in the structure. To study the influence of SSI on the plastic hinge rotation of the RC frame system, the absolute value of rotation (AVR) is obtained at the different storey levels. The absolute value of rotation (AVR) at a particular storey level is the summation of the plastic hinge rotations of all the elements (beams and columns) corresponding to that particular storey level. For the considered frame systems under different SPF conditions at the ultimate state, the AVR profile is shown in Figure 6.4. From the figure, it can be observed that for most of the frames, the influence of SSI on the AVR profiles is quite small. For short (3-storeyed and 6-storeyed) frame systems, only a slight reduction in AVR values

is observed above L1. For taller frame systems with 9 storeys, observable variation is seen for F9-3 and F9-5, while for 12-storeyed frames, the variation is observable for all the configurations. For these frames under SSI condition, AVR at L1 is relatively higher (highest for S1), while that at higher storey levels (where peak AVR develops), it is relatively lesser than that observed under FB condition. Frame systems F12-9 and F12-15 under weaker soil conditions (S1 and S2) exhibit peak AVR at L4, whereas for stiffer soils (S3 and S4) and FB condition, the peak AVR is exhibited at L7, thereby indicating a shift in the location of the impending collapse.

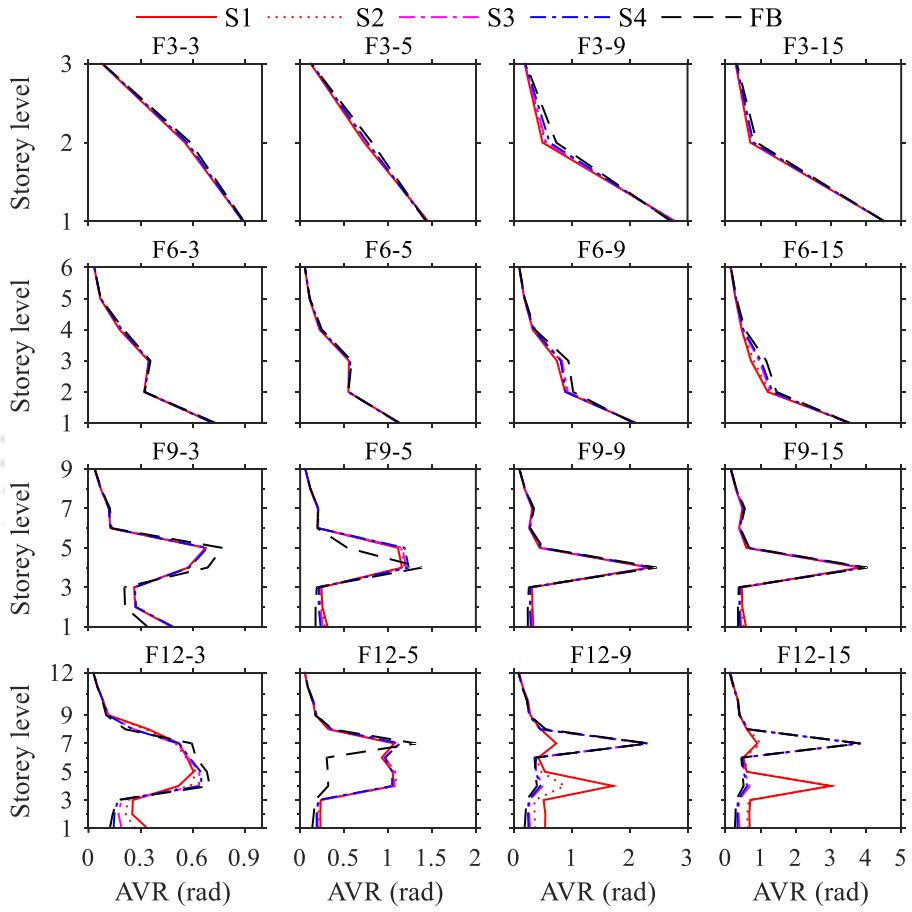

Figure 6.4 Influence of SSI on the absolute value of rotation (AVR) of the RC frame system of various configurations.

6.3.2 RC Wall-frame System

As in the case of frame systems, under the influence of SSI, various configurations of the RC wall-frame systems have been analysed to obtain the pushover curves, and the results have been compared with the fixed-base (FB) systems. Figures 6.5a-6.5d show the bilinear pushover curves of a few selected RC wall-frame systems under the different soil-pile foundation conditions; their respective inter-storey drift profiles, at the ultimate state, are

shown in Figures 6.5e-6.5h. The major observations are discussed in the following paragraphs.

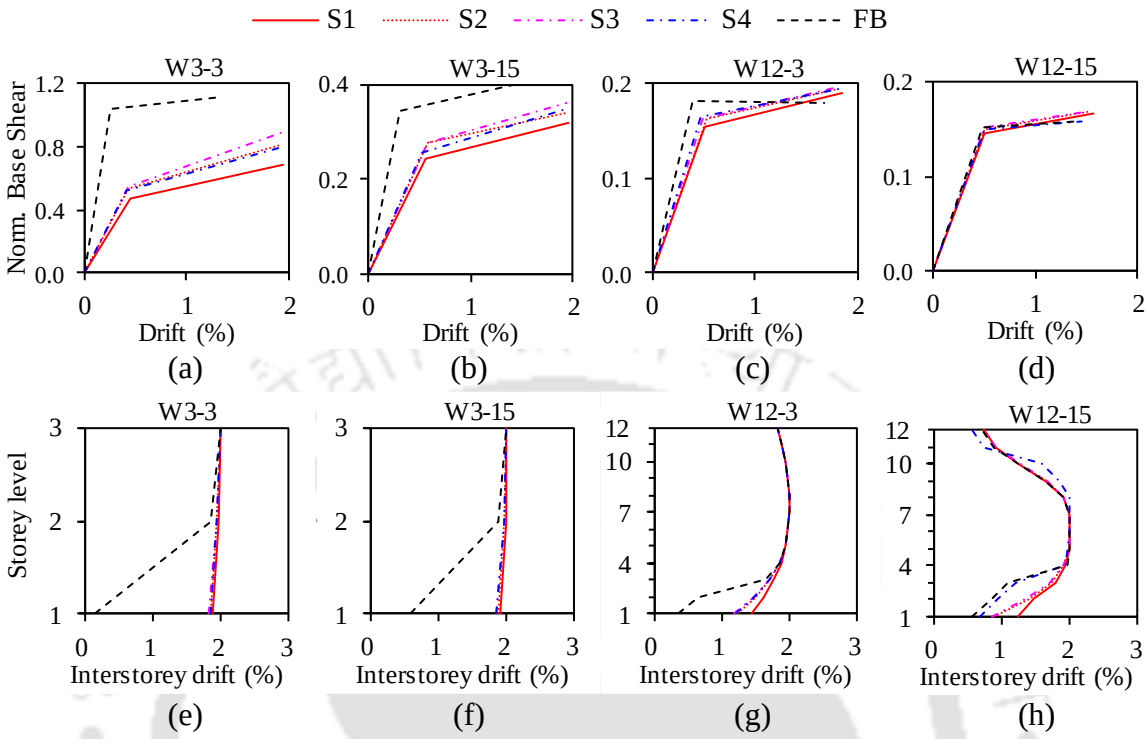

Figure 6.5 Influence of SSI on lateral load behaviour: pushover curves for (a) F3-3, (b) F3-15, (c) F12-3, and (d) F12-15; Inter-storey drift profiles for (e) F3-3, (f) F3-15, (g) F12-3, and (h) F12-15.

From the Figures 6.5a-6.5d, the pushover curves of the RC wall-frame systems under SSI conditions show significant variation in the yield and maximum shear capacities from that observed for FB condition, unlike that observed for RC framed systems. For e.g., V_{max} for W3-3 varies between 0.69-1.11 for S1 to FB conditions, while for W3-15, the same varies between 0.32-0.40 for S1 to FB conditions. Similarly, for W12-3, V_{max} varies between 0.19-0.18 for S1 to FB conditions, while for W12-15, the variation in V_{max} is observed between 0.17-0.16. The variation in the yield drift (Δ_y) for the wall-frame systems have been observed to be quite evident. For e.g., for W3-3, Δ_y is observed to lie between 0.44-0.26 for S1 to FB conditions, while that for W3-15, it varies between 0.57-0.31. For W12-3, slightly reduced variation in Δ_y is observed, between 0.52-0.4 for S1 to FB conditions; however, for W12-15, the variation is still negligible, ranging between 0.5-0.48 for S1 to FB conditions. Significant variation in ultimate drifts (Δ_u) is observed for W3-3 (1.95-1.33 for S1 to FB conditions) and F3-15 (1.96-1.491 for S1 to FB conditions). However, the variation in Δ_u is reduced for W12-3 (1.86-1.68 for S1 to FB conditions) and W12-15 (1.57-

1.4 for S1 to FB conditions). From the foregoing observations, it can be noted that for both shorter and taller RC wall-frame systems, under FB conditions, Δ_u is relatively smaller as compared to that observed under SSI conditions, the difference being lesser for taller systems. For instance, for W3-3 and W3-15 under SSI conditions, Δ_u is obtained as 1.95 and 1.96, which is respectively reduced to 1.33 and 1.49 under FB conditions. However, for W12-3 and W12-15, Δ_u under SSI conditions is 1.86 and 1.57, which reduces by a relatively smaller margin to 1.68 and 1.4, respectively. For 3-storeyed wall-frame system, under SSI conditions, Δ_u exhibits insignificant variation upon increasing the width from 3 bays to 15 bays (for S1 condition, Δ_u changes from 1.95 to 1.96); although, under FB condition, Δ_u increases from 1.33 to 1.49. Nevertheless, for 12-storeyed wall-frame systems, Δ_u exhibits a reduction upon increasing the width from 3 bays to 15 bays for SSI as well as FB conditions (for S1 condition, Δ_u changes from 1.86 to 1.57, while for FB condition, Δ_u changes from 1.68 to 1.4).

Figures 6.5e-6.5h respectively show the inter-storey drift (ISD) profile for W3-3, W3-15, W12-3, and W12-15, under different SPF conditions. It can be observed that although the variation under the different SPF conditions is not significant towards the higher storey levels, however, at L1, the ISD under FB condition is significantly lower in comparison to the SSI condition. For these RC wall-frames, it can be observed that the ISD profiles possess larger values under S1 conditions as compared to that obtained for FB condition. This is the cause for the wall-frame systems exhibiting higher Δ_u under SSI than that observed under FB condition. The peak ISD for 3-storeyed wall-frame system develops at the top storey level (L3); however, for 12-storeyed wall-frame system, the peak ISD develops at intermediate storey levels (L4-L8). The ISD profiles of these wall-frames possess the highest values under maximum SSI influences (S1) and lowest under the FB condition. On comparing the ISD profiles of the 3-storeyed wall-frames with narrow (W3-3) and wide (W3-15) configuration, it can be observed that, for all SPF conditions, similar ISD profiles develop in terms of shape and magnitude. This causes the 3-storeyed wall-frames to exhibit similar Δ_u upon increasing the width (from 3 bays to 15 bays). For 12-storeyed wall-frame systems, under all SPF conditions, ISD profiles of the narrower configuration (W12-3) exhibit larger ISD values at several storey levels (above L7) as compared to the wider configuration (W12-15). This causes 12-storeyed wall-frames to exhibit a reduction in the Δ_u upon increasing the width (from 3 bays to 15 bays).

The pushover curves and ISD profiles of other RC wall-frame systems are shown in Figure 6.6a and 6.6b, respectively, and a qualitative discussion is presented herein. From Figure 6.6a, it can be observed that for almost all the RC wall-frame specimens, those under S1 condition have the lowest base shear capacity, while those under FB condition exhibited the highest magnitudes. This is obvious as, under the FB condition, it is expected that the foundation system will attract larger forces as compared to that under the SSI cases. Moreover, the variation in V_{max} is observed to be the largest for W3-3 (most stiff) and least for W12-15 (most flexible). Moreover, for a fixed height of the wall-frame system, V_{max} reduces upon increasing the width from 3 bays (relatively stiff) to 15 bays (relatively flexible). This indicates that the effect of incorporating soil-foundation flexibility is more influential for a stiffer system. Among the SSI cases, for a few instances, the wall-frame system under the S3 condition exhibits larger V_{max}. For instance, it can be observed that corresponding to W3-3, W3-5, W3-9, and W6-3, V_{max} is larger under S3 condition when compared to that obtained from other SSI conditions. The influence of SSI on Δ_y is quite observable for most of the configurations and is marginal for a select few (e.g., W9-9, W9-15, W12-9, and W12-15). Similarly, the influence of SSI on Δ_u is observable for most of the configurations and is negligible for W9-3, W9-5, and W9-9 wall-frames.

From Figure 6.6b, it can be observed that for the considered specimens, the variation in the ISD profile is negligible at higher storey levels. However, at L1 level, significant variation is observed, with the exception of 9-storeyed wall-frame systems, wherein negligible variation is observed even at L1 level. For 3-storeyed wall-frame systems, the ISD at L1 level does not show significant variation under the different SSI conditions, although they are significantly higher than that obtained for the FB conditions. For 6-storeyed wall-frame systems, the ISD at L1 is largest for S1 followed by S3, S2, S4, and is the least for FB condition. For 9-storeyed wall-frame systems, the variation in ISD at L1, for various support conditions (SSI or FB), is observed to be very small. This is attributed to a similar magnitude of inelasticity developed at that level for the different SPF conditions. For 12-storeyed wall-frame systems, under the different SPF conditions, significant variation in ISD at L1-L3 is observed with the largest being at L1 level. In some cases, when compared with less stiff soil conditions, larger ISD is observed for stiffer soil conditions (e.g., for W12-9, at L1 level, ISD for S4 condition is larger than that obtained for S3 condition).

Figure 6.7 shows the AVR profiles of the various RC wall-frame systems under different SPF conditions. As mentioned earlier for RC frame systems, similarly, the absolute value of rotation (AVR) at a storey level in the wall-frame systems, is the summation of the plastic hinge rotation of all the beams, column and shear wall elements. With the exception of 9-storeyed frame, the AVR profiles for wall-frame systems exhibit significant variation at the lower storey levels (particularly L1). It can be observed that in comparison to the FB condition, the presence of SSI causes a significant increase in AVR at L1, which is observed to be maximum for the poorest soil condition (S1). At other storey levels, for several specimens, FB condition exhibits slightly larger AVR values (e.g., at L2 for W3-3, W3-5, and W3-15; at L2 for W6-9; and, at multiple storey levels for W9-3, W9-5, W9-9, W9-15, W12-3, W12-5, and W12-9). For a number of specimens, it is observed that at L1 level, AVR for frames resting on stiffer soil conditions is observed to be higher than that obtained for frames resting on poorer soil conditions. For example, corresponding to W6-3, W6-5, W6-9, and W6-15, AVR for S4 is larger than that obtained for S2 condition; while, corresponding to W12-9 RC wall-frame, AVR for S4 is larger than that obtained for S3 condition.

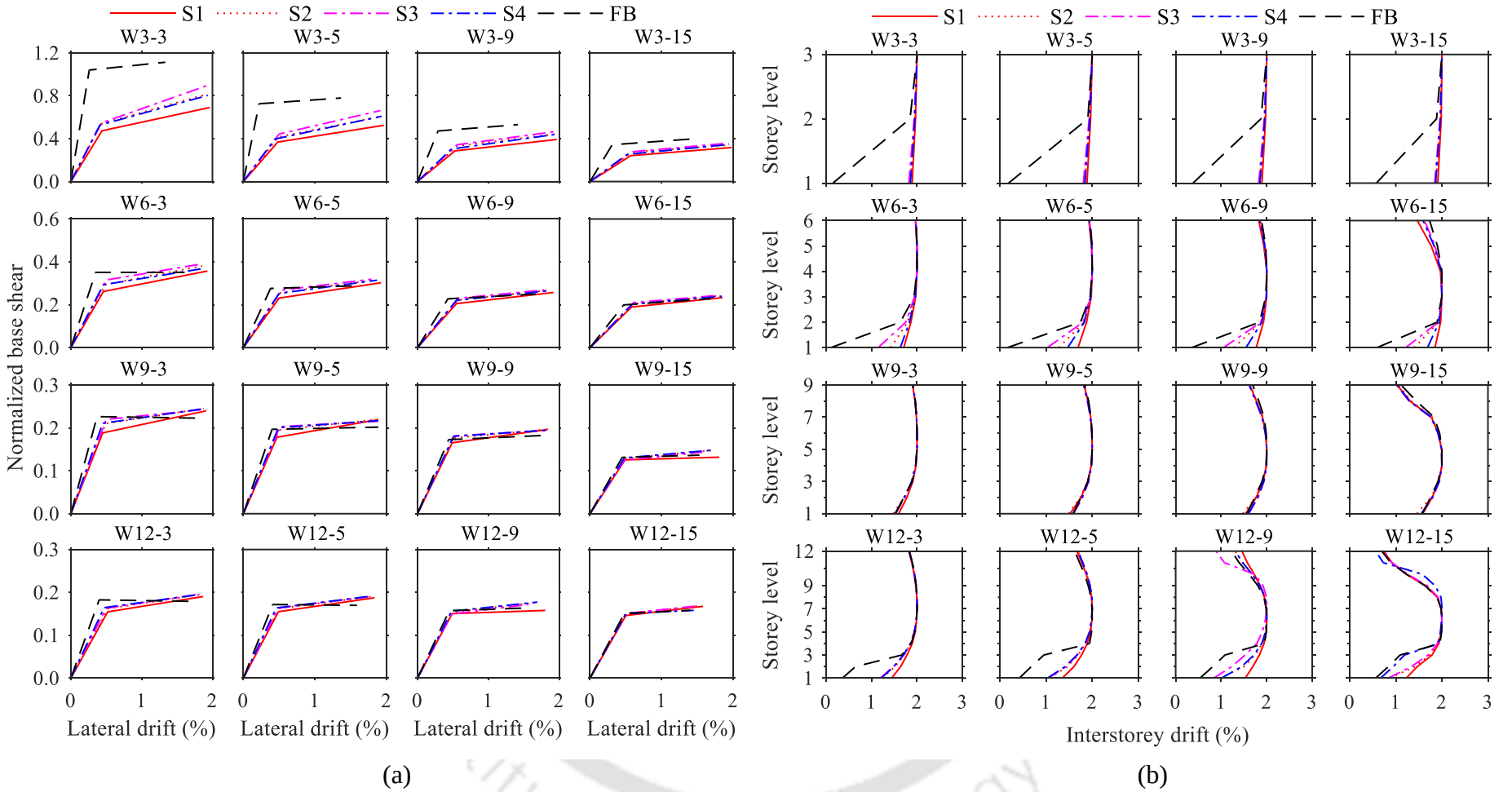

Figure 6.6 Influence of SSI on inelastic behaviour of RC wall-frame systems: (a) pushover curves, and (b) inter-storey drift profile.

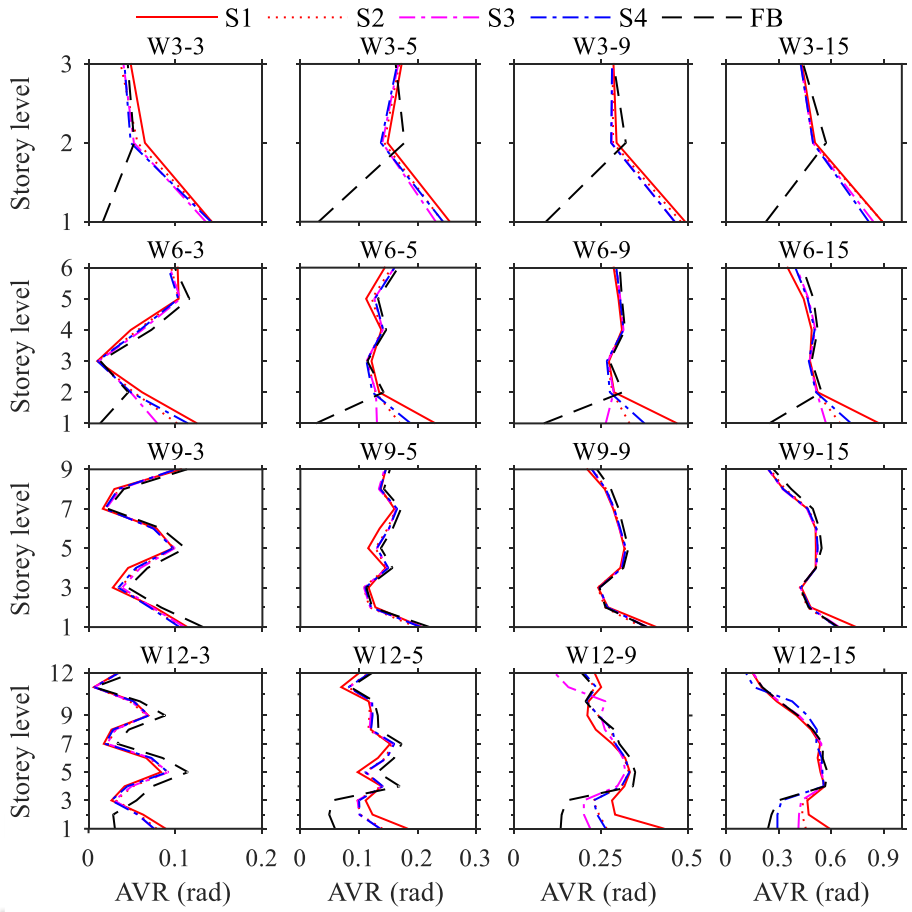

Figure 6.7 Influence of SSI on the absolute value of rotation (AVR) of RC wall-frame systems of various configurations.

6.4 BEHAVIOUR OF SOIL-PILE-FOUNDATION SYSTEM

The behavior of the substructure system may significantly influence the behaviour of the superstructure system. The response of the soil-pile-foundation system for the RC frame and RC wall-frame system may be different owing to the variation in the response of the superstructure. Moreover, for a particular type of system, different configurations of the superstructure and substructure may lead to a variation of response. The following sub-sections discuss the influence of SSI on the rocking of the pile-group foundation and the inelastic rotation in the piles supporting the RC frame and RC wall-frame systems at their ultimate state.

6.4.1 RC Frame System

Foundation rocking is an important response parameter that is influenced by the response of the superstructure, and at the same time, influences the superstructure response as well. The magnitude of rocking exhibited may be influenced by the magnitude of axial load transferred onto the group. Under lateral loading, the different foundation groups experience varying magnitudes of axial forces. For RC frame systems, four groups of pile foundation are considered wherein two belong to the exterior most columns (E' with least compression and E with the highest compression), and the other two belong to the innermost columns (I' with relatively lesser compression and I with relatively higher compression).

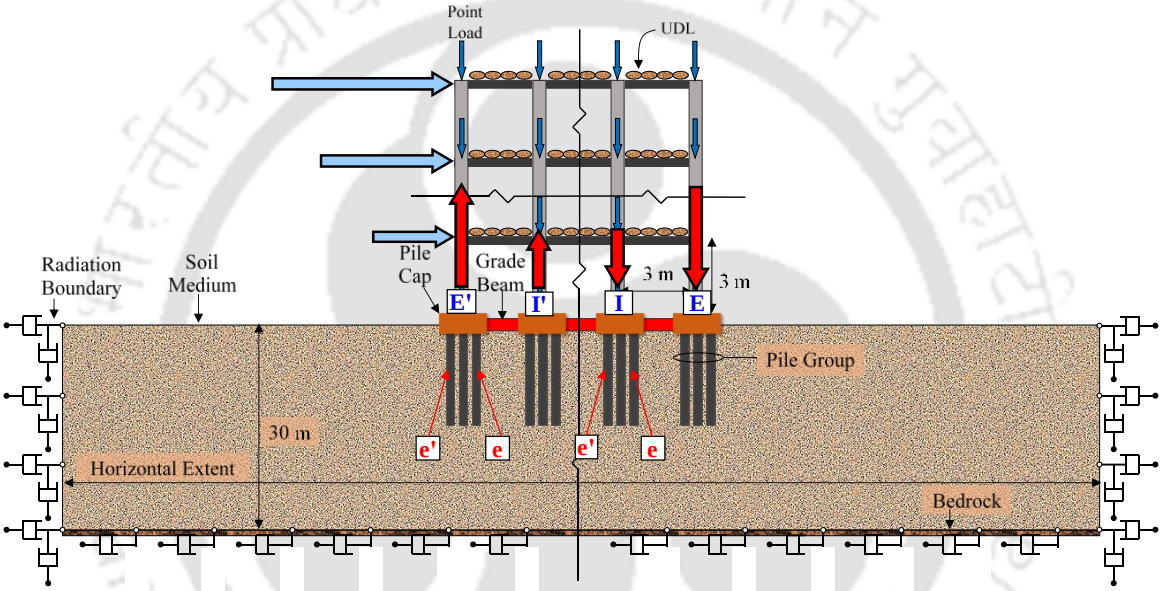

Figure 6.8 Schematic illustration showing the different pile groups and the different piles within a pile group.

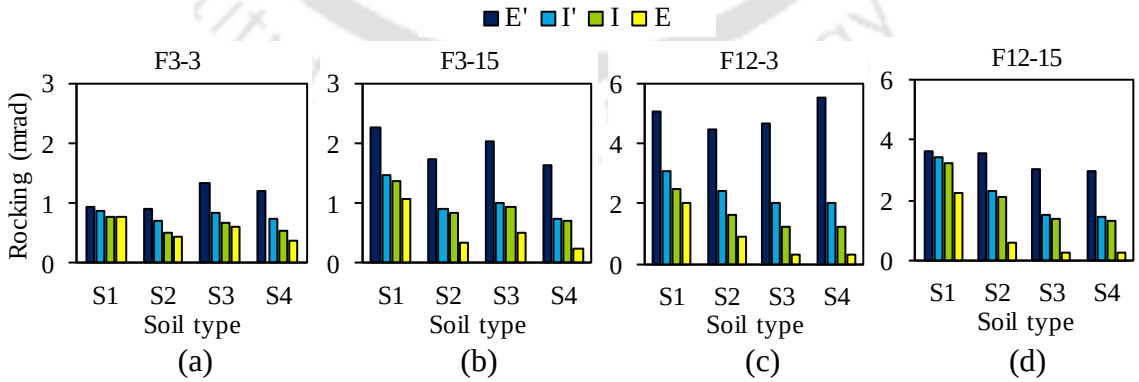

Figure 6.9 Pile group rocking at different locations for (a) F3-3, (b) F3-15, (c) F12-3, and (d) F12-15.

A schematic illustration of these pile groups is shown in Figure 6.8. For F3-3, Figure 6.9a shows the rocking of various pile groups under different soil conditions. It can be observed

that corresponding to each soil type (S1 to S4), pile group E' and E exhibit the largest and least magnitude of rocking respectively, while the groups I and I' exhibit intermediate rocking. This is because the columns on E' and E impart the least and largest compressive loads, respectively, while the columns on I and I' impart intermediate magnitude of compressive load. Moreover, the rocking exhibited by all the groups (E', E, I and I') having piles with smaller length and stiffer soil condition (S3) is observed to be higher than that observed for the case of the group possessing piles with relatively larger length but weaker soil condition (S2). Similarly, the rocking exhibited by E' in the S4 condition is larger than that under the S2 condition. It is worth recapitulating that considering the same structural configuration and same load imparted by the structure, as per the design requirement, the length of the pile group changes based on the foundation soils. For a poorer soil, in order to sustain the load imparted by the building frame, longer piles would be automatically required. Figure 6.9b shows the rocking of the pile groups under various soil conditions for F3-15. Although for this frame, the pattern of rocking observed for each soil type is similar to that observed for F3-3 (rocking reduces from E' to I', to I, and is least for E), it can be observed that the magnitude of rocking for F3-15 is larger. Moreover, for this frame, the rocking of the pile groups under S3 is larger than that under S2. Figure 6.9c shows the rocking of pile groups of F12-3 and, as observed for 3-storeyed frames, for this frame as well, the rocking is largest for E', lowest for E and intermediate for I' and I. Under all the soil conditions, the rocking exhibited by pile group E' is observed to be significantly higher than that exhibited by group E, and that the difference becomes more pronounced as the soil becomes stiffer (for which the length of the piles is reduced). When compared with F12-3, the magnitude of rocking for F12-15 is reduced significantly for E' with a marginal change in the other groups (Figure 6.9d).

The rocking of the pile foundation in the case of the other RC frame systems is shown in Figure 6.10. It can be observed that for all the configurations and soil conditions, the pile groups E' (under least compression) exhibit highest rocking, while the pile groups E (under largest compression) exhibit the least rocking features. For short frame systems (3-storeyed and 6-storeyed frames), the magnitude of rocking exhibited in the pile groups is larger for wider configurations than the narrower ones. The reason for such a phenomenon is explained as follows. For short frames (3-storeyed and 6-storeyed frames), it was observed (reported earlier) that the maximum inelasticity developed near the base of the superstructure level. Moreover, the narrower configurations exhibited larger ISD values

even at storey levels other than the ones wherein collapse is imminent. Since the superstructure in the wider frames develops lesser inelasticity, it allows for the development of larger rotation to be incurred at the base level, thereby causing larger rocking. For taller frame systems (9-storeyed and 12-storeyed frames), the phenomenon is further complex. On increasing the width (from 3 bays to 15 bays), the magnitude of rocking for pile group E' reduces, whereas it increases for the other groups. The explanation for this phenomenon is twofold. As observed earlier, taller frames exhibited imminent collapse at higher storey levels but not at the base. For narrower configurations, large ISD values developed at multiple storey levels, however for the wider configurations, large ISD values tend to get concentrated at the levels of imminent collapse. The development of concentrated failure in wider frames, firstly, induces the frame to achieve ultimate state at lower values of roof drifts, which causes a reduction in the rocking of E' as compared to the narrower frames. Secondly, upon increasing the width, the spread of nonlinearity, being limited to the storey where collapse is imminent, allows larger force[**] to be transferred at the base, which causes an increase in the rocking of pile groups I', I and E. For several frame specimens, it is observed that the pile group E', having a smaller length, exhibits larger rocking under stiffer soil conditions (S3 or S4) in contrary to the group under weaker soil conditions (S1 or S2) but having larger lengths (e.g., F3-3, F3-5, F3-9, F3-15, F6-3, F6-5, F6-9, F9-3, F9-5, F9-9, F12-3, F12-5 and F12-15). For almost all the configurations (except 3-storeyed frames), the rocking exhibited by pile group I', I, and E gets reduced for stiffer soil conditions. This is because on increasing the soil stiffness, the confinement action is increased, thereby reducing the possibility of rocking action within the group.

[**]The larger magnitude of force transferred to the base for wider frame is evident from the normalized pushover curves, and as an example, it can be noted that for S1 condition, V_{max} for F12-3 is 0.15 whereas the same is 0.16 for F12-15.

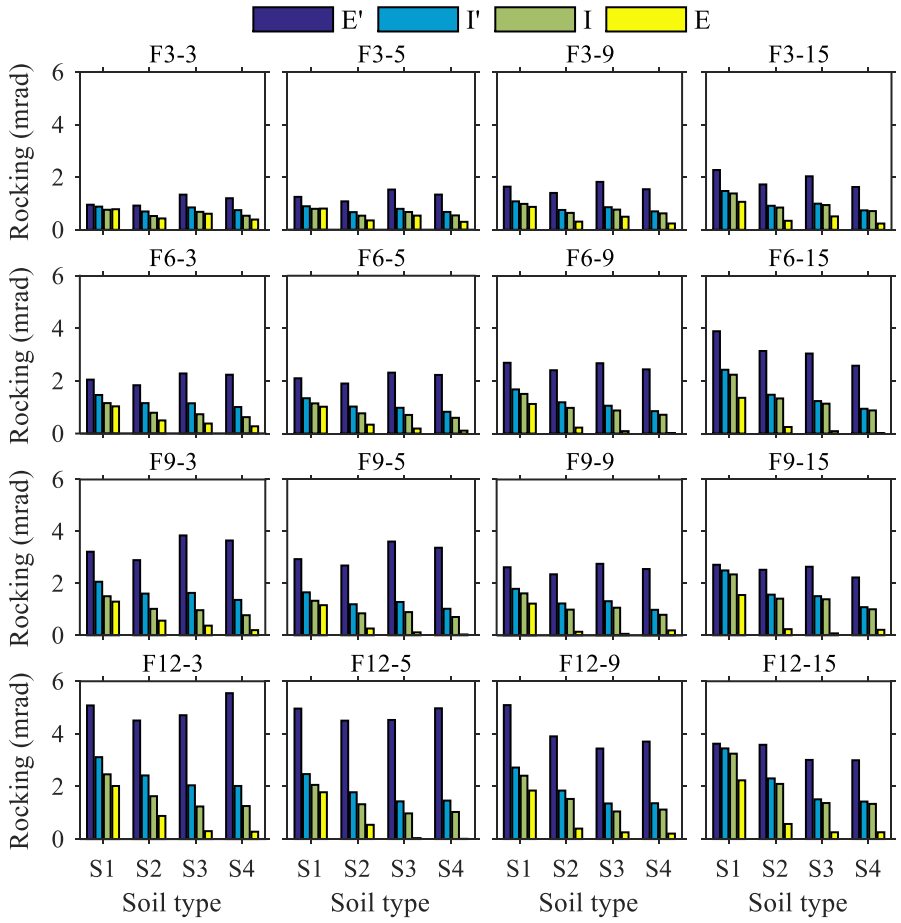

Figure 6.10 Influence of SSI on pile group rocking.

The lateral loads on the frame cause the foundation to rock, leading to plastic deformation in the piles, which in turn influences the rocking. Corresponding to each frame configuration, the pile length and diameter vary under different soil conditions. To examine critically the plastic behaviour of piles under different soil conditions, the plastic rotation along the length of the pile is obtained for the pile groups possessing maximum and minimum compressive load (group E' and group E). As shown in Figure 6.8, corresponding to a particular group, the piles possessing lesser compression are demarcated as ‘e’’ while those having higher compression are demarcated with label ‘e’. Moreover, to indicate the soil condition for the pile, a suffix indicating the soil type is utilized (for e.g., within a group, pile possessing least compression in S1 soil condition is labelled as e'_S1; similarly, the pile possessing highest compression in S3 soil condition is labelled as e_S3). Figure 6.11a shows the plastic rotation along the length of the piles of group E' under different soil conditions for the F3-3 frame. For group E' corresponding to F3-15 (Figure 6.11b), wherein the peak value of rotation is highest under S1, the foundation rocking is larger under S3 condition. Moreover, the magnitude is highest for S3, followed by S4, S2, and S1 conditions, which

can be correlated with the magnitude of foundation rocking. This is attributed to the fact that under S3 condition, the piles exhibited larger rotation near the top of the pile, thereby resulting in a larger magnitude of rocking of the group. As observed earlier for F12-3, the rocking of group E' was the largest under S4. Similarly, the magnitude of peak rotation was also observed to be highest for S4 (Figure 6.11c). Additionally, although the peak rotation in pile for S1 was smaller than that for S3 or S2, the rocking under S1 was observed to be larger. This is attributed to the substantial magnitude of rotation that was distributed over the length of the pile (for S2, S3, and S4 conditions, the rotation was concentrated in the top part of the pile with a very insignificant magnitude over the remaining portions). For F12-15, the piles exhibit a large magnitude of plastic rotation towards the bottom of the piles (Figure 6.11d).

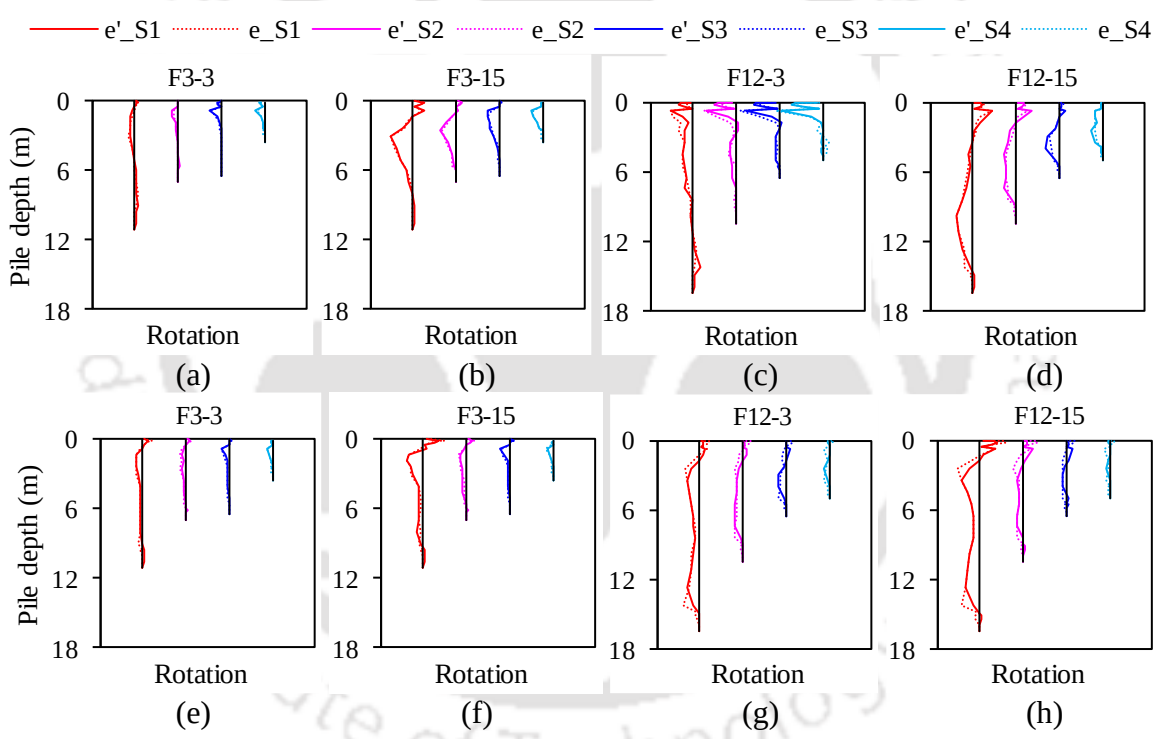

Figure 6.11 Plastic rotation in piles under different soil conditions: pile group E of (a) F3-3, (b) F3-15, (c) F12-3, and (d) F12-15; pile group E' of (e) F3-3, (f) F3-15, (g) F12-3, and (h) F12-15.

This is because for F12-15, the ultimate state is achieved at relatively lower drifts wherein the release of compressive loads is lesser. Under this condition, upon being subjected to lateral deformations, the piles develop a different profile, and inelasticity develops at relatively larger depths. This is also the cause for the reduced magnitude of rocking for pile group E', as observed earlier. Figures 6.11e-6.11h show the plastic rotations of pile group E for the frames F3-3, F3-15, F12-3, and F12-15, respectively. Similar to group E', for group

E, as well, the magnitude of rocking can be correlated with the plastic rotation developed in the piles. For both groups, E' and E, the profile of plastic rotation and the magnitude of peak rotation are similar for piles e and e' under the different soil conditions.

The plastic rotation in the piles, e' and e, for pile group E' and E of the other RC frame systems are shown in Figures 6.12a and 6.12b, respectively. As observed from the figure, the plastic rotations of the piles vary for the different soil conditions corresponding to the various frames. The magnitude of plastic rotation in the piles, corresponding to a particular soil condition, can be correlated with the magnitude of rocking experienced by the pile group. For e.g., corresponding to pile group E' (Figure 6.12a) of the 6-storeyed frames, it can be observed that the largest magnitude of plastic rotation is experienced by the piles of F6-15 and least by that of F6-3. Furthermore, the largest magnitude of rocking (Figure 6.10) is exhibited by pile group E' of F6-15 and least by that of F6-3. Additionally, larger rocking is exhibited in those pile foundation groups wherein the piles exhibit large plastic rotations very near the top of the pile. For example, corresponding to pile group E' (Figure 6.12a), the larger magnitude of rocking is observed in frames F9-3 and F9-5, wherein the piles exhibited larger plastic rotations near the top of the piles in comparison to that observed in F9-9 and F9-15. Similar observations can be made for F12-3 and F12-5 frames as well. For some cases corresponding to pile group E' (which experience release of compressive loads), it was observed that the rocking of the foundation group was larger under stiffer soil condition as compared to that of the weaker soil conditions. This can be explained as follows. Piles in the stiffer soil conditions experience larger restraint with the increase in depth. However, towards the top of the pile, the restraint developed under reduced compressive loads is not that high. Moreover, the piles under stiffer soil conditions possess smaller sections. Under these circumstances, the piles in the stiffer soil, on being subjected to lateral deformations, exhibit larger plastic rotation near the top of the pile, thereby producing larger rocking in the pile group.

In general, it can be observed that the plastic rotation in the piles of group E is lesser than that of the piles of group E'. This causes the rocking of pile group E to be lesser than that of pile group E' (see Figure 6.10). This is attributed to the fact that the pile group E experiences an increase in compressive loads, thereby increasing the level of confinement in the soil, which causes a reduction in the development of plastic rotations. Additionally, for group E, it can be observed that for almost all the configurations, the piles under S2, S3,

and S4 conditions exhibit significantly lesser plastic rotations compared to that of S1 condition. This is because the enhancement in the confinement effect is larger for the stiffer soil conditions (S2, S3, and S4), thereby inhibiting the development of plastic rotations within them. It can also be observed that corresponding to pile group E, the piles exhibiting larger rotation along the length results in the larger rocking of the pile group. For example, in the 9-storeyed frame (Figure 6.12b), it can be observed that the piles belonging to F9-15 develop large plastic rotation distributed over the length, thereby exhibiting a larger magnitude of rocking (Figure 6.10) as compared to that of the F9-3 frame. This is observed notably for piles under S1 condition, as for piles under S2, S3, and S4 conditions, the very less rocking is exhibited owing to the larger confining action being generated under the compressive forces).

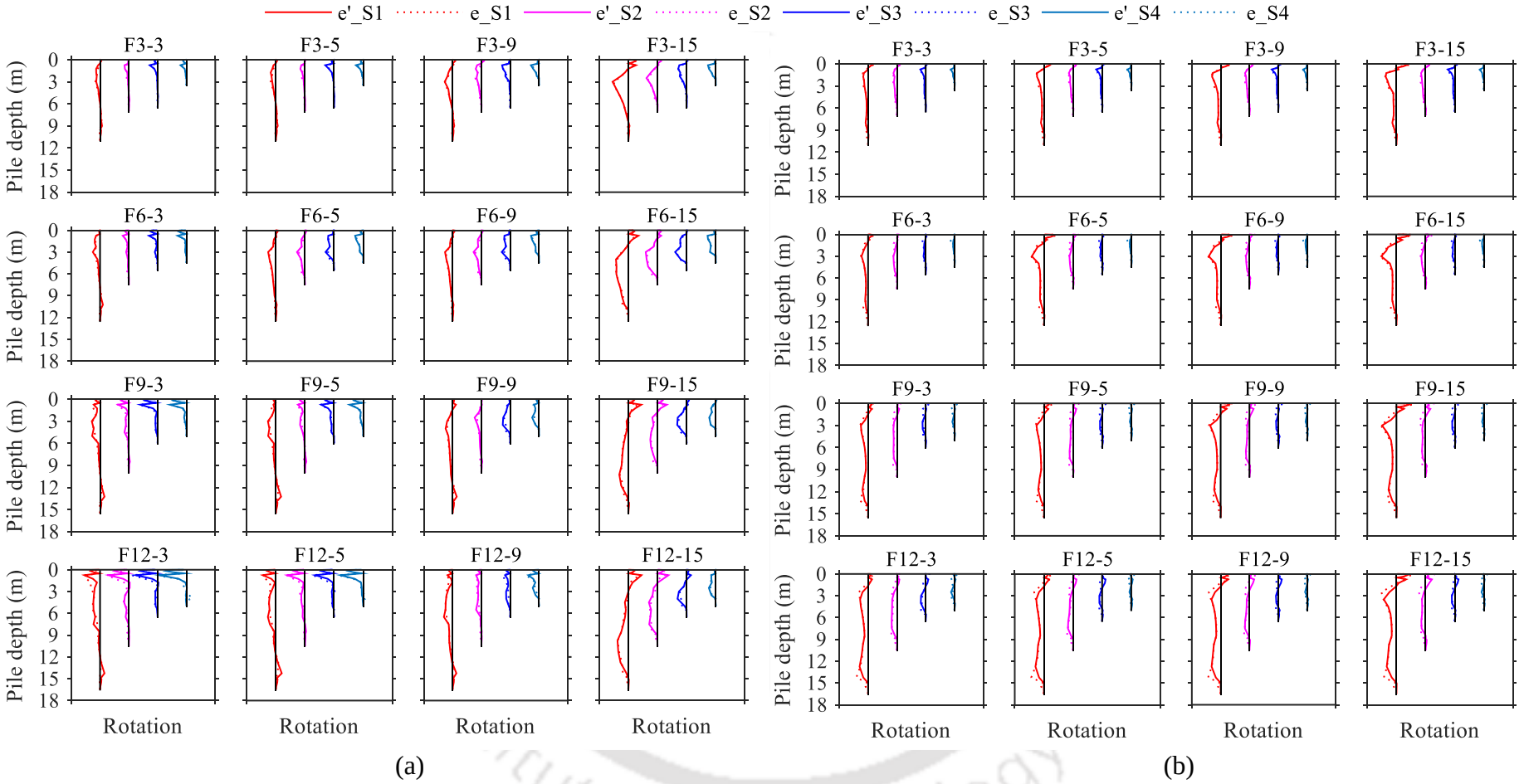

Figure 6.12 Influence of SSI on plastic pile rotation in (a) E' pile group, and (b) E pile group, for different RC frames.

6.4.2 RC Wall-frame System

For the RC wall-frame systems, the pile foundation groups are classified into three types. The pile groups under the exterior most columns, experiencing least and highest compression, are labelled as E' and E, respectively. The pile group under the shear wall are labelled as W. Figure 6.13a shows the rocking of the pile groups under the columns and the shear wall for the various RC wall-frame systems. For all the frames, it is observed that the pile group under the shear wall (W) exhibits a higher magnitude of rocking as compared to that of the pile group under the columns (E' and E). This is because, as compared to the columns, the shear wall is a stiffer member and attracts larger forces and moments, thereby leading to higher rocking. Moreover, it can be observed that the magnitude of rocking is largest for 3-storeyed wall-frame systems, and reduces as the height of the wall-frame system is increased. This is because the taller frames attract lesser forces (see Figure 6.6a). In general, corresponding to a particular height, upon increasing the width of the frame, the magnitude of forces is reduced. However, for some cases, the magnitude of rocking is yet high (e.g., the rocking corresponding to 3-storeyed and 6-storeyed frames). This is because of the similar magnitude of ISD developed at L1 corresponding to the different widths of the wall-frame systems. In general, the magnitude of rocking reduces upon increasing the stiffness of the soil (S1 to S3). Barring a few exceptions (F12-5, F12-9, and F12-15), for almost all the wall-frame systems, it can be observed that the magnitude of rocking is larger for stiffer soil (S4 condition) as compared to the weaker soil (S3 condition). For almost all the wall-frame systems (except 3-storeyed frames), it can be observed that upon increasing the width of the systems, the magnitude of rocking for S4 condition increases, and the same can be related to the lesser magnitude of ISD developed by the wall-frame systems at L1 level (see Figure 6.6b). For shorter wall-frame systems, such variation is not observed, as corresponding to the different widths, the ISD at L1 is similar. Similar to that observed in the framed systems, for wall-frame systems as well, the rocking exhibited by E' is larger than that exhibited by E. For most of the cases, upon increasing the stiffness of the soil, the magnitude of rocking in the pile group E' reduces. For a few cases corresponding to 6, 9, and 12 storeyed systems, it is observed that the rocking exhibited by the group E' is higher under stiffer soil condition (S4) as compared to the weaker soil conditions (S2 and S3).

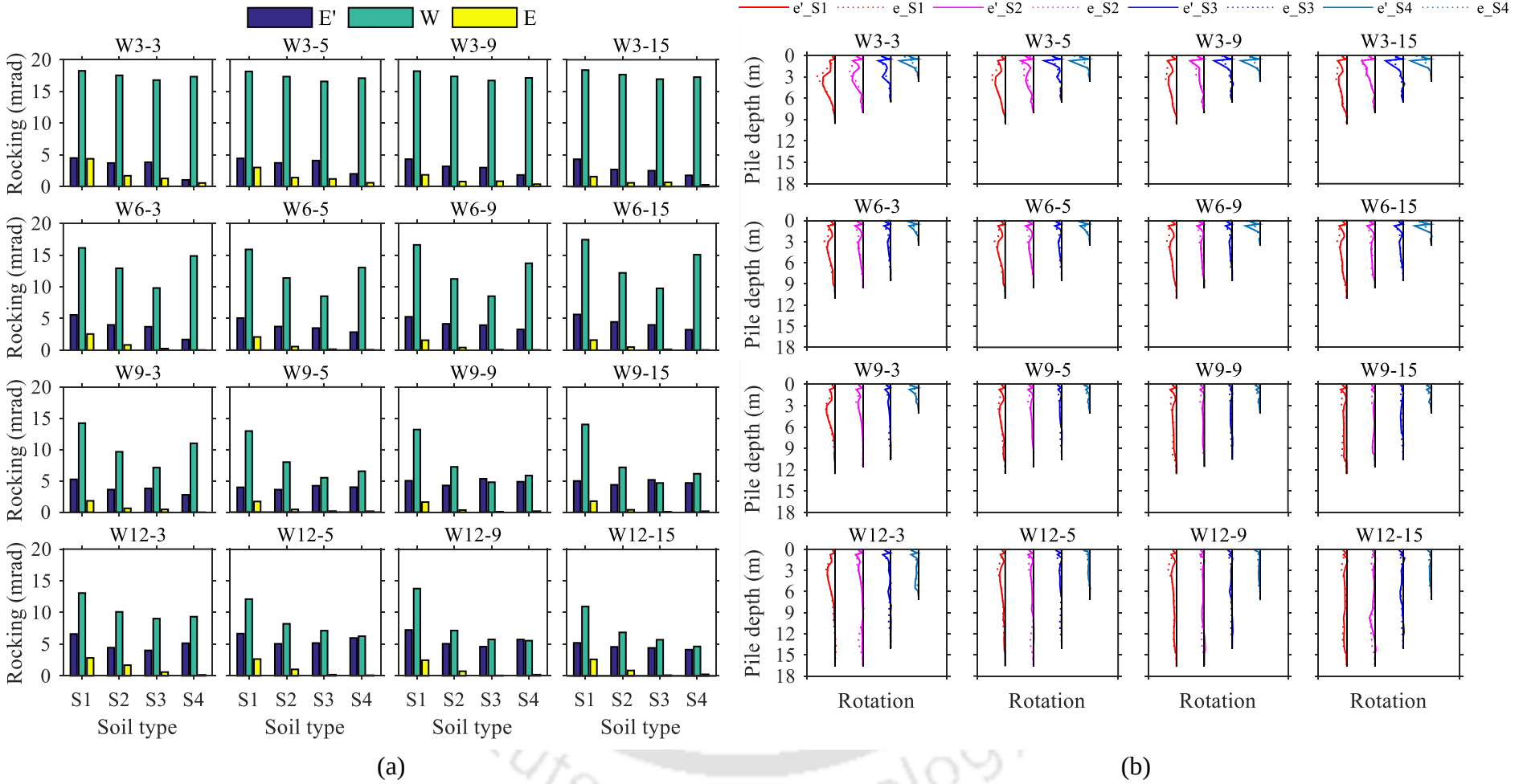

Figure 6.13 Influence of SSI on pile foundation behaviour of the RC wall-frame systems: (a) pile group rocking, and (b) plastic rotation in pile of group W.

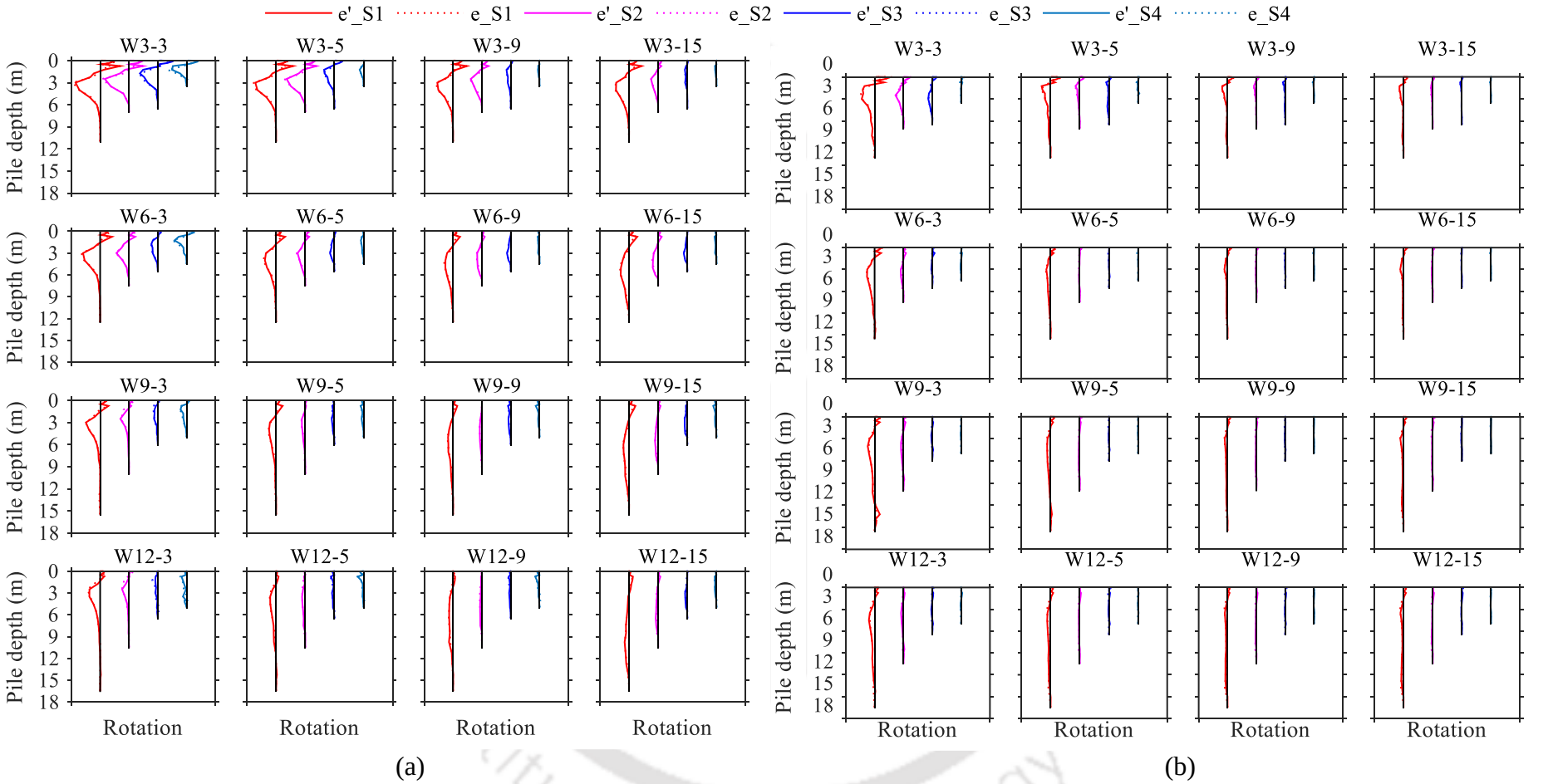

Figure 6.14 Influence of SSI on plastic pile rotation in (a) pile group E', and (b) pile group E, for RC wall-frame systems.

The plastic rotation in the piles group W under the wall-frame systems of various configurations is shown in Figure 6.13b. The plastic rotation in the piles, corresponding to 3-storeyed wall-frame systems, is observed to be the highest, whereas, that corresponding to 12-storeyed wall-frame systems is observed to be the lowest. Moreover, corresponding to a particular height of wall-frame, the plastic rotation in the piles of the wall-frame systems of smaller widths (3 bays and 5 bays) is observed to be larger as compared to that of the ones corresponding to larger widths (9 bays and 15 bays). This is more prominent for 6, 9, and 12-storeyed wall-frame systems. For most frames, the piles for S1 and S4 conditions show a relatively larger magnitude of peak rotation and thereby exhibit higher magnitudes of rocking experienced by the foundation group under these soil conditions. Piles in S1 soil conditions show higher rotation owing to the inability of the weaker soil to provide confinement action, thereby allowing the pile to deform significantly. On the other hand, piles in S4 soil conditions possess a smaller section. Moreover, the confinement at the top portion of the pile is less. On being subjected to lateral deformations, the piles exhibit larger inelasticity that is concentrated in the upper portion, thereby allowing larger rocking of the foundation group. The piles e' and e exhibit similar magnitude and plastic rotation profile for all the configurations. The magnitude of rocking experienced by the foundation can be correlated with the magnitude of plastic rotations exhibited by the piles of the group and is applicable for all the considered wall-frame configurations.

The plastic rotation along the length of the piles belonging to pile group E' and E is shown in Figure 6.14a and 6.14b, respectively. It can be observed that the magnitude of rotation for the different pile groups is different for the various considered wall-frame configurations, which can be correlated with the base shear at the ultimate state. The highest plastic rotation is observed for the piles corresponding to W3-3 for which the magnitude of base shear is highest. On the other hand, the least magnitude of plastic rotation is observed for W12-15 for which the magnitude of base shear is lowest. For a particular height of wall-frame and type of soil condition, on increasing the width of the frame, owing to the development of a lesser magnitude of base shear, the plastic pile rotation gets reduced. In general, for any particular wall-frame configuration, piles in S1 condition undergo the highest plastic rotation, and those with S4 condition undergo least plastic rotation (this is prominently visible for pile group E). For a few cases, it was observed earlier that the pile groups in S4 soil exhibit rocking larger than that for S3 condition. The cause for such behaviour has already been explained earlier while discussing similar observations for piles

of group W. Compared to the magnitude of plastic rotation in the piles belonging to group E', the magnitude of plastic rotation in piles belonging to group E is observed to be lesser. This is due to the increased compressive loads in the former group, which leads to an increase in confinement provided to the piles. The magnitude and profile of plastic rotation for e' and e are almost similar for most of the cases, and as observed for all other pile cases, they can be correlated with the magnitude of rocking experienced by the foundation for the considered specimens.

6.5 Influence of SSI on Ductility Capacity

The presence of soil-pile foundation system causes the plastic behavior of the superstructure systems to be different from its fixed-base behavior. This results in the modification of the ductility capacity of the superstructure. In the following subsections, the influence of SSI on the ductility capacity of the various considered RC frame and RC wall-frame systems is discussed.

6.5.1 RC Frame System

The ductility capacity ($\mu_c = \Delta_u / \Delta_y$) of a structural system depends on the magnitude of ultimate and yield drift. As already observed earlier, under different SPF conditions, these drifts vary. Figures 6.15a-6.15d show the ultimate drifts (Δ_u) of the considered frame systems for the various soil conditions. It can be observed that upon increasing the width of the frame systems, the ultimate drift values reduce for all the SPF conditions. For e.g., for 3-storeyed RC frame system under FB condition, on increasing the width from 3 bays to 15 bays, Δ_u reduces from 2.85 to 2.02. Similarly, for 12-storeyed frames under S1 condition, increasing the width from 3 bays to 15 bays results in the reduction of Δ_u from 2.69 to 1.26. The observation holds true for all the frames with different soil conditions (S1 to S4). The variation of Δ_u under different SSI conditions is observed for all the considered frame specimens. Compared to the 12-storeyed frame system, the ultimate drift is relatively less in 3, 6, and 9-storeyed frame systems. For e.g., the maximum variation in Δ_u for 3-storeyed frame system (corresponding to F3-9) is observed to vary from 1.99-2.17 for S1 to FB conditions. Similarly, for 6-storeyed frame system (corresponding to F6-15) and 9-storeyed frame system (corresponding to F9-5), the same varies from 1.65-1.92 and 1.73-1.31, respectively. However, for a 12-storeyed frame system (corresponding to F12-5), the same is found to vary from 2.13-1.31 for S1 to FB conditions. Moreover, for shorter RC frame

systems (3-storeyed and 6-storeyed frames), under FB condition, Δ_u is found to be higher than that observed for the SSI conditions. However, for taller RC frame systems (9-storeyed and 12-storeyed), Δ_u is lower for FB condition than that observed for the SSI conditions.

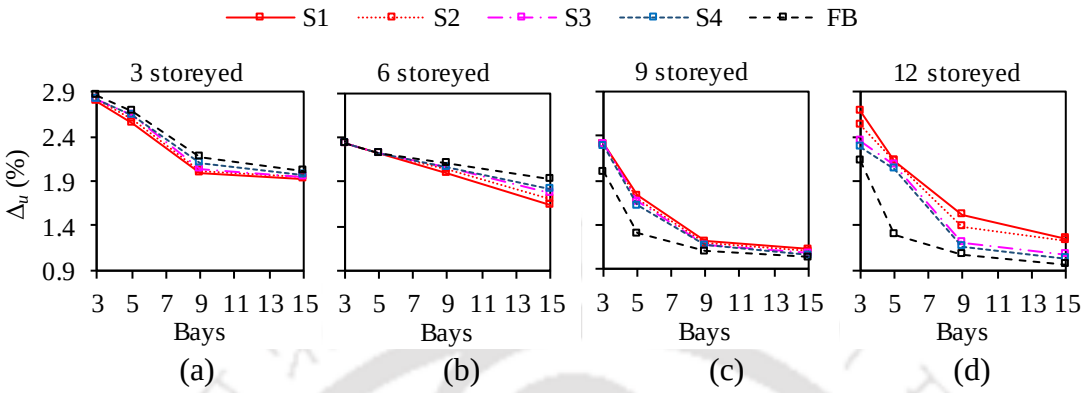

Figure 6.15 Influence of SSI on ultimate drift of RC frame systems with different widths and heights: (a) 3 storeys, (b) 6 storeys, (c) 9 storeys, and (d) 12 storeys.

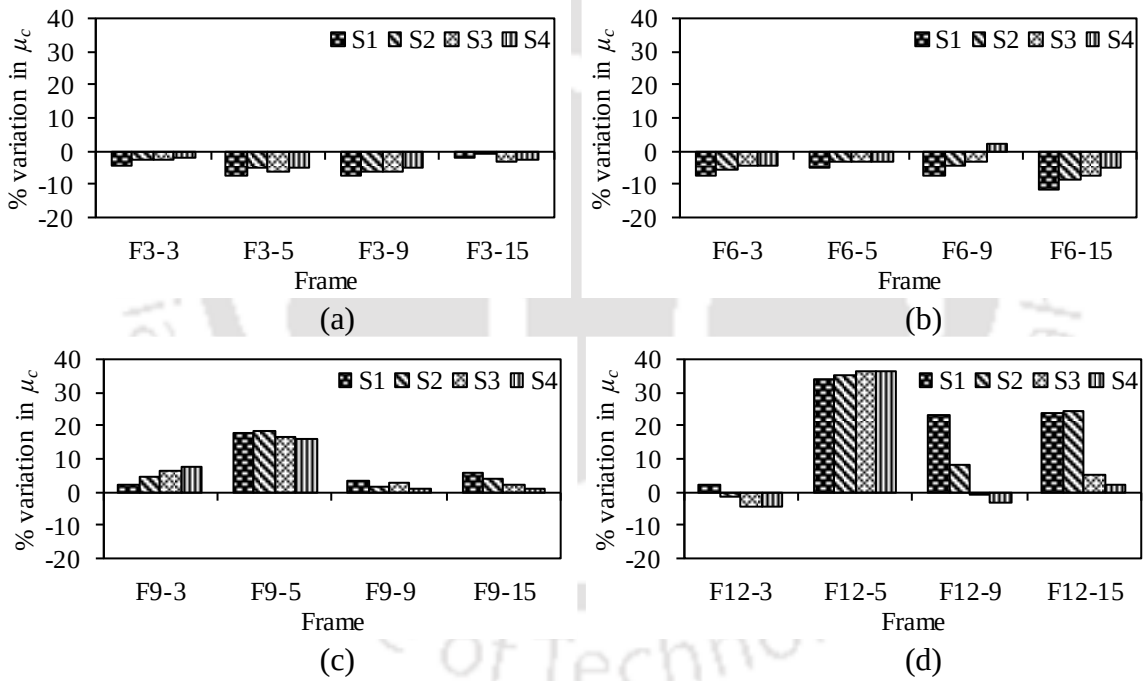

Figure 6.16 Variation in ductility capacities under the influence of SSI for RC frame systems with (a) 3 storeys, (b) 6 storeys, (c) 9 storeys, and (d) 12 storeys.

From the obtained ultimate and yield drifts, the ductility capacities are estimated under different SPF conditions, and its variation, with respect to the FB condition, for the various RC framed systems is shown in Figure 6.16a to 6.16d. It can be observed that for shorter frames (3-storeyed and 6-storeyed), corresponding to almost all the cases, SSI reduces the ductility capacity of the systems. This is because, for these frame systems, SSI causes Δ_u to reduce (see Figure 6.15a and 6.15b). In general, due to the larger magnitude of

reduction in Δ_u, the reduction in ductility capacity is observed to be higher for weaker soil conditions (S1 and S2) as compared to the stiffer soil conditions (S3 and S4). For instance, corresponding to 3-storeyed frame systems, the largest reduction in ductility capacity (8%) is observed for F3-5 for S1 condition, for which the decrease in Δ_u was highest. Similarly, corresponding to 6-storeyed frame systems, the largest reduction (12%) in ductility capacity is observed for F6-15 for S1 condition. For taller frames (9-storeyed and 12-storeyed), barring a few exceptions, SSI increases the ductility capacity of the systems. This is because, for these frame systems, SSI causes Δ_u to increase (Figures 6.15c and 6.15d). The largest increase in the ductility capacity is observed for F9-5 (19%) and F12-5 (37%). This is because, corresponding to these frames, the increase in the ultimate drift under the SSI condition is observed to be the highest (Figures 6.15c and 6.15d). Not for all the cases, the increase in the ductility capacity is highest for weaker soil conditions (S1 and S2). Rather, for some frames, the increase in ductility capacity is highest for stiffer soil conditions (S3 and S4), although the increase in ultimate drift is highest for the weaker soil conditions (S1 and S2). For e.g., corresponding to F9-3 and F12-5 frames, the increase in the ductility capacity is highest for S4 and lowest for S1 condition. This is because, for these frames, the ultimate drift exhibited under different soil conditions is of similar order; however, the yield drift under stiffer soil conditions is relatively lesser, thereby exhibiting a larger increase in the ductility capacity. Corresponding to some of the 12-storeyed frames (F12-3 under S2, S3, and S4 conditions; F12-9 under S4 condition), the decrease in ductility capacity is observed; although, for these cases, the ultimate drifts are larger compared to the fixed-base condition. This is because, for these cases, for the mentioned soil conditions, the frames exhibit larger yield drifts as compared to the FB condition, thereby reducing the ductility capacity.

6.5.2 RC Wall-frame System

Figures 6.17a-6.17d show the ultimate drifts (Δ_u) of the considered RC wall-frame systems for the various soil conditions. It can be observed that for 3-storeyed and 6-storeyed wall-frame systems, for SSI conditions, increasing the width of the wall-frame system results in a negligible change in Δ_u, however the same increases for FB condition. For e.g., upon increasing the width of the 3-storeyed wall-frame system from 3 bays to 15 bays, Δ_u remains unchanged at about 1.95 for S1 condition, but increases from 1.33 to 1.48 for FB condition. For 9-storeyed and 12-storeyed wall-frame systems, Δ_u reduces for SSI as well as FB

conditions. For all the considered wall-frame specimens, SSI exhibits larger Δ_u compared to that of the FB case (except for W9-3, W9-5, and W9-9 for which Δ_u under the SSI and FB cases are almost similar). Moreover, the increase in Δ_u under the influence of SSI is the largest for 3-storeyed wall-frame systems and least for 9-storeyed wall-frame systems.

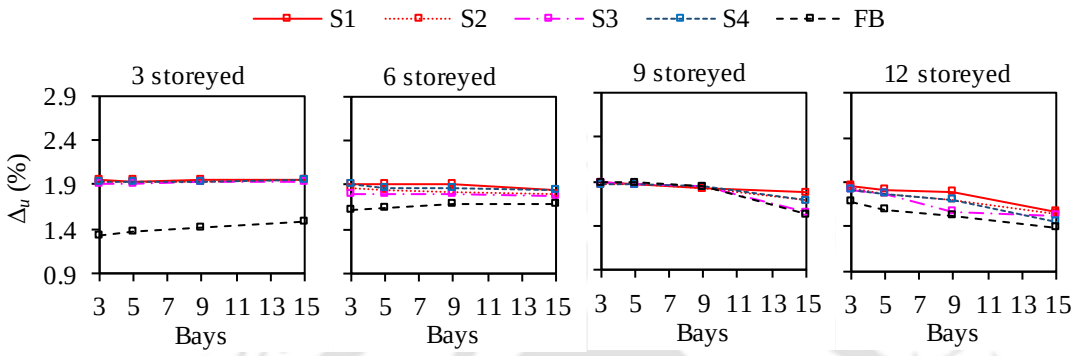

Figure 6.17 Influence of SSI on the ultimate drift of RC wall-frame systems with different widths and heights: (a) 3 storeys, (b) 6 storeys, (c) 9 storeys, and (d) 12 storeys.

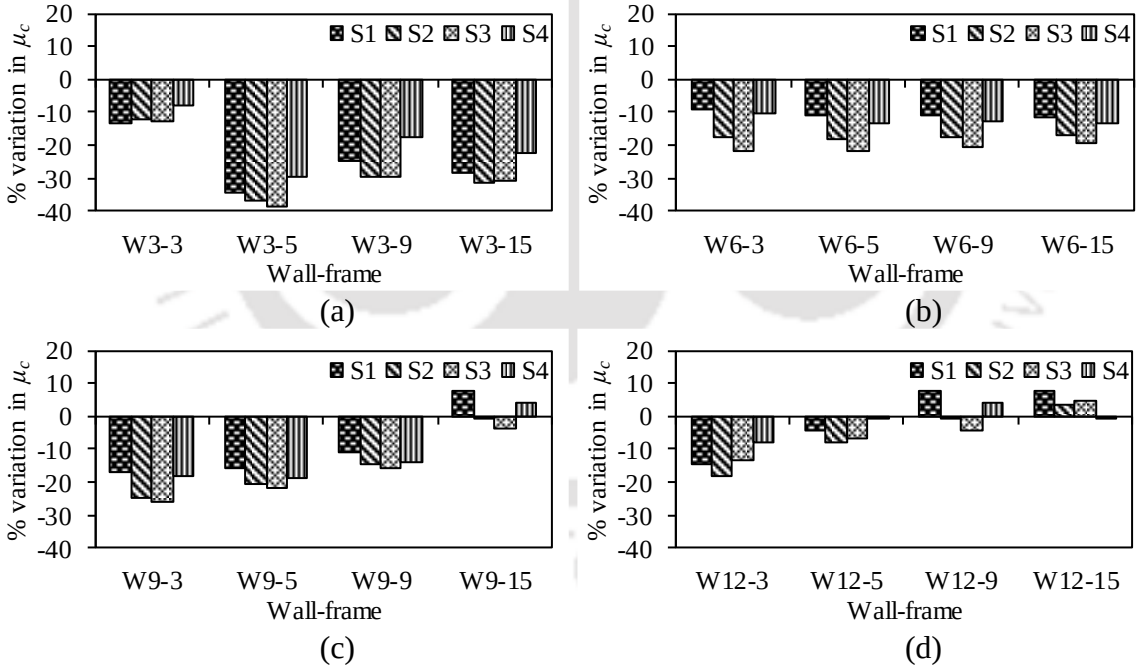

Figure 6.18 Variation in ductility capacity under the influence of SSI for RC wall-frame systems with (a) 3 storeys, (b) 6 storeys, (c) 9 storeys, and (d) 12 storeys.

The variations in the ductility capacity of the considered wall-frame specimens with respect to the FB condition are shown in Figures 6.18a to 6.18d. It can be observed that for all the 3-storeyed and 6-storeyed wall-frame systems and most of the 9-storeyed and 12-storeyed systems, the ductility capacity reduces under SSI effects, although the ultimate

drifts were higher for these frames. This is because, compared to the FB condition, the yield drifts exhibited by these systems were higher under SSI conditions, which caused an overall reduction in the ductility capacity. It can be observed that for several cases, the magnitude of reduction is observed to increase upon increasing the stiffness of the soil from S1 to S3 condition. On further increasing the stiffness to S4 condition, however, the change in the magnitude of reduction in the ductility capacity is observed to be slightly lesser. This is because the increase in the stiffness of the soil from S3 to S4 condition causes a slight increase in ultimate drift, thereby exhibiting a relatively lesser reduction in ductility capacity. The largest reduction for 3-storeyed system was observed to be 39% (W3-5 under S3 condition); for 6-storeyed system, the same was about 22% (W6-3 under S3 condition); for 9-storeyed system, it was about 26% (W9-3 under S3 condition); and for 12-storeyed system, the same was about 18% (W12-3 under S2 condition). For a few wider configurations corresponding to 9-storeyed and 12-storeyed wall-frame systems, an increase in the ductility capacity was observed (e.g., W9-15 under S1 and S4 conditions; W12-9 under S1 and S4 conditions; W12-15 under S1, S2, and S3 conditions). This is because, for these cases, the ultimate drifts increased without a significant increase in yield drifts. The maximum increase in the ductility capacity was observed to be about 8% for F12-9 under the S1 condition.

6.6 Effect of Shear wall on Framed buildings

This section studies the change in the plastic behaviour of RC frame systems supported on pile foundation due to the inclusion of RC shear wall while considering SSI conditions of the foundation-soil system. Since the focus is more on the modification in the behaviour, the phenomenon is highlighted with the help of limited results only. The results corresponding to 6-storey 5-bay and 12-storey 5-bay systems located on one particular type of soil (S2 condition) are studied to assess the influence of shear wall of RC frame systems with and without SSI effects. These configurations are chosen to be representative of frames with two different heights (namely short and tall configurations) possessing an intermediate width founded on moderately soft soil conditions. In the present study, nonlinear static analysis is carried out considering the lateral load pattern resembling the first mode of vibration of the structural system. Therefore, it is worth discussing the influence of shear wall on the natural vibrational characteristics a-priori, which is an essential component influencing the plastic response.

6.6.1 Modification in the Natural Vibrational Characteristics

Incorporating shear wall in an RC frame causes a change in the fundamental natural period and modifies the mode shape, which governs the distribution of the developed forces at various storey levels within the frame system. The presence of the shear wall in an RC frame system increases the lateral stiffness of the overall frame system, thereby reducing the natural period. This reduction may vary as per the prevalence of SSI effects. Figure 6.19a shows the reduction of the natural period due to the presence of the shear wall in the considered 6-storeyed and 12-storeyed RC frames, with and without SSI effects. The natural periods of the 6-storeyed and 12-storeyed frame system, without the shear wall and in the absence of SSI effects (T_{FB}), are 1.06 s and 1.44 s, respectively. Similarly, the natural periods of the frame system, without the shear wall and with SSI effects (T_{SSI}), are 1.10 s and 1.60 s, respectively. For a particular height of the frame, incorporating SSI effects makes the system flexible. It can be noted that due to the presence of SSI effects, the increase in the natural period of the RC frame is about 4% and 11% for 6-storeyed and 12-storeyed frame systems, respectively. Moreover, upon increasing the height, the frame system becomes relatively more flexible with and without SSI effects. The reductions in the natural period due to shear wall, of the 6-storeyed frame system, are 24% and 58%, with and without SSI effects, respectively. Similarly, the corresponding reductions for the 12-storeyed frame system are 14% and 30%, respectively, with and without the SSI effects. It can be observed that the reduction in the natural period of 6-storeyed frame is larger than that of the 12 storeyed frame. This indicates that when SSI effects are absent, the RC frame would attract larger seismic forces due to the presence of shear wall, and the effect is larger for a stiffer frame system.

Along with the natural period, the presence of shear wall also modifies the natural mode of vibration of the RC frame. Figures 6.19b and 6.19c show the influence of the presence of shear wall, with and without SSI, on the normalized mode shapes of the 6-storeyed and 12-storeyed RC frames, respectively. 'F_FB' indicates the mode shape profile of frame without shear wall and without SSI effects. The addition of shear wall to the frame significantly modifies the mode shape, as shown by 'W_FB'. The mode shape profile of the frame without shear wall and with SSI effects is indicated by 'F_SSI'. The incorporation of shear wall into the frame, while incorporating SSI effects, also modifies the mode shape profile, although to a relatively lesser degree, as indicated by 'W_SSI'. The modification in the mode shape profile on the incorporation of shear wall, with and without SSI effects, is

larger for 6-storeyed frame as compared to the 12-storeyed frame. The alteration in the mode shape profile provides an estimate of the variation in the distribution of forces that would arise at various storey levels in the frame due to the presence of shear wall when subjected to lateral loads.

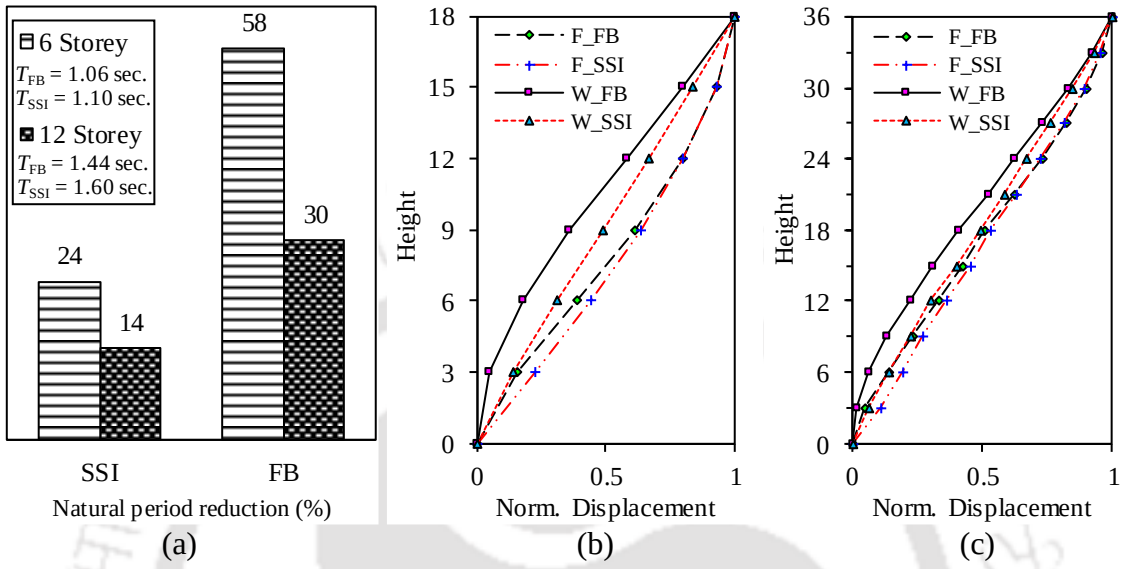

Figure 6.19 Details of natural vibration analysis of RC frame depicting the influence of shear wall on (a) fundamental natural period, (b) natural vibrational mode of the 6 storeyed frame, and (c) natural vibrational mode of the 12 storeyed frame.

6.6.2 Modification in the Global Inelastic Behaviour

Figures 16.20a and 16.20b show the influence of shear wall, with and without SSI effects, on the inelastic behaviour of the 6-storeyed and the 12-storeyed RC frame, respectively. It can be observed that the presence of shear wall modifies (a) the yield and ultimate base shear, (b) the effective lateral stiffness, and (c) the yield and ultimate drifts. The observation holds valid for both the frames of different heights. For the 6-storeyed frame, the increase in the yield base shear is 57% and 70%, with and without SSI effects, respectively. Similarly, for the 12-storeyed frame, the increase in yield base shear is 12% and 25%, with and without SSI effects, respectively. The increase in the ultimate base shear for the 6-storeyed frame is 82% and 70%, with and without the SSI effects, respectively. Similarly, for the 12-storeyed frame, the increase in the ultimate base shear is 28% and 17%, with and without the SSI effects, respectively. The increase in the yield base shear and ultimate base shear is relatively larger for the 6-storeyed frame as compared to that of the 12-storeyed frame. Moreover, it can be observed that the increase in yield base shear is relatively lesser with SSI effects; however, the increase in the ultimate base shear is relatively larger with

SSI effects. The observation holds equally good for the 6-storeyed and the 12-storeyed frame.

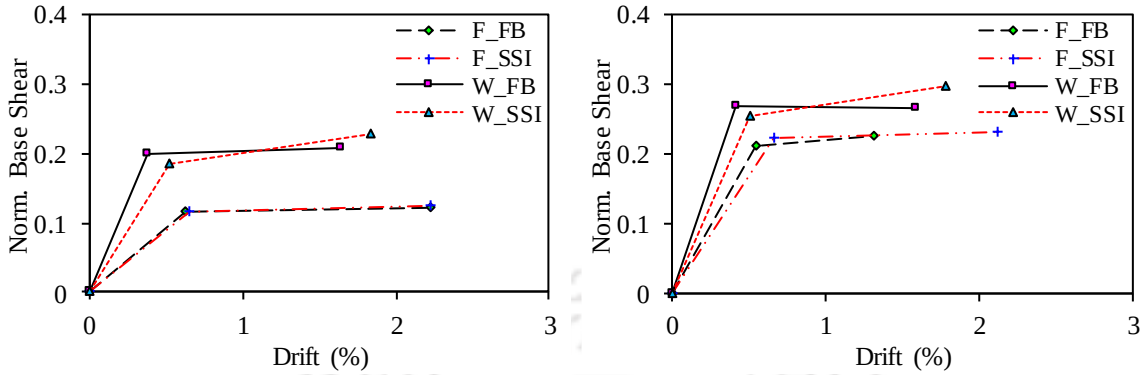

Figure 6.20 Influence of shear wall on RC frame with and without soil-pile foundation interaction on nonlinear static response of (a) 6 storeyed frame, and (b) 12 storeyed frame.

The influence of shear wall on the increase in effective lateral stiffness of the frame is evaluated and is shown in Figure 6.21a. For the 6-storeyed frame, the increase in effective lateral stiffness is 96% and 183%, with and without SSI effects, respectively. Similarly, the increase in effective lateral stiffness of the 12-storeyed frame is 49% and 69%, with and without SSI effects, respectively. The increase in the effective lateral stiffness is larger for 6-storeyed frame as compared to the 12-storeyed frame. It can be observed that the influence of shear wall on the effective lateral stiffness is relatively lesser while considering the SSI effects. On incorporating the shear wall, frames exhibit a larger change in the natural period and effective lateral stiffness, thereby exhibiting an increase in the yield and ultimate base shear. The magnitude of the increase in base shear is influenced by the presence of SSI effects. The increase in the yield base shear is relatively lesser with SSI effects; however, the increase in ultimate base shear is relatively larger. This is due to two primary reasons. Firstly, the RC frame without SSI effects attracts larger forces and undergoes higher damage as compared to the frame with SSI effects, thereby causing a larger increase in yield base shear but lesser increase in ultimate base shear. Secondly, the foundation of the RC frame with SSI effects also participates in the inelastic behaviour that causes less damage in the frame, thereby increasing its ability to exhibit larger load resisting ability at higher inelastic deformation.

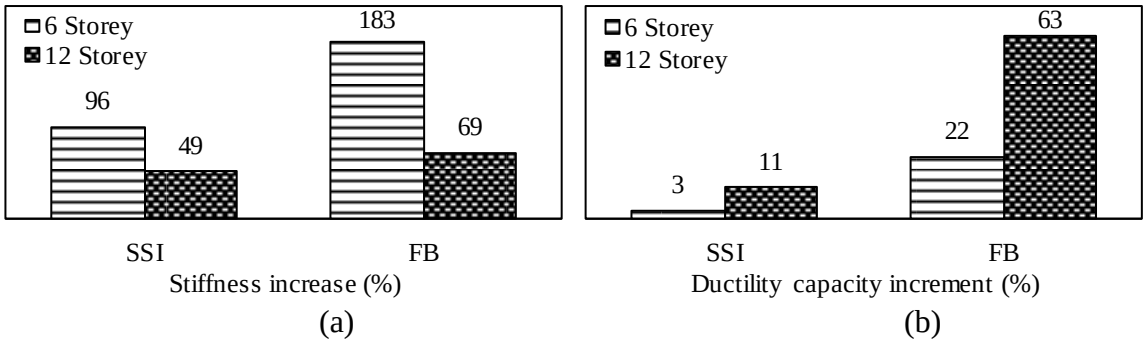

Figure 6.21 Influence of shear wall on RC frame with and without soil-pile foundation interaction on (a) lateral stiffness, and (b) ductility capacity.

As already observed, on the addition of the shear wall, the lateral load resistance and effective lateral stiffness are modified, both in the presence and in the absence of SSI effects. Shear wall also modifies the lateral displacement response of the RC frame, as observed in Figures 6.20a and 6.20b, in terms of yield and ultimate drifts. This ultimately influences the ductility capacity of the frame. The presence of shear wall increases the ductility capacity of the frame, as shown in Figure 6.21b. For the 6-storeyed frame, the increase in the ductility capacity is 3% and 22%, with and without SSI effects, respectively. Similarly, for the 12-storeyed frame, the increase is about 11% and 63%, with and without SSI effects, respectively. The increase in ductility capacity is larger for the relatively flexible frame (12-storeyed) compared to the relatively stiffer frame (6-storeyed). Moreover, it can be observed that the increase in the ductility capacity is lesser when SSI effects are incorporated. For the stiffer frame, it is possible for the inelasticity to develop at relatively lesser drifts, thereby allowing larger mobilization of the ductility contribution due to the shear wall and exhibiting larger ductile behavior before the collapse. For frames with SSI, due to the inelasticity developing at relatively higher drifts, the opportunity available for the shear wall to mobilize its ductile behaviour is reduced, thereby exhibiting a relatively lesser increase in the ductility capacity.

6.7 SUMMARY

Allowing inelastic behaviour on account of ductility is an integral component of the modern-day earthquake resistant design philosophy of building structures. The soil-pile foundation inevitably contributes and, thus, modifies the inelastic response and ductility capacity of the buildings. In this chapter, the influence of SSI on the inelastic behaviour and its subsequent effect on the ductility capacity of RC frame and RC wall-frame systems is investigated. Further, the role of the shear wall in modifying the inelastic behaviour and ductility capacity is also studied. The main summaries from the present study are as follows:

- The inelastic behaviour under the influence of SSI is modified considerably for stiffer systems with weaker soil conditions. In the present study, the stiffer wall-frame systems exhibited a larger change in the inelastic behaviour due to the presence of soil-pile foundation system. Stiffer wall-frame systems, due to the large magnitude of forces attracted by the stiff shear wall, induce larger deformations at the base of the superstructure, which is complied to a larger extent by the pile foundations on weaker soil conditions. For frame systems, due to the absence of a very stiff member like a shear wall, relatively lesser forces and deformations are induced at the superstructure base, thereby exhibiting a lesser influence of SSI on the inelastic response. Compared to shear wall, column sections incur large inelastic deformations, thereby curbing the transfer of large magnitude of rotations onto the soil-pile foundation, and hence exhibiting lesser SSI effects for frame systems.
- The ultimate drifts exhibited by a structure is dependent on the inter-storey drift profile. Depending on the inherent behaviour, the superstructure may exhibit ISD profile and ultimate drifts under the influence of SSI to be larger or lesser than that for the fixed-base condition. The influence of SSI is to impart flexibility at the base and reduce the magnitude of inelasticity (ISD) within the superstructure. In the present study, the RC frame systems with short heights tend to satisfy the ISD criteria for imminent collapse near the superstructure base (at the expense of the inelastic deformation in the soil-pile foundation system), while exhibiting ISD profile and ultimate drifts to be lesser than that under the fixed-base condition. Taller RC frame systems, on the other hand, tend to satisfy the collapse criteria at levels higher than the superstructure base. For this behaviour, it is required to undergo larger drifts to satisfy the collapse criteria, thereby exhibiting the ISD profile and ultimate drifts larger than that observed under the fixed-base condition.
- Due to the presence of the stiff shear wall member, RC wall-frame systems exhibit significant variation in the yield drifts under the influence of SSI. Moreover, the wall-frame systems tend to satisfy the collapse criteria at a level higher than at the superstructure base. Under SSI effects, the wall-frame systems exhibit a significant increase of ISD at the bottom storey level, thereby exhibiting ultimate drifts larger than that observed under fixed-base condition.
- Wider frames, having a larger number of members at each storey level, possess larger redundancy; thereby, inhibit large ISD values except at the storey developing the

impending collapse. Narrower frames, on the other hand, develop large ISD values at the storeys where collapse is not imminent as well. This causes the frames with narrower configurations to exhibit larger ultimate drifts, which reduces upon increasing the width of the frames corresponding to a particular height.

- The magnitude of plastic hinge deformation (in the form of AVR profiles at ultimate state) is observed to correspond with the ISD profiles while exhibiting lesser plastic hinge deformations for short RC frame systems under the influence of SSI. For taller frame systems under SSI effects, the plastic hinge deformations at the bottom storey are observed to be higher, while at higher storeys, the same is lesser than that observed under fixed-base condition. RC wall-frame systems under SSI effects exhibit significantly larger plastic hinge deformations at the base of the superstructure than that observed under fixed-base conditions.
- Pile groups sustaining larger compressive loads exhibit lesser rocking. This is due to the increase in the confinement effect under increased compressive loads.
- The nature and magnitude of inelasticity within the superstructure influences the magnitude of rocking. Larger inelasticity within the superstructure causes more rotations within the superstructure, thereby reducing the magnitude of rocking in the pile foundation group, and vice-versa.
- Inelasticity concentrated in the superstructure causes the system to achieve ultimate state at relatively lesser drifts, thereby reducing the magnitude of rocking in the pile foundations, and vice-versa.
- The magnitude of plastic rotation in the piles, corresponding to a particular soil condition, can be correlated with the magnitude of rocking experienced by the pile group. Additionally, the pile foundation groups, wherein the piles exhibit large plastic rotations very near the top of the pile, exhibit larger rocking.
- RC frame and RC wall-frame systems on weaker soils exhibit larger inelasticity in the pile foundations, owing to the inability of the weaker soil to exhibit higher restraint due to the lack of confinement
- Under reduced compressive loads, piles with smaller sections (generally found in stiffer soil conditions) may experience less restraint towards the top of the pile. On being subjected to lateral loading, these piles exhibit large inelastic rotations near the top of the pile giving rise to large rocking in the pile group.

- Piles of the group possessing larger compressive loads, exhibit lesser plastic rotations, owing to the increase in confinement along the length of the pile. Compared to very weak soils, this effect is much more pronounced for piles under relatively stiffer soil conditions.
- Pile group under the shear wall exhibits a larger magnitude of rocking as compared to that of the pile group under the columns, owing to the presence of the wall as a stiff member. Moreover, the exhibition of rocking is larger for the stiffer systems that attract larger forces.
- Pile groups below the shear wall, found in very weak and very stiff soil conditions, exhibit a higher magnitude of rocking. Very weak soil conditions, owing to their inability to provide confinement action allowing the piles to develop larger plastic rotations. On the other hand, piles under very stiff soil conditions owing to a smaller section and less magnitude of confinement at the top, exhibit larger plastic rotations concentrated in the uppermost portion of the pile. Under both circumstances, a larger rocking of the foundation group is exhibited.
- Due to the modification in the inelastic behaviour, the ductility capacity of the RC frame under the influence of SSI is modified. The ductility capacity is influenced by the yield and ultimate drifts. For RC frame systems, yield drifts are not significantly altered under SSI effects. Moreover, for shorter height frame systems, the ultimate drift is reduced due to SSI effects, thereby exhibiting a reduction in ductility capacity, which is observed to be larger for weaker soil conditions. For taller frames, ductility capacity increases under the influence of SSI as the ultimate drifts are higher under SSI effects. The increase is generally larger for weaker soil conditions. However, under exceptional cases, the same is also found larger for stiffer soil conditions, especially wherein slightly larger influence on yield drift is conceived.
- Most RC wall-frame systems exhibit an increase in the yield and ultimate drifts, thereby causing an overall decrease in ductility capacity. The magnitude of reduction in the ductility capacity increases with an increase in the stiffness of the soil. Under very stiff soil conditions, the pile foundations tend to undergo slightly larger inelasticity, owing to the smaller sections causing slightly larger drifts to be mobilized before satisfying the collapse criteria. This leads to a slight reduction in the ductility capacity for frames resting on stiffer soil conditions. For the cases wherein the yield drifts are much less

influenced compared to ultimate drifts, the increment in the ductility capacity is experienced.

- To study the influence of shear wall on the inelastic behaviour of RC frame systems, with and without SSI effects, the modification in the natural vibrational characteristics was studied concisely. Shear wall influences the natural vibration characteristics by reducing the natural period and modifying the mode shape profile of the RC frame. The modification is relatively higher for a stiffer frame as compared to a flexible one. Moreover, the modification is relatively lesser for frames where SSI effects are duly incorporated.
- The modification in the natural vibrational characteristics alters the inelastic behavior of the RC frame. Shear wall increases the effective lateral stiffness, which causes an increase in the yield and ultimate base shear in the RC frame. Such an increase is observed to be higher for stiffer frame systems.
- The increase in the yield base shear is relatively lesser with SSI effects, although the increase in ultimate base shear is relatively larger. This is because the frames without SSI effects attract larger forces and undergo higher damage as compared to the frame with SSI effects. This causes a larger increase in yield base shear but a lesser increase in ultimate base shear. Moreover, the foundation of the frame incorporating SSI effects also participates in the inelastic behaviour, which causes less damage in the frame, thereby increasing its ability to exhibit larger load resisting ability at ultimate drifts.
- The presence of shear wall tends to increase the ductility capacity of RC frames, and it is larger for the relatively flexible frame as compared to the relatively stiffer one. For the frame without SSI effects, inelasticity develops at relatively lesser drifts, thereby allowing a larger contribution of ductility from the shear wall and exhibiting extensive ductile behaviour before the collapse. For frames with SSI, due to the inelasticity developing at relatively higher drifts, the possibility of mobilization of ductile behavior in the shear wall is reduced, thereby exhibiting a relatively lesser increase in the ductility capacity.

Chapter 7
INFLUENCE OF SSI ON INELASTIC BEHAVIOUR: ASSESSMENT OF DUCTILITY DEMANDS

CONTENTS

7.1 OVERVIEW

During the shaking of an earthquake, a structural system is subjected to inelastic deformations, thereby causing damage to the system. The imposition of the inelastic deformations can be assessed by evaluating the ductility demands. The ductility demands can be assessed at both the local (elemental) and the global (structural) level. It can be understood that greater ductility demands at the local level could lead to the system to exhibit greater ductility demands at the global level. For the same shaking, the ductility demands are modified due to the presence of soil-pile foundation flexibility as compared to those obtained for the fixed base system. This is because the inelastic behavior of the structural system is modified under the influence of SSI. The extent of this modification may be influenced by the type of structure, its configuration, and the prevailing soil-pile foundation conditions. In the present chapter, the influence of SSI on the inelasticity in the

superstructure is studied with the help of local level inelastic response (of the plastic hinge regions) of the several** RC frame and RC wall-frame systems. Subsequently, the influence of SSI on the local and global ductility demands is assessed. The magnitude of ductility demands can be directly correlated with the damage incurred to the structure.

7.2 METHODOLOGY FOR ASSESSING DUCTILITY DEMANDS

For assessing ductility demands, the various configurations of the RC frame and RC wall-frame systems under the influence of SSI, are subjected to lateral loads using ground motion as the seismic input. The inelastic response of the SSI and fixed base system is determined by means of conducting nonlinear time history analysis. The influence of SSI is studied by comparing the ductility demands of the SSI system with that of the fixed base (FB) systems at the local and global levels.

At the local level, the ductility demands are assessed through curvatures developed at the plastic hinge sections of the various elements (beams, columns, and shear wall) subjected to the input seismic shaking. Normalized curvature ductility demand defined as the ratio of the curvature ductility demand with and without SSI is used in the present study for assessing the influence of SSI on ductility demands. The mathematical expression is shown in Eq. 7.1,

$$\bar{\mu}_c = \frac{\mu_{c,SSI}}{\mu_{c,FB}} \tag{7.1}$$

where $\mu_{c,SSI}$ and $\mu_{c,FB}$ is the curvature ductility demand of a section under SSI and FB condition, respectively, and is estimated as the curvature demand (ϕ_d) normalized with respect to the yield curvature of the section (i.e., $\mu_c = \phi_d / \phi_y$).

At the global level, displacement ductility demands of the frame and wall-frame systems (for the top-level displacement) corresponding to the different configurations are assessed with the help of normalized displacement ductility demand ($\bar{\mu}_d$) - response reduction factor (R_μ) relationships. R_μ is the ratio of the maximum base shear developed in the linear elastic system to that of the inelastic system, and $\bar{\mu}_d$ is the ratio of the ductility

**Note: The various configurations have been introduced in Chapter 5. In this chapter, the study is focused on the systems supported by pile foundation comprising three-pile group.

demand imposed onto the SSI system to that of the fixed base system. Mathematically $\bar{\mu}_d$ is expressed as shown in Eq. 7.2,

$$\bar{\mu}_d = \frac{\mu_{d,SSI}}{\mu_{d,FB}} \tag{7.2}$$

where, $\mu_d = \Delta_d / \Delta_y$, is the displacement ductility demand imposed onto the system.

7.3 SEISMIC INPUT

For studying the influence of SSI on ductility demands, lateral loading is applied in the form of ground motion shaking. Before applying the seismic motion onto the RC frame and RC wall-frame systems, it is essential to modify the input ground motions so that it possesses an acceptable level of damaging potential towards the structural system under consideration. This modification can be carried out by scaling the real records such that its spectral acceleration (corresponding to the natural period of the structural system) matches that of the considered hazard spectrum. Alternatively, the real records can be modified to match its spectrum with that of the hazard spectrum. Naumoski et al. (2006) concluded that the structural response obtained by applying artificial accelerograms that are compatible with the design spectrum was similar to that obtained by applying real records scaled to the design spectrum. The choice of scaling also influences the number of ground motions required to obtain the response within an acceptable level of confidence. Gascot and Montejo (2016) highlighted the fact that the use of spectrum compatible motions would reduce dispersion in the elastic response spectra of the input ground motions. This results in reduced variability in the output of the time-history analysis. Thus, a smaller number of records are required by the analyst. Similarly, Hancock et al. (2008) concluded that spectrally matching accelerograms significantly reduced the required number of records to estimate an expected response. They found that only two numbers of spectrally matched records are required to predict the drift and rotation with a confidence level of 64%. Jun (2013) studied the effect of input ground motions for nonlinear seismic response analysis of building structures. It was concluded in the study that simulated ground motions that are compatible with the design spectrum provide better stability in the response quantities than the real recorded ground motions.

In the present study, three ground motion records have been selected for conducting a nonlinear time-history analysis of the considered building frames, with and without the

influence of SSI. For convenience, in the present chapter, the motions are labelled as GM1, GM2, and GM3. GM1 is the 1940 Imperial Valley earthquake recorded at the station 'El Centro Array #9'; GM2 is the 1994 Northridge earthquake recorded at the station 'Castaic - Old Ridge Route'; and, GM3 is the 1979 Imperial Valley earthquake recorded at the station 'El Centro - CA Array Station 2 Keystone Road'. The current study utilizes the spectra prescribed for response spectrum analysis in IS 1893: Part 1 (2016) as the hazard spectrum. The ground motions are assumed to be recorded at the rock outcrop and have been matched with the hazard spectrum using the SeismoMatch software (Seismosoft, 2018). Spectrum compatible motions are considered for the analysis, as it is intended that the various considered structural systems should experience a shaking corresponding to a defined level of hazard. Figure 7.1 shows the average and individual response spectra of the ground motions that have been modified to match the desired hazard spectrum. Each motion is scaled to seven different levels of shaking, equally spaced within the range 0.12-0.48g; thereby corresponding to the hazard level (as specified in IS-1893 Part 1, 2016) ranging from 0.33-1.33 times the maximum considered earthquake (MCE). The soil profile is excited at the base by a horizontal force time-history, which is proportional to the known velocity time-history of the ground motion (Joyner and Chen, 1975). It is noted that due to the consideration of an elastic half-space, the outcropping rock motion could be directly applied at the base of the soil model (Kwok et al., 2007).

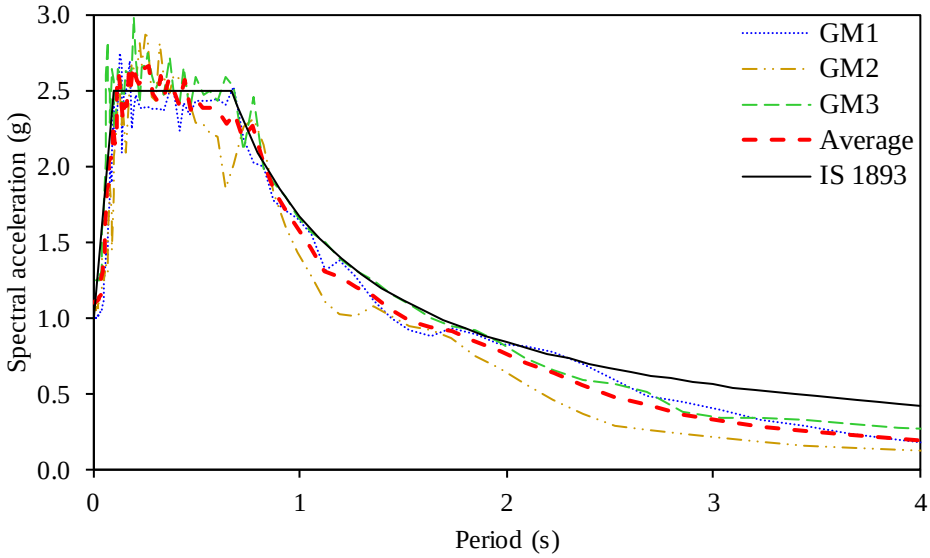

Figure 7.1 Response spectra of the ground motions after modification to match with the design spectrum of IS 1893 Part 1 (2016).

7.4 GROUND RESPONSE ANALYSIS

In order to study the effect of SSI, it is essential to compare the response of the structural system under flexible SSI condition with that of the FB condition. Moreover, for the SSI system, the seismic input is applied at the bedrock level; however, for a fixed base system, the input is applied at the base of the superstructure level. Owing to the presence of soil layer, the seismic input exhibits amplification in the acceleration as it propagates from the bedrock to the free field surface. Prior to analysing the fixed base system, this amplification in acceleration needs to be accounted for, and the corresponding amplified time-history should be applied at the base of the FB system. For this scenario, free field ground response analysis (GRA) has been carried out on the considered free-field soil domain using the selected motions scaled to the different intensity levels.

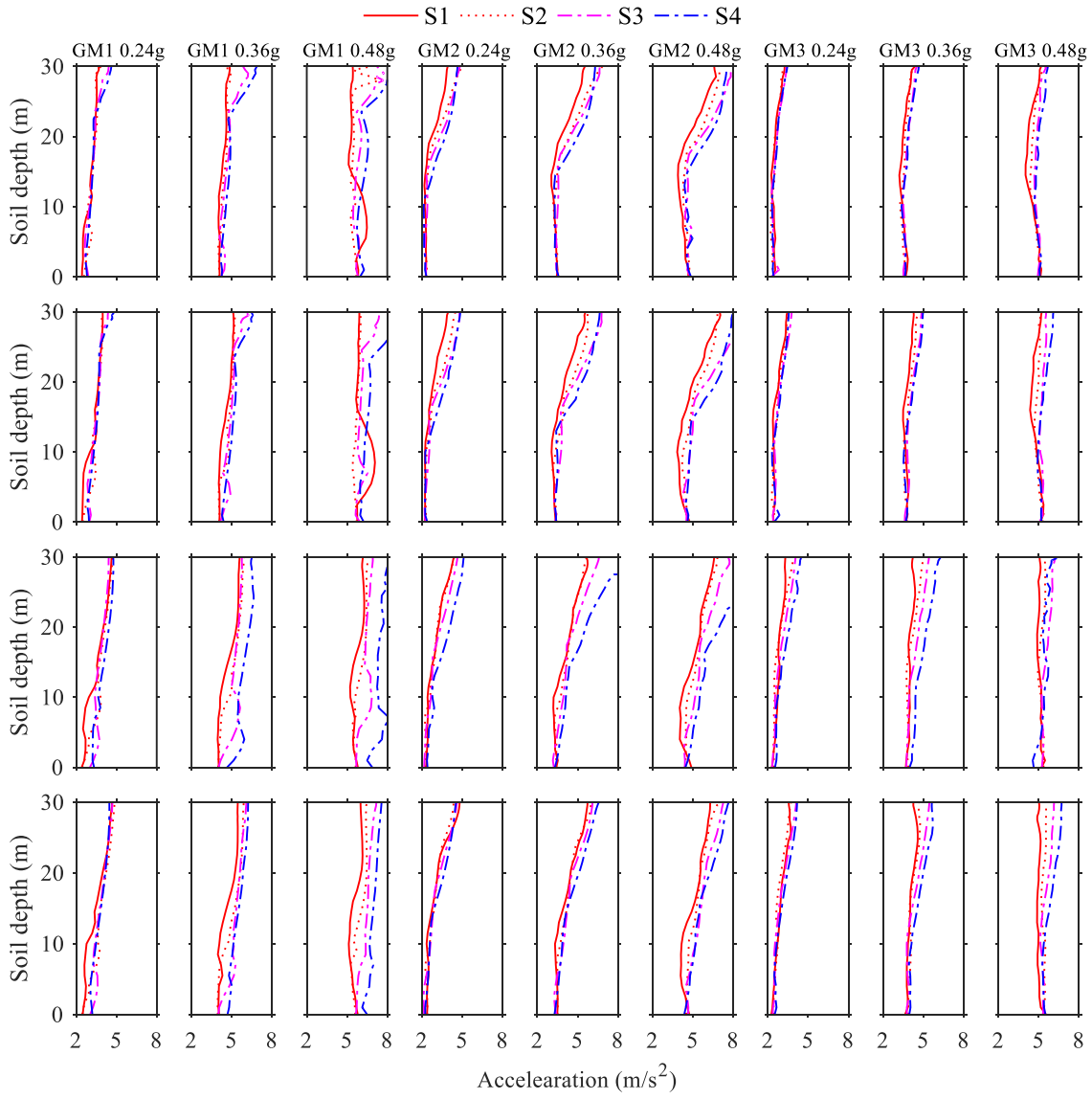

Figure 7.2 Ground response analysis to obtain free field peak acceleration to be applied to the fixed base model.

A total number of 1,344 ground response analyses (GRA) have been performed and the acceleration amplification in the soil domain, corresponding to some typical cases, as shown in Figure 7.2. For each soil domain, the acceleration time-history used for conducting fixed base analysis is scaled to match the peak acceleration at the free field soil surface (obtained from GRA). In the present study, each specimen is analysed under the influence of SSI; and, for each structure-soil configuration, its corresponding fixed-base analysis is also carried out. The peak dynamic response of a particular entity is obtained by considering the average of the peak values determined from the three input ground motions. A total number of 5,376 nonlinear time-history analyses have been conducted, and the results are discussed in the following sections.

7.5 Influence of SSI on Dynamic Inelastic Response

The influence of SSI on the dynamic inelastic response is studied by assessing the extent of inelasticity developed in the predefined inelastic zones (plastic hinges). FEMA 356 prescribes the criteria for performance evaluation of the various RC elements. Three performance states are prescribed, namely (a) Immediate Occupancy (IO), (b) Life Safety (LS), and (c) Collapse Prevention (CP). In the present study, the same has been utilized for assessing the inelastic response in the elements of the structural system. For convenience, the inelastic response is classified based on the extent of inelasticity exhibited by the plastic hinges as follows:

Stage 1: At this stage, the plastic hinges exhibit approximately elastic behavior and the performance is within the IO state.

Stage 2: At this stage, the plastic hinges exhibit the inelasticity to lie between IO and LS states. This stage is indicated by blue colour [●, ▬].

Stage 3: At this stage, the plastic hinges exhibit the inelasticity to lie between LS and CP states. This stage is indicated by pink colour [●, ▬].

Stage 4: At this stage, the plastic hinges exhibit the performance to lie beyond the CP state. This stage is indicated by red colour [●, ▬].

The influence of SSI on the dynamic inelastic response of RC frame and RC wall-frame buildings is discussed in the following subsections. Since at very low shaking intensity (0.12g), the inelasticity is not well developed within the RC frame and RC wall-frame systems, therefore, for the purpose of observation, results corresponding to intermediate (0.24g) and high intensities (0.48g) of shaking are discussed.

7.5.1 RC Frame System

Corresponding to intermediate shaking intensity, the frame members in most specimens exhibit inelasticity corresponding to stage 2 or above. The inelasticity developed, however, is observed to be lesser for the frames under the influence of SSI. For the sake of clarity, results corresponding to some of the specimens are discussed in the following. Figures 7.3a and 7.3b show the inelasticity developed in the plastic hinges of F3-5 under S1 and S4, respectively. The corresponding FB models are shown in Figures 7.3d and 7.3e. It can be observed that under the SSI condition, the columns at L1 exhibit stage 2 or stage 3 level of inelasticity with a lesser number of overall locations developing inelasticity. However, under FB condition, the columns at L1 exhibit stage 4 inelasticity and, compared to SSI condition, more number of locations develop stage 2 inelasticity. Figure 7.3c shows the plastic hinges for F3-15 under S1, and the corresponding FB model is shown in Figure 7.3f. It can be observed that under SSI, apart from the bottom, the top locations in the columns at L1 exhibit stage 3 or stage 4 inelasticity. However, under FB condition, the top locations in columns at L1 exhibit stage 2 inelasticity. Additionally, under FB condition, several beams at L1 exhibit stage 2 inelasticity whereas, that under SSI are at stage 1. Figure 7.4a shows the plastic hinges in F6-15 under S1, and that of the corresponding FB model is shown in Figure 7.4b. It can be observed that under FB condition, several frame members at the higher storey level exhibit stage 2 inelasticity, which is absent for the columns of the frame under SSI. Moreover, it can be observed that at the bottom of several columns at L1, the frame under SSI exhibits stage 3 and stage 4 inelasticity. However, at the corresponding locations in the frame under the FB condition, only stage 2 inelasticity is exhibited. Figure 7.5a shows the plastic hinges for F12-15 under S1, and the corresponding plastic hinges under FB condition is shown in Figure 7.5b. It can be observed that the beams in the frame under FB condition develop inelasticity at more number of locations, and exhibit a greater level of inelasticity (stage 2 for beams at L1-L3; stage 3 for beams L7-L9). Under SSI condition, the inelasticity in beams at L1-L3 is at stage 1, and that at L7-L9 is at stage 2. The foregoing results (corresponding to intermediate shaking) indicate that under SSI, the RC frame systems may develop lesser inelasticity compared to that under FB condition. Moreover, under SSI conditions, locally, the frame members may exhibit a greater extent of inelasticity. Although this may not contribute to the exhibition of higher displacements at the global level, however, it could lead to the development of unsafe conditions.

At high shaking intensity, the frame members in most of the specimens exhibit inelasticity corresponding to stage 4. The results of the discussed RC frame specimens corresponding to 0.48g shaking intensity are shown in Figures 7.6-7.8. For each of the frames, it can be observed that the number of plastic hinges developed is similar for SSI and FB conditions; however, the extent of inelasticity exhibited is greater under SSI condition. For example, in Figure 7.6a, it can be observed that the bottom of the columns at L2 are at stage 4 while that under FB condition (shown in Figure 7.6d) are at stage 2. A similar observation is made for F3-15 under S1 shown in Figures 7.6c and 7.6f. In Figures 7.7a and 7.7b, it can be observed that the frames under SSI exhibit greater inelasticity in beams and columns when compared with that under FB condition. In Figures 7.8a and 7.8b, it can be observed that the frames under SSI exhibit greater inelasticity in columns at L8 and L1 when compared with that under fixed base condition. The results (corresponding to high shaking) indicate that under SSI, the members of the RC frame systems develop greater inelasticity compared to that under FB condition.

7.5.2 RC Wall-frame System

In RC wall-frame systems, under intermediate shaking (0.24g), the beams and columns develop less amount of inelasticity, both with and without the influence of SSI. However, compared to FB condition, wall-frame systems under SSI exhibit greater inelasticity at bottom locations in the columns at L1 and in the beams adjacent to the shear wall. Additionally, the shear wall exhibits lesser inelasticity at the base of the shear wall under SSI compared to that under FB conditions. For the sake of clarity, results corresponding to some of the specimens are discussed in the following. Figures 7.9a and 7.9b show the plastic hinges in W3-9 and W3-15 respectively under S1; and their corresponding FB models are shown in Figures 7.9c and 7.9d. It can be observed that for the models under SSI, columns at L1 and beams adjacent to shear wall develop stage 2 inelasticity that is significantly reduced in the corresponding FB models. However, under FB condition, the shear wall develops greater inelasticity. This is because, under SSI, the soil-pile foundation flexibility reduces the forces under the shear wall by allowing the shear wall to rock. This rocking, in turn, imposes additional rotation in the beams adjacent to the shear wall and onto the columns at L1. Under FB condition, the rocking of the shear wall is restrained, thereby attracting a large magnitude of forces and simultaneously reducing the magnitude of forces in the columns. A similar observation holds true for other configurations and has been highlighted, as shown in Figures 7.10 to 7.13. Similar observation has been reported by

Marzban et al. (2014), where the authors observed intensification of beam end rotations in RC shear wall-frames under SSI.

For high shaking intensity (0.48g) under the SSI condition, the beams and columns develop significantly high inelasticity (stage 4). The inelasticity developed in the shear wall is absent for short frames while that for taller frames is very limited. Under FB condition, the inelasticity in the shear wall is developed, which in turn inhibits the development of inelasticity in beams and columns. The results of the RC wall-frame specimens discussed for intermediate shaking are discussed for high shaking intensity in the following. Figure 7.14a and 7.14b show the plastic hinges in W3-9 and W3-15, respectively under S1; and their corresponding FB models are shown in Figures 7.14c and 7.14d. It can be observed that for the models under SSI, several columns and beams exhibit stage 4 inelasticity, whereas that under fixed base is negligible. The shear wall, however, undergoes a greater amount of inelasticity under FB condition. A similar observation holds true for other configurations shown in Figures 7.15 to 7.18. Under softer soil conditions, the beams and columns tend to develop a greater magnitude of inelasticity, especially in the columns at L1 and beams adjacent to the shear wall (for instance, compare Figures 7.16a and 7.16b). Additionally, under FB condition, the shear wall tends to develop significantly high inelasticity compared to that under SSI (compare Figures 7.17a-7.17d with Figures 7.17e-7.17h). Inelasticity in the shear wall causes significant inelasticity in the beams and columns. For example, comparing Figures 7.17g with 7.17h, it can be observed that the beams and columns at the top three storey levels develop greater inelasticity for the case wherein the shear wall develops greater inelasticity over the height. In Figures 7.18a and 7.18b, it can be observed that at L7, the shear wall in the wall-frame system under SSI exhibits greater inelasticity whereas that at L1, the extent of inelasticity is more under FB condition. The development of greater inelasticity in the shear wall at a higher storey level under SSI causes the beams and columns in the immediate higher storeys to develop greater inelasticity. The results indicate that the RC wall-frame systems under SSI could exhibit greater inelasticity in the frame members owing to the additional drifts induced due to rocking of the shear wall. The allowed rocking under SSI reduces the inelasticity in the shear wall at L1 however, at higher storey levels, greater inelasticity may develop. This, in turn, could give rise to additional inelastic deformations in the frame members of the storeys located in the immediate higher vicinity.

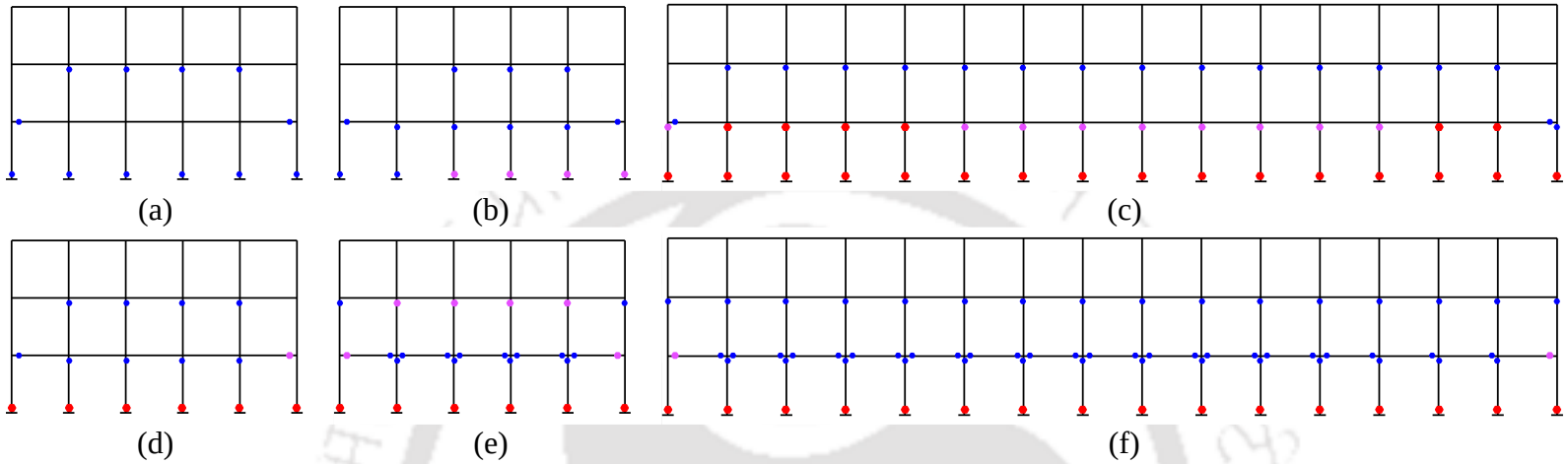

Figure 7.3 Inelastic response of plastic hinges in RC frame system (shaking intensity 0.24g) shown for (a) F3-5 under S1, (b) F3-5 under S4, and (c) F3-15 under S1. Corresponding fixed base response shown for (d) F3-5 under S1, (e) F3-5 under S4, and (f) F3-15 under S1.

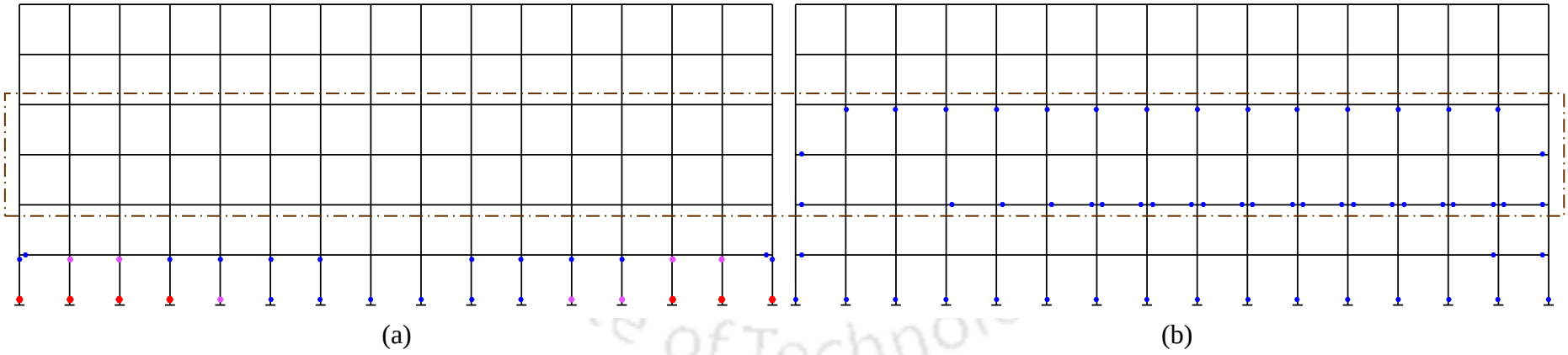

Figure 7.4 Inelastic response of plastic hinges in RC frame system (shaking intensity 0.24g) for (a) F6-15 under S1, and (b) its corresponding fixed base response.

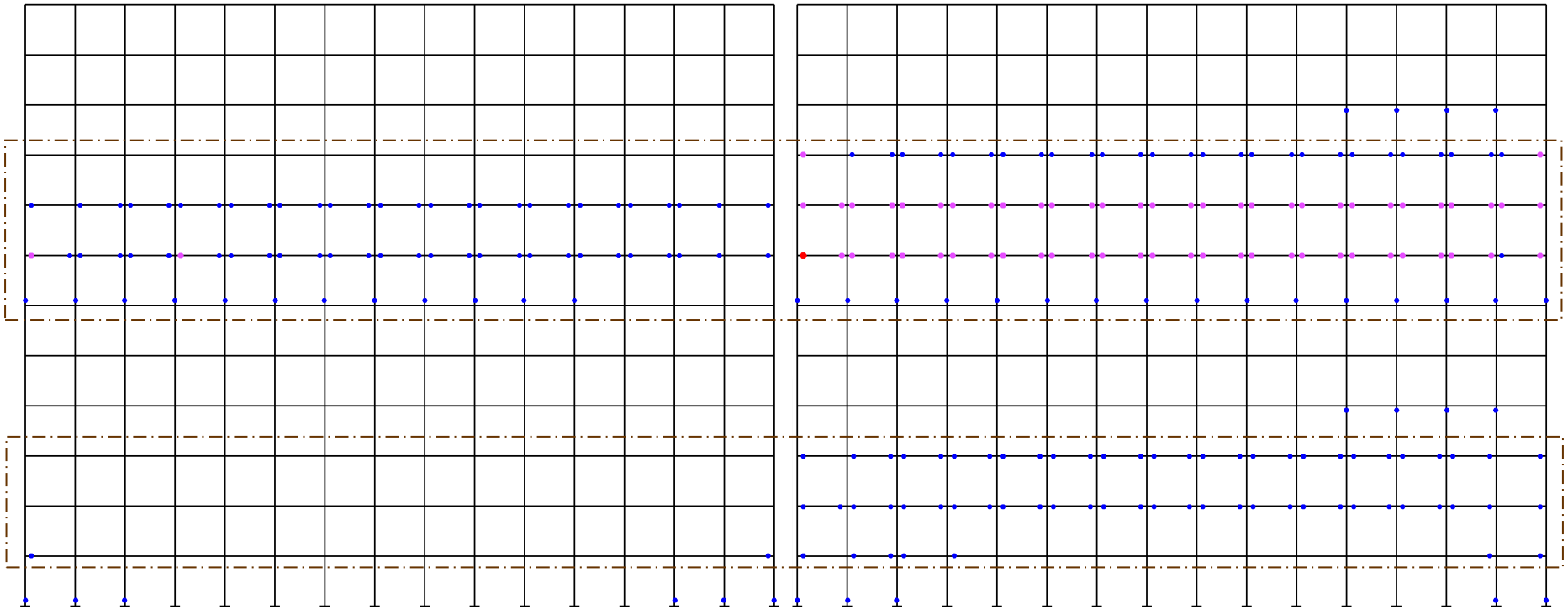

(a) (b)

Figure 7.5 Inelastic response of plastic hinges in the RC frame system (shaking intensity 0.24g) shown for (a) F12-15 under S1, and (b) its corresponding fixed-base response.

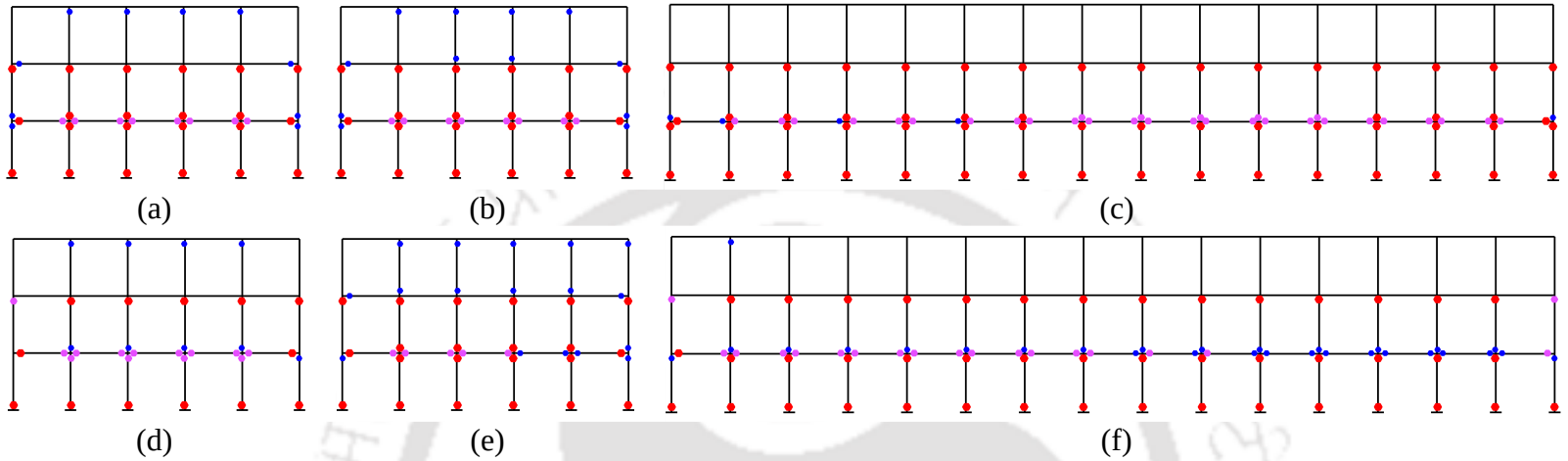

Figure 7.6 Inelastic response of plastic hinges in RC frame system (shaking intensity 0.48g) shown for (a) F3-5 under S1, (b) F3-5 under S4, and (c) F3-15 under S1. Corresponding fixed base response shown for (d) F3-5 under S1, (e) F3-5 under S4, and (f) F3-15 under S1.

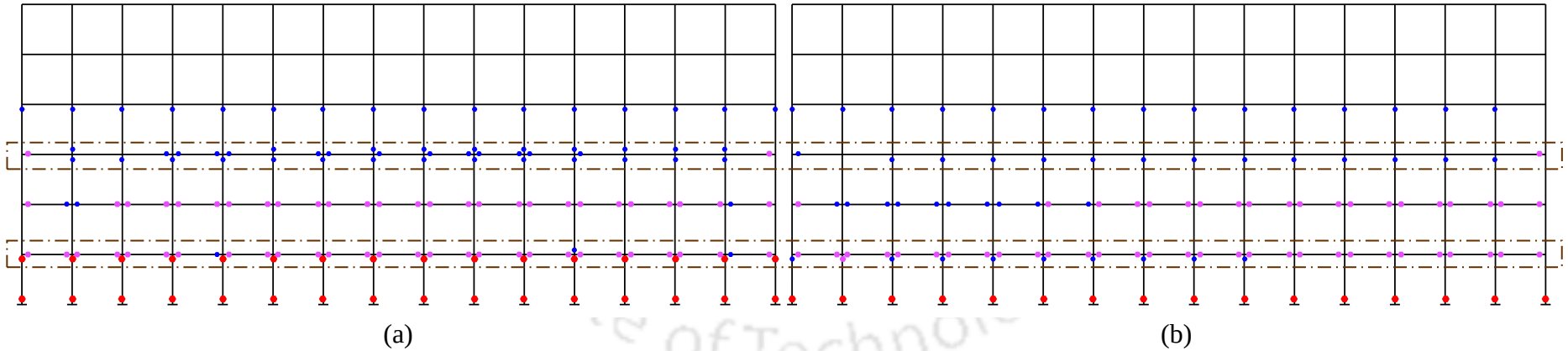

Figure 7.7 Inelastic response of plastic hinges in RC frame system (shaking intensity 0.48g) shown for (a) F6-15 under S1, and (b) its corresponding fixed base response.

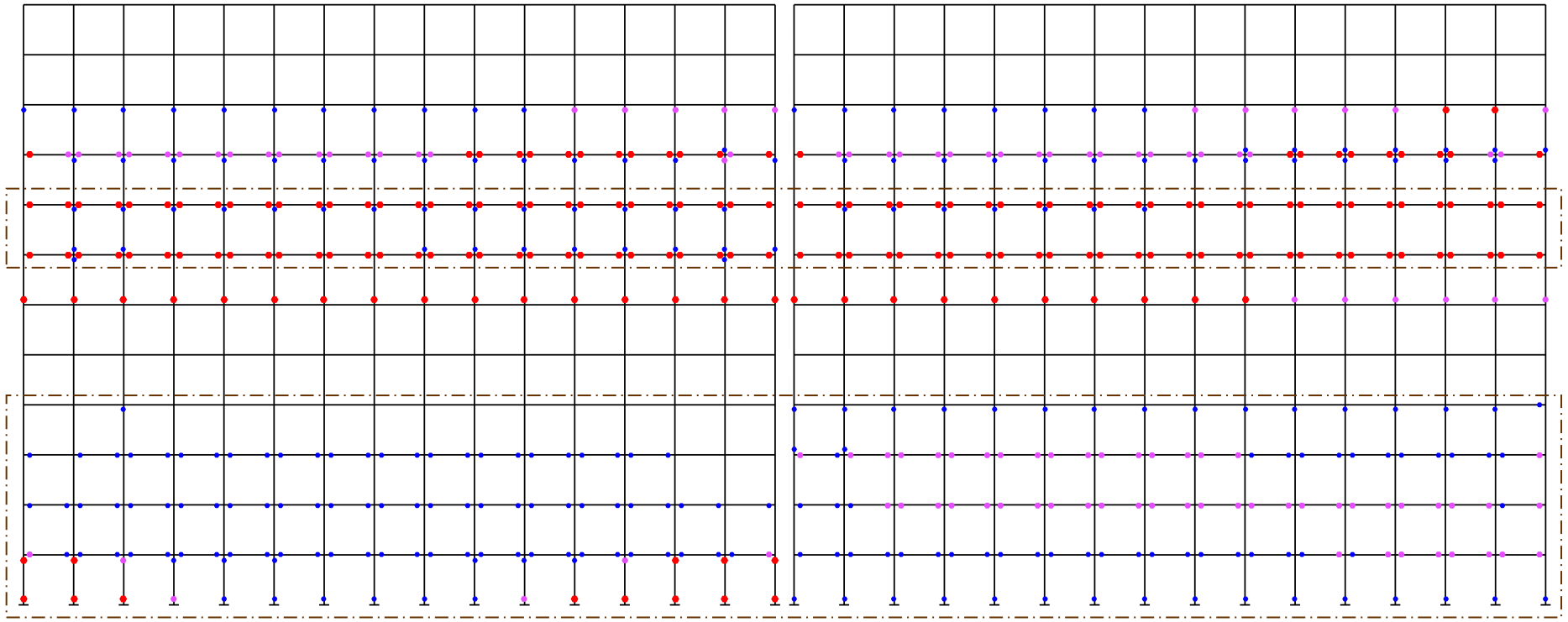

(a) (b)

Figure 7.8 Inelastic response of plastic hinges in the RC frame system (shaking intensity 0.48g) shown for (a) F12-15 under S1, and (b) its corresponding fixed-base response.

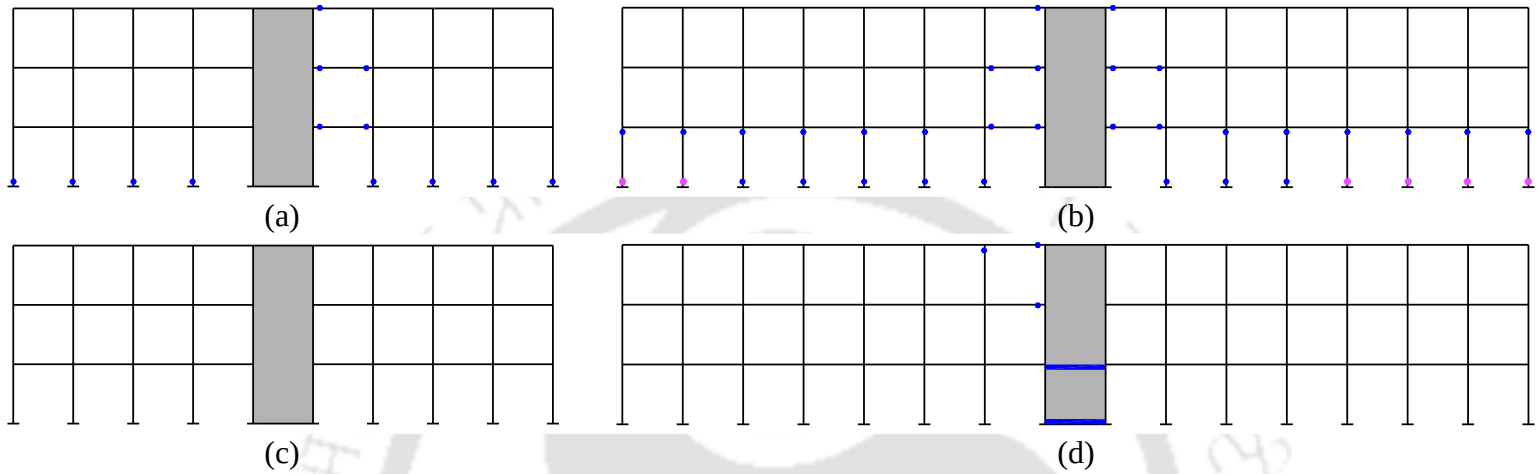

Figure 7.9 Inelastic response of plastic hinges in RC wall-frame system (shaking intensity 0.24g) shown for (a) W3-9 under S1, (b) W3-9 under S1. Corresponding fixed base response shown for (d) W3-9 under S1, and (e) W3-15 under S1.

Figure 7.10 Inelastic response of plastic hinges in RC wall-frame system (shaking intensity 0.24g) W6-15 under (a) S1, and (b) its corresponding fixed base response.

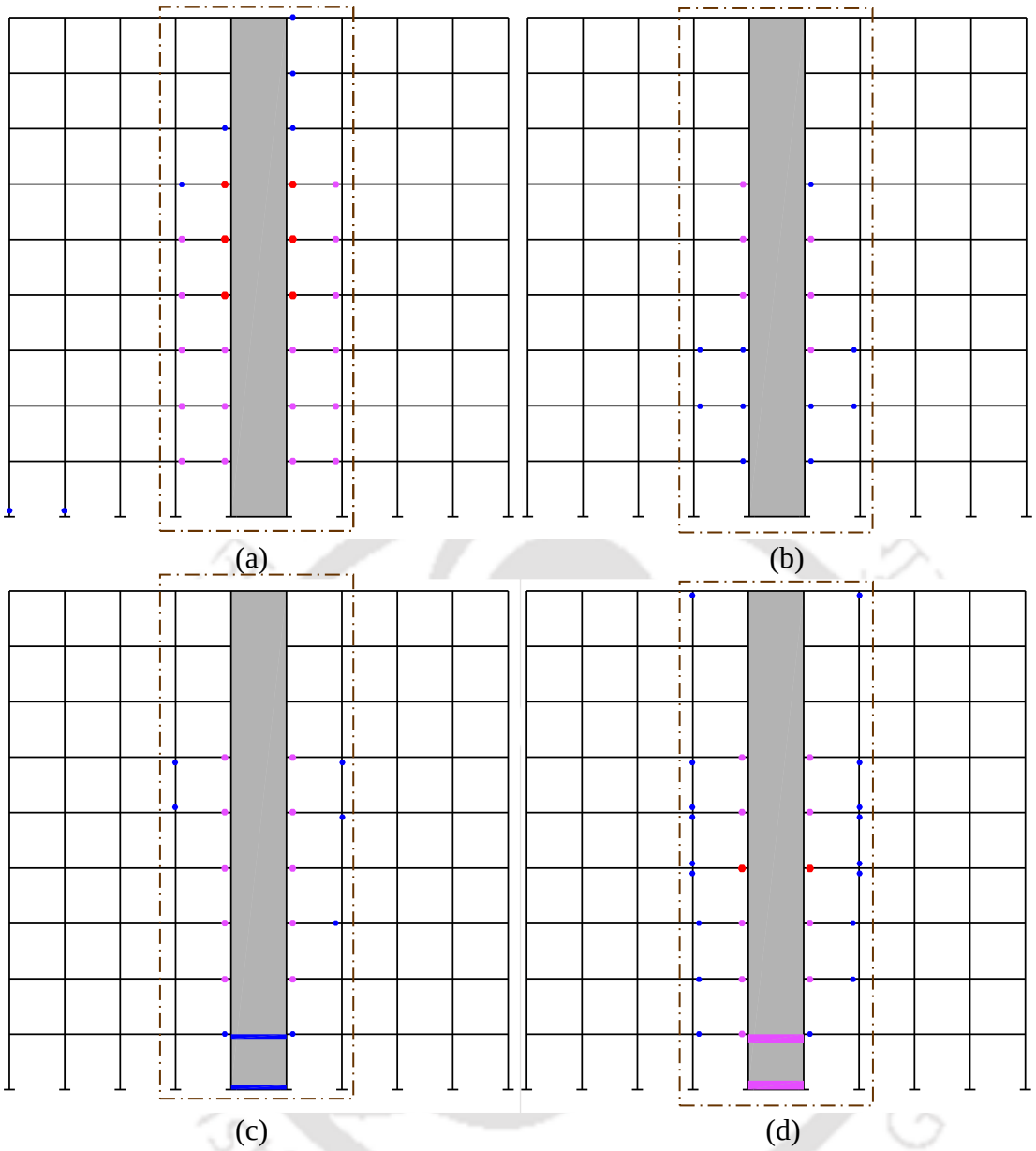

Figure 7.11 Inelastic response of plastic hinges in RC wall-frame system (shaking intensity 0.24g) shown for W9-9 under (a) S1, and (b) S4. Corresponding fixed base response shown for W9-9 under (c) S1, and (d) S4.

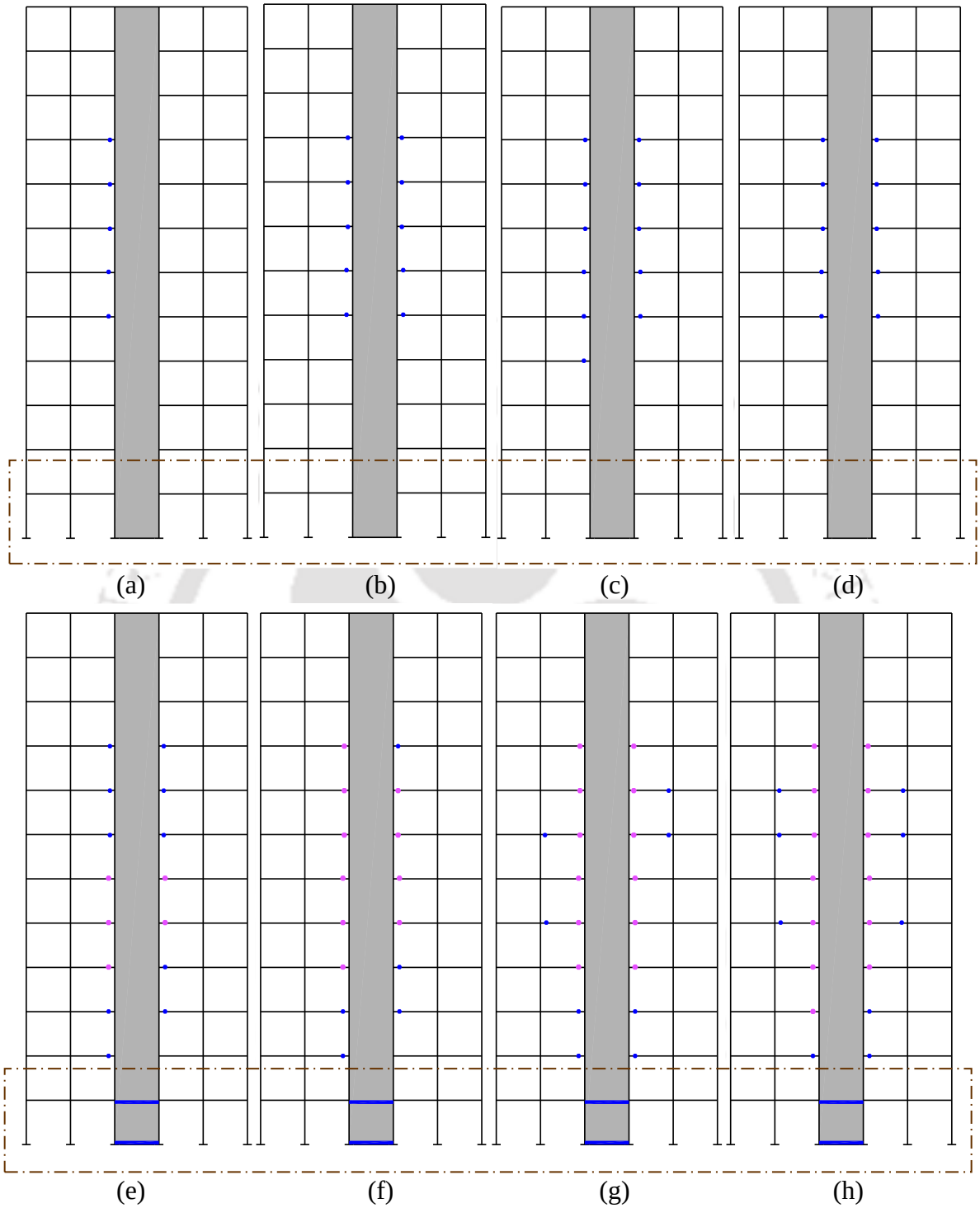

Figure 7.12 Inelastic response of plastic hinges in RC wall-frame system (shaking intensity 0.24g) shown for F12-5 under (a) S1, (b) S2, (c) S3, and (d) S4. Corresponding fixed base response of F12-5 under (e) S1, (f) S2, (g) S3, and (h) S4.

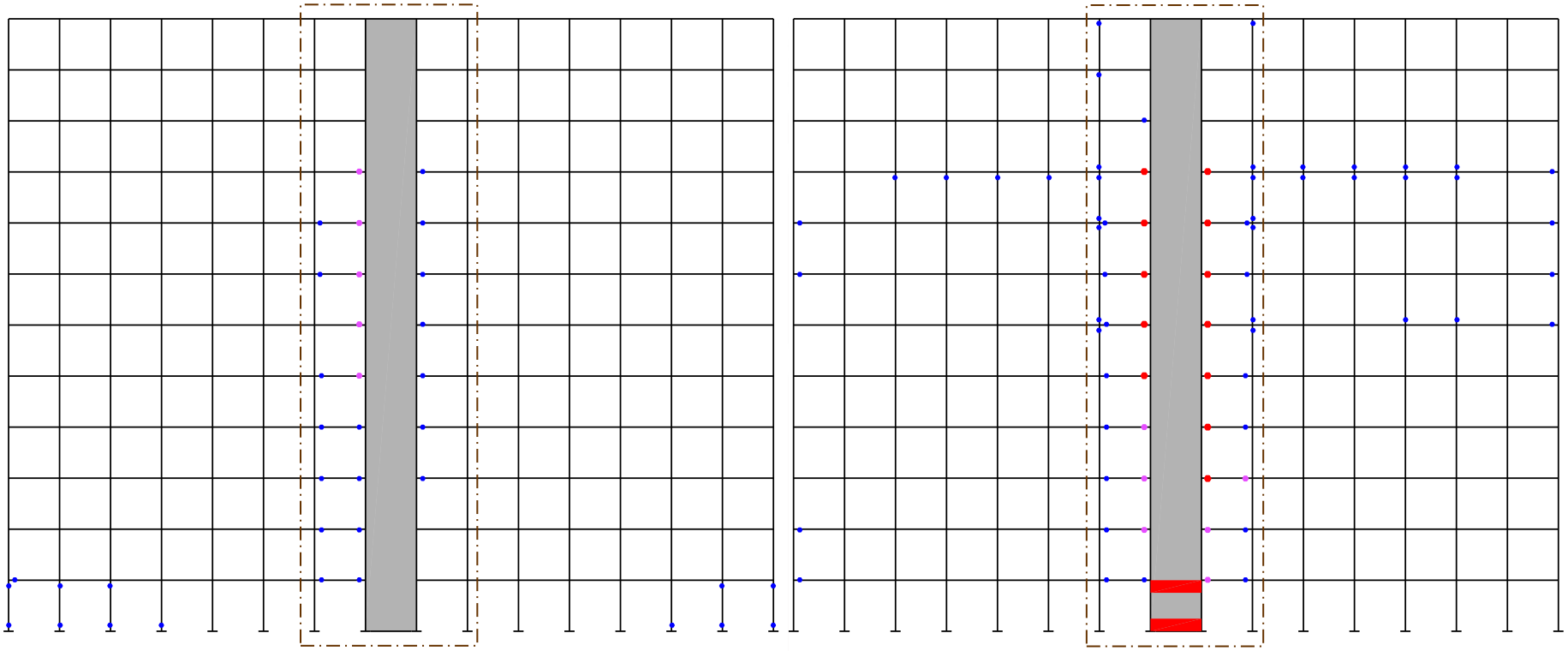

(a) (b)

Figure 7.13 Inelastic response of plastic hinges in RC wall-frame system (shaking intensity 0.24g) shown for F12-15 under (a) S1, and (b) its corresponding fixed base response.

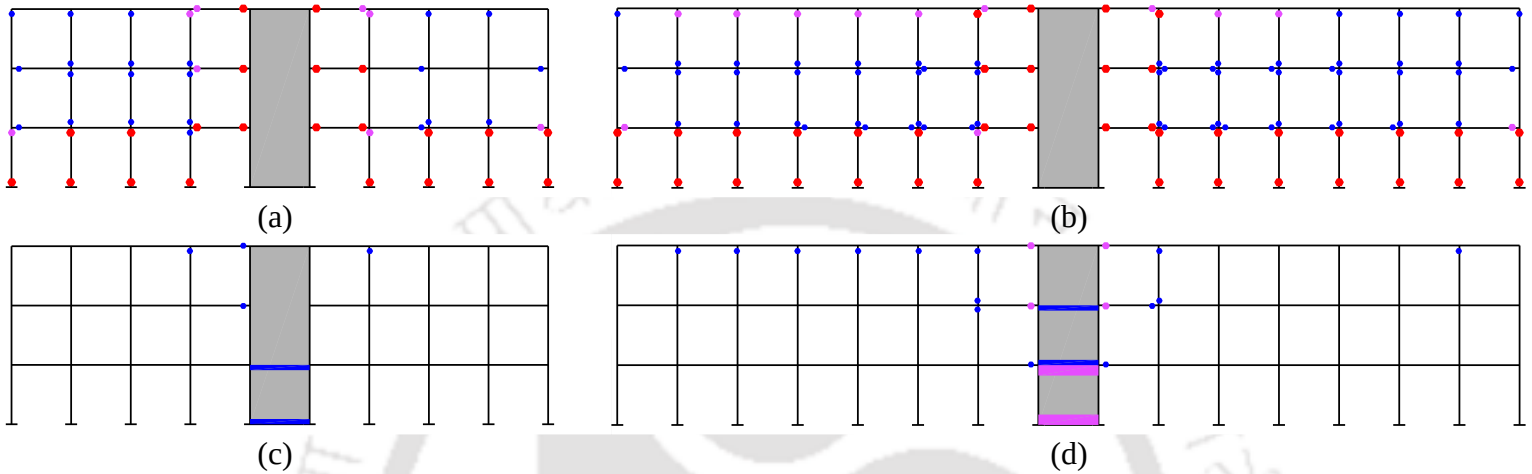

Figure 7.14 Inelastic response of plastic hinges in RC wall-frame system (shaking intensity 0.48g) shown for (a) W3-9 under S1, and (b) W3-9 under S1. Corresponding fixed base response shown for (d) W3-9 under S1, and (e) W3-15 under S1.

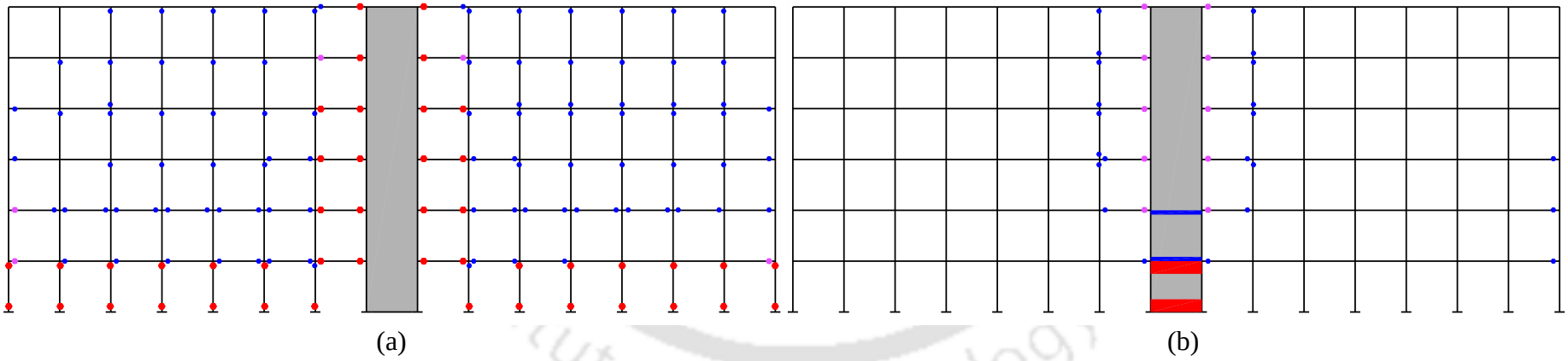

Figure 7.15 Inelastic response of plastic hinges in RC wall-frame system (shaking intensity 0.48g) shown for W6-15 under (a) S1, and (b) its corresponding fixed base response.

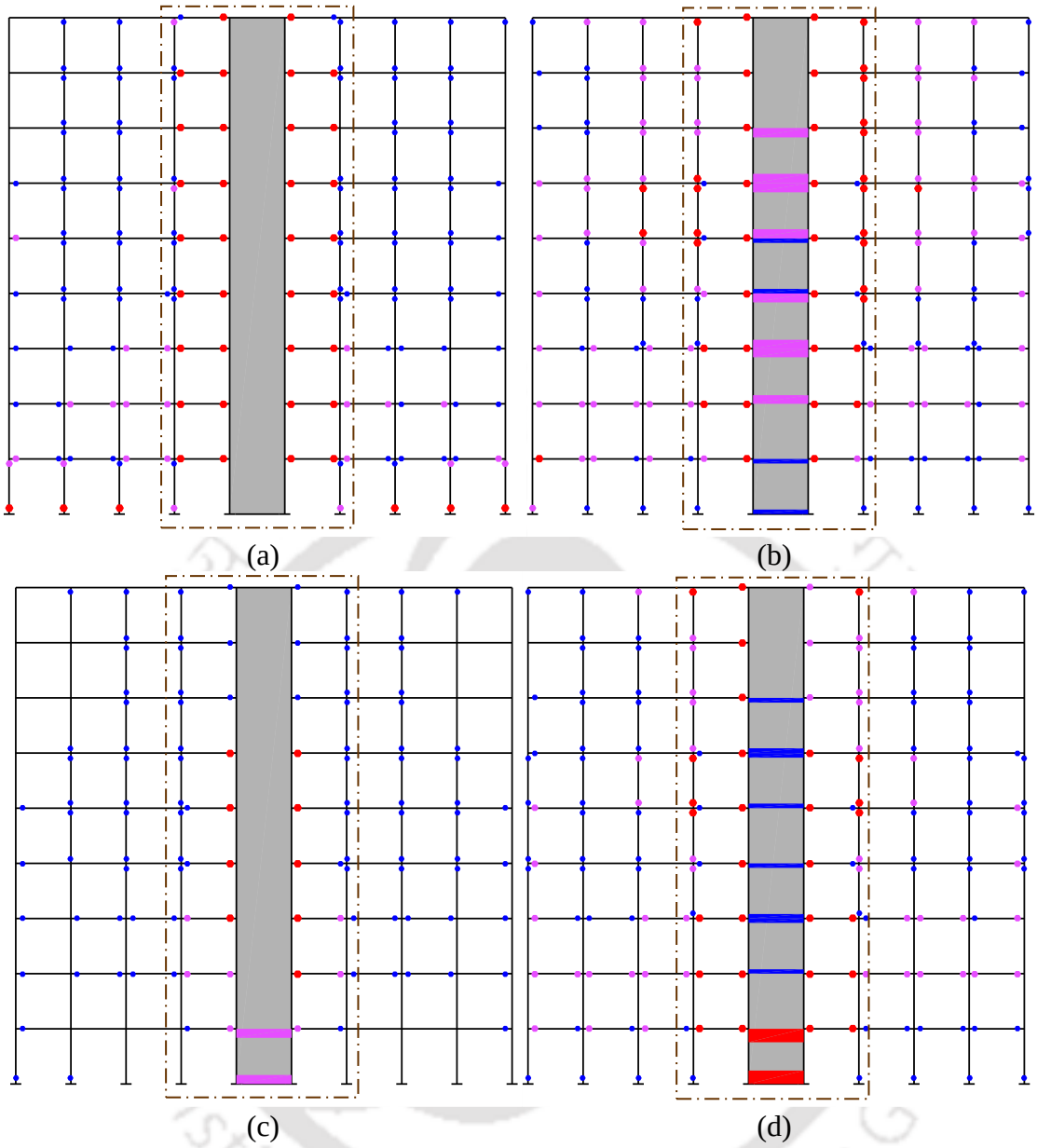

Figure 7.16 Inelastic response of plastic hinges in RC wall-frame system (shaking intensity 0.48g) shown for W9-9 under (a) S1, and (b) S4. Corresponding fixed base response shown for W9-9 under (c) S1, and (d) S4.

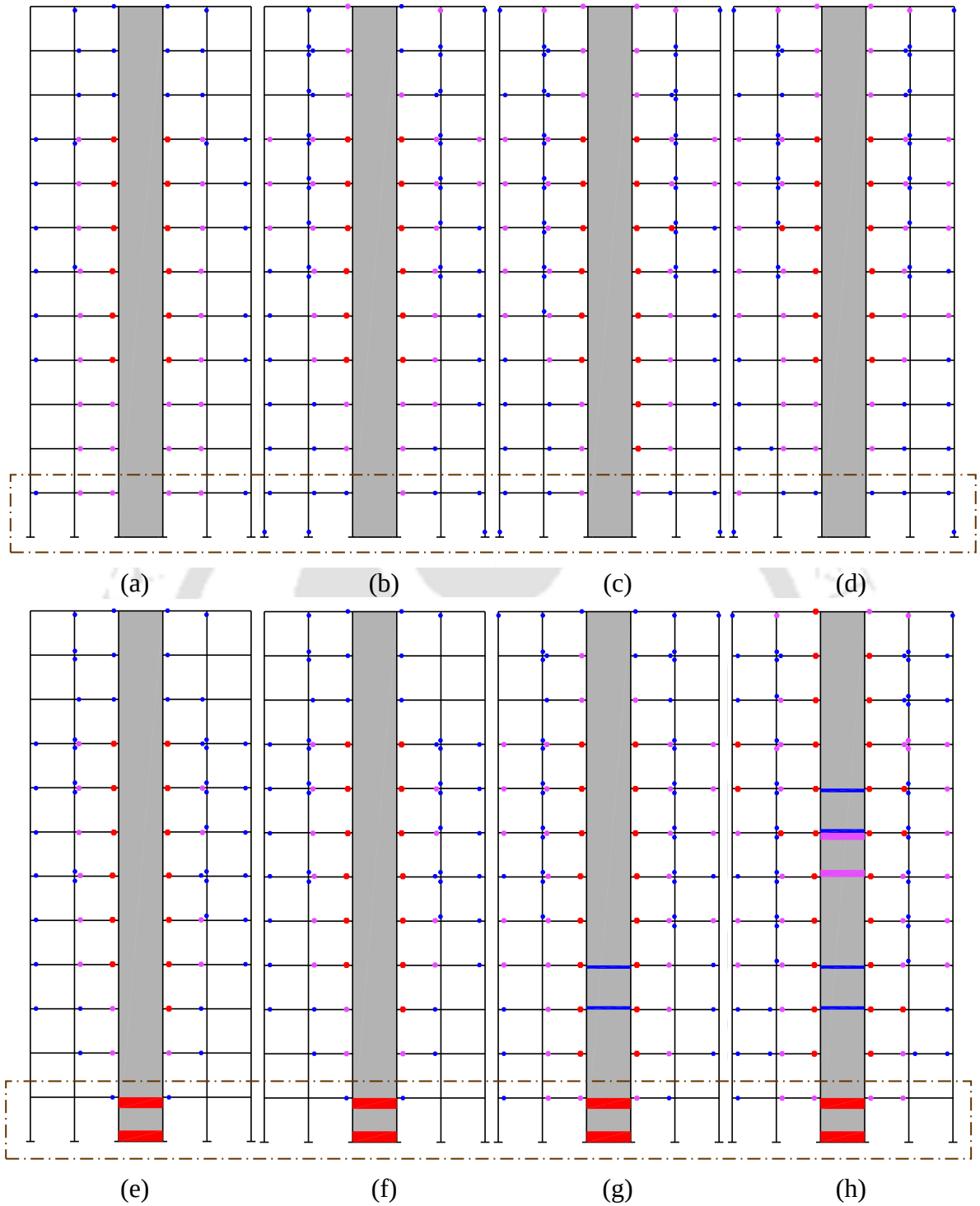

Figure 7.17 Inelastic response of plastic hinges in RC wall-frame system (shaking intensity 0.48g) shown for F12-5 under (a) S1, (b) S2, (c) S3, and (d) S4. Corresponding fixed base response of F12-5 under (e) S1, (f) S2, (g) S3, and (h) S4.

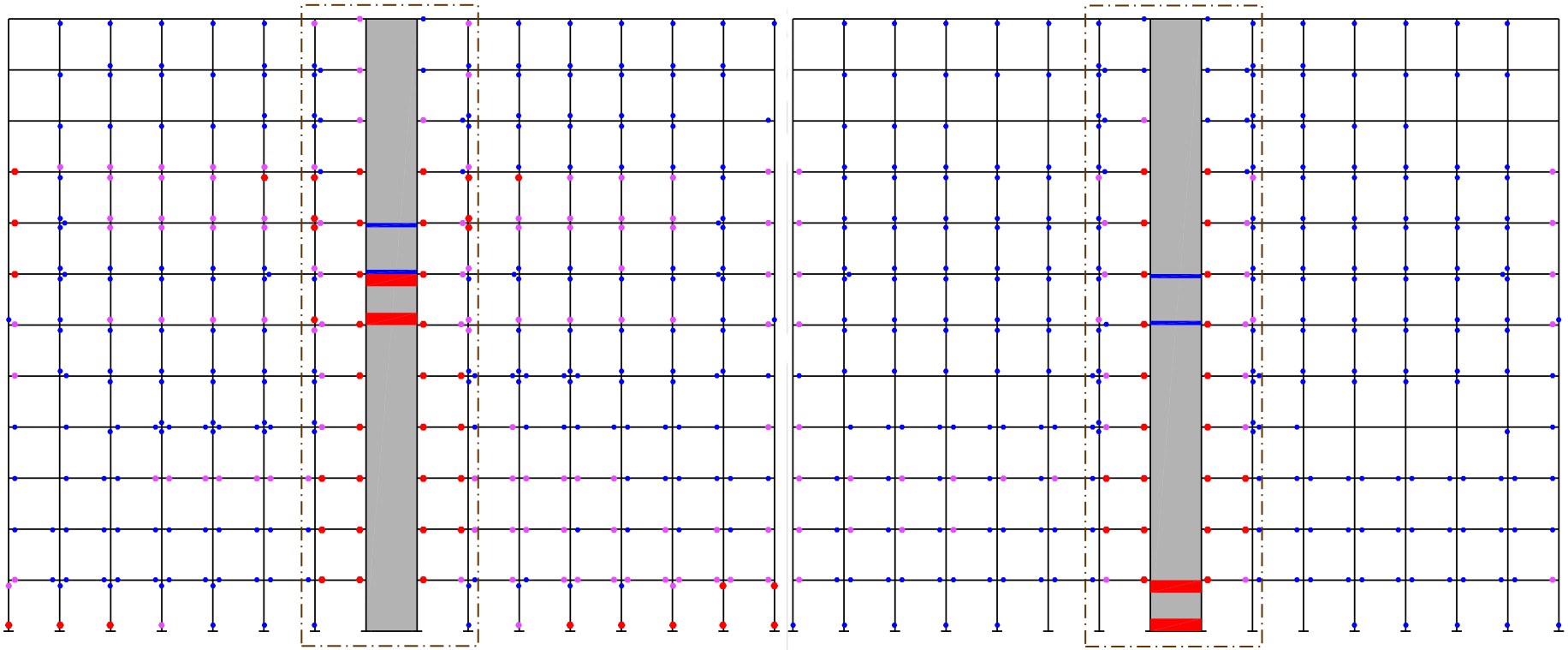

(a) (b)

Figure 7.18 Inelastic response of plastic hinges in RC wall-frame system (shaking intensity 0.48g) shown for F12-15 under (a) S2, and (b) its corresponding fixed base response.

7.6 INFLUENCE OF SSI ON DUCTILITY DEMANDS

The results of the analysis cases obtained to study the influence of SSI on the local and global ductility demands are discussed in the following sections.

7.6.1 Local Demands

As already discussed, the influence of SSI on local ductility demands is studied with the help of normalized curvature ductility demand $\bar{\mu}_c$, in the structural elements at the different storey levels of the RC frame and RC wall-frame systems. For any particular section, $\bar{\mu}_c > 1$ indicates that the curvature ductility demand under the influence of SSI is greater than that under FB condition. The mobilization of this condition with the curvature demands imposed being lower than the yield curvature of the section may not be sufficient to induce a detrimental instance. This is because the sectional response would remain essentially elastic. Therefore, the influence of SSI on local ductility demands would be detrimental when the following conditions develop simultaneously.

1. Curvature ductility demands of elements under the influence of SSI are greater than 1, i.e., $\mu_{c,SSI} > 1$ In other words, the section has undergone an inelastic response.
2. Curvature ductility demands imposed onto the elements under the influence of SSI must be greater than that imposed under FB condition, i.e., $\frac{\mu_{c,SSI}}{\mu_{c,FB}} = \bar{\mu}_c > 1$.

For any particular section, the simultaneous fulfillment of these two conditions leads to the development of detrimental instances for the element section. It is worth mentioning that while studying the storey wise variation in $\bar{\mu}_c$, the average ductility demand of the frame members is considered. The following subsections discuss the influence of SSI on the local ductility demands in the sections of the load resisting elements of the RC frame and RC wall-frame systems.

7.6.1.1 RC Frame System

In this section, the influence of SSI on the local ductility demands in the members of the RC frame system is discussed. Figures 7.19a-7.19d respectively show the storey wise distribution of $\bar{\mu}_c$ in the columns of F3-3, F3-15, F12-3, and F12-15 subjected to intermediate (0.24g) intensity of shaking under different soil conditions. The detrimental instances are marked by red bubbles. It can be observed that for F3-3 no detrimental instance

develops although at L3, $\bar{\mu}_c > 1$ for the weaker soil conditions (S1 and S2). This is because the sectional response is elastic (in other words, the curvatures developed under SSI are less than the yield curvature of the section, i.e., $\phi_{d,SSI} < \phi_y$). Similarly, for F3-15, no detrimental instance develops under the stiffer soil conditions (S2, S3, and S4), however, under S1 detrimental instance is observed at L1. For F12-3 detrimental instance develops at L10 under S1 and that for F12-15, develops for all soil types at L1 but at higher storey level; the detrimental instances are observed for the stiffest soil condition (S4).

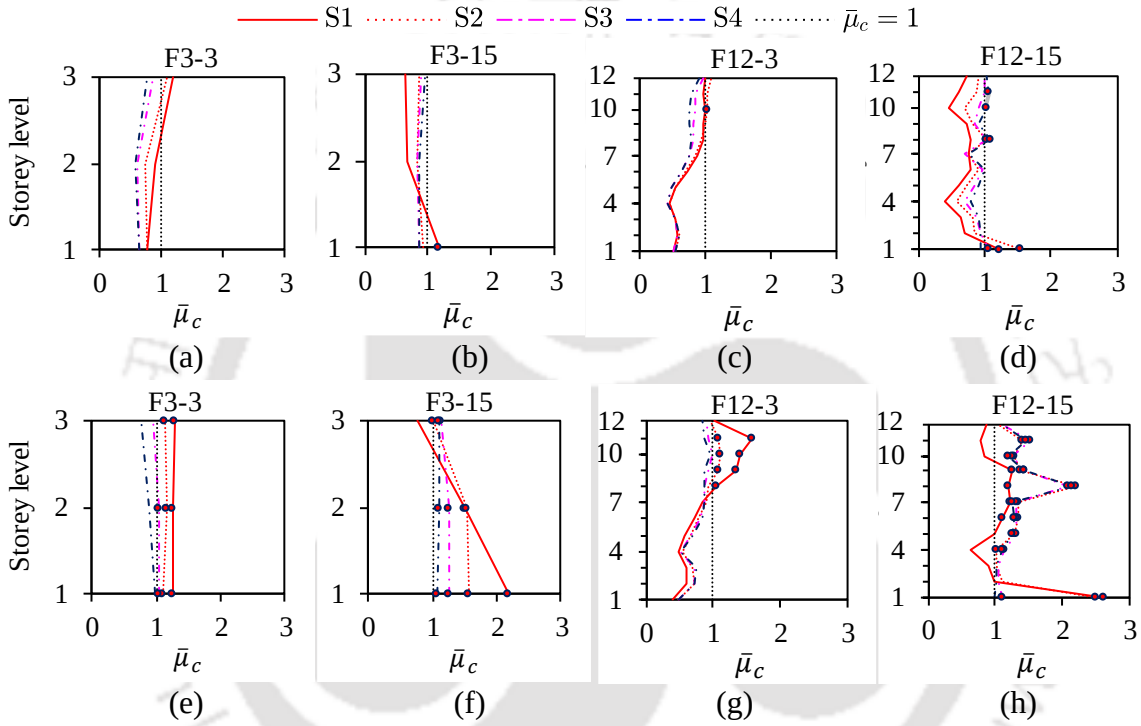

Figure 7.19 Influence of SSI on average $\bar{\mu}_c$ in column sections at various storey levels of RC frame systems (a) F3-3, (b) F3-15, (c) F12-3, and (d) F12-15 for ground motion intensity 0.24g; (e) F3-3, (f) F3-15, (g) F12-3, and (h) F12-15 ground motion intensity 0.48g.

Figures 7.19e-7.19h respectively show the storey wise distribution of $\bar{\mu}_c$ in the columns of F3-3, F3-15, F12-3, and F12-15 subjected to the high intensity of shaking (0.48g) under the different soil conditions. It can be observed that at high shaking intensity, frames F3-3 and F3-15 exhibit more number of detrimental instances at various storey levels for most soil conditions. Moreover, it can be observed that the magnitude of exceedance $\bar{\mu}_c > 1$ is greater for softer soil conditions (S1 and S2) compared to stiffer soil conditions (S3 and S4). Similarly, for F12-3, detrimental instances develop at higher storey levels corresponding to the weaker soil conditions (S1 and S2). For F12-15 under S1 and S2, the detrimental

instances develop with a very large magnitude of $\bar{\mu}_c$ at L1 and relatively smaller magnitude at higher storey levels. Under S3 and S4, the magnitude of $\bar{\mu}_c$ (for the detrimental cases) is significantly lower at L1, but at a higher storey level, it is much greater when compared with that under S1.

The storey wise distribution of $\bar{\mu}_c$ in columns of other configurations is shown in Figures 7.20a and 7.20b corresponding to intermediate (0.24g) and high (0.48g) intensity of shaking, respectively. In general, it can be observed that a greater magnitude of the peak $\bar{\mu}_c$ is exhibited under weaker soil conditions (mostly for S1 followed by S2). For stiffer soil conditions (S3 and S4), the peak $\bar{\mu}_c$ is relatively less. For intermediate shaking intensity (Figure 7.20a), $\bar{\mu}_c$ for columns, in frames with narrow widths (3 bay, 5 bay), it is mostly less than unity at lower stories of the frame and is close to unity for higher storey levels. This indicates that at lower storey levels, the difference in the magnitude of inelasticity under SSI and FB conditions is greater compared to that at higher storey levels. For frames with larger widths (9 bay and 15 bay), $\bar{\mu}_c$ is relatively close or exceeds unity at lower storey levels exhibiting detrimental instances under softer soil conditions (S1 and S2). For stiffer soil conditions (S3 and S4), the frames may exhibit detrimental instances at higher storey levels also. This indicates that the local ductility demands are significantly modified under different soil conditions. It is to be noted that corresponding to intermediate shaking intensity, only very few detrimental instances are observed in the various RC frame systems. Moreover, the increase in the ductility demands ranges from 5% to 76%.

For the high intensity of the shaking (Figure 7.20b), a large number of detrimental instances are observed in each specimen under the various soil profiles considered. Corresponding to a particular height, narrow frames exhibit detrimental instances with the peak $\bar{\mu}_c$ at higher storey levels that are greater for relatively weaker soil conditions (S1 and S2). Wider frames exhibit a greater number of detrimental instances distributed over the height of the frame for all the soil conditions. Moreover, the wider frames develop peak $\bar{\mu}_c$ at L1, which is greater under weaker soil conditions (S1 and S2). On increasing the width of the frame, the peak $\bar{\mu}_c$ developed shifts towards lower storey levels, and it is more pronounced for the weaker soil conditions (S1 and S2). For stiffer soil conditions (S3 and S4), however, peak $\bar{\mu}_c$ may develop at higher storey levels. It is worth mentioning that in

a past study by Ghandil and Behnamfar (2018) on intermediately wide (20 m) moment-resisting frame (MRF) systems, a similar observation was made wherein SSI increased the ductility demands in the lower stories. The foregoing observations indicate that influence of SSI on ductility demands could be detrimental for all types of building frame configurations. For narrow configurations, SSI could cause a detrimental increase in the local ductility demands of the columns at higher storey levels that is greater for weaker soil conditions. For wider frames under weaker soil conditions, SSI could cause a detrimental increase in local ductility demands at lower storey levels. However, for a wider frame under stiffer soil conditions, SSI is more detrimental for columns at higher storey levels. The maximum increase in the local ductility demands ranges from 14% to 163%.

As for columns, the storey wise distribution of $\bar{\mu}_c$ for beams is obtained for the various configurations of frame systems under the various soil conditions and are shown in Figures 7.21a and 7.21b respectively for intermediate (0.24g) and high (0.48g) intensity of shaking. As observed for column members, for beams too in general, it can be observed that the greatest $\bar{\mu}_c$ is exhibited under weaker soil conditions (mostly for S1 followed by S2) and that for stiffer soil conditions (S3 and S4) is relatively less. Higher intensity of shaking results in the development of a larger number of detrimental instances at the various storey levels. It can be observed that unlike for columns, for beams, the influence of SSI on $\bar{\mu}_c$ is comparatively less. However, irrespective of the structural elements, the observations indicate that local ductility demands may increase at one or more storey levels. This increase is greater for weaker soil conditions under the higher intensity of shaking, which leads to the exhibition of a larger number of detrimental instances and greater inelasticity in the RC frame systems.

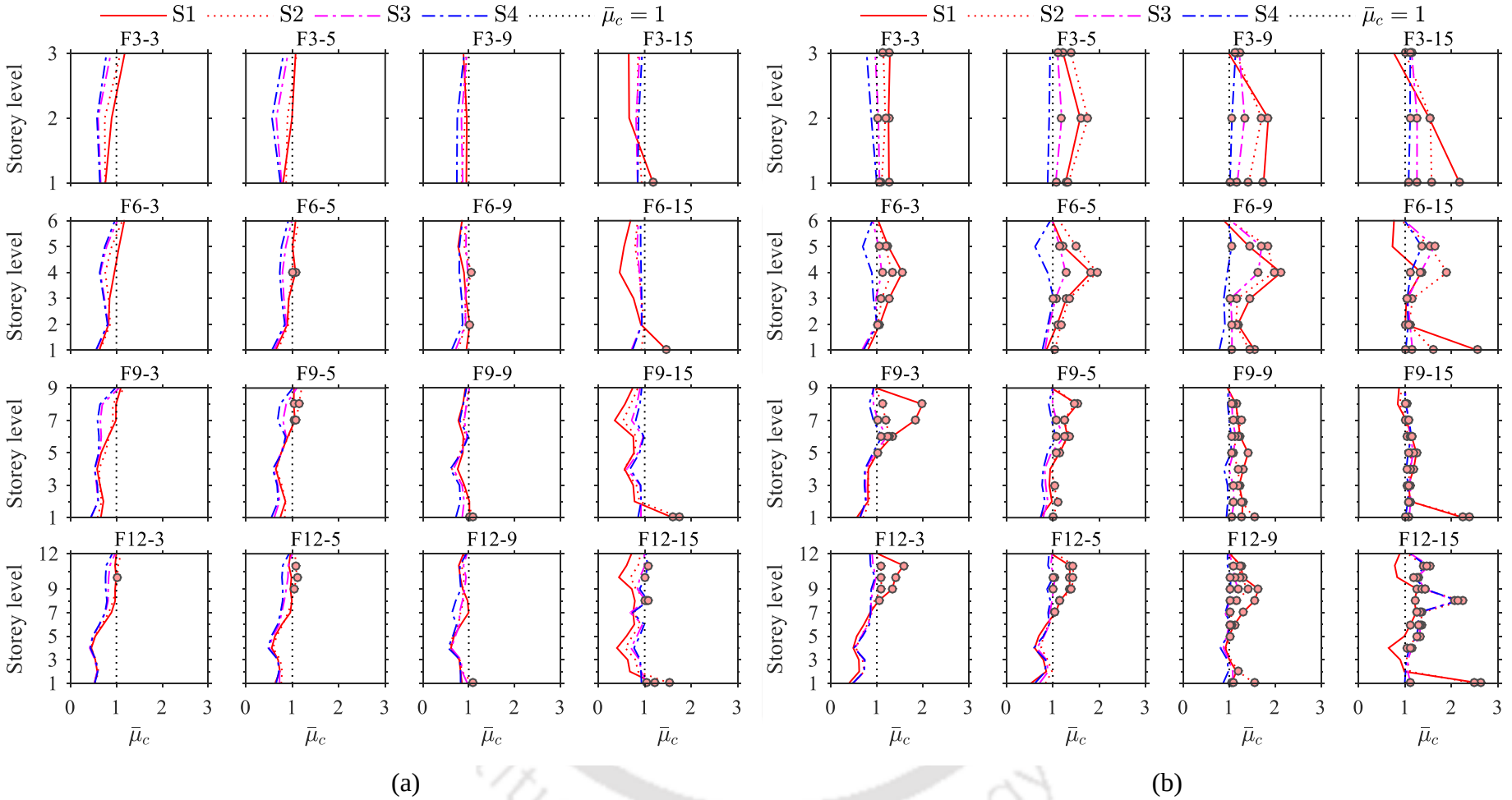

Figure 7.20 Influence of SSI on average $\bar{\mu}_c$ in column sections at various storey levels of RC frame systems under ground motion intensities (a) 0.24g, and (b) 0.48g.

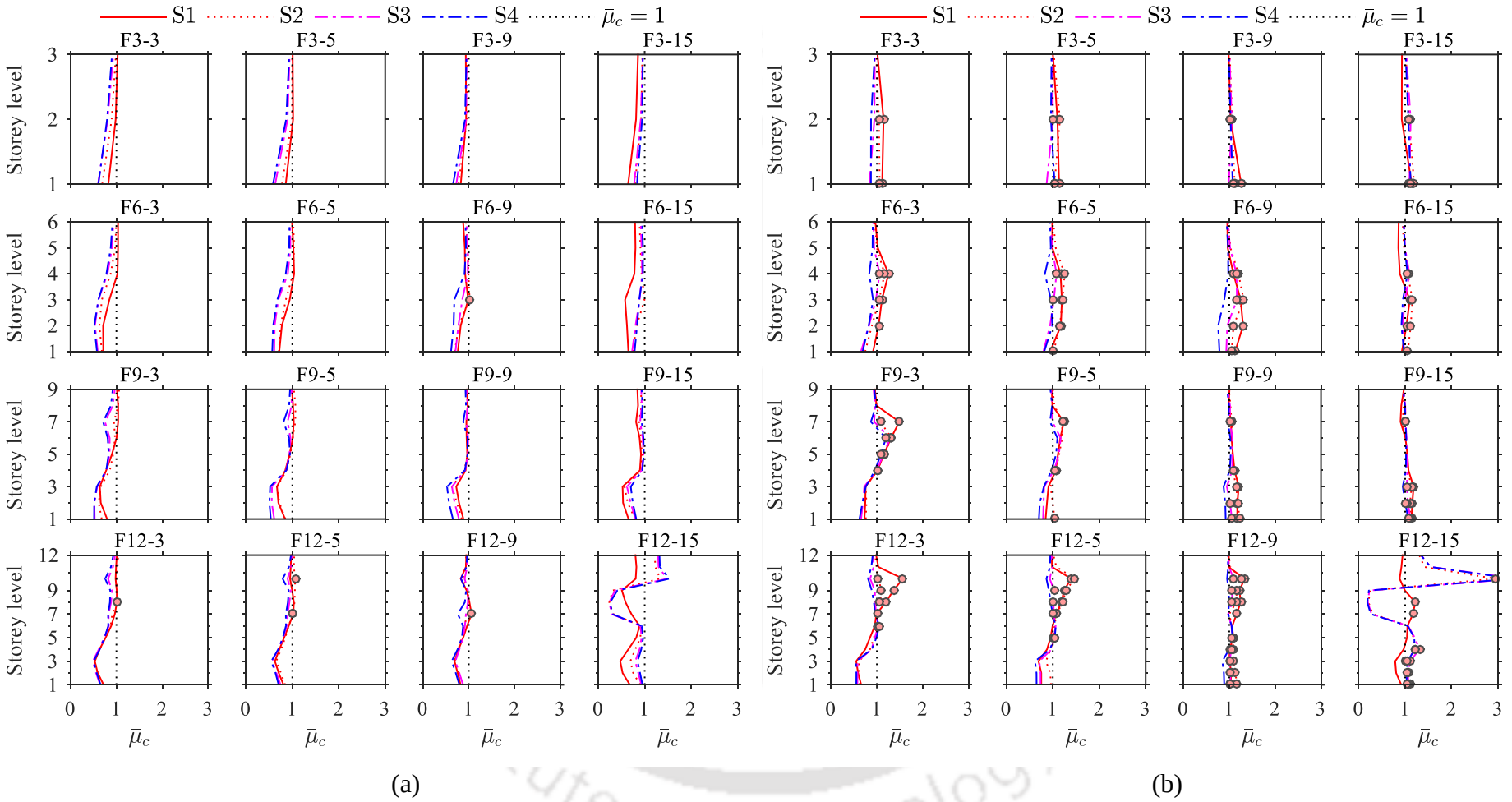

Figure 7.21 Influence of SSI on average $\bar{\mu}_c$ in beams sections at various storey levels of RC frame systems under ground motion intensities, (a) 0.24g, and (b) 0.48g.

7.6.1.2 RC Wall-frame System

The storey wise distribution of $\bar{\mu}_c$ in columns of the various RC wall-frame systems under different soil conditions corresponding to intermediate (0.24g) and high (0.48g) intensities of shaking is shown in Figures 7.22a and 7.22b respectively. It can be observed that $\bar{\mu}_c$ is generally highest for the weakest soil condition (S1 followed by S2) and relatively less for stiffer soil condition (S3 and S4). In general, it can be observed that peak $\bar{\mu}_c$ is developed at L1 for all the considered configurations under intermediate and high shaking intensities. Moreover, it is highest for 3 storeyed configurations (W3-3, W3-5, W3-9, and W3-15) followed by 6 storeyed, 9 storeyed, and 12 storeyed wall-frame systems. For the intermediate intensity of shaking (Figures 7.22a), it can be observed that very few detrimental instances are observed, which mostly develop at L1 and for weaker soil conditions (S1 and S2). Additionally, for narrow configurations (3 bay and 5 bay) it is observed that no detrimental instances develop since the sectional response is largely elastic. However, a higher intensity of shaking leads to the development of more cases of detrimental instances. For very narrow configurations (3 bay), very few detrimental instances develop mostly for the weaker soil conditions. This is because very narrow configurations are relatively stiffer due to the greater shear-wall area ratio. For the other configurations, it is observed that detrimental instances are observed at several storey levels with peaks at L1. This is because, under SSI conditions, greater flexibility is imparted to the base of the wall that imposes additional demands on the columns due to frame action. It may also be noted that greater exceedance of $\bar{\mu}_c$ above unity is observed for stiffer systems with softer soil conditions. The maximum increase in the local ductility demands in the columns for the detrimental instances could range from 450% to 300% for very stiff to flexible wall-frame configuration, respectively.

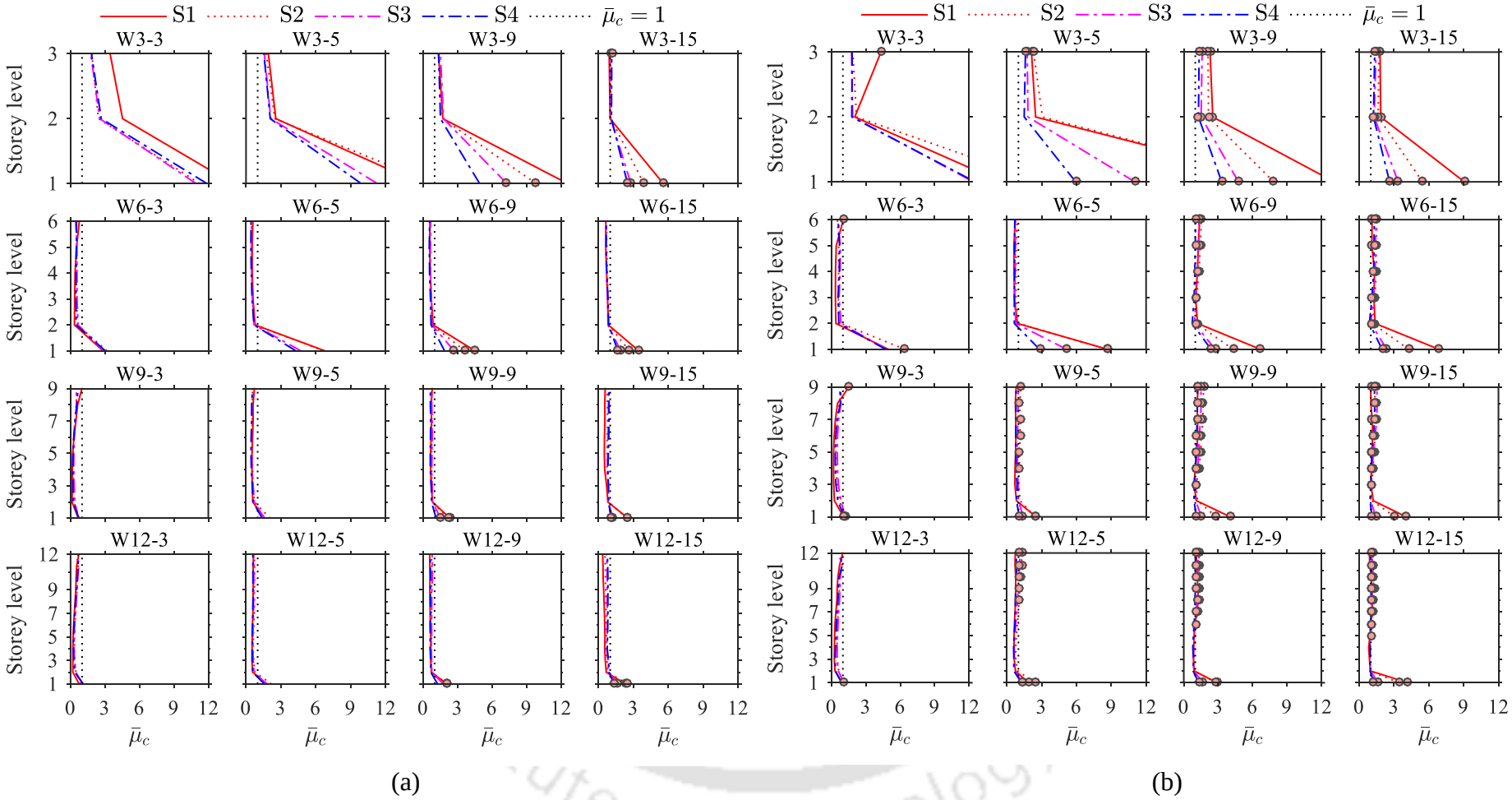

Figure 7.22 Influence of SSI on average $\bar{\mu}_c$ in column sections at various storey levels of RC wall-frame systems under ground motion intensities (a) 0.24g, and (b) 0.48g.

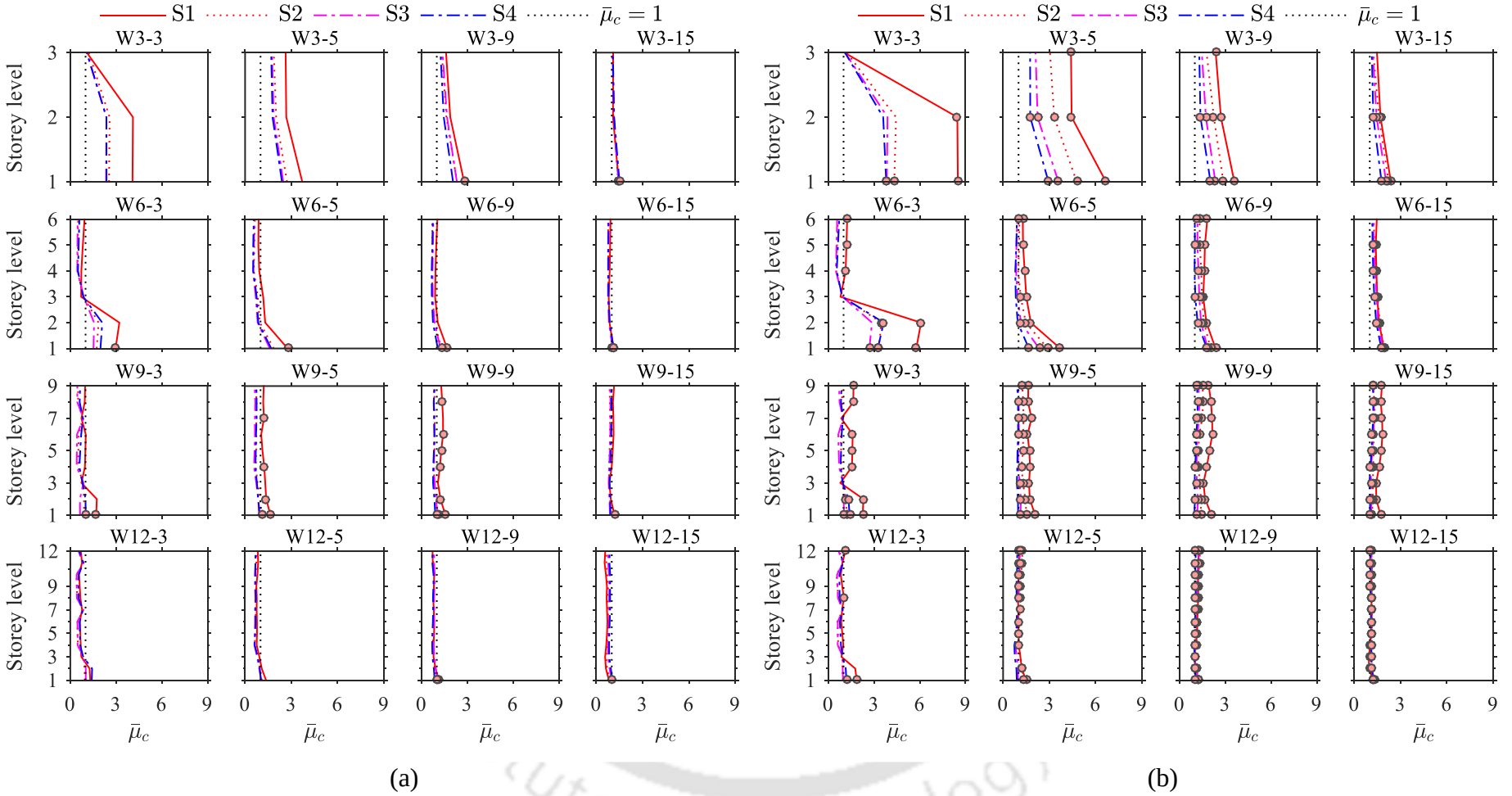

Figure 7.23 Influence of SSI on average $\bar{\mu}_c$ in beam sections at various storey levels of RC wall-frame systems under ground motion intensities (a) 0.24g, and (b) 0.48g.

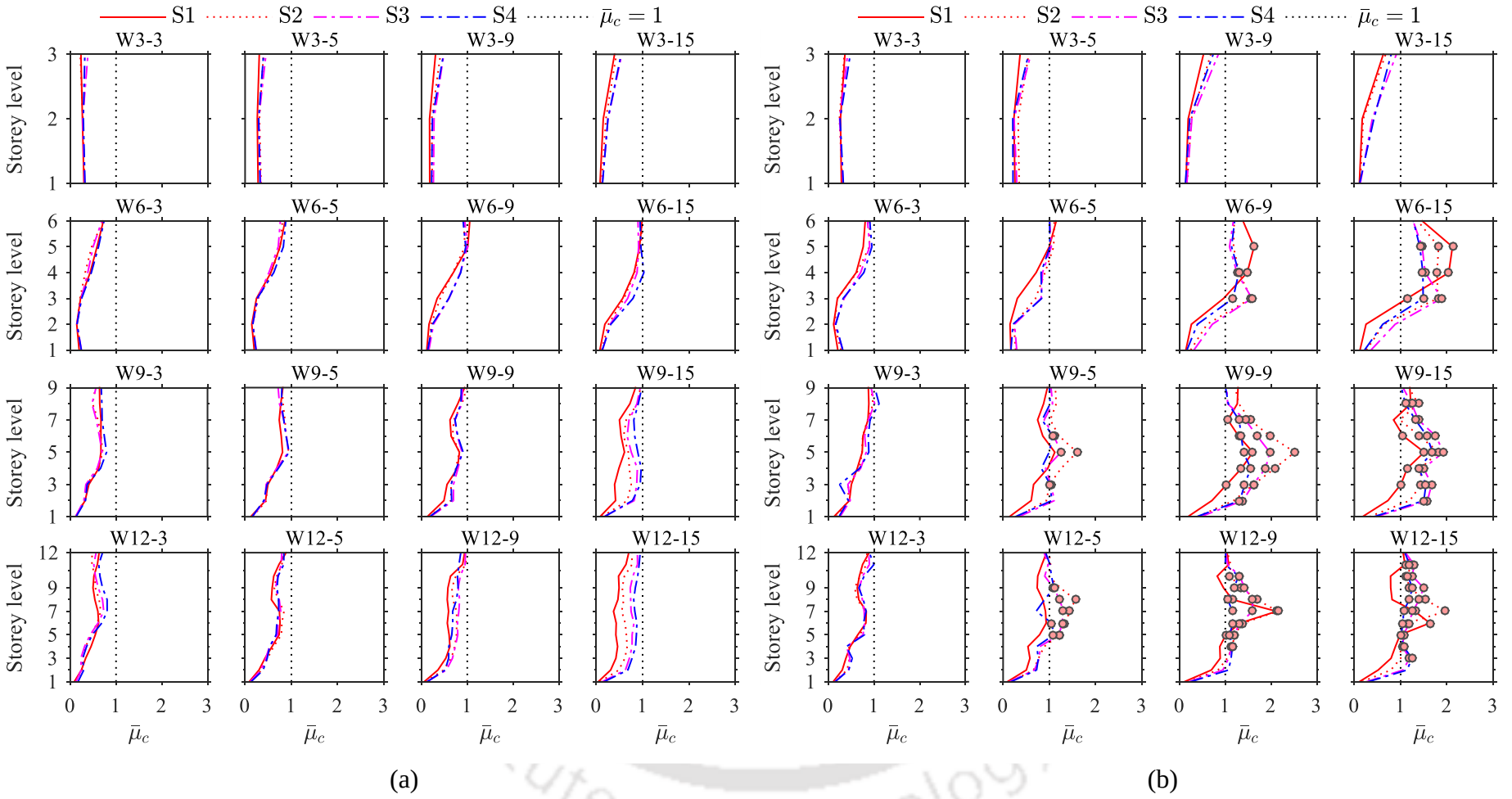

Figure 7.24 Influence of SSI on average $\bar{\mu}_c$ in shear wall sections at various storey levels of RC wall-frame systems under ground motion intensities (a) 0.24g, and (b) 0.48g.

The storey wise distribution of $\bar{\mu}_c$ in the beams of the various wall-frame systems under the different soil conditions corresponding to intermediate (0.24g) and high (0.48g) shaking intensities is shown in Figures 7.23a and 7.23b respectively. As for columns, in beams too, the peak $\bar{\mu}_c$ is greatest for weaker soil conditions (mostly for S1 followed by S2) and relatively lesser for stiffer soil condition (S3 and S4). In general, it can be observed that $\bar{\mu}_c$ is greatest at L1 for all the considered configurations. For frames with narrow configuration (3 bay) apart from L1, beams at L2 also exhibit greater $\bar{\mu}_c$. For the intermediate intensity of shaking, it can be observed that the number of detrimental instances is significantly less compared to that at high shaking intensity for the considered configurations. The detrimental instances could exhibit a maximum increase in the local ductility demands in the beams ranging from 140% for very stiff configuration to 90% for flexible configuration. It can be observed that a greater increase in the local ductility demands is observed for stiffer systems with softer soil conditions. A similar observation was made by Marzban et al. (2014).

The storey wise distribution of $\bar{\mu}_c$ in the shear wall of the various wall-frame systems under the different soil conditions corresponding to intermediate (0.24g) and high (0.48g) intensities of shaking is shown in Figures 7.24a and 7.24b respectively. For shear walls, $\bar{\mu}_c$ is generally greatest for stiffer soil conditions (mostly for S4 and S3) and relatively less for weaker soil condition (S1 and S2). This is because the effect of SSI is to introduce flexibility at the wall base that is higher for weaker soil conditions. Therefore, the reduction in the curvature demand is also higher for the weaker soil conditions. It can be pointed out that similar observation was made by Carbonari et al. (2012) in their study wherein compared to FB condition, SSI led to a reduction of seismic forces under the shear wall and was greater for weaker soil conditions. Moreover, at intermediate shaking intensity, $\bar{\mu}_c$ for the shear wall is invariably less than unity for all the wall-frame systems considered. It can be observed that $\bar{\mu}_c$ is particularly less for the lower storey levels of the wall-frame systems and at L1 $\bar{\mu}_c$ is greatly less than unity. At higher storey levels for all soil conditions $\bar{\mu}_c$ is relatively closer to unity. This is because, at higher storey levels, the frame action dominates, and the influence of the allowed flexibility at the base of the wall gets reduced, thereby causing curvature ductility demand under the SSI case to be similar to that of the fixed base case.

At higher shaking intensity, it can be observed that many detrimental instances develop for the wall-frame configurations W6-9, W6-15, W9-5, W9-9, W9-15, W12-5, W12-9, and W12-15. For relatively stiffer systems in which the shear wall area ratio is relatively greater (W3-3, W3-5, W3-9, W3-15, W6-3, W6-5, W9-3, and W12-3), no detrimental instance develops and $\bar{\mu}_c$ is less than unity at all storey levels under all soil types. For the configurations that exhibit detrimental instances, it can be observed that for weaker soil conditions (S1 and S2), the detrimental instances are distributed over a lesser number of stories, but may exhibit peak $\bar{\mu}_c$ magnitudes to be relatively higher. For stiffer soil conditions (S3 and S4), the detrimental instances are distributed over a larger number of stories with relatively lower magnitudes of peak $\bar{\mu}_c$. The maximum increase in the local ductility demands in the shear wall ranges from 50% to 150% for stiff to flexible configurations.

7.6.2 Global Demands

In this section, the influence of SSI on global ductility demands is examined with the help of the displacement ductility demand-response reduction factor ($\mu_d - R_\mu$) relationship. From the nonlinear time history analysis, the displacement ductility demands (μ_d) imposed onto the various considered RC frame and RC wall-frame systems have been obtained corresponding to different levels of inelasticity. The increased levels of inelasticity within the structural system are represented by increased values of the response reduction factors (R_μ). On increasing the level of nonlinearity, the displacement ductility demands also increase, which leads to the ascending nature of $\mu_d - R_\mu$ the relationship for the RC frame and RC wall-frame systems. Moreover, to clearly examine the effect of SSI on the global ductility demands, normalized displacement ductility demand ($\bar{\mu}_d$) is obtained, which is mathematically expressed as shown in Eq. 7.2. The following subsections discuss the influence of SSI on the global ductility demands of the RC frame and RC wall-frame system.

7.6.2.1 RC Frame System

Figure 7.25a shows the $\mu_d - R_\mu$ relationship for the various configurations of RC frame systems with and without the influence of SSI. For all the configurations, it can be observed that for low values of R_μ, the displacement ductility demands (μ_d) with and without SSI are of a similar order. However, for higher values R_μ, it can be observed that μ_d under the

influence of SSI is greater than that under FB condition. For several configurations (F3-9, F6-3, F6-5, F6-9, F6-15, F9-9), μ_d under SSI is higher than that under FB condition even at relatively lower values of R_μ. For other configurations (F3-3, F3-5, F3-9, F3-15, F9-5, F9-15) μ_d under SSI is greater than that under FB condition at relatively higher values of R_μ. For a few configurations (F9-3, F12-3, F12-5, F12-9, F12-15), the increase in μ_d under SSI is not observed distinctly. Rather, it can also be observed that for some cases at low values R_μ, the ductility demands under the influence of SSI are observed to be lesser compared to that under fixed base condition.

The influence of SSI on individual soil type is studied by obtaining the $\bar{\mu}_d$ with R_μ for the various RC frame system and shown in Figure 7.25b. For all the configurations, it can be observed that corresponding to low values of R_μ, $\bar{\mu}_d$ is either close to or less than unity. This indicates that at lower levels of nonlinearity, the ductility demands under the influence of SSI may be lesser than those under FB condition. Moreover, at high values of R_μ, $\bar{\mu}_d$ is greater than unity for most configurations under the different soil conditions. This indicates that at a higher level of nonlinearity, the influence of SSI is to increase the ductility demands. Zhou et al. (2004) showed that the global displacement ductility demands of RC framed structure shares a positively increasing relationship with curvature ductility demands. In this regard, the behaviour of the obtained $\mu_d - R_\mu$ relation can be understood by relating with the local curvature ductility demands and is explained with the help of an example in the following. Corresponding to F3-9, it was observed (Figure 7.20a) that at intermediate shaking intensity, the local curvature ductility demands in the column under SSI are mostly lower than that under FB condition. This results in an exhibition of lower values of displacement ductility (μ_d) under SSI compared to FB conditions as observed for intermediate values of R_μ. At high shaking intensity (see Figure 7.20b), it can be observed that the local curvature ductility demands in the columns under SSI are greater than that under FB condition. This leads to higher values of displacement ductility (μ_d) under SSI compared to FB condition, as observed for higher values of R_μ. For most cases, the increase in displacement ductility demands corresponding to higher values of R_μ is observed to be greater for weaker soil conditions (S1 and S2). However, for a few cases, it is observed to be greater for stiffer soil conditions (F9-15, F12-3, F12-9, F12-15). For e.g., corresponding

to F12-15, $\bar{\mu}_d$ under S4 is greater than that under other soil conditions. This is because these frames exhibit higher curvature ductility demands under stiffer soil conditions when compared to that under weaker soil conditions, as observed from Figures 7.20a and 7.20b.

7.6.2.2 RC Wall-frame System

The $\mu_d - R_\mu$ relationship for RC wall-frame systems is obtained for the various configurations with and without the influence of SSI and is shown in Figure 7.26a. It can be observed that for most of the very stiff wall-frame systems (W3-5, W3-9, W3-15, W6-3), the ductility demands exhibited under the influence of SSI are lower than those under fixed base condition. For several other configurations (W6-5, W6-9, W6-15, W12-9, W12-15), the ductility demands under the influence of SSI are lower than those under FB condition for low values of R_μ. However, for higher values of R_μ, the global displacement ductility demands under SSI are observed to be higher than those under FB condition. For a few configurations (W9-3, W9-5, W9-9, W9-15, W12-3, W12-5) the displacement ductility demands under the influence of SSI are higher than that under FB condition for low as well as higher values of R_μ. The $\bar{\mu}_d - R_\mu$ relationship between the various RC wall-frame system is shown in Figure 7.26b. For most configurations, it can be observed that at low R_μ, $\bar{\mu}_d$ is close to unity. However, corresponding to high R_μ values, $\bar{\mu}_d$ is greater than unity (indicating an increase in global ductility demands under the influence of SSI). This is because at higher shaking intensity, greater inelasticity develops under SSI (discussed in the previous sections), leading to the exhibition of higher global ductility demands. For W3-9, W3-15, and W6-3, it can be observed that $\bar{\mu}_d$ is less than unity for a broad range of R_μ. This is because corresponding to these configurations, the fixed-base system develops greater nonlinearity as it attracts greater forces compared to the SSI model. For W3-3 and W3-5 corresponding to low values of R_μ significantly high increase in $\bar{\mu}_d$ is observed. This is because the system behaves elastically, and the increase in demand is due to the inelastic deformation of the soil-pile foundation system leading to the global displacement demand of these systems being very much higher than that of the corresponding fixed-base systems. At higher values of R_μ, an increase in nonlinearity in the fixed base system causes a reduction in $\bar{\mu}_d$. On further increasing R_μ, the global demands increase in the SSI system owing to the development of high inelasticity in the SSI system. For most of the systems $\bar{\mu}_d$ is less than unity for low R_μ but exceeds unity at higher values of R_μ. This is because, at

higher levels of inelasticity, the local curvature ductility demands in the columns of the RC wall-frame systems under SSI cases are observed to be higher (see Figures 7.22a and 7.22b). Moreover, under the influence of SSI, the rocking of the shear wall is allowed, which induces additional demands onto the RC wall-frame systems.

7.6.3 Note on Detrimental Scenarios

Examination of the dynamic inelastic behavior (section 7.4) revealed that under high shaking intensity, the RC frame and RC wall-frame systems exhibit greater inelasticity under the influence of SSI (compared to FB cases). This observation was further substantiated by examining the local and global ductility demands under the influence of SSI. It was observed that for most of the configurations of the RC frame and RC wall-frame systems corresponding to low R_μ values, the global ductility demands under the influence of SSI are smaller than that under FB condition. However, for larger values of R_μ (increased value of R_μ signifies greater level on inelasticity), it is observed that the global ductility demands under the influence of SSI exceed that of the FB system. Therefore, from the observations, it can be stated that SSI could lead to detrimental scenarios for the cases where greater magnitudes of inelasticity could arise. Hence, it is essential to examine and verify the superstructure response by considering nonlinear SSI under such circumstances. This can be done by identifying the level of superstructure inelasticity for which SSI must be incorporated for analysis. For each of the cases considered in the present study, the values of R_μ for which global ductility demands under the influence of SSI exceed that of the FB system are obtained and shown in Figures 7.27 and 7.28 for RC frame and RC wall-frame systems respectively. It can be observed that baring a few cases, for each of the specimens, the variation in R_μ under the different soil conditions is very less. Moreover, except for a few configurations, the value of R_μ is of a similar order. The average values of R_μ for which the global ductility demands under SSI exceed that of the FB condition is obtained for RC frame and RC wall-frame systems and has been found to be about 2. From the present study, the following is recommended. The inelastic behaviour of the fixed base system can be analysed under the expected hazard level and, subsequently, R_μ can be obtained. The inelastic response of the considered structural system should be verified by incorporating SSI effects if the value of R_μ obtained under the FB case is greater than 2.

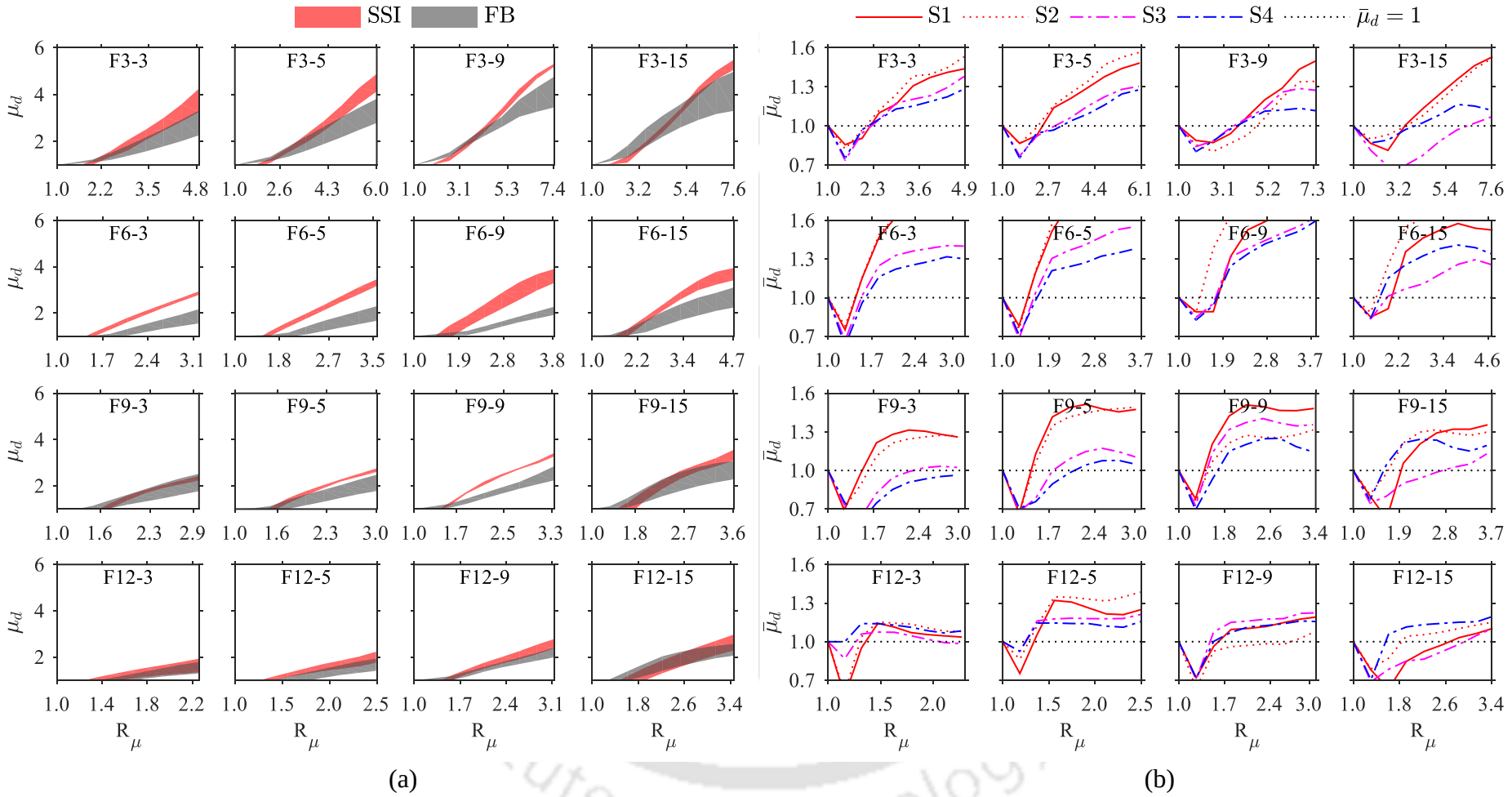

Figure 7.25 Influence of SSI on global ductility demands of RC frame systems with various configurations shown in the form of (a) $\mu_d - R_\mu$ relationships, and (b) $\bar{\mu}_d - R_\mu$ relationships.

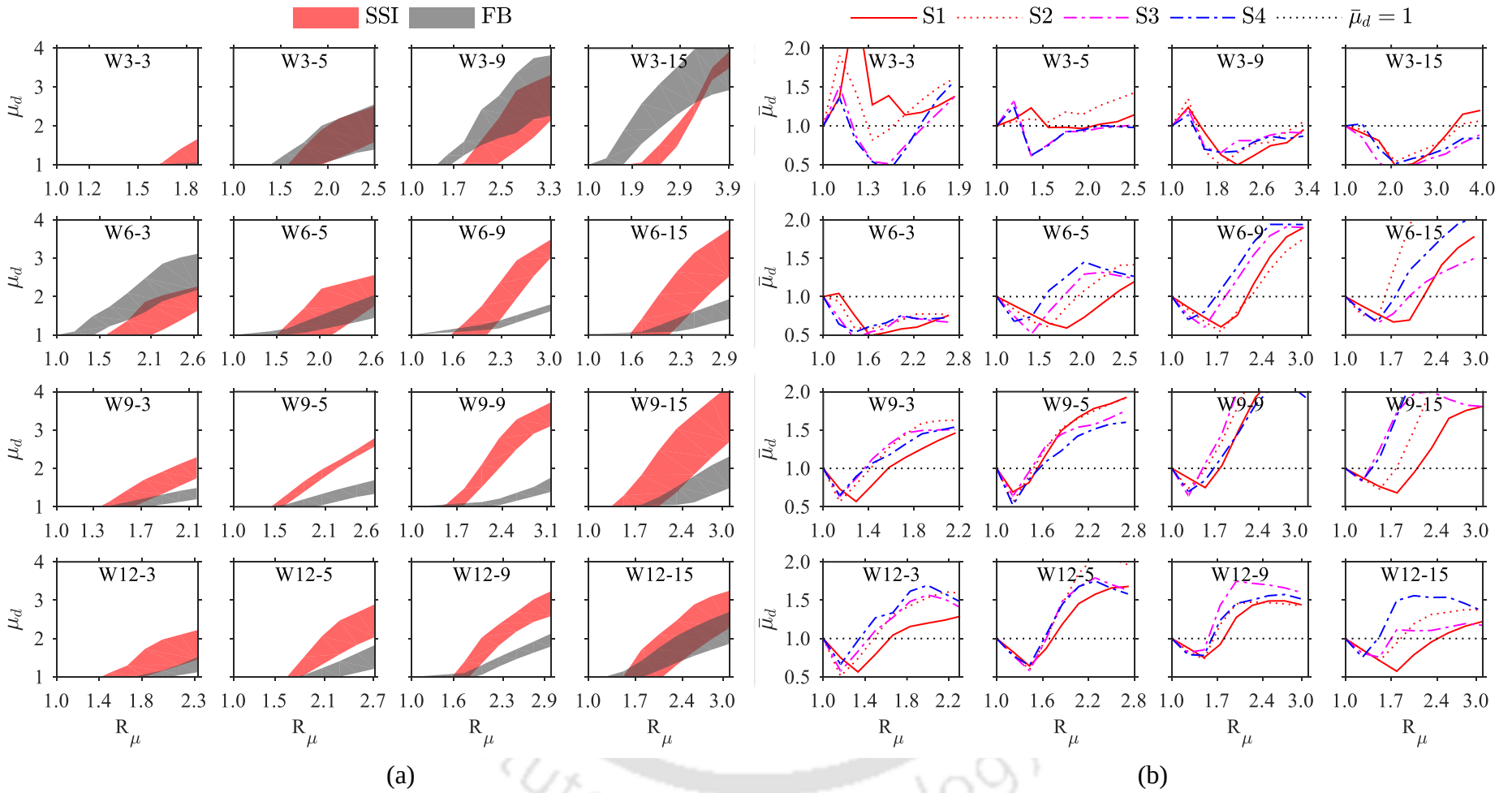

Figure 7.26 Influence of SSI on global ductility demands of RC wall-frame systems with various configurations shown in the form of (a) $\mu_d - R_\mu$ relationships, and (b) $\bar{\mu}_d - R_\mu$ relationships.

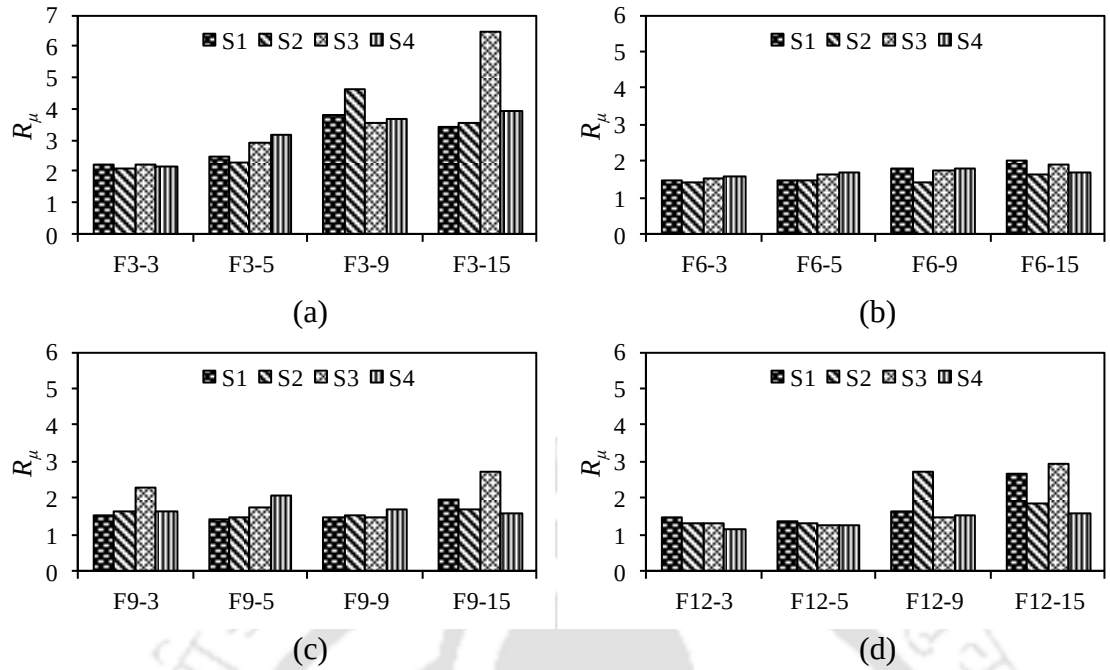

Figure 7.27 Value of R_μ beyond which global ductility demands under the influence of SSI exceed that of the FB condition for RC frame system having (a) 3 storeys, (b) 6 storeys, (c) 9 storeys, and (d) 12 storeys.

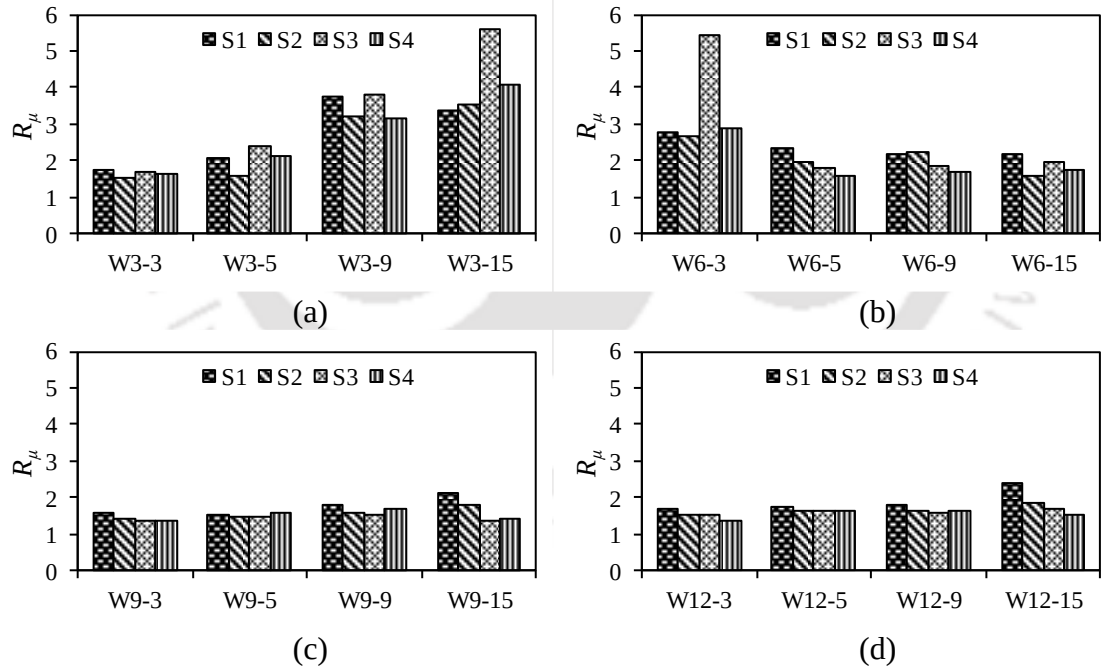

Figure 7.28 Value of R_μ beyond which global ductility demands under the influence of SSI exceed that of the FB condition for RC wall-frame system having (a) 3 storeys, (b) 6 storeys, (c) 9 storeys, and (d) 12 storeys.

7.7 SETTLEMENTS UNDER SEISIMC VIBRATIONS

This section studies the foundation settlement in the RC frame and RC wall-frame systems under seismic vibrations. During seismic shaking, the vibrations introduced into the SSI system cause a change in the void ratio of the soil. Moreover, the rocking motions introduced into the superstructure system also causes the soil, in the vicinity of the foundation, to experience additional loads and vibrations. Corresponding to fame systems, these vibrations may vary under the column members leading to the exhibition of differential settlements. Settlements of differential nature may pose great implications onto the superstructure system. Angular distortion (δ/l) is the common parameter by which the severity of the differential settlement is measured. It is the ratio of the differential settlement (δ) between two foundations and their distance (l) (typically the bay width). In the present study, the RC frame and RC wall-frame systems supported on the different soil-pile foundations, subjected to seismic excitations of varying intensities, experience differential settlements. Corresponding to a particular structural configuration, the maximum angular distortion (δ_{max}/l) introduced due to vibration and rocking is observed at the end of the dynamic analysis. The maximum angular distortion for the various RC frame systems subjected to a shaking intensity of 0.36g is shown in Figures 7.29a-7.29d. It can be observed for the frame systems the δ_{max}/l is within 0.1% (i.e., 0.001). Moreover, it can also be observed that the magnitude of maximum angular distortion for the different frame systems under soil conditions (corresponding to a particular structural configuration) is comparable.

Corresponding to RC wall-frame systems, the differential settlement is observed to be the greatest under the shear wall (since it is under the highest amount of gravity loads and also exhibits large amount of rocking as shown in Figure 6.13a). The maximum angular distortion for the various RC wall-frame systems subjected to a shaking intensity of 0.36g is shown in Figures 7.30a-7.30d. It can be observed for the wall-frame systems the δ_{max}/l is of higher order (maximum of about 2%, i.e., 0.02). Moreover, it can also be observed that corresponding to a particular configuration, the magnitude is highest for the loosest (weakest) soil type S1. On increasing the stiffness of the soil from S1 to S3, the maximum angular distortion reduces. However, on further increasing the stiffness of the soil to S4, the maximum angular distortion, again, increases. This is because the length of the pile foundations under S4 condition is reduced and is not embedded deep into the soil. The soil near the surface is relatively loose and the SSI induced vibrations onto the pile causes greater exhibition of differential settlements.

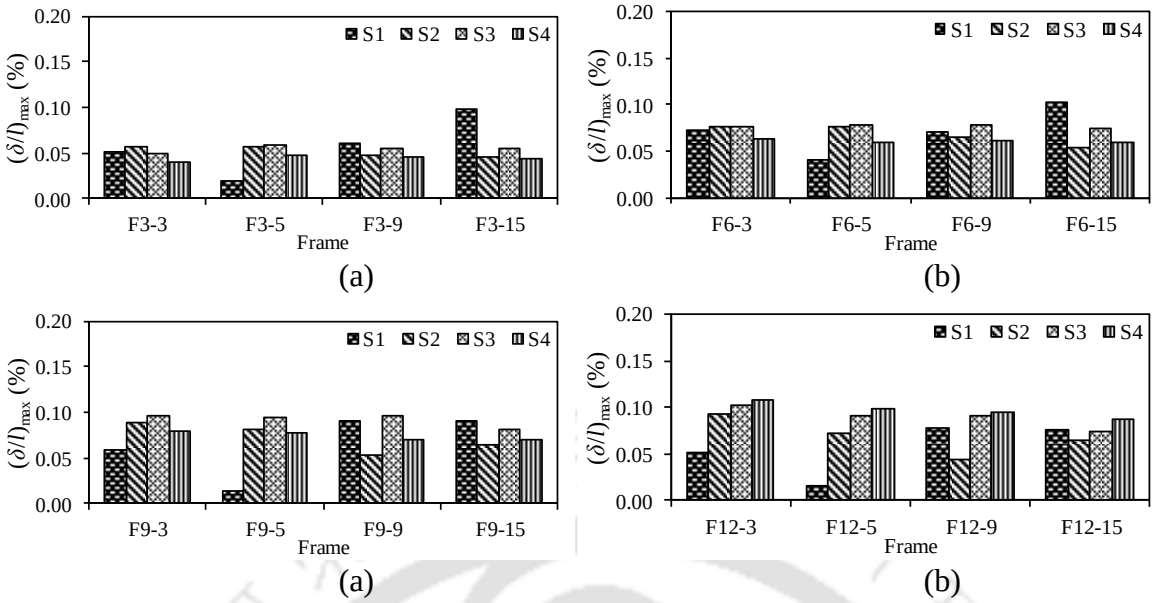

Figure 7.29 Variation in (δ_{max}/l) due to seismic vibrations (of intensity 0.36g) and rocking under different soil conditions for RC frame systems with (a) 3 storeys, (b) 6 storeys, (c) 9 storeys, and (d) 12 storeys .

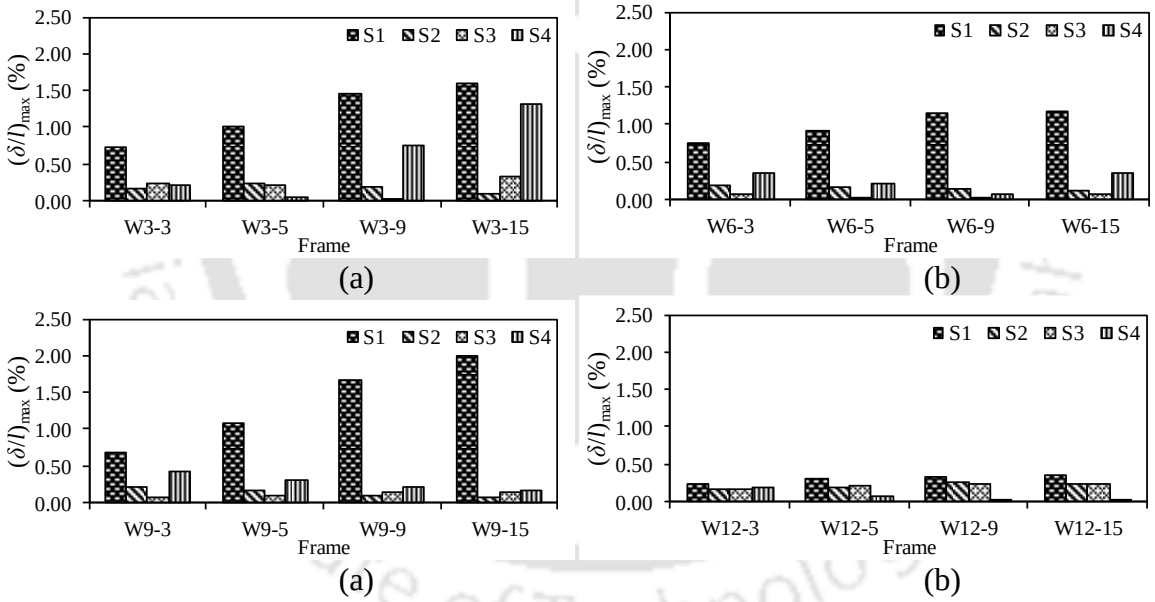

Figure 7.30 Variation in (δ_{max}/l) due to seismic vibrations (of intensity 0.36g) and rocking under different soil conditions for RC wall-frame systems with (a) 3 storeys, (b) 6 storeys, (c) 9 storeys, and (d) 12 storeys

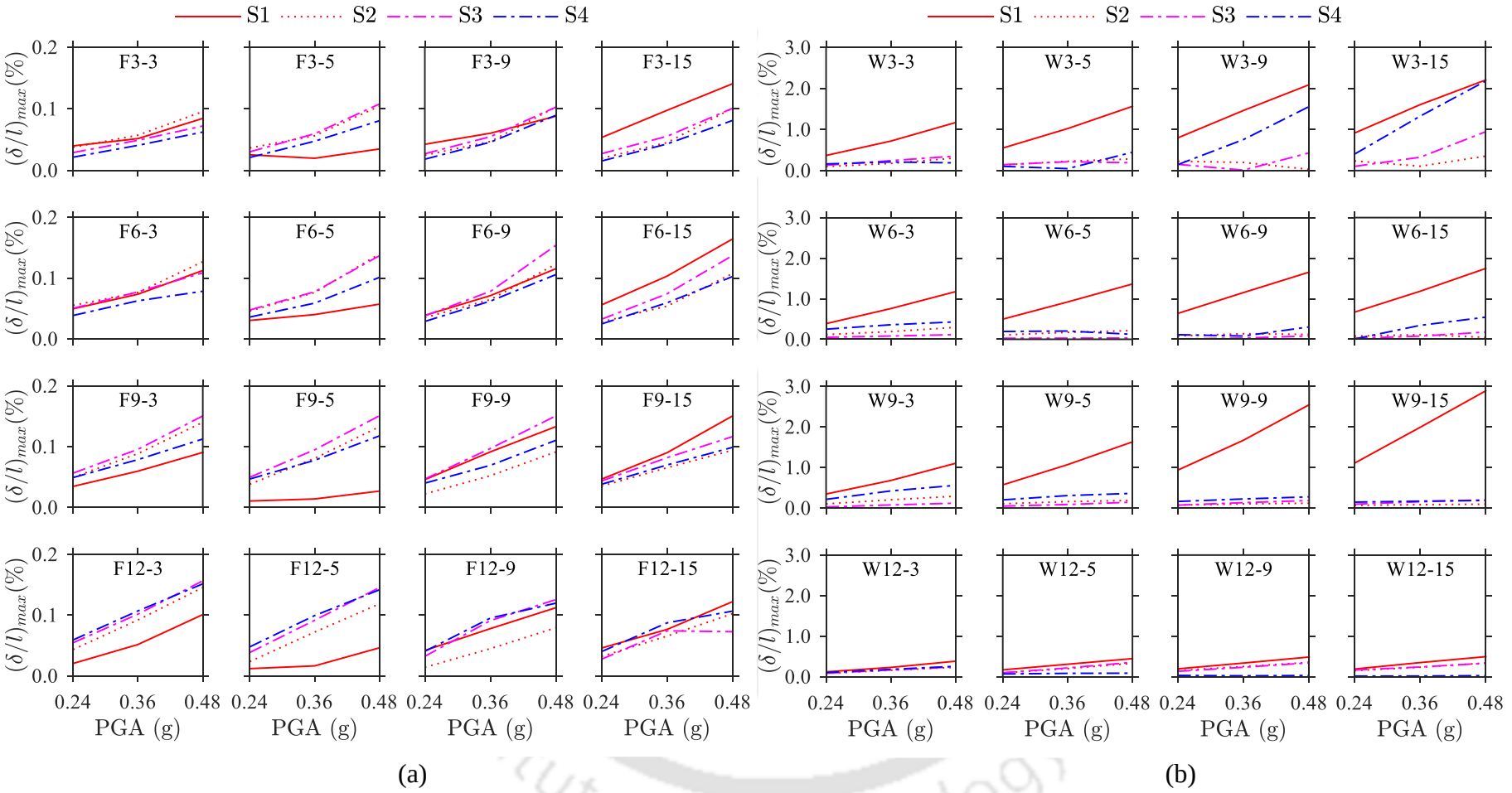

Figure 7.31 Variation in (δ_{max}/l) with PGA under different soil conditions for (a) RC frame systems and (b) RC wall-frame systems..

The variation of maximum angular distortion (δ_{max}/l) with the intensity of shaking is also observed for the different configurations of RC frame and RC wall-frame systems under the different soil-pile foundation conditions and is shown in Figure 7.31a and 7.31b respectively. From the figure, it can be observed that the relationship of maximum angular distortion (δ_{max}/l) with PGA is an increasing one for the different soil-pile foundation conditions. This is because the greater intensity of shaking induces higher magnitude of vibrations and rocking into the SSI system leading to an increase in the maximum angular distortion. The observation holds true for the different configurations of both the RC frame and RC wall-frame systems.

7.8 Effect of Shear wall on Frame Buildings

This section studies the change in the local behaviour of RC frame systems with pile foundation on the inclusion of the RC shear wall considering SSI. Since the focus is more on the modification in the behaviour, the phenomenon is highlighted with the help of limited results only. The results corresponding to two configurations (namely 6 storey 5 bay system and 12 storeyed 5 bay system) located on one type of soil (S2) are studied in this section to assess the influence of the shear wall on RC frame systems with and without SSI effects.

7.8.1 Modification in Local Behaviour

As seen in the previous chapter, the shear wall modifies the natural vibrational characteristics and the mode shape profile of an RC frame building. This may lead to a modification in the member or local level response for the different frame members. The local level response is assessed in terms of the rotational demand (θ_d) developed in the inelastic region (plastic hinge) of the column and beam members. The average value of the demand is obtained for a particular storey level, and its profile at various storey levels is obtained. Figures 7.32a and 7.32c show the variation of average rotational demand (θ_d) in the columns at various storey levels in the 6 storeyed and the 12 storeyed frames respectively on incorporating shear wall into the system. Similarly, Figures 7.32b and 7.32d show the variation of the average rotational demand (θ_d) in the beams at the various storey levels in the 6 storeyed and the 12 storeyed frames respectively. It can be observed that the presence of shear wall influences the rotational demands (θ_d) in the frame members, and the extent of change depends on the frame height, member type (columns or beams), storey level, and the SSI effects.

For the 6 storeyed frame, shear wall reduces θ_d in columns at L1, and the reduction is about 27% and 91% with and without SSI effects, respectively. At L6, the shear wall increases θ_d in the columns by about 80% and 218% with and without SSI effects, respectively. The presence of the shear wall causes a reduction in θ_d in columns at L1 and the reduction is relatively less for the frame with SSI effects. At L6, the shear wall significantly increases θ_d in columns for the frame without SSI effects, however, for the frame with SSI effects, the increase is relatively less. At other intermediate storey levels (L2-L5), shear wall causes a similar reduction of θ_d in the columns with maximum reductions of about 70% and 54% with and without SSI effects respectively. In the beams, shear wall reduces θ_d at L1 by 45% and 79% with and without SSI effects respectively, however, at L6, it increases θ_d by about 137% and 206%. At other intermediate storey levels, shear wall reduces θ_d in beams with a maximum reduction of 66% in the frame with SSI effects. For the frame without SSI effects, the presence of shear wall reduces θ_d at L2-L3 (with a maximum reduction of about 72%), however, at L4 and L5, the presence of shear wall increases θ_d by about 39%.

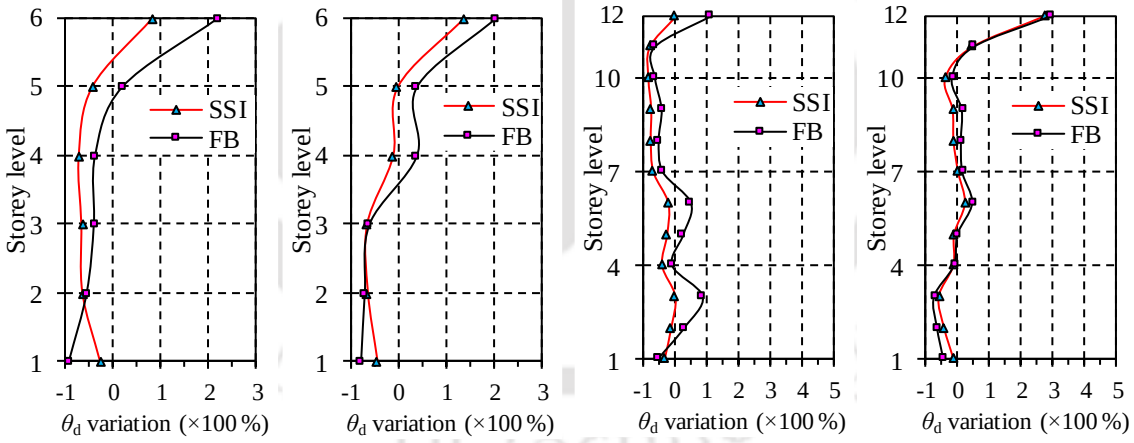

Figure 7.32 Influence of shear wall on RC frame with and without soil-pile foundation interaction on the variation of average plastic hinge rotational demands at various storey levels in (a) columns and (b) beams of the 6 storeyed frame, (c) columns, and (d) beams of the 12 storeyed frame.

As observed for the 6 storeyed frame, in the 12 storeyed frame also, shear wall reduces θ_d in columns at L1, and the reductions are about 31% and 50% with and without SSI effects respectively. At L12, the presence of shear wall increases θ_d in the columns by about 3% and 115% with and without SSI effects respectively. The presence of shear wall causes a

reduction in θ_d in columns at L1, and the reduction is relatively less for frames with SSI effects. At L12, shear wall increases θ_d in columns, and the percentage increase for frame without SSI effects is several times that of the frame with SSI effects. At other intermediate storey levels (L2-L11), shear wall causes a reduction of θ_d at most storey levels exhibiting a maximum reduction of about 79% and 60% for frames with and without SSI effects, respectively. Moreover, for the frame without SSI effects, θ_d is observed to have increased at some of the lower storey levels with a maximum of about 95%. In the beams, shear wall reduces θ_d at L1 by 15% and 43% with and without SSI effects respectively, however, at L12, it increases θ_d by about 271% and 291%. At other intermediate storey levels in the frame with SSI effects, shear wall reduces θ_d in beams (except at L6 and L11 where it increases by 21% and 42% respectively) with a maximum reduction of 61%. For the frame without SSI effects, shear wall reduces θ_d at L2-L5 (with a maximum reduction of about 72%), however, at L6-L11, shear wall increases θ_d with a maximum of about 49%.

Shear wall is equally effective in the reduction of θ_d in beams and columns at the bottom storey of 6 storey as well as 12 storey frame without SSI effects. For frames with SSI effects, the reduction in θ_d of columns is greater for a stiffer frame (6 storey) compared to the flexible frame (12 storey) as for stiffer frames, the shear wall causes a greater reduction in the rotational demands and is more effective in capturing the rotational demands. For the frames with SSI, the reduction of θ_d in the beams at the bottom storey due to the shear wall is greater for the stiffer frame (6 storey) compared to the flexible frame (12 storey). This is because SSI causes greater rotation of columns for stiffer frames forcing the beams to comply with the assumed deformed profile, thereby increasing the demands in the beams. On incorporation of the shear wall, this imposed demand due to the inherent flexibility of the frame is reduced to a greater margin for the stiffer frames.

On incorporating shear wall, at the top storey level, the RC frame experiences increased θ_d in the frame members. In the absence of the shear wall, the RC frame members at the top storey level exhibit lower θ_d. This can also be understood from the mode shape profile (Figures 6.19b and 6.19c) where it can be seen that the normalized inter-storey displacements at the top level are much less for frames without the shear wall. The presence of shear wall rigidity modifies the mode shape of the RC frame that causes greater

magnitudes of normalized inter-storey displacements at the top storey levels, thereby causing an increase in θ_d for beams and columns. The increase is greater for frames without SSI effects and can be related to its mode shape profile that shows higher normalized inter-storey displacements as compared to that of the frame with SSI effects. The increase in the rotational demands in the frame members of a relatively flexible frame is greater than that of the stiffer frame for beams and lesser for columns. This is because flexible frames tend to possess lesser magnitudes of normalized inter-storey displacements at the top storey which on the incorporation of the shear wall is increased by a greater magnitude as compared to that of a stiffer frame. Moreover, for frames without SSI, the increase in θ_d for columns is greater for a stiffer frame (6 storey) while the increase in θ_d for beams is much greater for the flexible frame (12 storey). Owing to the inherent deformation compliance of the frame, the demands in the beams are increased to a greater degree in flexible systems. On incorporating SSI in these frames, the magnitude of increase in θ_d, for the beams and columns, is relatively reduced. At intermediate storey levels, θ_d in columns and beams generally reduces towards the lower storey levels and may increase towards the top storey level, and it depends on the continuity of the θ_d variation profile (which is again in coherence with the mode shape profile) of the respective member for both with and without SSI effects.

7.9 SUMMARY

The incorporation of SSI modifies the inelastic behavior and consequently, the local and global ductility demands. In this chapter, the influence of SSI on the local and global ductility demands of RC frame and RC wall-frame systems is investigated. Further, the seismic vibration induced settlements under these superstructure was studied. Finally, the role of the shear wall in modifying the local behaviour of the RC frame is studied. The main conclusions drawn from the present chapter are as follows:

- For RC frame systems, SSI modifies the inelastic response at the plastic hinge locations of the superstructure. The influence of SSI could lead to the development of inelasticity at a lesser number of locations but the inelasticity could develop to a greater degree. At higher shaking intensity, however, both the number of locations and the extent of inelasticity could be higher under the influence of SSI.

- For RC wall-frame systems, SSI introduces flexibility at the shear wall base allowing it to deform (rock), thereby reducing the extent of inelasticity developed at the base of the shear wall compared to the fixed base models. This deformation, in turn, imposes additional rotation onto the columns at the base of the superstructure and the beams adjacent to the shear wall. At higher shaking intensity, the SSI effect is increased, leading to the possibility of development of greater inelasticity in the shear wall at higher storey levels that causes the beams and columns in the immediate higher storeys to develop greater inelasticity.
- For RC frame systems, the local ductility demands are modified with incorporation of SSI, and the effect is higher for weaker soil conditions. Under low shaking intensity (low level of inelasticity), the detrimental instances under SSI are relatively lesser. However, under high shaking intensity (higher level of inelasticity) higher number of detrimental instances could develop under the influence of SSI. For narrow frames, the increase in local ductility demands gets significantly increased at higher storey levels. For wider frames resting on weaker soil conditions, a greater number of detrimental instances could develop, with a significant increase in local ductility demands in the columns at lower storeys. For stiffer soil conditions, the local ductility demands in columns at higher storey levels could increase significantly at higher storey levels.
- For RC wall-frame systems, the local ductility demands in the columns and beams are significantly increased under the influence of SSI due to the allowance of deformations at the base of the system. Moreover, this effect is greater for weaker soil conditions. The increase in the local ductility demands in the columns for the detrimental instances could be of the order of several times. In the shear walls, the local ductility demands reduce significantly, especially at the lower storey levels owing to the influence of SSI. For very stiff configurations, the local ductility demands under the influence of SSI may be very much reduced. However, for relatively flexible systems, the local ductility demands may increase in the shear wall under SSI, giving rise to detrimental scenarios, especially under weaker soil conditions and at higher shaking intensity.
- The global ductility demands can be related to the local ductility demands. In the present study, in general, for both RC frame and RC wall-frame systems, it has been observed that at intermediate shaking intensity, local demands under SSI are lower and at higher shaking intensity are greater than that under FB condition. Similarly, the

global demands under SSI are observed to be lower for low R_μ and higher for greater R_μ than that under FB condition.

- The average maximum increase in the local ductility demands under SSI effects in columns of RC frame systems is about 50% while that for RC wall-frame systems is about 120%. Similarly, the average maximum increase in the global ductility demands under the influence of SSI for RC frame systems is about 35%, while that for the RC wall-frame system is about 60%. It can be noted that the increase in local curvature ductility demands under SSI is greater than the global displacement ductility demands. A similar outcome was seen in the study by Zhou et al. (2004) on RC frames.
- SSI could lead to detrimental scenarios for the cases where greater magnitudes of inelasticity could arise. Since conducting SSI analysis is time-consuming and expensive, the present study recommends conducting nonlinear SSI study and verifying the response of RC frame and RC wall-frame systems for which their fixed base models exhibit inelasticity with $R_\mu > 2$.
- Seismic vibrations leads to the exhibition of differential settlements of the pile group under the superstructure and has been assessed in terms of angular distortion. For RC frame systems, the maximum angular distortion corresponding to a particular configuration were observed to be comparable for the different soil types. Rocking due to shear wahh in RC wall-frame systems caused greater exhibition of angular distrotions, which was highest for the loosest (weakest) soil type S1. Due to reduced pile lengths in very stiff soil condition (S4), the RC wall-frame systems exhibited increased angular distortions. The magnitude of angular distortions exhibited by the SSI system increases with the shaking intensity.
- Shear wall modifies the mode shape of the RC frame, causing a variation of the local demands (plastic hinge rotation) in the frame members at various storey levels that are prominently visible at the bottom and top storey levels.
- At bottom storey level: Shear wall reduces the rotation demand in columns and beams, and the reduction is greater for frames without SSI effects. Moreover, in the presence of SSI effects, shear wall causes a greater reduction of rotational demands in columns of flexible frames, whereas the reduction in beams is greater for stiffer frames.
- At top storey level: Shear wall rigidity modifies the mode shape to develop greater magnitudes of normalized inter-storey displacements leading to an increase in the rotational demands of the beams and columns. The increase in the rotational demands

is greater in columns of the stiffer frame, whereas that for the beam is greater for the relatively flexible frame. Moreover, in the absence of SSI effects, shear wall causes a greater increase in the rotational demands in the columns of stiffer frames, whereas for beams, it is greater for flexible frames. SSI effects reduce the extent of variation in the rotational demands in the beams and columns.

- At intermediate storey level: The variation of the rotational demands in columns and beams, due to shear wall, generally reduce towards the bottom storey level and may increase towards the top storey level; and the variation can be related to the normalized inter-storey displacements of the respective mode shape profiles.
- Shear wall can significantly modify the behaviour of RC frames, and the suitability of incorporating shear wall needs to be assessed judiciously by accounting several factors influencing the decision making, such as the properties of the frame, presence of SSI effects, and influence on the seismic response parameters.

This page has been intentionally left blank.

Chapter 8
SUMMARY, CONCLUSION AND FUTURE SCOPE

CONTENTS

8.1 OVERVIEW

Construction of Reinforced Concrete (RC) buildings has gained great popularity in the urban areas. These buildings are constructed with or without the presence of RC shear walls and are known as RC frame systems and RC wall-frame systems, respectively. Depending on the relative stiffness of the foundation substructure and foundation soil, soil-structure interaction (SSI) may intricately govern the combined response of the structure, footing, and the soil. The conventional approach is to neglect the influence of SSI and consider the system to be fixed at the base. However, if the supporting soil foundation medium provides flexibility, then the building's elastic and inelastic response may be significantly influenced by SSI effects. The present study is focussed on assessing the influence of soil-structure interaction on the seismic behaviour (elastic and inelastic) of RC frame and RC wall-frame buildings supported on pile foundations. In this chapter, a brief summary of the entire study is provided, and the major conclusions have been outlined. Based on the study, possible recommendations have been suggested. Finally, the limitations and possible scopes of future work are listed.

8.2 SUMMARY

The present research aims at studying the influence of soil-structure interaction (SSI) on the seismic behavior of RC frame and RC wall-frame buildings supported on pile foundations. The seismic behavior is investigated by means of an exhaustive numerical study with the help of the finite element software framework, OpenSEES (Mazzoni et al., 2009). The entire study is divided into the following parts:

***Preliminary study*:** Initially, a preliminary numerical study is carried out to establish the efficacy of the numerical models for investigating the influence of SSI on the RC frame and RC wall-frame systems. This includes mesh sensitivity study, checking the numerical model for possible anomalies (spurious oscillations under dynamic loading), and validating the numerical response obtained from the adopted numerical modelling approach with that of the past studies.

***Development of a modelling approach for rigorous numerical study*:** A rigorous numerical study involving detailed modelling with advanced features capable of simulating nonlinear behavior could be quite expensive from the aspects of computation, storage, and time. For this, it is essential to develop a modelling approach that would be helpful in reducing the computational costs and time, without influencing the accuracy. In the present study, a strategic approach has been outlined to arrive at the optimum normalized length of soil domain to be considered for soil-structure interaction studies. Based on exhaustive finite element simulations, normalized root mean square error (*NRMSE*) for various domain lengths is obtained for various structural widths and soil types. With the aid of bilinear fit to the *NRMSE* plots, normalized optimum soil domain lengths have been obtained. Adopting these lengths for developing the numerical models ensures significant saving in computational time and effort without hampering the accuracy of the results.

***Influence of SSI on elastic behavior*:** Natural period, an important parameter for characterizing the dynamic behaviour, has significant relevance in the context of elastic seismic behaviour of the structural system. The presence of the soil-foundation system inevitably induces SSI effects onto the structural system, thereby leading to a change in the natural period of the fixed-base system. In the present study, the influence of SSI on the natural period of RC frame and RC wall-frame systems supported on pile foundation has been studied to provide accurate estimates of the effective natural period (T_{SSI}) of several configurations of the superstructure and soil-pile foundation systems. The change in the

fixed-base natural period, under the influence of SSI for the frames, was quantified in terms of the modification factor (*MF*), which is expressed as the ratio of the effective natural period (T_{SSI}) to the fixed-base natural period (T_F) of the building frame. A parametric study was conducted to identify the influence of various input parameters of the SSI system on the *MF*. Higher magnitude of *MF* indicated the greater influence of the SSI effects. Subsequently, a feed-forward back-propagation artificial neural network (ANN) model has been adopted to develop a predictive relationship for obtaining the modification factor (*MF*). This would lead to a quick and easy determination of effective natural period (T_{SSI}) of RC frame and RC wall-frame systems supported on pile foundations.

***Influence of SSI on Inelastic behavior*:** Allowing of inelastic behaviour on account of ductility is an integral component of the modern-day earthquake resistant design philosophy of buildings structures. The soil-pile foundation inevitably contributes and thus modifies, upon the inelastic response, which forms an important aspect of performance-based assessment and design. Therefore, in the present study, the influence of SSI on the inelastic response is assessed, as given below.

- ***Assessment of ductility capacity*:** The influence of SSI on the inelastic behaviour is studied by investigating the lateral load behaviour of RC frame and RC wall-frame systems considering SSI. Based on the induced degree of inelasticity, the role of soil-pile foundation system in modifying the lateral load behaviour is studied, which in turn influences the yielding and ultimate response of the superstructure system. Subsequently, the extent of modification in the ductility capacity, due to the modified yield and ultimate response of the superstructure system, is assessed. Further, the role of shear wall in modifying the inelastic behaviour and ductility capacity of RC frame systems is also studied concisely.
- ***Assessment of ductility demands*:** The modification in the ductility demands due to SSI effects is an outcome of the modification of the inelastic response of the structural system. The influence of SSI on the degree of inelasticity developed in the plastic hinge regions of the structural members of the RC frame and RC wall-frame building is examined. The consequent impact on the local and global ductility demands is investigated. Further, the role of the shear wall in modifying the local behaviour (element level) of the RC frame system is also studied.

8.3 CONCLUSIONS

The main conclusions drawn from the present study are categorically presented in the following.

Numerical modeling for SSI studies

- The optimum domain length of soil domain (Ω) is estimated for numerical SSI studies. For studies on RC frame buildings, beyond the estimated Ω, the overall response on the SSI system is affected by insignificant changes (less than 10%), while the computational efficacy is immensely improved (minimum 96% for the present study).
- A generalized set of robust, practically feasible, and efficient predictive relationships are provided for Ω, expressed as a function of structural or foundation width and the PGA of the strong motion.
- For SSI problems subjected to higher PGA strong motion, the magnitude of Ω is higher and vice-versa. Ω is virtually independent of the soil type. Moreover, SSI problems comprising smaller structural widths require larger Ω, and vice-versa.

Influence of SSI on elastic behaviour

- The incorporation of SSI modifies the fixed-base natural period of the structural system, which is expressed in terms of modification factor (*MF*).
- RC frame and RC wall-frame systems resting on loose soil exhibit greater *MF* (greater SSI effects), which reduces for stiffer soil conditions. Taller RC frame systems and stiffer RC wall-frame systems exhibit greater SSI effects. For the latter case, SSI effects are more pronounced for pile foundations possessing greater flexibility (S_H).
- RC frame and RC wall-frame systems comprising columns supported on single pile exhibit greater SSI effects as compared to the same supported by a pile group due to an additional rocking stiffness induced by group action.
- For the RC frame and RC wall-frame systems, the developed ANN prediction model predicts the modification factor (*MF*) with noticeable accuracy, with a maximum error of less than 10% as compared to the same obtained using existing expressions.
- Sensitivity analysis indicates that the overall influence of input parameters on *MF* comprises 42% contribution from the soil-pile foundation properties and 58% contribution from the structural properties.

Influence of SSI on inelastic behaviour

- In RC frame systems, the absence of a very stiff member (such as a shear wall) leads to greater inelasticity in columns (hence curbing the transfer of large magnitude of rotations onto the soil-pile foundation). Thus, RC frame systems manifest lesser SSI effects.
- The shorter-height RC frame systems exhibit ISD profile and ultimate drifts to be lesser under the influence of SSI. However, taller RC frame systems exhibit otherwise.
- Under the influence of SSI, shorter-height RC frame systems exhibit lesser plastic hinge deformations. Under SSI effects, taller RC frame systems exhibit higher plastic hinge deformations at the bottom storey(s), while the same is lesser at higher stories.
- Wider RC frames exhibit inelasticity concentrated at the storey level, while in narrower frames, the inelasticity is more distributed; thus, the latter exhibits greater ultimate drifts.
- Irrespective of the height of an RC wall-frame system, due to the presence of the stiff shear wall member, incorporation of SSI exhibit greater ultimate drifts than that observed for FB condition.
- The influence of SSI on the inelastic behaviour is greater for comparatively stiffer RC wall-frame systems supported on pile foundations embedded in weaker soil conditions.
- As compared to the FB condition, under SSI effects, RC wall-frame systems exhibit significantly greater plastic hinge deformations at the base of the superstructure.
- When subjected to greater compressive loads, the pile group exhibit lesser rocking due to the increased confinement effect. RC frame and RC wall-frame systems that are founded on weaker soil exhibit greater inelasticity in the pile foundations due to the lack of confinement.
- Larger magnitudes of inelasticity in the superstructure reduce rocking in the pile group, and vice versa.
- Pile groups exhibit greater rocking, in case the comprising piles exhibit large inelastic rotations at or very near their top.
- Under reduced compressive loads, piles with smaller sections (generally founded in stiffer soil conditions) experience lesser restraint towards the top, thereby exhibiting large inelastic rotations causing larger rocking in the pile group.
- Owing to the inherent stiffness of the shear wall, the pile group under the shear wall exhibits a greater amount of rocking as compared to those supporting a column.

Influence of SSI on ductility capacity

- Due to the influence of SSI, modification in the inelastic behaviour, in turn, modifies the ductility capacity of the RC frame, and RC wall-frame systems.
- Owing to the incorporation of SSI, shorter RC frame systems exhibit a reduction in ductility capacity, more when they are supported by weaker soil. The response of taller RC frames is mostly otherwise. Except under specific cases, upon the incorporation of SSI, taller RC frame systems exhibit increased ductility capacity, more so when supported by weaker soil.
- Owing to the incorporation of SSI, most RC wall-frame systems exhibit an overall decrease in ductility capacity (due to an increase in yield and ultimate drifts), more so when placed on stiffer soils (wherein the piles exhibit greater inelasticity owing to the smaller sections). For other cases, wherein the yield drifts are much less influenced as compared to ultimate drifts, the ductility capacity increases under SSI effects.

Influence of SSI on ductility demands

- The influence of SSI on ductility demands is related to the inelastic response of the structural system.
- For RC frame systems subjected to intermediate shaking, incorporation of SSI leads to the development of larger degrees of inelasticity generated only at fewer locations. However, at higher shaking intensity, both the number of locations and the degree of inelasticity are generally higher.
- For RC wall-frame systems subjected to intermediate shaking, SSI reduces the extent of inelasticity developed at the base of the shear wall, thereby imposing additional rotation onto the columns at the base of the superstructure and the beams adjacent to the shear wall. However, at higher shaking intensity, the possibility of greater inelasticity in the shear wall at higher storey levels is likely to generate greater inelasticity in the beams and columns of the immediate higher storeys.
- Upon incorporating SSI, local ductility demands get modified to a greater extent in RC frame systems supported by weaker soil. Higher shaking intensity (i.e., higher level of inelasticity) raises the possibility of a higher number of detrimental instances.
- Upon incorporating SSI, narrower RC frame systems exhibit an increase in local ductility demands at higher storey levels. In wider RC frame systems resting on weaker and stiffer soils, the increase in local ductility demand is manifested at lower and upper stories respectively.

- Owing to the incorporation of SSI, RC wall-frame systems exhibit a significant increase in the local ductility demands of the columns and beams at the base, more so when the system is supported by weaker soil.
- Upon incorporating SSI, the shear wall in RC wall-frame systems exhibit a significant reduction in the local ductility demands at its base, more so for very stiff configurations. For flexible configurations, the local ductility demands in the shear wall at higher storey levels are likely to increase, especially when the wall-frame is supported by weaker soil and subjected to higher shaking intensities, thereby giving rise to detrimental scenarios.
- The global ductility demands are related to the local ductility demands. Upon incorporating SSI, for both RC frame and RC wall-frame systems, the global demands are lower for smaller R_μ, and vice-versa.
- Upon incorporating SSI, the average maximum increase in the local ductility demands in columns of RC frame systems is about 50%, while the same for RC wall-frame systems is about 1.2 times of the cases without the incorporation of SSI. Similarly, the corresponding magnitudes for global ductility demands are 35% and 60% for the RC frame systems and RC wall-frame systems, respectively.
- SSI could lead to detrimental scenarios owing to the generation of greater magnitudes of inelasticity. The present study recommends conducting nonlinear SSI study and verifying the response of RC frame and RC wall-frame systems for which their fixed base models exhibit inelastic behaviour with $R_\mu > 2$.

Effect of incorporating shear wall in RC frame system

- The incorporation of shear wall reduces the natural period and modifies the mode shape profile of an RC frame system. The modification is relatively higher for a stiffer frame, and vice versa. Upon incorporating SSI, the modification is relatively lesser, and vice versa.
- Incorporation of shear wall alters the inelastic behaviour of the RC frame by causing an increase in the yield and ultimate base shear; the alteration being higher for stiffer frames. Upon incorporating SSI, the increase in the yield base shear is relatively lesser, although the increase in the ultimate base shear is relatively higher.
- The presence of shear wall tends to increase the ductility capacity of RC frames, more so for relatively flexible frames. For an RC frame without incorporating SSI, the

presence of shear wall allows greater mobilization of the ductility, thereby exhibiting larger ductile behaviour before the collapse. With SSI incorporated, for RC frames, mobilization of ductile behaviour in the shear wall is reduced, thereby exhibiting a relatively lesser increase in the ductility capacity.

- Seismic vibrations causes differential settlements of the pile group under the superstructure which is greater for RC wall-frame systems due to the large amount of rocking exhibited by the shear wall. The magnitudes of differential settlments depends not only depends on the soil type but also on the pile geometry and the shaking intensity.
- Shear wall modifies the mode shape of an RC frame, causing a variation of the local demands (plastic hinge rotation) in the frame members at various storey levels, which are prominently visible at the bottom and top storey levels.
    - *At bottom storey level:* Shear wall reduces the rotation demand in columns and beams, more so when SSI is not incorporated in the analysis of RC frames. Upon incorporating SSI, shear wall causes a greater reduction of rotational demands in columns of stiffer frames, whereas for flexible frames, the reduction greater in the beams.
    - *At top storey level:* The presence of shear wall introduces greater magnitudes of normalized inter-storey displacements, thereby increasing rotational demands in the beams and columns. The increase is greater for the members of relatively flexible frames. In the absence of SSI, the increase is greater in the columns of stiffer frames, and beams of flexible frames. The incorporation of SSI reduces the extent of variation in the rotational demands in the beams and columns of the frame.
    - *At intermediate storey level:* In the presence of the shear wall, the variation in the rotational demand is related to the normalized inter-storey displacements of the respective mode shape profiles.
- Shear wall can significantly modify the behaviour of RC frames. The suitability of incorporating shear wall in framed structures needs to be judiciously assessed by accounting several factors influencing the decision-making such as the properties and configuration of the frame, presence of SSI effects, and influence on the seismic response parameters.

8.4 RECOMMENDATIONS FROM THE PRESENT STUDY

The prevalent notion of soil-structure interaction being beneficial is an oversimplification made by codes that could lead to detrimental scenarios. Based on studies, several past researchers have propounded the idea of considering SSI effects, and not ignoring it. In the present study as well, it has been seen that the phenomenon of soil-structure interaction can significantly influence RC frame and RC wall-frame systems supported on pile foundations and could give rise to conventionally unaccounted detrimental situations. However, in order to avoid spending greater computational time, the prevalent general practice ignores SSI effects and consider the superstructure system to be fixed at its base. Therefore, it is essential to have guidelines that would help the analysts in decision making as to whether or not to consider the SSI effects (linear and nonlinear). From the present study, the recommendations are outlined to facilitate the analysts with regards to the possible consideration of SSI effects. The analyst may carry out the following steps and follow the subsequently outlined recommendations.

Step 1: At the outset, the analyst should conduct a preliminary design/analysis, considering the structural system to be fixed at its base. The fixed-base natural period (T_F) of the structural system, along with the various response entities (base shear, drifts, sectional forces, etc.), is to be obtained in this process.

Step 2: Next, the analyst should obtain the pile-foundation soil parameters pertaining to the considered structural system. The modification in the fixed-base natural period, upon considering the influence of SSI, is to be estimated (in the form of modification factor, *MF*, using the mathematical expressions proposed in Chapter 5). Subsequently, the effective natural period (T_{SSI}) is to be obtained.

Step 3: Further, corresponding to the design hazard level, the analyst should perform a nonlinear dynamic analysis of the structure considered to be fixed at the base and obtain the inelastic response reduction factor (R_μ).

The effective natural period (T_{SSI}) obtained in Step 2 should be utilized by the analyst to make a judgement about the modification in the response, by comparing it with that obtained for the structural system obtained in Step 1. If the modification indicates a significant change in the response entities, then the analyst should proceed to check the magnitude of the response reduction factor obtained in Step 3. If $R_\mu > 2$, then, the inelastic

response of the considered structural system should be verified by incorporating nonlinear SSI effects. To numerically model SSI effects, the analyst should use the recommendations outlined in Chapter 4. That would be extremely helpful in saving computational expenses without hampering the accuracy of the results. The recommendation from the study are presented in the form of a flowchart and is shown in Figure 8.1.

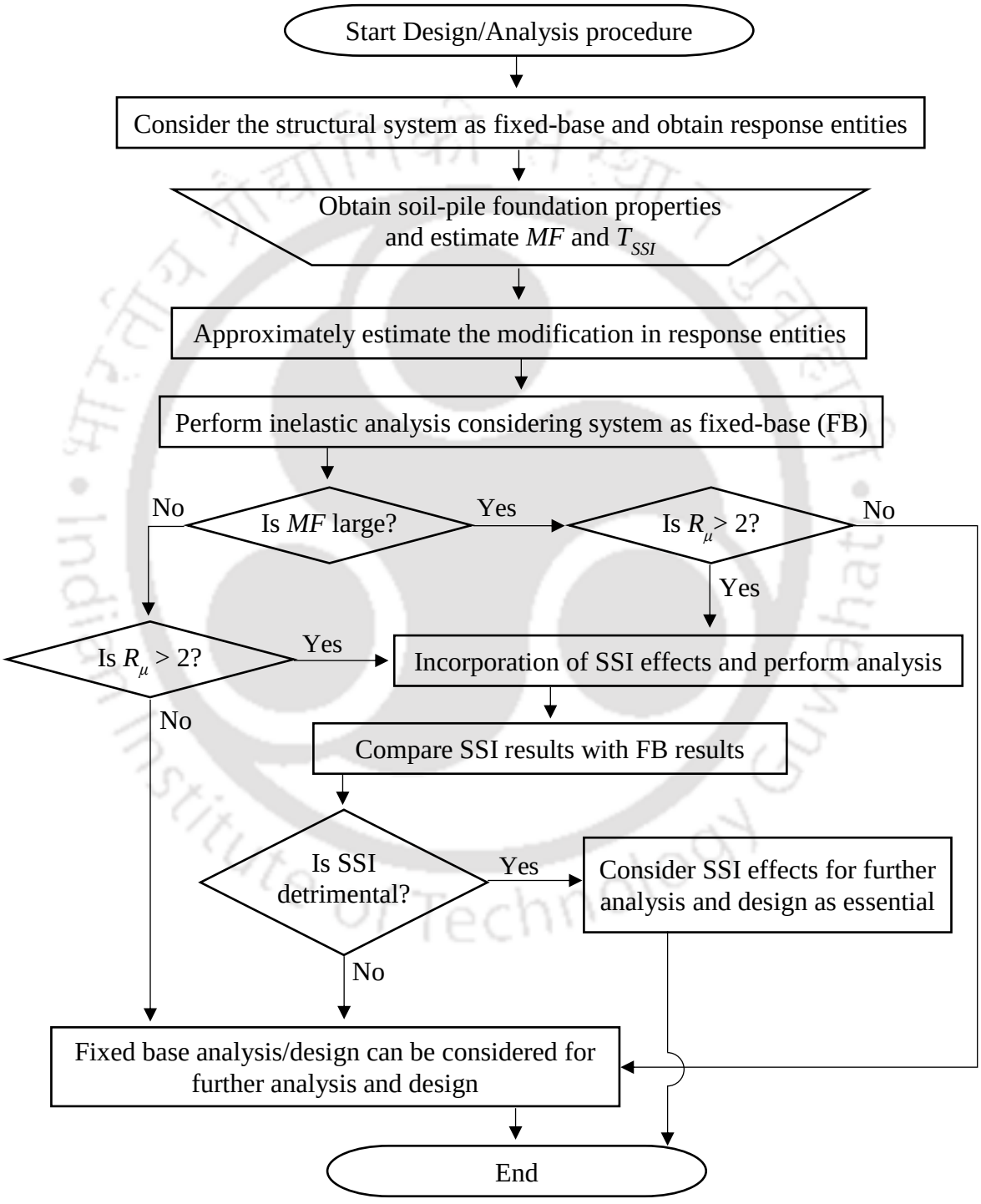

Figure 8.1 Strategy and recommendation for decision making on possible consideration of SSI effects.

8.5 LIMITATIONS OF THE PRESENT STUDY

This study has been carried out considering the RC frame and RC wall-frame systems that have been designed and conform to the relevant standard codes prescribed by BIS (Bureau of Indian Standards). The study may not be applicable to those special structures which do not conform to the codal provisions, and complete independent analyses may be required for such systems.

The present study has been conducted with the assumption that the water table lies at a far deeper level such that the foundation's response is not influenced by the seismic-induced excess pore-water pressure generation. However, for conditions wherein the water table is located at relatively shallower depths, the influence of pore-water pressure may substantially affect the stress-state of sandy soils and make them susceptible to liquefaction. In such cases, the conclusions drawn from this study may not be applicable and calls for complete analyses of such systems.

The presence of critical soil conditions such as layered soils with recognizably varying properties, soil conditions, arbitrary layering, and pile-soil separation during seismic action can play an influencing role in the SSI response. Under such circumstances, the pile-soil behavior can be unique to the specific soil condition, and conclusions drawn from this study may not be reflective of those conditions.

In the present study, P-δ effects have not been considered. Hence the conclusions drawn from this study are not applicable to cases where P-δ effects are influential (for e.g. buildings with larger storey height and slender columns). Additionally, the present study employs a deterministic approach. However, it is worth mentioning that, in reality, statistical variability exists, which is not addressed in the present study.

8.6 FUTURE SCOPE

The present study is carried out considering regular RC frame and RC wall-frame systems for which only limited cases have been adopted. This study can be applied to other types of buildings, which constitute a large portion of the building stock, for e.g., building with irregularities or Open Ground Storey buildings, Ordinary Moment Resisting Frame buildings, steel buildings, and others. Additionally, a higher number of cases that are representative of practical scenarios can be studied.

The influence of liquefaction on the inelastic response of the soil-pile-structural system could be studied by considering the influence of the water table (or the excess pore-water pressure generated during seismic motion). Therefore, the studies can be conducted for liquefaction prone soils submerged partially or fully by the water table.

A similar study under a probabilistic framework can be carried out, wherein the variations in the input parameters (material and geometric properties of the soil-pile-structure system) to account for uncertainty. This would also pave the path for probabilistic seismic fragility assessment of the structural system under the influence of SSI.

REFERENCES

Acharyya, R., and Dey, A. (2018). Assessment of bearing capacity for strip footing located near sloping surface considering ANN model. *Neural Computing and Applications*, 31(11), 8087–8100.

Acharyya, R., Dey, A., and Kumar, B. (2018). "Finite element and ANN-based prediction of bearing capacity of square footing resting on the crest of c-φ soil slope." *International Journal Geotechnical Engineering*, 14(2), 176–187.

Aldea, A., Iiba, M., Demetriu, S., and Kashima, T. (2007). "Evidence of soil-structure interaction from earthquake records at a high-rise building site in Bucharest." In: *4th International Conference on Earthquake Engineering*, Thessaloniki, Greece.

ASCE 7-05. (2006). *Minimum design loads for buildings and other structures (ASCE Standard ASCE/SEI 7–05)*, American Society of Civil Engineers, Virginia, USA.

ATC 3-06. (1978). *Tentative provisions for the development of seismic regulations for buildings*, Applied Technological Council, Report no. ATC3–06, California, USA.

ATC 40. (1996). *Seismic evaluation and retrofit of concrete buildings*, Applied Technology Council, Report no. ATC–40, California, USA.

Badry, P., and Satyam, N. (2016). "An efficient approach for assessing the seismic soil structure interaction effect for the asymmetrical pile group." *Innovative Infrastructure Solutions*, 1(8), 1–19.

Balkaya, C., Yuksel, S. B., and Derinoz O. (2012). "Soil-structure interaction effects on the fundamental periods of the shear-wall dominant buildings." *The Structural Design of Tall and Special Buildings*. 21(6), 416–430.

Behera, R. N., Patra, C. R., Sivakugan, N., and Das, B. M. (2013a). "Prediction of ultimate bearing capacity of eccentrically inclined loaded strip footing by ANN: Part I." *International Journal of Geotechnical Engineering, ASCE*, 7(1), 36–44.

Behera, R. N., Patra, C. R., Sivakugan, N., and Das, B. M. (2013b). "Prediction of ultimate bearing capacity of eccentrically inclined loaded strip footing by ANN: Part II." *International Journal of Geotechnical Engineering, ASCE*, 7(2), 165–172.

Berger, E., Mahi S. A., and Pyke, R. (1977). "Simplified method for evaluating soil-pile-structure interaction effects." In: *Proceedings of the 9th Offshore Technology Conference*, Houston, Texas, 589–598.

Bhattacharya, K., and Dutta, S. C. (2004). "Assessing lateral period of building frames incorporating soil-flexibility." *Journal of Sound and Vibration*, 269(3), 795–821.

Bielak, J. (1978). "Dynamic response of non-linear building-foundation systems." *Earthquake Engineering and Structural Dynamics* 6(1), 17–30.

Bielak, J., Loukakis, K., Hisada, Y., and Yoshimura, C. (2003). "Domain Reduction Method for Three-Dimensional Earthquake Modeling in Localized Regions, Part I:

Theory." *Bulletin of the Seismological Society of America*, 93(2), 817-824. doi:10.1785/0120010251.

Blaney, G. W., and O'Neill, M. W. (1986). "Measured lateral response of mass on single pile in clay." *Journal of Geotechnical Engineering, ASCE*, 112(4), 443–457.

Boulanger, R. W., Curras, C. J., Kutter, B. L., Wilson, D. W., and Abghari, A. (1999). "Seismic soil-pile-structure interaction experiments and analyses." *Journal of Geotechnical and Geoenvironmental Engineering, ASCE*, 125(9), 750–759.

BSSC. (1997). *NEHRP recommended provisions for seismic regulations for new buildings and other structures*, Building Seismic Saftey Council, Washington, DC, USA.

Capuani, D., Klein, R., Antes, H., and Tralli, A. (1995). "Dynamic soil-structure interaction of coupled shear walls by boundary element method." *Earthquake Engineering and Structural Dynamics*, 24(6), 861–879.

Carbonari, S., Dezi, F., and Leoni, G. (2011). "Linear soil–structure interaction of coupled wall–frame structures on pile foundations." *Soil Dynamics and Earthquake Engineering*, 31(9), 1296–1309.

Carbonari, S., Dezi, F., and Leoni, G. (2012). "Nonlinear seismic behaviour of wall-frame dual systems accounting for soil–structure interaction." *Earthquake Engineering and Structural Dynamics*, 41(12), 1651–1672.

Çelebi, E., Firat, S., and Çankaya, I. (2006). "The evaluation of impedance functions in the analysis of foundations vibrations using boundary element method." *Applied Mathematics and Computation*, 173(1), 636–667.

Celebi, M., and Safak, E. (1991). "Seismic response of TransAmerica buiklding. I: Data and preliminary analysis." *Journal of Structural Engineering, ASCE*, 117(8), 2389–2404.

Chatterjee, P., and Basu, B. (2008). "Some analytical results on lateral dynamic stiffness for footings supported on hysteretic soil medium." *Soil Dynamics and Earthquake Engineering*, 28(1), 36–43.

Chen, A. T. F. (1985). "Transmitting boundaries and seismic response." *Journal of Geotechnical Engineering, ASCE*, 111(2), 174–180.

Chopra, A. K. (2011). *Dynamics of Structures-Theory and Applications to Earthquake Engineering*, Pearson Education, Inc., Noida, U.P., India.

Chuhan, Z., Xinfeng, C., and Guanglun, W. (1999). "A coupling model of FE-BE-IE-IBE for non-linear layered soil-structure interactions." *Earthquake Engineering and Structural Dynamics*, 28(4), 421–441.

Cook, R. D., Malkus, D. S., Plesha, M. E., and Witt, R. J. (1989). *Concepts and applications of finite element analysis*, Wiley, New York, USA.

Cundall, P. A., Kunar, R. R., Carpenter P. C., and Marti J. (1978). "Solution of infinite dynamic problems by finite modelling in the time domain." In: *Second International Conference on Applied Numerical Modelling*, 339–351.

Das, S. K., and Basudhar, P. K. (2006). "Undrained lateral load capacity of piles in clay using artificial neural network." *Computers and Geotechnics*, 33(8), 454–459.

Datta, T. K. (2010). *Seismic analysis of structures*, John Wiley & Sons, New Jersey.

Deeks, A. J., and Randolph, M. F. (1994). "Axisymmetric time-domain transmitting boundaries." *Journal of Engineering Mechanics, ASCE*, 120(1), 25–42.

del Distrito Federal G (2004). "Normas técnicas complementarias para diseño por sismo." *Gaceta Oficial del Gobierno del*, Mexico.

Dezi, F., Carbonari, S., and Leoni. G. (2009). "A model for the 3D kinematic interaction analysis of pile groups in layered soils." *Earthquake Engineering and Structural Dynamics*, 38(11), 1281–1305.

Dobry, R., and Gazetas, G. (1986). "Dynamic response of arbitrarily shaped foundations." *Journal of Geotechnical Engineering, ASCE*, 112(2), 109–135.

Dobry, R., and Gazetas, G. (1988). "Simple method for dynamic stiffness and damping of floating pile groups." *Geotechnique*, 38(4), 557–574.

Dutta, S. C., and Roy, R. (2002). "A critical review on idealization and modeling for interaction among soil–foundation–structure system." *Computers and Structures*, 80(20), 1579–1594.

Dutta, S. C., Bhattacharya, K., and Roy, R. (2004). "Response of low-rise buildings under seismic ground excitation incorporating soil-structure interaction." *Soil Dynamics and Earthquake Engineering*, 24(12), 893–914.

Eilouch, M. A., and Sandhu, R. S. (1986). "A mixed method for transient analysis of soil-structure interaction under SH-motion." *Earthquake Engineering and Structural Dynamics*, 14(4), 499–516.

Elgamal, A., Yang, Z., Parra, E., and Ragheb, A. (2003), "Modeling of cyclic mobility in saturated cohesionless soils." *International Journal of Plasticity*, 19(6), 883– 905.

Eurocode 8 Part 1. (2004). "Design of structures for earthquake resistance Part 1: General rules, seismic actions and rules for buildings (EN 1998–1: 2004)." *European Committee for Normalization (CEN)*, Brussels, Belgium.

FEMA 356. (2000). *Prestandard and commentary for the seismic rehabilitation of buildings*, Federal Emergency Management Agency, Washington, DC, USA.

FEMA 440. (2005). "Improvement of nonlinear static seismic analysis procedures." *Applied Technical Council*, Redwood City, California, USA.

FEMA 450 (2003). *NEHRP recommended provisions for seismic regulations for new buildings and other structures Part 1: Provisions*, Building Seismic Saftey Council, Washington, DC, USA.

Filippou, F.C., Popov, E.P., and Bertero, V.V. (1983) "Effects of Bond Deterioration on Hysteretic Behavior of Reinforced Concrete Joints." Report EERC 83-19, Earthquake Engineering Research Center, University of California, Berkeley.

Gajan, S., Raychowdhury, P., Hutchinson, T. C., Kutter, B. L., and Stewart, J. P. (2010). "Application and validation of practical tools for nonlinear soil-foundation interaction analysis." *Earthquake Spectra*, 26(1), 111–129.

Ganainy, H., and El Naggar, M. H. (2009). "Seismic performance of three-dimensional frame structures with underground stories." *Soil Dynamics and Earthquake Engineering*, 29(9), 1249–1261.

Garson, G. D. (1991). "Interpreting neural-network connection weights." *AI Expert*, 6(4), 46-51.

Gascot, R. L., and Montejo, L. A. (2016)." Spectrum-compatible earthquake records and their influence on the seismic response of reinforced concrete structures." *Earthquake Spectra*, 32(1), 101–123.

Gazetas, G. (1983). "Analysis of machine foundation vibrations: state of the art." *International Journal of Soil Dynamics and Earthquake Engineering*, 2(1), 2–42.

Gazetas, G. (1984a). "Seismic response of end-bearing single piles." *International Journal of Soil Dynamics and Earthquake Engineering*, 3(2), 82–93.

Gazetas, G. (1991a). "Formulas and charts for impedances of surface and embedded foundations." *Journal of Geotechnical Engineering, ASCE*, 117(9), 1363–1381.

Gazetas, G. (1991b). "Foundation vibrations." In: *Foundation engineering handbook*, Springer, Boston, MA, 553-593.

Gazetas, G. (1996). *Soil dynamics and earthquake engineering- case studies*. Athens (in Greek), Simeon Publication.

Gazetas, G., and Dobry, R. (1984a). "Horizontal response of piles in layered soils." *Journal of Geotechnical Engineering, ASCE*, 110(1), 20–40.

Gazetas, G., and Dobry, R. (1984b). "Simple radiation damping model for piles and footings." *Journal of Engineering Mechanics, ASCE*, 110(6), 937–956.

Gazetas, G., and Dobry, R. (1984c). "Simple radiation damping model for piles and footings." *Journal of Engineering Mechanics, ASCE*, 110(6), 937–956.

Gentela, S. R. (2011). *Influence of soil-structure interaction on seismic behaviour of reinforced concrete integral bridge piers*. M. Tech thesis, Indian Institute of Technology Guwahati.

Gerolymos, N., and Gazetas, G. (2006). "Development of Winkler model for static and dynamic response of caisson foundations with soil and interface nonlinearities." *Soil Dynamics and Earthquake Engineering*, 26(5), 363–376.

References

Ghaboussi J., Sidarta D. E., and Lade P. V. (1994). "Neural network based modelling in geomechanics." In: *Computer methods and advances in geomechanics*, Rotterdam Publishing, Balkema, 153–164.

Ghandil, M., and Behnamfar, F. (2017). "Ductility demands of MRF structures on soft soils considering soil-structure interaction." *Soil Dynamics and Earthquake Engineering*, 92, 203–214.

Ghosh, S., and Wilson, E. (1969). "Dynamic stress analysis of axisymmetric structures under arbitrary loading." Report no. EERC 69–10, University of California, Berkeley.

Godbole, P., Viladkar, M., and Noorzaei, J. (1990). "Nonlinear soil-structure interaction analysis using coupled finite-infinite elements." *Computers and Structures*, 36(6), 1089–1096.

Goh, A. T. C. (1994). "Seismic liquefaction potential assessed by neural networks." *Journal of Geotechnical Engineering, ASCE*, 120(9),1467–1480.

Gomes, A., and Appleton, J. (1997). "Nonlinear cyclic stress-strain relationship of reinforcing bars including buckling." *Engineering Structures*, 19(10), 822–826.

Guéguen, P., and Bard, P. Y. (2005). "Soil-structure and soil-structure-soil interaction: experimental evidence at the Volvi test site." *Journal of Earthquake Engineering*, 9(05), 657–693.

Guéguen, P., Bard, P. Y., and Chávez-Garc'ia, F. J. (2002). "Site-City Seismic Interaction in Mexico City-Like Environments: An Analytical Study." *Bulletin of the Seismological Society of America*, 92(2), 794–811.

Hadjian, A. H., Luco, J. E., and Tsai, N. C. (1974). "Soil-structure interaction: continuum or finite element?" *Nuclear Engineering and Design*, 31(2), 151–167.

Hagan, M. T., and Menhaj, M. B. (1994). "Training feedforward networks with the Marquardt algorithm." *IEEE transactions on Neural Networks*, 5(6), 989–993.

Häggblad, B., and Nordgren, G. (1987). "Modelling nonlinear soil-structure interaction using interface elements, elastic-plastic soil elements and absorbing infinite elements." *Computers and Structures*, 26(1-2), 307–324.

Halabian, A., El Naggar, M., and Vickery, B. (2002). "Nonlinear seismic response of reinforced-concrete free-standing towers with application to TV towers on flexible foundations." *The Structural Design of Tall Buildings*, 11(1), 51–72.

Hamdia, K. M., Ghasemi, H., Zhuang, X., Alajlan, N., and Rabczuk, T. (2018). "Sensitivity and uncertainty analysis for flexoelectric nanostructures." *Computational Methods in Applied Mechanics and Engineering*, 337, 95–109.

Hamdia, K. M., Silani, M., Zhuang, X., He, P., and Rabczuk T (2017). "Stochastic analysis of the fracture toughness of polymeric nanoparticle composites using polynomial chaos expansions." *International Journal of Fracture*, 206(2), 215–227.

Han, Y. (2002). "Seismic response of tall building considering soil-pile-structure interaction." *Earthquake Engineering and Engineering Vibration* 1(1), 57–64.

Hancock, J., Bommer, J. J., and Stafford, P. J. (2008). "Numbers of scaled and matched accelerograms required for inelastic dynamic analyses." *Earthquake Engineering and Structural Dynamics*, 37(14), 1585–1607.

Heidebrecht, A., Henderson, P., Naumoski, N., and Pappin, J. (1990). "Seismic response and design for structures located on soft clay sites." *Canadian Geotechnical Journal*, 27(3), 330-341.

Hilber, H. M., Hughes, T. J., and Taylor, R. L. (1977). "Improved numerical dissipation for time integration algorithms in structural dynamics", *Earthquake Engineering and Structural Dynamics*, 5(3), 283–292.

Hokmabadi, A. S., Fatahi B., and Samali, B. (2014). "Assessment of soil–pile–structure interaction influencing seismic response of mid-rise buildings sitting on floating pile foundations." *Computers and Geotechnics*, 55, 172–186.

IS 13920. (2016). *Indian standard ductile detailing of reinforced concrete structures subjected to seismic forces- code of practice*, Bureau of Indian Standards, New Delhi, India.

IS 1893 Part 1. (2016). *Indian standard criteria for earthquake resistant design of structures, part 1: General provisions and buildings*, Bureau of Indian Standards, New Delhi, India.

IS 2911Part 1/Sec 1. (2010). *Indian standard design and construction of pile foundations-code of practice: concrete piles*, Bureau of Indian Standards, New Delhi, India.

IS 456. (2000). *Indian standard plain and reinforced concrete- code of practice*, Bureau of Indian Standards, New Delhi, India.

IS 875 Part 2. (1987). *Indian standard code of practice for design loads (other than earthquake) for building and structures: Imposed loads*, Bureau of Indian Standards, New Delhi, India.

Iwan, W. D. (1967). "On a class of models for the yielding behavior of continuous and composite systems." *Journal of Applied Mechanics, ASME*, 34, 612–617.

Jingbo, L., and Yandong, L. (1998). "A direct method for analysis of dynamic soil-structure interaction based on interface idea." *Developments in Geotechnical Engineering*, 83, 261-276.

Joyner, W. B., and Chen, A. T. (1975). "Calculation of nonlinear ground response in earthquakes." *Bulletin of the Seismological Society of America*, 65(5), 1315–1336.

JSCE. (2007). *Guidelines for Concrete No. 15: Standard Specifications for Concrete Structures*, Japan Society of Civil Engineers, Tokyo, Japan.

Jun, D. H. (2013). "Seismic response of R/C structures subjected to simulated ground motions compatible with design spectrum." *The Structural Design of Tall and Special Buildings*, 22(1), 74–91.

Kampitsis, A. E., Sapountzakis, E. J., Giannakos, S. K., and Gerolymos, N. A. (2013). "Seismic soil–pile–structure kinematic and inertial interaction—A new beam approach." *Soil Dynamics and Earthquake Engineering*, 55, 211–224.

Kausel, E. (1988). "Local transmitting boundaries." *Journal of Engineering Mechanics*, 114 (6), 1011–1027.

Kausel, E. (2010). "Early history of soil-structure interaction." *Soil Dynamics and Earthquake Engineering*, 30(9), 822–832.

Kausel, E., Roesset, J. M., and Wass, G. (1975). "Dynamic analysis of footings on layered media." *Journal of the Engineering Mechanics Division*, 101, 679–693.

Kavitha, P. E., Beena, K. S., and Narayanan, K. P. (2016). "A review on soil-structure interaction analysis of laterally loaded piles." *Innovative Infrastructure Solutions*, 1(1), 1–55.

Kavvadas, M., and Gazetas, G. (1993). "Kinematic seismic response and bending of free-head piles in layered soil." *Geotechnique*, 43(2), 207–222.

Kazaz, I. (2013). "Analytical study on plastic hinge length of structural walls." *Journal of Structural Engineering, ASCE*, 139(11), 1938–1950.

Kempton, J. J., and Stewart, J. P. (2006). "Prediction equations for significant duration of earthquake ground motions considering site and near-source effects." *Earthqake Spectra*, 22(4), 985–1013.

Kent, D. C., and Park, R. (1971). "Flexural members with confined concrete." *Proceedings, ASCE*, 97(ST7), 1969–1990.

Ko. Y. F., and Phung, C. (2014). "Nonlinear static cyclic pushover analysis for flexural failure of reinforced concrete bridge columns with combined damage mechanisms." *Acta Mechanica*, Springer, 225, 477–492.

Kolay, C. (2009). "Seismic analysis of Bridge abutment-soil systems." Ph.D. Thesis, Indian Institute of Technology Kanpur.

Kolay, C., Prashant, A., and Jain, S. K. (2013). "Nonlinear dynamic analysis and seismic coefficient for abutments and retaining walls." *Earthquake Spectra*, 29(2), 427–451.

Kramer, S. L. (1996). *Geotechnical earthquake engineering*. Prentice-Hall, New York, USA.

Kraus, I., and Džakić, D. (2013). "Soil-structure interaction effects on seismic behaviour of reinforced concrete frames." In: *50 years Skopje Earthquake-50 years of European Earthquake Engineering*, 1–8.

Krishnan, R., Gazetas, G., and Velez, A. (1983). "Static and dynamic lateral deflexion of piles in non-homogeneous soil stratum." *Geotechnique*, 33(3), 307–325.

Kuhlemeyer, R. L., and Lysmer, J. (1973). "Finite element method accuracy for wave propagation problems." *Journal of Soil Mechanics and Foundation Division, ASCE,* 99(SM5), 421–427.

Kumar, S., and Prakash, S. (2004). "Estimation of fundamental period for structures supported on pile foundations." *Geotechnical and Geological Engineering,* 22, 375–389.

Kunar, R., and Rodriguez-Ovejero, L. (1980). "A model with non-reflecting boundaries for use in explicit soil-structure interaction analyses." *Earthquake Engineering and Structural Dynamics,* 8(4), 361–374.

Kutanis, M., and Elmas, M. (2001). "Non-linear seismic soil-structure interaction analysis based on the substructure method in the time domain." *Turkish Journal of Engineering and Environmental Sciences,* 25(6), 617–626.

Kwok, A. O., Stewart, J. P., Hashash, Y. M., Matasovic, N., Pyke, R., Wang, Z., and Yang, Z. (2007). "Use of exact solutions of wave propagation problems to guide implementation of nonlinear seismic ground response analysis procedures." *Journal of Geotechnical and Geoenvironmental Engineering, ASCE,* 133(11), 1385–1398.

Lee, S. C. (2003). "Prediction of concrete strength using artificial neural networks." *Engineering Structures,* 25(7), 849–857.

Lou, M., Wang, H., Chen, X., and Zhai, Y. (2011). "Structure-soil-structure interaction: Literature review." *Soil Dynamics and Earthquake Engineering,* 31(12), 1724-1731.

Lu, X., Chen, B., Li, P., and Chen, Y. (2003). "Numerical analysis of tall buildings considering dynamic soil-structure interaction." *Journal of Asian Architecture and Building Engineering,* 2(1), 1–8.

Luco, J., Trifunac, M., and Wong, H. (1988). "Isolation of soil-structure interaction effects by full-scale forced vibration tests." *Earthquake Engineering and Structural Dynamics,* 16(1), 1–21.

Lysmer, J., and Kuhlemeyer, R. L. (1969). "Finite dynamic model for infinite media." *Journal of Engineering Mechanics Division, ASCE,* 95(4), 859–878.

Lysmer, J., and Kuhlemeyer, R. L. (1969). "Finite Dynamic Model for Infinite media." *Journal of Engineering Mechanics Division, ASCE,* 95, 859–877.

Lysmer, J., and Waas, G. (1972). "Shear waves in plane infinite structures." *Journal of Engineering Mechanics*.

Makris, N., and Gazetas, G. (1992). "Dynamic pile-soil-pile interaction. Part II: lateral and seismic response." *Earthquake Engineering and Structural Dynamics,* 21(2), 145–162.

Mansour, M. Y., Dicleli, M., Lee, J. Y., and Zhang J (2004). "Predicting the shear strength of reinforced concrete beams using artificial neural networks." *Engineering Structures,* 26(6), 781–799.

Marzban, S., Banazadeh, M., and Azarbakht, A. (2014). "Seismic performance of reinforced concrete shear wall frames considering soil–foundation–structure interaction." *The Structural Design of Tall and Special Buildings*, 23(4), 302–318.

MathWorks. (2001). *Matlab user's manual. Version 2015A*. The MathWorks, Inc., Natick, USA.

Matinmanesh, H., and Asheghabadi, M. S. (2011). "Seismic analysis on soil-structure interaction of buildings over sandy soil." *Procedia Engineering*, 14, 1737–1743.

Mazzoni, S., McKenna, F., Scott, M., and Fenves, G. (2009). "Open system for earthquake engineering simulation user command language manual—OpesnSeesVersion 2.0." Pacific Earthquake Engineering Research Center, University of California, Berkeley, USA.

Meek, J., and Veletsos, A. (1974). "Simple models for foundations in lateral and rocking motion." In: *5th World Conference on Earthquake Engineering*, 2610-2631.

Meli, R., Faccioli, E., Murià-Vila, D., Quaas, R., and Paolucci, R. (1998). "A study of site effects and seismic response of an instrumented building in Mexico City." *Journal of Earthquake Engineering*, 2(1), 89-111

Menegotto, M., and Pinto, P. E. (1973). "Method of analysis for cyclically loaded reinforced concrete plane frames including changes in geometry and non-elastic behavior of elements under combined normal force and bending moment." IASBE Proceedings, pp. 15–22, Lisbon, Portugal.

Momeni, E. R., Nazir, D., Armaghani, J., and Maizir, H. (2014). "Prediction of pile bearing capacity using a hybrid genetic algorithm-based ANN." *Measurement*, 57, 122–131.

Mondal, A., Ghosh, S., and Reddy, G.R. (2013). "Performance-based evaluation of the response reduction factor for ductile RC frames." *Engineering structures*, 56, 1808–1819.

Mondal, G., Prashant, A., and Jain, S. K. (2012). "Simplified seismic analysis of soil–well–pier system for bridges". *Soil Dynamics and Earthquake Engineering*, 32(1), 42–55.

Mroz, Z. (1967). "On the description of anisotropic work hardening." *Journal of the Mechanics and Physics of Solids*, 15(3), 163–175.

Muria-Vila, D., Taborda, R., and Zapata-Escobar, A. (2004) "Soil-structure interaction effects in two instrumented tall buildings." In: *13th World Conference on Earthquake Engineering*, Vancouver, Canada.

Mylonakis, G., and Gazetas, G. (2000). "Seismic soil-structure interaction: beneficial or detrimental?" *Journal of Earthquake Engineering*, 4 (3), 277–301.

Mylonakis, G., Nikolaou, A., and Gazetas, G. (1997). "Soil-pile-bridge seismic interaction: kinematic and inertial effects. Part I: soft soil." *Earthquake Engineering and Structural Dynamics*, 26(3), 337–359.

Nadjai, A., and Johnson, D. (1996). "Elastic analysis of spatial shear wall systems with flexible bases." *The Structural Design of Tall Buildings*, 5(1), 55–72.

Nagendra, M., and Sridharan, A. (1984). "Footing response to horizontal vibration." *Journal of Engineering Mechanics, ASCE,* 110(4), 648–654.

Nakamura, N. (2009). "Nonlinear response analyses of a soil-structure interaction system using transformed energy transmitting boundary in the time domain." *Soil Dynamics and Earthquake Engineering*, 29(5), 799–808.

Nateghi-A, F., and Rezaei-Tabrizi, A. (2013). "Nonlinear dynamic response of tall buildings considering structure–soil–structure effects." *The Structural Design of Tall and Special Buildings*, 22(14), 1075-1082.

Naumoski, N., Saatcioglu, M., Lin, L., and Amiri-Hormozaki, K. (2006). "Evaluation of the effects of spectrum-compatible seismic excitations on the response of medium-height reinforced concrete frame buildings." *Canadian Journal of Civil Engineering*. 33(10), 1304–19.

Nguyen, Q. V., Fatahi, B., and Hokmabadi, A. S. (2016). "The effects of foundation size on the seismic performance of buildings considering the soil-foundation-structure interaction." *Structural Engineering and Mechanics*, 58 (6), 1045–1075.

NIST GCR 12-917-21 (2012). "Soil-structure-interaction for building structures". *National Institute of Standards and Technology*, Gaithersburg, MD, USA.

Nogami, T., Otani, J., Konagai, K., and Chen, H. L. (1992). "Nonlinear soil-pile interaction model for dynamic lateral motion." *Journal of Geotechnical Engineering, ASCE*, 118(1), 89–106.

Novak, M., and Sheta, M. (1980). "Approximate approach to contact effects of piles." In: *Dynamic response of pile foundations: Analytical aspects, ASCE,* 53–79.

Oliveto, G., and Santini, A. (1993). "A simplified model for the dynamic soil-structure interaction of planar frame-wall systems." *Engineering Structures* 15(6), 431–438.

Padrón, L. A., Aznárez, J. J., and Maeso, O. (2009). "Dynamic structure–soil–structure interaction between nearby piled buildings under seismic excitation by BEM–FEM model." *Soil Dynamics and Earthquake Engineering*, 29(6), 1084–1096.

Pala, M., Caglar, N., Elmas, M., Cevik, A., and Saribiyik, M. (2008). "Dynamic soil-structure interaction analysis of buildings by neural networks." *Construction and Building Materials*, 22(3), 330–342.

Parra, E. (1996). "Numerical modeling of liquefaction and lateral ground deformation including cyclic mobility and dilation response in soil systems." Ph.D. thesis, Dept. of Civil Engineering, Rensselaer Polytechnic Institute, Troy, New York, USA.

Paulay T., and Priestley M. J. N., (1992). Seismic Design of Reinforced Concrete and Masonry Buildings. John Wiley & Sons, Inc., New York, USA.

References

PEER Database (Pacific Earthquake Engineering Research Center). *PEER ground motion database*, University of California, Berkeley, CA. (http://ngawest2berkeley.edu/).

Poulos, H. G., and Davis, E. H. (1990). *Pile foundation analysis and design*, Krieger Publication, Malabar.

Prevost, J. H. (1985). "A simple plasticity theory for frictional cohesionless soils." *Soil Dynamics and Earthquake Engineering*, 4(1), 9–17.

Randolph, M. F. (1981). "The response of flexible piles to lateral loading." *Geotechnique* 31(2), 247–259.

Raychowdhury, P., and Singh, P. (2012). "Effect of non-linear soil-structure interaction on seismic response of low-rise SMRF buildings." *Earthquake Engineering and Engineering Vibration*, 11(4), 541–551.

Rayhani, M. H., and El Naggar, M. H. (2008). "Numerical modeling of seismic response of rigid foundation on soft soil." *International Journal of Geomechanics*, 8(6), 336–346.

Reddy, J. N. (1993). *An introduction to the finite element method*. New York, USA: McGraw-Hill.

Renzi, S., Madiai, C., and Vannucchi, G. (2013), "A simplified empirical method for assessing seismic soil-structure interaction effects on ordinary shear-type buildings." *Soil Dynamics and Earthquake Engineering*, 55, 100–107.

Roesset, J. M. (2013). "Soil structure interaction the early stages." *Journal of Applied Science and Engineering* 16(1), 1–8.

Roesset, J. M., and Ettouney, M. M. (1977). "Transmitting boundaries: a comparison." *International Journal for Numerical and Analytical Methods in Geomechanics*, 1(2), 151–176.

Rovithis, E. N., Pitilakis, K. D., and Mylonakis, G. E. (2009). "Seismic analysis of coupled soil-pile-structure systems leading to the definition of a pseudo-natural SSI frequency." *Soil Dynamics and Earthquake Engineering*, 29(6), 1005–1015.

Roy, J., Kumar, A., and Choudhury, D. (2018). "Natural frequencies of piled raft foundation including superstructure effect." *Soil Dynamics and Earthquake Engineering*, 112, 69–75.

Sáez, E., Lopez-Caballero, F., and Modaressi-Farahmand-Razavi A. (2013). "Inelastic dynamic soil–structure interaction effects on moment-resisting frame buildings." *Engineering Structures*, 51, 166–177.

Scott, B. D., Park, R., and Priestley, M. J. N. (1982). "Stress-strain behavior of concrete confined by overlapping hoops at low and high strain rates". *ACI Journal*, 79, 13–27.

Seismosoft. (2018). SeismoMatch — A computer program for spectrum matching of earthquake records.

Smith, W. D. (1974). "A nonreflecting plane boundary for wave propagation problems." *Journal of Computational Physics*, 15(4), 492–503.

Spacone, E., Filippou, F. C., and Taucer, F. F. (1996a). "Fibre beam-column model for non-linear analysis of R/C frames: part I. Formulation." *Earthquake Engineering and Structural Dynamics*, 25(7), 711–725.

Spacone, E., Filippou, F. C., and Taucer, F. F. (1996b). "Fibre beam-column model for non-linear analysis of R/C frames: part II. Applications." *Earthquake Engineering and Structural Dynamics*, 25(7), 727–742.

Stevens, D. J., and Krauthammer, T. (1988). "A finite difference/finite element approach to dynamic soil-structure interaction modelling." *Computers and Structures*, 29(2), 199–205.

Syed, N. M., and Maheshwari, B. K. (2017). "Non-linear SSI analysis in time domain using coupled FEM–SBFEM for a soil–pile system." *Géotechnique*, 67(7), 572-580.

Tabatabaiefar, H. R., and Massumi, A. (2010). "A simplified method to determine seismic responses of reinforced concrete moment resisting building frames under influence of soil-structure interaction." *Soil Dynamics and Earthquake Engineering* 30(11), 1259–1267.

Tabatabaiefar, S. H. R., Fatahi, B., and Samali, B. (2013). "Seismic behavior of building frames considering dynamic soil-structure interaction." *International Journal of Geomechanics, ASCE*, 13(4), 409–420.

Tang, Y., and Zhang, J. (2011) "Probabilistic seismic demand analysis of a slender RC shear wall considering soil-structure interaction effects." *Engineering Structures*, 33(1), 218–229.

Thomsen IV, J. H., and Wallace, J. W. (2004). "Displacement-based design of slender reinforced concrete structural walls—experimental verification." *Journal of Structural Engineering, ASCE*, 130(4), 618–630.

Tomeo, R., Pitilakis, D., Bilotta, A., and Nigro, E. (2018). "SSI effects on seismic demand of reinforced concrete moment resisting frames." *Engineering Structures*, 173, 559–572.

Trifunac, M. D., and Brady, A. G. (1975). "A study on the duration of strong earthquake ground motion." *Bulletin of Seismological Society of America*, 65(3), 581–626.

Veletsos, A. S., and Meek, J. W. (1974). "Dynamic behaviour of building-foundation systems." *Earthquake Engineering and Structural Dynamics*, 3(2), 121–138.

Vivek, B., and Raychowdhury, P. (2017). "Influence of SSI on period and damping of buildings supported by shallow foundations on cohesionless soil." *International Journal of Geomechanics*, 17(8), 04017030.

Vu-Bac, N., Lahmer, T., Zhuang. X., Nguyen-Thoi, T., and Rabczuk, T. (2016). "A software framework for probabilistic sensitivity analysis for computationally expensive models." *Advances in Engineering Software*, 100, 19–31.

Wang, S. (1992). "Coupled boundary and finite elements for dynamic structure (3D)-foundation-soil interaction." *Computers and Structures*, 44(4), 807–812.

Wang, S., Kutter, B. L., Chacko, M. J., Wilson, D. W., Boulanger, R. W., and Abghari, A. (1998). "Nonlinear seismic soil-pile structure interaction." *Earthquake Spectra*, 14(2), 377–396.

Wegner, J., Yao, M., and Zhang, X. (2005). "Dynamic wave-soil-structure interaction analysis in the time domain." *Computers and Structures*, 83(27), 2206–2214.

Weissman, K., and Prevost, J. H. (1991). "Results and analysis of soil-structure interaction experiments performed in the centrifuge." *Earthquake Engineering and Structural Dynamics*, 20(3), 259–274.

Wolf, J. P. (1986). "A comparison of time-domain transmitting boundaries." *Earthquake Engineering and Structural Dynamics*, 14, 655–673.

Wolf, J. P. (2003). *The scaled boundary finite element method*. John Wiley & Sons, USA.

Wolf, J. P., and Darbre, G. R. (1984). "Dynamic stiffness matrix of soil by the boundary-element method: Conceptual aspects." *Earthquake Engineering and Strctural Dynamics*, 12(3), 385–400.

Wolf, J. P., and Somaini, D. R. (1986). "Approximate dynamic model of embedded foundation in time domain." *Earthquake Engineering and Structural Dynamics*, 14(5), 683–703.

Yamahara, H. (1970). "Ground motions during earthquakes and the input loss of earthquake power to an excitation of buildings." *Soils and Foundations*, 10(2), 145–161.

Yang, Z. (2000). "Numerical modeling of earthquake site response including dilation and liquefaction." Ph.D. dissertation, Dept. of Civil Engineering and Engineering Mechanics, Columbia University, New York.

Yang, Z., Elgamal, A., and Parra, E. (2003). "Computational model for cyclic mobility and associated shear deformation." *Journal of Geotechnical and Geoenvironmental Engineering, ASCE*, 129(12), 1119–1127.

Yang, Z., Lu, J., and Elgamal, A. (2008). "OpenSees Soil Models and Solid-Fluid Fully Coupled Elements," *User's Manual. Ver*, vol. 1.

Yegian, M. K., Chang, C. Y., Mullen, C. L., and Mylonakis, G. (2001). "Soil-structure Interaction under Dynamic Loading for Both Shallow and Deep Foundations." In: *Fourth International Conference on Recent Advances in Geotechnical Earthquake Engineering and Soil Dynamics and Symposium in Honor of Professor WD Liam Finn*, San Diego, California, USA.

Yun, C. B., Kim, D. K., and Kim, J. M. (2000). "Analytical frequency-dependent infinite elements for soil-structure interaction analysis in two-dimensional medium." *Engineering Structures*, 22(3), 258–271.

Zdravkovic, L., and Kontoe, S. (2008). "Some issues in modelling boundary conditions in dynamic geotechnical analysis." In: *12th International Conference of International Association for Computer Methods and Advances in Geomechanics*, India, 1–6.

Zhang, Y., Conte, J. P., Yang, Z., Elgamal, A., Bielak, J., and Acero, G. (2008). "Two-dimensional nonlinear earthquake response analysis of a bridge-foundation-ground system." *Earthquake Spectra*, 24(2), 343–86.

Zhang, Y., Yang, Z., Bielak, J., Conte, J.P., and Elgamal, A. (2003), "Treatment of seismic input and boundary conditions in nonlinear seismic analysis of a bridge ground system." In: *Proceedings of the16th ASCE Engineering Mechanics Conference*, 16–18, University of Washington, Seattle, USA.

Zhou, J., He, F., and Liu, T. (2014). "Curvature ductility of columns and structural displacement ductility in RC frame structures subjected to ground motions." *Soil Dynamics and Earthquake Engineering*, 63, 174–183.

Appendix A
SIZE AND REINFORCEMENT DETAILS OF THE RC FRAME AND WALL-FRAME SYSTEMS

A.1 OVERVIEW

This appendix provides the details of the columns, beams, shear walls, and pile foundations of the various configurations used in the present study. The various configuration studied in this work are already described in Chapter 5, and relevant Indian Standards have been utilized for the purpose of analysis and design. The following subsection briefly describes the design basis of the superstructure and foundation members of the RC frame and RC wall-frame systems. The cross-sectional details (member sizes and details of the longitudinal and shear reinforcement) are also provided in a tabular format to facilitate readability.

A.2 DESIGN BASIS AND MEMBER DETAILS

The RC frame and RC wall-frame systems are designed as per the provisions of the relevant codes issued by the Bureau of Indian Standards (BIS). The intended use of the frames is assumed to be for residential purposes, and the gravity loading is estimated as per IS 875 (Part 2) (1987). The super-imposed dead load considered as 3 kN/m^2, and the assumed live load as 3 kN/m^2. A uniformly distributed load of 5 kN/m, representing the weight of the unreinforced brick masonry infill wall, is imposed on the beams of the frame. The seismic forces on the superstructure are calculated as per the provisions of IS 1893 (Part 1) (2016), considering the structure to be located in Seismic Zone V as per Indian Seismic Zoning map. For design purposes, the natural period of the structure is estimated as per Eq. (A.1).

$$T_a = \frac{0.075H^{0.75}}{\sqrt{A_{we}}} \tag{A.1}$$

In the above expression, A_{we} is the total effective area of shear walls in the first storey of the building and is calculated using Eq. (A.2) as,

$$A_{we} = \sum_{i=1}^{N_w} \left[A_{wi} \left\{ 0.2 + \left(\frac{L_{wi}}{H} \right)^2 \right\} \right] \tag{A.2}$$

where H is the height of the building frame, A_{wi} is the effective cross-sectional area of the wall 'i' in the first storey of the building frame (in m^2), L_{wi} is the length of shear wall in the first storey in the direction of lateral forces (in m), and N_w is the number of shear walls in the considered direction of shaking. The design base shear at the bottom of the superstructure is calculated as shown in Eq. (A.3),

$$V_d = \frac{Z}{2} \times \frac{I}{R} \times \frac{S_a}{g} \times W \tag{A.3}$$

where Z is the zone factor (0.36 for Zone V), I is the importance factor of the structure (1 for residential building), R is the response reduction factor (5 for ductile moment-resisting frames), S_a is the spectral acceleration obtained using Eq. (A.4), and W is the seismic weight of the structure.

$$\frac{S_a}{g} = \begin{cases} 2.5 & 0s < T_a \le 0.67s \\ 1.67 / T_a & 0.67s < T_a \le 4s \\ 0.42 & T_a > 4s \end{cases} \tag{A.4}$$

The design of frame and shear wall sections corresponding to each superstructure configuration has been carried out for the estimated gravity and seismic loads as per the provisions of IS 456 (2000) and IS 13920 (2016). For a particular height of the building frame, the dimensions of the frame and shear wall sections are kept to be the same for different structural widths. Table A.1 shows the details of the columns and beam members, and Table A.2 shows the details of the shear wall and boundary elements for various storey heights and storey levels. The grade of concrete (f_{ck}) and rebar (f_y) used for the design of all concrete members is M30 in the present study, and the elastic modulus of concrete is obtained as $E_c = 5000 \times (f_{ck})^{0.5}$ MPa (IS 13920, 2016). The estimated gravity and seismic loads at the base of the superstructure level are used for the design of pile foundation under the columns and shear wall. The provisions of IS 2911 Part1/Sec 1 (2010) have been used for the design of the pile foundations under gravity and seismic loading. Details of pile foundation supporting the column members are shown in Table A.3, and those supporting the shear wall are shown in Table A.4. Pile foundation supporting the shear wall comprises a group of 6 piles for all structural configurations, and the distance between adjacent piles

in a group under columns is kept to be three times the diameter of the individual pile, as per the practice.

Table A.1 Details of RC frame members

No. of Stories	Storey level	Column					Beam				
		Size (mm×mm)	Main reinf.		Shear reinf.		Size (mm×mm)	Main reinf.		Shear reinf.	
			ϕ (mm)	no.	ϕ (mm)	s_v (mm)		ϕ (mm)	no.	ϕ (mm)	s_v (mm)
3	Upto 3	300×300	12	4+4	8 8	75 170	200×280	20† 20*	2 2	8	100
6	Upto 3	350×350	16	4+4	8 8	75 170	200×350	20† 12*	3 3	8	100
	3 to 6	350×350	16 12	4 4	8 8	75 170	200×350	20† 12*	3 3	8	100
9	Upto 3	450×450	16	4+4	8 8	75 170	250×400	20† 12*	4 3	8	100
	3 to 6	400×400	16 12	4 4	8 8	75 200	250×400	20† 12	4 3	8	100
	6 to 9	350×350	16 12	4 4	8 8	75 220	250×350	20† 12*	3 3	8	100
12	Upto 3	500×500	20 16	4 4	8 8	75 170	250×450	25 16*	3 2	8	90
	3 to 6	450×450	16	4+4	8 8	75 200	250×450	25† 16*	3 2	8	90
	6 to 9	400×400	16	4+4	8 8	75 220	250×400	20† 12*	4 3	8	100
	9 to 12	400×400	16 12	4 4	8 8	75 250	200×350	20† 12*	3 3	8	100

Note: ϕ is rebar diameter, † indicates tensile reinf., ∗ indicates compressive reinf. and reinf. is the abbreviation for reinforcement

Table A.2 Details of RC shear walls

No. of Stories	Storey level	Shear wall details					Boundary element details				
		t_w (mm)	Vertical reinf.		Horizontal reinf.		Size (mm×mm)	Main reinf.		Shear reinf.	
			ϕ (mm)	no.	ϕ (mm)	s_v (mm)		ϕ (mm)	no.	ϕ (mm)	s_v (mm)
3	Upto 1	200	12	10*	12	280	500×500	25 20	4 4	8	100
	1 to 3	200	12	10	12	280	300×300	12 12	4 4	8	100
6	Upto 1	200	12	10*	12	280	500×500	25 20	4 4	8	100
	1 to 3	200	12	10	12	280	350×350	16 16	4 4	8	100
	3 to 6	150	12	10	12	300	350×350	16 12	4 4	8	100
9	Upto 1	200	12	10*	12	260	500×500	25 20	4 4	8	100
	1 to 3	150	12	10	12	260	450×450	16 16	4 4	8	100
	3 to 6	150	12	10	12	300	400×400	16 12	4 4	8	100
	6 to 9	150	12	10	12	300	350×350	16 12	4 4	8	100
12	Upto 1	200	12	10*	12	230	500×500	25 20	4 4	8	100
	1 to 3	150	12	10	12	230	500×500	20 16	4 4	8	100
	3 to 6	150	12	10	12	300	450×450	16 16	4 4	8	100
	6 to 9	150	12	10	12	300	400×400	16 16	4 4	8	100
	9 to 12	150	12	10	12	300	400×400	16 12	4 4	8	100

Note: ϕ is rebar diameter, † indicates tensile reinf., ∗ indicates compressive reinf. and reinf. is the abbreviation for reinforcement

Table A.3 Details of pile groups supporting frame members

No. of Stories	Loose Soil S1		Medium soil S2		Med. dense soil S3		Dense soil S4	
	Pile length (m)	Pile dia. (mm)	Pile length (m)	Pile dia. (mm)	Pile length (m)	Pile dia. (mm)	Pile length (m)	Pile dia. (mm)
				Pile group of three				
3	11.0	300	7.0	300	6.5	250	3.5	250
6	12.5	400	7.5	400	5.5	350	4.5	300
9	15.5	450	10.0	450	6.0	400	5.0	350
12	16.5	500	10.5	500	6.5	450	5.0	400
				Pile group of two				
3	12.0	350	8.0	350	6.0	300	3.5	300
6	12.0	500	9.5	450	6.0	400	5.0	350
9	15.0	550	12.0	500	7.5	450	5.5	400
12	16.5	600	10.0	600	6.5	450	5.0	400
				Single pile				
3	15.0	450	9.0	450	6.0	400	4.5	350
6	16.0	600	13.0	550	7.5	500	5.5	450
9	15.5	750	14.0	650	8.5	600	7.0	500
12	18.0	800	16.0	700	12.5	600	7.5	550

Table A.4 Details of pile groups supporting RC shear walls.

No. of Stories	Loose Sand S1		Medium sand S2		Med. dense sand S3		Dense sand S4	
	Pile length (m)	Pile dia. (mm)	Pile length (m)	Pile dia. (mm)	Pile length (m)	Pile dia. (mm)	Pile length (m)	Pile dia. (mm)
3	11.0	250	7.0	250	7.5	200	3.5	200
6	12.5	350	8.5	350	6.5	300	6.5	250
9	17.0	400	11.5	400	8.0	350	7.0	300
12	16.5	500	13.5	450	9.5	400	7.0	350

This page has been intentionally left blank.

Appendix B
LATERAL LOAD PROFILES FOR PUSHOVER ANALYSIS

B.1 OVERVIEW

For conducting displacement-based nonlinear pushover analysis, it is essential to deform the structural system conforming to its natural vibrational characteristic. In the present study, the fundamental mode of vibration has been utilized for deforming the structural system. The fundamental mode shape profile is applied as a lateral load pattern for conducting the pushover analysis. This appendix provides the details of the lateral load profile, utilized for conducting pushover analysis, of the various configurations of RC frame and RC wall-frame systems under different soil conditions considered in this study. Other details of the pushover analysis are provided in Chapter 6.

B.2 LATERAL LOAD PROFILES FOR PUSHOVER ANALYSIS

The mode shape corresponding to the fundamental mode of vibrations has been utilized as the lateral load profile for conducting the pushover analysis of the various RC frame and RC wall-frame systems under the different soil-pile-foundation conditions. The fundamental mode shape profiles have been obtained by conducting Eigen analysis. Tables B.1-B.4 shows the fundamental mode shapes of the various RC frame configuration under the various soil-pile-foundation conditions. Similarly, Tables B.5-B.8 shows the fundamental mode shapes of the various RC wall-frame systems under the different soil-pile foundation conditions.

Table B.1 Mode shape profile for 3 storey RC frame system

	3 Bay					5 Bay				
	Soil Type					Soil Type				
Storey	S1	S2	S3	S4	FB	S1	S2	S3	S4	FB
1	0.40	0.38	0.37	0.36	0.32	0.42	0.39	0.36	0.37	0.32
2	0.77	0.76	0.75	0.74	0.74	0.78	0.77	0.68	0.76	0.73
3	1.00	1.00	1.00	1.00	1.00	1.00	1.00	1.00	1.00	1.00
	9 Bay					15 Bay				
	Soil Type					Soil Type				
Storey	S1	S2	S3	S4	FB	S1	S2	S3	S4	FB
1	0.45	0.41	0.40	0.38	0.33	0.47	0.43	0.41	0.39	0.33
2	0.79	0.78	0.77	0.76	0.74	0.80	0.79	0.78	0.77	0.74
3	1.00	1.00	1.00	1.00	1.00	1.00	1.00	1.00	1.00	1.00

Table B.2 Mode shape profile for 6 storey RC frame system

	3 Bay					5 Bay				
	Soil Type					Soil Type				
Storey	S1	S2	S3	S4	FB	S1	S2	S3	S4	FB
1	0.22	0.20	0.19	0.18	0.16	0.25	0.23	0.21	0.20	0.16
2	0.43	0.42	0.41	0.40	0.39	0.46	0.44	0.43	0.42	0.39
3	0.63	0.62	0.62	0.61	0.60	0.65	0.64	0.63	0.63	0.61
4	0.79	0.79	0.79	0.79	0.79	0.81	0.80	0.80	0.80	0.80
5	0.92	0.92	0.92	0.92	0.92	0.93	0.93	0.93	0.92	0.93
6	1.00	1.00	1.00	1.00	1.00	1.00	1.00	1.00	1.00	1.00
	9 Bay					15 Bay				
	Soil Type					Soil Type				
Storey	S1	S2	S3	S4	FB	S1	S2	S3	S4	FB
1	0.27	0.24	0.23	0.21	0.17	0.30	0.27	0.24	0.22	0.17
2	0.48	0.46	0.45	0.44	0.40	0.50	0.48	0.46	0.45	0.40
3	0.67	0.66	0.65	0.64	0.62	0.69	0.67	0.66	0.65	0.62
4	0.83	0.82	0.81	0.81	0.80	0.84	0.83	0.82	0.81	0.80
5	0.94	0.93	0.93	0.93	0.93	0.94	0.94	0.93	0.93	0.93
6	1.00	1.00	1.00	1.00	1.00	1.00	1.00	1.00	1.00	1.00

Table B.3 Mode shape profile for 9 storey RC frame system

	3 Bay					5 Bay				
	Soil Type					Soil Type				
Storey	S1	S2	S3	S4	FB	S1	S2	S3	S4	FB
1	0.14	0.13	0.12	0.11	0.07	0.17	0.15	0.13	0.11	0.08
2	0.26	0.25	0.24	0.23	0.20	0.29	0.27	0.25	0.24	0.20
3	0.38	0.37	0.36	0.35	0.33	0.41	0.39	0.38	0.37	0.33
4	0.51	0.49	0.49	0.48	0.47	0.53	0.52	0.51	0.50	0.48
5	0.62	0.61	0.61	0.61	0.60	0.65	0.63	0.63	0.62	0.61
6	0.73	0.72	0.72	0.72	0.71	0.75	0.74	0.73	0.73	0.72
7	0.84	0.83	0.84	0.83	0.84	0.85	0.85	0.85	0.85	0.84
8	0.93	0.93	0.93	0.93	0.94	0.94	0.94	0.94	0.94	0.94
9	1.00	1.00	1.00	1.00	1.00	1.00	1.00	1.00	1.00	1.00
	9 Bay					15 Bay				
	Soil Type					Soil Type				
Storey	S1	S2	S3	S4	FB	S1	S2	S3	S4	FB
1	0.20	0.17	0.15	0.13	0.08	0.24	0.19	0.16	0.14	0.08
2	0.32	0.29	0.27	0.26	0.21	0.34	0.31	0.29	0.27	0.21
3	0.43	0.41	0.39	0.38	0.64	0.46	0.43	0.41	0.39	0.34
4	0.56	0.54	0.53	0.52	0.48	0.59	0.56	0.54	0.53	0.49
5	0.67	0.65	0.64	0.64	0.61	0.69	0.67	0.66	0.65	0.62
6	0.76	0.75	0.75	0.74	0.73	0.78	0.77	0.76	0.75	0.73
7	0.87	0.86	0.86	0.85	0.85	0.88	0.87	0.86	0.86	0.85
8	0.95	0.95	0.95	0.95	0.94	0.95	0.95	0.95	0.95	0.95
9	1.00	1.00	1.00	1.00	1.00	1.00	1.00	1.00	1.00	1.00

Table B.4 Mode shape profile for 12 storey RC frame system

	3 Bay					5 Bay				
	Soil Type					Soil Type				
Storey	S1	S2	S3	S4	FB	S1	S2	S3	S4	FB
1	0.10	0.09	0.08	0.07	0.04	0.13	0.11	0.09	0.08	0.05
2	0.18	0.17	0.16	0.15	0.12	0.21	0.19	0.18	0.17	0.13
3	0.26	0.25	0.24	0.23	0.20	0.29	0.27	0.26	0.25	0.21
4	0.34	0.34	0.33	0.32	0.29	0.38	0.36	0.35	0.34	0.31
5	0.43	0.42	0.42	0.41	0.38	0.46	0.45	0.44	0.43	0.40
6	0.51	0.51	0.50	0.50	0.47	0.54	0.53	0.52	0.52	0.49
7	0.61	0.60	0.60	0.60	0.58	0.64	0.63	0.62	0.62	0.60
8	0.70	0.70	0.70	0.70	0.70	0.73	0.72	0.72	0.72	0.71
9	0.79	0.79	0.79	0.79	0.79	0.82	0.81	0.81	0.81	0.81
10	0.87	0.87	0.87	0.87	0.88	0.89	0.89	0.89	0.89	0.89
11	0.94	0.95	0.94	0.95	0.95	0.95	0.95	0.95	0.95	0.96
12	1.00	1.00	1.00	1.00	1.00	1.00	1.00	1.00	1.00	1.00
	9 Bay					15 Bay				
	Soil Type					Soil Type				
Storey	S1	S2	S3	S4	FB	S1	S2	S3	S4	FB
1	0.16	0.14	0.11	0.10	0.05	0.19	0.16	0.13	0.10	0.05
2	0.24	0.22	0.20	0.18	0.14	0.27	0.25	0.21	0.19	0.14
3	0.32	0.30	0.28	0.27	0.22	0.35	0.33	0.30	0.28	0.23
4	0.41	0.39	0.37	0.36	0.32	0.44	0.42	0.39	0.37	0.33
5	0.49	0.48	0.46	0.45	0.42	0.52	0.50	0.48	0.46	0.42
6	0.57	0.55	0.54	0.54	0.51	0.59	0.58	0.56	0.55	0.51
7	0.66	0.65	0.64	0.64	0.62	0.68	0.68	0.66	0.65	0.62
8	0.76	0.75	0.74	0.74	0.73	0.77	0.77	0.75	0.75	0.73
9	0.84	0.83	0.83	0.82	0.82	0.85	0.85	0.84	0.83	0.82
10	0.91	0.90	0.90	0.90	0.90	0.92	0.91	0.91	0.91	0.90
11	0.96	0.96	0.96	0.96	0.96	0.97	0.96	0.96	0.96	0.96
12	1.00	1.00	1.00	1.00	1.00	1.00	1.00	1.00	1.00	1.00

Table B.5 Mode shape profile for 3 storey RC wall-frame system

	3 Bay					5 Bay				
	Soil Type					Soil Type				
Storey	S1	S2	S3	S4	FB	S1	S2	S3	S4	FB
1	0.31	0.31	0.31	0.31	0.15	0.30	0.30	0.30	0.30	0.15
2	0.66	0.65	0.65	0.65	0.52	0.65	0.65	0.65	0.65	0.53
3	1.00	1.00	1.00	1.00	1.00	1.00	1.00	1.00	1.00	1.00
	9 Bay					15 Bay				
	Soil Type					Soil Type				
Storey	S1	S2	S3	S4	FB	S1	S2	S3	S4	FB
1	0.30	0.30	0.30	0.30	0.15	0.31	0.30	0.30	0.30	0.15
2	0.65	0.65	0.65	0.65	0.53	0.65	0.65	0.65	0.65	0.53
3	1.00	1.00	1.00	1.00	1.00	1.00	1.00	1.00	1.00	1.00

Table B.6 Mode shape profile for 6 storey building frame with shear wall

	3 Bay					5 Bay				
	Soil Type					Soil Type				
Storey	S1	S2	S3	S4	FB	S1	S2	S3	S4	FB
1	0.14	0.14	0.14	0.14	0.05	0.15	0.14	0.14	0.14	0.05
2	0.30	0.30	0.30	0.30	0.17	0.32	0.61	0.30	0.31	0.18
3	0.48	0.47	0.47	0.48	0.35	0.50	0.49	0.48	0.49	0.36
4	0.66	0.65	0.65	0.66	0.56	0.67	0.67	0.67	0.67	0.58
5	0.83	0.83	0.83	0.83	0.78	0.85	0.84	0.84	0.84	0.80
6	1.00	1.00	1.00	1.00	1.00	1.00	1.00	1.00	1.00	1.00
	9 Bay					15 Bay				
	Soil Type					Soil Type				
Storey	S1	S2	S3	S4	FB	S1	S2	S3	S4	FB
1	0.14	0.15	0.15	0.15	0.05	0.16	0.15	0.15	0.15	0.06
2	0.31	0.32	0.32	0.32	0.19	0.34	0.33	0.33	0.33	0.21
3	0.49	0.50	0.50	0.51	0.38	0.53	0.52	0.52	0.52	0.41
4	0.67	0.68	0.68	0.69	0.60	0.71	0.70	0.70	0.70	0.62
5	0.84	0.85	0.85	0.85	0.81	0.86	0.86	0.86	0.86	0.82
6	1.00	1.00	1.00	1.00	1.00	1.00	1.00	1.00	1.00	1.00

Table B.7 Mode shape profile for 9 storey building frame with shear wall

	3 Bay					5 Bay				
	Soil Type					Soil Type				
Storey	S1	S2	S3	S4	FB	S1	S2	S3	S4	FB
1	0.08	0.09	0.08	0.09	0.03	0.09	0.09	0.08	0.09	0.03
2	0.19	0.19	0.19	0.19	0.10	0.20	0.20	0.19	0.20	0.11
3	0.31	0.30	0.30	0.30	0.20	0.32	0.31	0.31	0.32	0.21
4	0.43	0.42	0.42	0.42	0.32	0.44	0.44	0.43	0.44	0.35
5	0.55	0.54	0.54	0.54	0.46	0.56	0.56	0.56	0.56	0.48
6	0.67	0.66	0.66	0.66	0.60	0.68	0.68	0.67	0.68	0.62
7	0.78	0.78	0.78	0.78	0.74	0.79	0.80	0.79	0.79	0.76
8	0.89	0.89	0.89	0.89	0.87	0.90	0.90	0.90	0.90	0.89
9	1.00	1.00	1.00	1.00	1.00	1.00	1.00	1.00	1.00	1.00
	9 Bay					15 Bay				
	Soil Type					Soil Type				
Storey	S1	S2	S3	S4	FB	S1	S2	S3	S4	FB
1	0.09	0.09	0.09	0.09	0.03	0.09	0.09	0.09	0.09	0.04
2	0.21	0.20	0.20	0.20	0.11	0.21	0.21	0.20	0.20	0.13
3	0.33	0.32	0.32	0.32	0.23	0.34	0.33	0.33	0.33	0.25
4	0.46	0.45	0.45	0.45	0.37	0.47	0.47	0.46	0.46	0.39
5	0.58	0.58	0.57	0.58	0.51	0.60	0.59	0.58	0.59	0.53
6	0.70	0.69	0.69	0.69	0.64	0.71	0.71	0.70	0.70	0.66
7	0.81	0.80	0.80	0.81	0.77	0.82	0.82	0.81	0.81	0.79
8	0.91	0.91	0.91	0.91	0.89	0.91	0.91	0.91	0.91	0.90
9	1.00	1.00	1.00	1.00	1.00	1.00	1.00	1.00	1.00	1.00

Table B.8 Mode shape profile for 12 storey building frame with shear wall

	3 Bay					5 Bay				
	Soil Type					Soil Type				
Storey	S1	S2	S3	S4	FB	S1	S2	S3	S4	FB
1	0.06	0.06	0.06	0.06	0.01	0.06	0.06	0.06	0.06	0.02
2	0.13	0.13	0.13	0.12	0.05	0.14	0.14	0.14	0.13	0.06
3	0.21	0.20	0.20	0.20	0.12	0.21	0.22	0.22	0.21	0.13
4	0.29	0.29	0.28	0.28	0.19	0.31	0.30	0.30	0.30	0.22
5	0.38	0.37	0.37	0.37	0.28	0.41	0.40	0.40	0.39	0.31
6	0.47	0.46	0.46	0.46	0.38	0.50	0.49	0.49	0.49	0.41
7	0.56	0.55	0.55	0.55	0.49	0.59	0.58	0.58	0.58	0.57
8	0.65	0.65	0.65	0.65	0.59	0.67	0.67	0.67	0.67	0.68
9	0.74	0.74	0.74	0.74	0.70	0.76	0.76	0.76	0.76	0.73
10	0.83	0.83	0.83	0.83	0.81	0.84	0.84	0.84	0.85	0.83
11	0.92	0.92	0.92	0.92	0.91	0.93	0.93	0.93	0.93	0.92
12	1.00	1.00	1.00	1.00	1.00	1.00	1.00	1.00	1.00	1.00
	9 Bay					15 Bay				
	Soil Type					Soil Type				
Storey	S1	S2	S3	S4	FB	S1	S2	S3	S4	FB
1	0.07	0.06	0.06	0.06	0.02	0.07	0.06	0.06	0.06	0.02
2	0.15	0.14	0.14	0.14	0.07	0.15	0.14	0.14	0.14	0.08
3	0.24	0.22	0.22	0.23	0.15	0.24	0.23	0.23	0.23	0.116
4	0.33	0.32	0.32	0.32	0.24	0.34	0.33	0.32	0.32	0.26
5	0.42	0.41	0.41	0.42	0.34	0.44	0.42	0.42	0.42	0.36
6	0.51	0.50	0.50	0.51	0.44	0.53	0.52	0.51	0.51	0.46
7	0.61	0.60	0.60	0.61	0.55	0.63	0.61	0.61	0.61	0.57
8	0.70	0.69	0.69	0.71	0.66	0.72	0.71	0.71	0.71	0.68
9	0.79	0.78	0.78	0.79	0.76	0.82	0.80	0.80	0.79	0.77
10	0.86	0.86	0.86	0.87	0.85	0.88	0.87	0.87	0.87	0.86
11	0.94	0.93	0.93	0.94	0.93	0.94	0.94	0.94	0.94	0.94
12	1.00	1.00	1.00	1.00	1.00	1.00	1.00	1.00	1.00	1.00

This page has been intentionally left blank.

Appendix C
RAYLEIGH DAMPING

C.1 OVERVIEW

As already discussed in Chapter 3, it is possible for the numerical solution to exhibit spuriousness during a nonlinear analysis of the SSI system. To capture these oscillations, numerical damping can be incorporated. However, even after the incorporation of the numerical damping, the spurious oscillations may not necessarily be captured. Additionally, it is quite essential to simulate the various frictional losses occurring during the vibration of an SSI system. Under such circumstances a small amount of Rayleigh damping can prove to be quite useful in capturing the spurious oscillations and, at the same time, simulating various frictional losses. The basics of the Rayleigh damping have already been elaborately discussed in Chapter 3 and hence are not reproduced here. This appendix provides the details of Rayleigh damping utilized for conducting nonlinear time history analysis in Chapter 7.

C.2 RAYLEIGH DAMPING

In the present study, a small amount (3% for soil and 5% for structure) of Rayleigh damping has been incorporated for capturing the spurious oscillations and simulating the various frictional losses during the vibration of the SSI system. Table C.1 shows the Rayleigh damping coefficients for soil corresponding to the different conditions. Tables C.2 and C.3 show the Rayleigh damping coefficients for the various configuration of RC frame and RC wall-frame systems respectively.

Table C.1 Rayleigh damping coefficients for soil elements

Soil Type	Avg. v_s (m/s)	ζ_n (%)	ω_1 (rad/s)	ω_2 (rad/s)	a_0	a_1
S1	193	3	10.11	30.32	0.45	0.0015
S2	212	3	11.10	33.30	0.50	0.0014
S3	240	3	12.57	37.70	0.57	0.0012
S4	270	3	14.14	42.41	0.64	0.0011

Table C.2 Rayleigh damping coefficients used for frame building

No. of Storeys	Bay	ζ_n (%)	ω_1 (rad/s)	ω_2 (rad/s)	a_0	a_1
3	3	5	9.38	196.35	0.90	0.0005
	5	5	8.85	125.66	0.83	0.0007
	9	5	8.98	73.92	0.80	0.0012
	15	5	8.89	48.33	0.75	0.0017
6	3	5	6.24	51.50	0.56	0.0017
	5	5	6.20	49.87	0.55	0.0018
	9	5	6.17	48.71	0.55	0.0018
	15	5	6.15	47.96	0.55	0.0018
9	3	5	5.49	39.77	0.48	0.0022
	5	5	5.52	38.79	0.48	0.0023
	9	5	5.55	38.31	0.48	0.0023
	15	5	5.55	37.85	0.48	0.0023
15	3	5	4.58	32.56	0.40	0.0027
	5	5	4.69	32.22	0.41	0.0027
	9	5	4.76	31.89	0.41	0.0027
	15	5	4.79	31.73	0.42	0.0027

Table C.3 Rayleigh damping coefficients used for wall-frame building

No. of Storeys	Bay	ζ_n (%)	ω_1 (rad/s)	ω_2 (rad/s)	a_0	a_1
3	3	5	39.77	255.41	3.44	0.0003
	5	5	31.89	152.88	2.64	0.0005
	9	5	24.74	86.07	1.92	0.0009
	15	5	19.88	55.60	1.46	0.0013
6	3	5	13.96	233.58	1.32	0.0004
	5	5	11.95	152.14	1.11	0.0006
	9	5	10.18	89.76	0.91	0.0010
	15	5	9.11	55.21	0.78	0.0016
9	3	5	8.89	139.63	0.84	0.0007
	5	5	8.05	106.68	0.75	0.0009
	9	5	7.21	77.38	0.66	0.0012
	15	5	6.68	59.28	0.60	0.0015
15	3	5	6.58	88.50	0.61	0.0011
	5	5	6.27	71.40	0.58	0.0013
	9	5	5.82	56.10	0.53	0.0016
	15	5	4.43	46.20	0.40	0.0020

PUBLICATIONS

Journal

Sharma, N., Dasgupta, K., and Dey, A. (2020). "Investigation on the natural period of RC frame with shear wall supported on soil-pile foundation system and its prediction using artificial neural network." *Journal of Earthquake Engineering* (*Taylor and Francis*). doi:10.1080/13632469.2020.1824876.

Sharma, N., Dasgupta, K., and Dey, A. (2020). "Natural period of reinforced concrete building frames on pile foundation considering seismic soil structure interaction effects." *Structures* (*Elsevier*), 27, 1594–1612. doi:10.1016/j.istruc.2020.07.010.

Sharma, N., Dasgupta, K., and Dey, A. (2020) "Optimum lateral extent of soil domain length for dynamic SSI analysis of RC framed buildings on pile foundations" *Frontiers in Structural and Civil Engineering* (*Springer*), 14(1), 62–81. doi:10.1007/s11709-019-0570-2.

Sharma, N., Dasgupta, K., and Dey, A. (2018). "A state-of-the-art review on seismic SSI studies on building structures." *Innovative Infrastructure Solutions* (*Springer*), 3(1), 22. doi:10.1007/s41062-017-0118-z.

Sharma, N., Dasgupta, K., and Dey, A. (To be submitted) "Assessment of inealstic seismic response and ductility demands of RC frame and RC wall-frame systems under the influence of soil structure interaction."

Sharma, N., Dasgupta, K., and Dey, A. (To be submitted). "Influence of soil-structure interaction on the ductility capacity of RC frame and RC wall-frame systems."

Book Chapter

Sharma, N., Dasgupta, K., and Dey, A. (2020). "Seismic behaviour of RC building frame considering soil-structure interaction effects." In *Advanced Topics in Structural Vibration*, Ed. S. Dutta, E. Inan, S. K. Dwivedy, Springer, Singapore. 157–170: ISBN No. 978-981-15-5862-7.

Sharma, N., Dasgupta, K. and Dey, A. (2018). "Importance of inclusion of soil structure interaction studies in design codes." In *Recent Advances in Structural Engineering*, Vol. 2, Ed. A. Rama Mohan Rao, K. Ramanjaneyulu, Springer, Singapore, 233–244: ISBN No. 978-981-13-0365-4.

Conference

Dey, A., Sharma, N. and Dasgupta, K. (2020). "Influence of shear wall on seismic response of RC frame buildings on pile foundation considering SSI." In *17th World Conference in Earthquake Engineering*, 13-18 September 2020, Sendai, Japan.

Sharma, N., Dasgupta, K., and Dey, A. (2018). "Seismic SSI effects on fundamental period of reinforced concrete frame with shear wall." In *Proceedings of the 11th Structural*

Engineering Convention, 19-21 December 2018, Paper No. 20180391_R1, Jadavpur University, Kolkata, India.

Sharma, N., Dasgupta, K., and Dey, A. (2018). "Natural period of RC buildings considering seismic soil structure interaction effects." In *16th Symposium on Earthquake Engineering*, 20-22 December 2018, Paper No. 275, IIT Roorkee, India.

Sharma, N., Dasgupta, K., and Dey, A. (2017). "Nonlinear static behaviour of RC-building frame under lateral loads considering soil structure interaction effects." In *Indian Geotechnical Conference*, 14-16 December 2017, Paper No. Th12_729, IIT Guwahati, India.

Sharma, N., Dasgupta, K., and Dey, A. (2016). "Finite element modeling intricacies for SSI studies." In *6th International Conference on Recent Advances in Geotechnical Earthquake Engineering and Soil Dynamics*, 1-6 August 2016, Paper No. 43, IIT Roorkee Extension Center, Greater Noida, India.

Sharma, N., and Dasgupta, K. (2015). "Review of seismic soil-structure interaction with pile foundation." In *UKIERI Workshop on Seismic Requalification of Pile Supported Structures (SRPSS)*, 7-9 January 2015, IIT Guwahati, India.